ES&T

Toxicants in ecosystems

P.E.T. ORGANICS.
NOW YOU CAN FINALLY SEE
HOW YOUR LAB COMPARES.

Only the new P.E.T. Organics Program from APG gives you a measure of importance. For the first time, Analytical Products Group, who has operated the only interlaboratory Performance Evaluation Program in the country for the past seven years, is extending this valuable service to include the GC and GC/MS 600 Series Methods.

By using the P.E.T. Organics standards, you can evaluate the performance of your laboratory against other labs throughout the country. With blind samples at two levels, the P.E.T. Program has the ability to evaluate your laboratory fairly and impartially. Our summary reporting format gives you the answers you need while maintaining complete confidentiality.

The P.E.T. Program works. More than 500 laboratories throughout the U.S. and Canada use this program as their external QA source. The addition of P.E.T. Organics for Volatiles, Acids, Base/Neutrals, and Pesticides brings you a new level of control in the important area of Quality Assurance for Organic Analysis. To put the P.E.T. Organics Program to work for you, order your first standards set today. Contact Analytical Products Group, Inc., 2730 Washington Blvd., Belpre, OH 45714.

Toll-free
1-800-272-4442
(In Ohio:
1-614-423-4200,
FAX: 1-614-423-5588)

APG
Analytical Products Group, Inc.
The measure of quality

CIRCLE 4 ON READER SERVICE CARD

APG Analytical Products Group, Inc.

Customer Code: 9736

Parameter: Benzene

Your Result:
Spike Value:
Mean of Reporting Laboratories:
Actual Standard Deviation:
Number Reporting:
Average % Recovery:
Your % Recovery:
Your Result Was:
Deviations from the Mean:
Comment:

Parameter: 1,2 Dichlorobenzene

Your Result:
Spike Value:
Mean of Reporting Laboratories:
Actual Standard Deviation:
Number Reporting:
Average % Recovery:
Your % Recovery:
Your Result Was:
Deviations from the Mean:
Comment:

Spike Compounds

Level 1 ug/L   Level 2   Page: 1

10.000   56.000
8.960   54.280
9.501   58.112
2.073   15.159
136.040   48
111.607   107.060
0.241   103.169
                    0.139

ES&T

CONTENTS

Volume 24, Number 1, January 1990

FEATURES

VIEWS

REGULATORY FOCUS

DEPARTMENTS

UPCOMING

RESEARCH

ห้องสมุดกรมวิทยาศาสตร์บริการ

–5 กพ 2533

Changes at *ES&T*

This month *ES&T* welcomes three new Associate Editors: Dr. Ron Hites of Indiana University, Dr. Joseph Suflita of the University of Oklahoma, and Dr. Walter Giger of the Swiss Federal Institute for Water Resources and Water Pollution Control (EAWAG). They join Dr. John Seinfeld of the California Institute of Technology and Dr. Philip Singer of the University of North Carolina at Chapel Hill.

Our principal purpose in increasing the corps of associate editors is to provide more expert coverage of the broad range of papers submitted to *ES&T*, to give more personal attention to the review process, and to attempt to decrease the time from initial submission to first decision. One of the most important functions of the associate editors will be in the selection of reviewers. The review process is the cornerstone of our editorial policy. Nothing is more important in the assurance of a quality journal than the review of a manuscript by peers. Successful review begins with the correct choice of reviewers. This, in turn, is determined by the knowledge of the associate editor and by the corps of reviewers available to the journal. The expertise of our associate editors, and the fact that they will be choosing reviewers in the future, should improve the quality of the reviews we are getting and speed the time of the review process by minimizing "zero reviews," the return of a manuscript with no review.

During the coming months the editorial staff will make a concerted effort to interact with reviewers to assist them in improving the quality of their reviews. In some cases reviews are truly excellent, but unfortunately many times they are superficial. Undoubtedly this is often due to hectic schedules and the press of many professional duties. Journals such as *ES&T* are very beholden to reviewers for contributing their time on a volunteer basis. Nonetheless, serving as a reviewer is part of the professional obligation of all who wish to publish in the scientific literature. What we at *ES&T* hope is that we can encourage all reviewers who accept this duty to give some thought to how they review papers and to approach this task with the same degree of care and thoroughness they use when they prepare a paper for submission.

Another significant change in the editorial review process will be that the editors will communicate directly with authors regarding revisions that are recommended for their manuscripts. We feel that authors deserve a careful and individualized analysis of their papers by a scientific editor who is familiar with the field, can interpret the views of reviewers, and can make a conscientious decision on its disposition.

The editors look forward to the coming year as we install the new process for review of manuscripts. Undoubtedly there will be glitches as we change the manner in which manuscripts are handled, but in the long run we expect that the quality of the process will be improved and, we hope, the time from receipt of a manuscript to publication will be decreased.

0013-936X/89/0924-0003$02.50/0 © 1989 American Chemical Society

Environ. Sci. Technol., Vol. 24, No. 1, 1990 **3**

ES&T
CURRENTS

INTERNATIONAL

Representatives of 71 nations attending a conference on global warming failed to specify levels at which man-made carbon dioxide emissions should be stabilized and by how much they should be reduced. The majority of representatives wanted to pass a resolution that calls on industrialized nations to hold CO_2 emissions at current levels and curtail them by 20% within an as-yet unspecified number of years. The stabilization and reduction provisions were deleted under pressure from U.S. and Japanese representatives. The U.S. position is that stabilization should be achieved "as soon as possible," but that cuts in CO_2 should be decided on only after more research on causes of global warming. Participants at the conference, held in Noordwijk, Holland, in November, did agree on the need to reforest 30 million acres per year and for a treaty on global warming by 1992.

An international campaign to stop large-scale extinction of plant and animal species has been launched by the World Resources Institute (WRI, Washington, DC), the United Nations Environment Programme, and the World Conservation Union. A WRI report, "Keeping Options Alive," issued in late October, predicts that if current rates of extinction continue, 25% of the world's flora and fauna could disappear within 25–50 years. The report notes that threats of extinction are not confined to tropical regions. For example, in Florida and the Pacific Northwest, logging, man-made changes in water drainage, and pollution are destroying several plant and animal species such as the Florida panther and unique species of mushrooms. The three organizations have begun a conservation campaign with consultations in Bangkok, Thailand, and hope to evolve a final strategy to be presented at a world meeting in 1992.

Lithuania has become a major center of environmentally active "Green Party" activity in the U.S.S.R. Lithuanian Green Party chairman Zigmas Vaisvila told the National Press Club Nov. 8 that members of his party oppose the operation of the RBMK 1500-MW nuclear power plant at Ignalina, 400 mi (640 km) west of Moscow. They note that the RBMK plant, which lacks containment facilities, is in the same class as the plant at Chernobyl that suffered the April 26, 1986 mishap; Ignalina, however, is 50% larger. Vaisvila also said that water pollution is so serious in Lithuania that all beaches on the Baltic Sea were closed to swimmers in the summers of 1988 and 1989, and that more than 70% of Lithuania's wastewater is untreated. He says that as Lithuania gains more autonomy, he expects vigorous legislative action aimed at environmental cleanup. Vaisvila, a member of the U.S.S.R. Congress of People's Deputies, told *ES&T* that Lithuania would welcome assistance from U.S. environmental professionals.
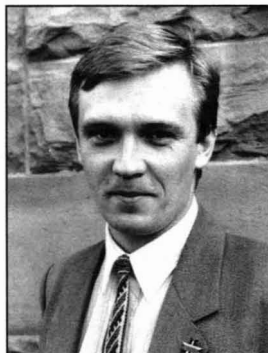
Vaisvila: With autonomy, cleanup

FEDERAL

The Forest Service is adopting a policy that would result in the preservation of about 50% of currently unprotected old-growth forest lands. Measures will include curtailing the patchwork clear-cutting of 25- to 40-acre tracts. The agency would permit cutting much larger tracts—40–1000 acres—in a manner that would leave other forest areas undisturbed for wildlife. Other steps will include keeping some trees and undergrowth in an otherwise clear-cut area to support future growth and accelerating research to assess the amount of old growth. A spokesman for the Wilderness Society has questioned the Forest Service's proposed policy by noting that there is no firm definition of old-growth forest.

EPA has field-tested its proposed revisions to the Superfund Hazard Ranking System (HRS) by inspecting 29 sites. Each site was scored on the basis of the revised HRS. Under the current HRS, the groundwater pathway scores highest, but under the revised system, first proposed Dec. 23, 1988, the surface water pathway scores higher. Also, although overall scores at the sites increased under the revisions, groundwater pathway scores decreased. Costs of doing inspections under the proposed revisions averaged about $175,000 a site, up from $110,000 under current practice. About 50% of the costs are for sampling and analysis. A report on the field test was issued Aug. 18, 1989; the final revisions to the HRS are expected in March 1990.

The Superfund program needs rebuilding from the ground up, according to a report, "Coming Clean—Superfund Problems Can Be Solved," issued in mid-October by the congressional Office of Technology Assessment (OTA). The report offers 38 ways to revamp the program. One example consists of finding alternatives for groundwater restoration: "Pumping it and treating it to remove contaminants is not reliable or predictable for anything but exceptionally simple situations." The report calls for Congress, the public, and EPA to develop a consensus on a detailed strategy for a multidecade Superfund program. "Simply tinkering with Superfund will not work," says OTA.

EPA will conduct a testing review of all conventional and alternative motor fuels under Section 211 of the Clean Air Act (CAA) and Section 4 of the Toxic Substances Control Act (TSCA). The testing review will encompass fuels such as gasoline, diesel, methanol, ethanol, compressed natural gas, and propane. EPA will determine whether fuels and fuel additives should be registered and tested by the registrants for health and environmental effects (CAA, Section 211), or whether fuels and additives are to be tested as

0013-936X/89/0924-0005$02.50/0 © 1989 American Chemical Society

Environ. Sci. Technol., Vol. 24, No. 1, 1990 **5**

chemical mixtures (TSCA, Section 4). The action is being taken in response to a petition from transportation organizations and manufacturers, under Section 21 of TSCA, requesting the agency to require manufacturers and processors of methanol to test that fuel under Section 4 of TSCA.

STATES

Much of the work in Texas that involves bioassays is being done at a research center at Texas A&M University (College Station) directed by Steve Safe. The objective of the research is to develop new methods to assess the toxic potential of chemical wastes in aquifers and in soils near landfills and Superfund sites. One of Safe's projects is to devise inexpensive bioassays to evaluate the impact of polychlorinated biphenyls (PCBs), dioxins, and certain other organic contaminants on animals such as rodents and fish. Another is to determine whether results of in vitro studies can be used to estimate in vivo effects of exposure to chemicals such as PCBs.

The city of Toledo, OH, is recycling sewage sludge into a fertilizer supplement at its Bayview Reclamation Plant, which started up in November. The plant uses a process developed by N-Viro Energy Systems (Toledo) that mixes sludge with kiln dust to pasteurize, stabilize, disinfect, deodorize, dry, and granulate the city's municipal wastewater sludge. The pasteurization process is the only one that immobilizes metals in the sludge, according to N-Viro president Pat Nicholson. The plant cost less than $3 million to construct, and operation and maintenance costs are estimated at $100 per dry ton. Previously, Toledo had to haul its sludge by truck to a landfill at a cost of about $8000 a day.

Seventeen states have passed laws requiring the coding of plastic bottles. Codes will identify the resin used in the bottles to make it easier for recyclers to identify the type of plastics they are recycling. Bottles containing 16 oz or more and rigid plastic containers that hold 8 oz or more will be subject to the laws. The codes used were published in July 1988 by the Society of the Plastics Industry (SPI, Washington, DC). Florida's law requiring SPI codes on bottles will be the first, and will go into effect July 1, 1990. Similar laws will take effect in 12 states in 1991 and in four more states in 1992.

The Illinois Environmental Protection Agency (IEPA) plans to extend its vehicle emissions testing program as part of the effort to solve the ozone problem in the Chicago metropolitan area. The current annual inspection program will be continued. Some urbanized areas not included in the current testing program could be added. These include Aurora, Elgin, and Joliet. Anti-tamper checks also may be implemented. Also, IEPA director Bernard Killian announced that the state has adequate capacity to manage hazardous waste expected to be generated by Illinois industries during the next 20 years. IEPA submitted this information to the federal EPA under Superfund requirements that each state submit a capacity assurance plan.
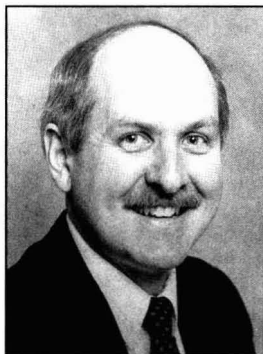
Killian: Can handle expected waste

Tucson, AZ, will use ozone to disinfect water at its new 150 million gal/day potable water treatment plant, scheduled for completion in late 1991. The plant will produce 6000 lb/day (2727 kg/day) of ozone with generators supplied by Emery Ozone Technology (Cincinnati, OH). According to Emery spokesman Jim Merritt, ozone is "particularly beneficial where surface water is used as the primary water source." He adds that its use reduces the formation of potentially carcinogenic trihalomethanes, which form when chlorine reacts with organic compounds dissolved in water. Excess ozone becomes oxygen before water leaves the treatment system.

SCIENCE

The Antarctic spring of 1989 showed the deepest ozone hole recorded so far—slightly deeper than the record hole of 1987. Scientists disagree, however, on whether and to what extent the plankton population of the Antarctic Ocean may be adversely affected by increased exposure to ultraviolet light, especially

UV-B. For example, Greg Mitchell of the Scripps Institution of Oceanography (La Jolla, CA) says that there have been huge blooms of phytoplankton despite the ozone hole, and he doubts that the UV-B had an adverse effect. On the other hand, Robert Bidigare of Texas A&M University ran tests in a tank and found that UV-B reduced the productivity of certain species of phytoplankton. He warned, however, that it is hard to extrapolate his results to the Antarctic Ocean, because there may be countervailing effects of turbid water or of natural protective screens produced by the phytoplankton itself.

How fast do contaminants move from the surface to groundwater tables? Purdue University scientists are trying to answer that question by measuring tritium that originated from nuclear atmospheric testing during the 1950s and 1960s. In studies in central Indiana, for instance, Steven Fritz and his team found that the tritium was percolating downward at about one foot (30.5 cm) a year. Fritz notes, however, that this technique is limited to use on flat soil or hilltops. Nevertheless, he says that the use of tritium can be a first step toward quantifying travel times of contaminants through soil zones. Results of Fritz's studies were presented Nov. 8 at the Geological Society of America's annual meeting in St. Louis.

TECHNOLOGY

Polychlorinated biphenyls (PCBs) can be decomposed faster when the natural biodegradation process is accelerated, according to scientists at General Electric (Schenectady, NY). They say that they will be able to test the process in the Hudson River within 24 months—more than one year ahead of schedule. Stephen Hamilton, GE's manager of corporate environmental science and technology, explains that his team found bacteria that "feed" on PCBs, and hopes to accelerate that natural process. GE scientist Daniel Abramowicz says that in laboratory tests, concentrations of Aroclor 1242, the most chlorinated PCB in the Hudson River, were reduced by more than 90% in 23 weeks. Both aerobic and anaerobic bacteria can be used, but the anaerobes work better on the more highly chlorinated PCBs. Abramowicz believes that a two-step process using both bacteria eventually can eliminate all PCBs in river sediments.

Clean-burning hydrogen—is it a viable fuel option for the future? When hydrogen is burned, it yields only about 50% of the energy that went into making it. Hydrogen could be a means of storing solar photovoltaic (PV) energy (the H_2 is obtained by electrolyzing water with PV energy). If solar power becomes cheap enough, the concept could make economic sense, despite the low energy returns of hydrogen, according to a report by the World Resources Institute (Washington, DC). The hydrogen could store the photovoltaic energy for use at night and on cloudy days. David Carlson of Solarex (Rockville, MD) estimates that to make enough hydrogen to replace natural gas in the nation's pipelines (15% efficient PV and 84% efficient hydrogen production) would require a desert area of 24,000 mi^2, about 7% of U.S. desert area.

One way to dispose of liquid plutonium waste may be to fuse it with sand at a temperature of 2000 °F (1083 °C) to immobilize it into a black glass-like material. That process will be tried at the Department of Energy's plutonium processing plant (Aiken, SC). If the trial succeeds, it could provide a means of cleaning up waste that has accumulated for nearly 40 years from the U.S. nuclear weapons program. About two-thirds of the nation's nuclear weapons waste is stored in Aiken and is estimated to contain about 800 million curies of radiation. Most of the remainder is stored in Hanford, WA. It is estimated that if the test succeeds, cleaning up the backlog of plutonium wastes in Aiken could take 15 years and cost $1.28 billion. Cleaning up all nuclear weapons waste could take at least 20 years and cost hundreds of billions of dollars. Plans are to store the vitrified wastes at Yucca Mountain, NV.

Anaerobic fermentation of municipal and industrial liquid and solid wastes can produce energy and chemicals as well as solve pollution problems, says Sam Ghosh of the University of Utah. A pilot plant that uses his two-phase system is in use in DuPage County, IL. Ghosh and DuPage County investigators say that the process destroys pathogenic bacteria, enteroviruses, and parasites and is not plagued with problems of foaming, overloading, and equipment instability. Also, organic wastes are converted to methane and to a solid residue useful as a medium-grade ammonia-containing fertilizer. Ghosh

PCB degradation model for Hudson River

Injection wells

Injection port for nutrients and organisms

Pump

Pumps

Sampling ports

Water

Sediment

Recirculating water
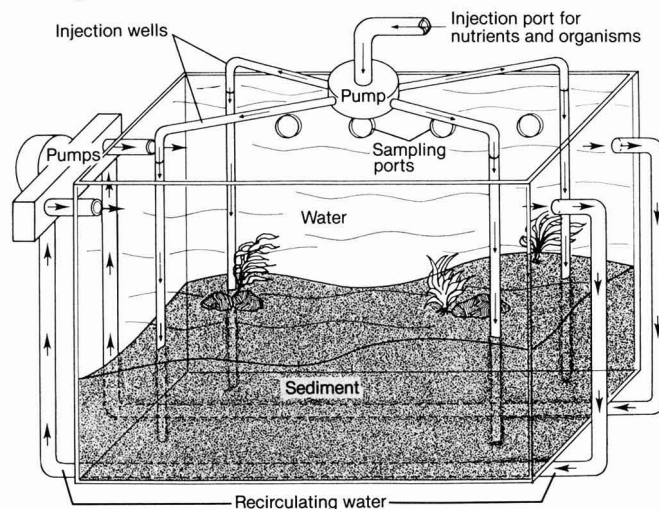
Source: General Electric.

says that his system can be used with many organic and biomass wastes. Results of pilot plant operations have impelled DuPage County officials to request approval from the Illinois Environmental Protection Agency for the construction of a full-scale water pollution control plant that uses Ghosh's process.

BUSINESS

JVC America (Tuscaloosa, AL) is the first user of a carbon-bed regeneration system developed by Airco Gases (Murray Hill, NJ). The carbon-bed system is combined with the existing Airco Solvent Recovery System (ASRS) to recover more than 95% of solvent vapors. It is designed to capture fugitive emissions. Currently EPA requires that 85% of solvents be recovered but has proposed a 93% recovery requirement. Michael Heil, Airco Gases' manager of solvent recovery systems, explains that anywhere the solvent might escape to the atmosphere, it is blanketed with nitrogen and forced back to the recovery system. Spokespersons for JVC say that the system started up in May 1988 and that they have recouped the cost of the system in less than one year. The company manufactures magnetic videotapes.

Much of the nation's coke-making and, eventually, steel-making industry will be shut down if more stringent air quality requirements under consideration by Congress

become law, Walter Williams, CEO of Bethlehem Steel, warned a House committee Oct. 19. He added that there is no sound scientific basis for stricter requirements and that "massive expenditures to achieve unrealistic standards. . . are just as harmful to the competitiveness of America's steel producers as are equally large subsidies to steel producers abroad." Williams told committee members that the steel industry has already spent billions of dollars to comply with the existing Clean Air Act and has acknowledged the need to control toxic air pollutants with maximum achievable control technology, even though this might cost billions more.

Sales of flue gas desulfurization (FGD) systems in the United States could exceed $10 billion during the 1990s, predicts Robert Conley, president of Pure Air (Allentown, PA). Conley also notes that if the Bush administration's proposed clean air legislation is passed, 85% of emission reductions will be required from 15 eastern, southern, and midwestern states and that costs could rise as high as $7 billion a year over the next 20 years. Conley estimates capital costs of FGD for a 500-MW power plant at $150/kWh. He also pegs the FGD market at about $2 billion/yr if any of the Clean Air legislation now before Congress becomes law. Pure Air is a joint venture of Air Products and Chemicals, Inc., and Mitsubishi Heavy Industries America.

Ecotoxicology

The study of the effects of chemicals on natural systems

The rapidly expanding science of ecotoxicology will be explored in a series of four articles. This series will cover the regulatory and scientific topics that are fundamental to the development of ecotoxicology.

Ecotoxicology can be defined as the study of the fate and effect of toxic agents in ecosystems. Ecotoxicology is the study of toxic effects on biota—particularly on communities and populations—and their interaction with processes controlling the functioning of defined ecosystems. Within this definition one may place the science of environmental toxicology.

The growth of ecotoxicology, like risk assessment, has paralleled the increased national awareness of the environment during the past two decades. The creation of the Federal Water Pollution Control Administration and EPA in the 1960s and early 1970s resulted in increased ecotoxicological research funding. The science is complex and addresses a broad range of issues that are frequently the focus of public concern and national and international policy.

The proliferation of water quality problems (e.g., elevated toxicant concentrations in fish tissue) makes painfully clear our lack of understanding of ecotoxicology and its role in maintaining ecosystem integrity. These problems, in some cases the result of intermedia pollutant transfer, are recognized as potentially catastrophic phenomena. This four-part series will explain the regulatory activities and research developments in aquatic and wildlife toxicology and will give a final perspective on maintaining ecosystem integrity.

The first article, by John Bascietto of the U.S. Department of Energy and Dexter Hinckley, James Plafkin, and Michael Slimak of EPA, provides an overview of applications of ecotoxicology through the various environmental regulatory acts and their respective EPA programs. Many ecological risk assessment protocols are modifications of methods used to characterize risk to public health. Unfortunately, these methods often lack environmental realism or validation and may not effectively measure ecosystem integrity. New directions within EPA reflect an increased emphasis on the role of sediments, biomarkers, and ecosystem assessments in regulating environmental pollutants.

In the second article, John Cairns of Virginia Polytechnic Institute and State University and Donald Mount of the EPA Environmental Research Lab in Duluth, MN, address aquatic toxicology from several perspectives. They discuss the problem of species extrapolation, whereby effects on a surrogate test species or multispecies system are related to in situ effects. They note that more standardized toxicity tests and multiassay test batteries are required to reduce extrapolation uncertainty. Future needs they identify include more ecosystem effect validation of test systems, predictive models addressing ecosystem functioning and resilience, and methods to assess ecological perturbations at hazardous-waste sites.

In the third article, wildlife toxicology is discussed by David Hoffman, Barnett Rattner, and Russell Hall of the Patuxent Wildlife Research Center in Laurel, MD. They review the various approaches used, both regulatory and new research developments, in assessing acute and chronic effects on wildlife. The approaches and problems associated with extrapolation between laboratory and field are addressed. They highlight the state of the art in contaminant interactions, stress effects, biomarkers, bioaccumulation, toxicokinetics, and validation studies.

Finally, in the fourth article, Hallet Harris and Paul Sager (University of Wisconsin–Green Bay), Henry Regier (Toronto University), and George Francis (University of Waterloo) discuss ecotoxicology from an ecosystem integrity standpoint, using studies of the Great Lakes as examples. The authors present a thought-provoking perspective on historical and current approaches to maintaining ecosystem integrity. They address the weaknesses of past efforts to regulate toxicants by controlling discharges from point sources and the critical research components involved in maintaining and monitoring ecosystem integrity. Complex socioeconomic issues and multiple interest groups are involved, and the social learning process plays a major role.

Our understanding of the critical role ecotoxicology plays in maintaining, degrading, or improving life is growing. I hope that the new developments, applications, and ideas presented in this *ES&T* series will both increase awareness and stimulate the science.

The outline of this series was written by G. Allen Burton, Jr., who suggested and coordinated the articles and encouraged fellow scientists to contribute to the series. Burton is an assistant professor of biological sciences, director of the Environmental Health Sciences Program, and associate director of the Toxicant Contaminant Research Program at Wright State University (Dayton, OH). He has authored or coauthored 30 publications on aquatic toxicology and environmental microbiology.

Ecotoxicity and ecological risk assessment

Regulatory applications at EPA

First part of a four-part series

John Bascietto
U.S. Department of Energy
Washington, DC 20585

Dexter Hinckley
James Plafkin
Michael Slimak
U.S. Environmental Protection Agency
Washington, DC 20460

Most of the laws under which EPA operates require protection of "human health and the environment," or words to that effect. Since its establishment in 1970, EPA has labored mightily to do both—protect health and protect the environment. However, resource constraints have forced many hard choices. Typically, those activities most closely related to identification and reduction of risks to human health have received the higher priority, leaving few dollars or staff for strictly environmental or ecological protection.

Despite these constraints, ecological risk assessment, based on ecotoxicity data, has been an important activity under many programs at EPA. The Office of Pesticides and Toxic Substances, for example, is concerned about potential impacts of pesticides and toxic chemicals on organisms, including aquatic and terrestrial communities. Its legal mandates come from the Federal Insecticide, Fungicide, and Rodenticide Act (FIFRA) and the Toxic Substances Control Act (TSCA).

The Office of Water is required by the Clean Water Act to restore and maintain the biological integrity of the nation's waters and, specifically, to ensure the protection and propagation of a balanced population of fish, shellfish, and wildlife. EPA also develops methods, including biological monitoring and assessment methods, for establishing and measuring water quality crite-

ria. These statutory requirements have encouraged the Office of Water to develop innovative approaches to ecological assessment.

The Office of Solid Waste and Emergency Response (OSWER) has responsibility for assessment of effects from solid waste and hazardous waste and for remediation of abandoned hazardous-waste sites under Superfund. Historically, OSWER guidance has focused primarily on health risks. However, national and site-specific strategies for remediation are now placing increased emphasis on ecological impacts as well, especially in the Superfund program.

We will now describe current approaches to ecological risk assessment used by the pesticides, toxics, and water programs and sketch new directions being explored by EPA.

Pesticides and toxic substances

Both programs under the Office of Pesticides and Toxic Substances, the Office of Pesticide Programs (OPP) and the Office of Toxic Substances (OTS), assess risks to ecological resources using an ecotoxicological approach: laboratory toxicity bioassays to determine hazard, determination of exposure either from monitoring data or predicted from models, and a comparison of exposure to hazard using the quotient method. In the quotient method, the exposure value is directly compared with a toxicity endpoint (e.g., concentration in water to an LC_{50} value; 10 ppm/100 ppm), the LC_{50}

TABLE 1
Data sources and assessment factors used by OTS[a] to evaluate need for testing of new chemicals

Data source available	Assessment factor to be applied
Structure-activity derived LC_{50} value	1000
Single LC_{50} value from chemical analog[b]	1000
Single test LC_{50} value for PMN[c]	1000
Two LC_{50} values for same analog (e.g., 1 fish, 1 algal test)	1000
Two LC_{50} values for PMN (e.g., 1 fish test, 1 invertebrate)	1000
Three LC_{50} values for same analog (fish, algae, invertebrate)	100
Five LC_{50} values for same analog (3 invertebrates, 2 fish)	100
Five LC_{50} values for the PMN (e.g., 3 algae, 2 fish)	100
Maximum acceptable toxic concentration for analog	10
Field study	1

[a]EPA's Office of Toxic Substances.
[b]"Analog" is a chemical similar to that proposed for production.
[c]"PMN" is the Premanufacture Notification describing the chemical.

value being the concentration lethal to 50% of a test population. The closer the quotient is to 1 (or greater), the higher the probability that an adverse effect will occur.

Interpreting this adverse effect, that is, the likelihood that what is observed in the lab will actually occur in the field, is one of the greatest uncertainties in both programs. Although each program derives it differently, the final result is the application of a safety factor to account for uncertainty.

The pesticide and toxic substances programs are similar in their approach to assessing ecological risk, but the quantity of data used to make assessments is strikingly different. TSCA assessments tend to be data-poor, with only limited ecological effects information being provided by the company submitting a premanufacture notification, whereas FIFRA assessments are usually data-rich. Why?

FIFRA is a registration law that gives EPA legal authority to require up-front testing. TSCA is not a registration law but, rather, a "review and approval law." A case must be made that a new chemical is likely to cause adverse health or ecological effects before any substantial testing can be required.

New chemicals under TSCA

Because of the large numbers of industrial chemicals that are assessed by OTS, a method was devised to ensure uniformity and consistency in identifying chemicals for testing to determine ecological hazard. Assessment factors are used in conjunction with the hazard assessment to derive concentrations of concern in aquatic media which, if equaled or exceeded, provide a basis for further testing. Assessment factors are numbers that are used to adjust standard toxicological measurements to

derive a "concern level."

An environmental concentration of concern is that concentration at which populations of organisms may be adversely affected under simulated or actual conditions of production, use, and disposal. The assessment factors take into account the uncertainties due to such variables as test species' sensitivity to acute and chronic exposures, laboratory test conditions, and age-group susceptibility. There are four assessment factors currently being used: 1, 10, 100, and 1000. Table 1 summarizes the application of assessment factors (1).

Assessment factors are not equivalent to safety factors. A safety factor is usually interpreted as being a margin of safety applied to a no-observed-effect level to produce a value below which exposures are presumed to be safe. Assessment factors are applied to acute or chronic toxicity values based on the type and quality of data available. They are used to arrive at a concentration that, if equaled or exceeded, could cause adverse effects. Assessment factors have been developed solely for the process of reviewing premanufacture notifications to identify those chemicals that require ecological testing to fully assess ecological risks.

Assessing pesticides under FIFRA

OPP follows four steps in a preliminary assessment of ecological risk: review and evaluate hazard data to identify the nature of the hazards; identify and evaluate the observed quantitative relationship between dose and response; identify the conditions of exposure (e.g., intensity, frequency, and duration of exposure); and combine the information on dose–response effects with that on exposure to estimate the probability that nontarget populations

will be adversely affected by actual use of the pesticide.

These steps result in the comparison of toxicological hazard data with exposure data. Typically, the toxicological hazard data may consist of acute LD_{50} (the *dose* lethal to 50% of a test population) and LC_{50} values, or chronic no-effect levels for a sensitive indicator species. Exposure data normally consist of model-based, estimated environmental concentrations (EEC) in the media of concern (i.e., water, soil, nontarget organism food items).

If the ratio of these input data (e.g., EEC/LC_{50}) equals or exceeds certain fixed criteria, a risk is inferred, and generally simulated or actual field testing is required to confirm the risk. In Table 2 are ecotoxicological assessment criteria containing specific safety factors that form the regulatory framework developed by EPA in 1975. This framework has been used to estimate the potential hazard of pesticides to nontarget organisms.

The framework was designed to provide a safety factor that would allow for differential variability among fish and wildlife species [2]. Many theoretical questions can be raised about the use of assessment criteria and safety factors in general. Currently, this framework is not used to predict the probability that the pesticide will cause significant adverse effects to nontarget organisms because the framework does not provide a mechanism for estimating uncertainty. Since 1985, the program has developed the weight-of-evidence approach for determining unreasonable ecological risk. This determination includes consideration of the quality and adequacy of the data, as well as the magnitude of the estimated or observed effect.

Both the toxics and the pesticides programs recognize that the ratio method for assessing risk has numerous weaknesses. For example: it does not adequately account for effects of incremental dosages; it does not compensate for differences between laboratory tests and field populations; it cannot be used for estimating indirect effects of toxicants (e.g., food chain interactions); it has an unknown reliability; it does not quantify uncertainties; and it does not adequately account for other ecosystem effects (e.g., predator–prey relationships, community metabolism, structural shifts, etc.). Therefore, the ratio method does not provide for a complete characterization of the magnitude of risk nor the degree of confidence associated with the characterization.

Assessing water quality

The Water Quality Act of 1987 (P.L. 100-4) amends the decade-old Clean Water Act and redirects its focus from

---

TABLE 2
Ecotoxicological assessment criteria for pesticides[a]

Presumption of no hazard	Presumption of hazard that may be mitigated by restricted use	Presumption of unacceptable hazard
Acute Toxicity		
Mammals		
$EEC^{b} < 1/5\ LC_{50}$ mg/kg/day $< 1/5\ LC_{50}$	$EEC \geq 1/5\ LC_{50}$ mg/kg/day $> 1/5\ LC_{50}$	$EEC \geq LC_{50}$
Birds		
$EEC < 1/5\ LC_{50}$	$1/5\ LC_{50} \leq EEC < LC_{50}$	$EEC \geq LC_{50}$
Aquatic organisms		
$EEC < 1/10\ LC_{50}$	$1/10\ LC_{50} \leq EEC < 1/2\ LC_{50}$ $EEC \geq 1/10\ LC_{50}$	$EEC \geq 1/2\ LC_{50}$
Chronic Toxicity		
$EEC < Chronic$ No effect level	N/A	$EEC \geq$ effect level (including reproductive)

[a]Adapted from Reference 2.
[b]Estimated environmental concentration. This is typically calculated using a series of simple nomographs to complex exposure models.

---

the technology approach, based on end-of-pipe standards, to full-scale implementation of the water quality approach, based on ambient receiving water standards. The new act requires detailed national assessments of: trophic status and trends in lakes (Section 314), waters needing additional nonpoint source controls to attain water quality standards (Section 319), and waters not meeting standards due to point and nonpoint sources of priority toxic pollutants [Section 304(l)].

Bodies of water not meeting applicable state standards must be listed in order of priority for control actions and management plans, and control strategies must be implemented to rehabilitate these degraded waters. In addition,

existing regulations are being updated to perpetuate this assessment process and to tighten controls on toxics. Proposed revisions to the Water Quality Management Regulation (3) would formalize the listing and reporting of water quality-limited segments, and the Water Quality Standards Regulation (4) will likely, for the first time, require all states to adopt criteria for the priority toxic pollutants.

State water quality standards form the backbone of the water quality-based approach, and biological endpoints often are the basis of such standards. Because the Clean Water Act declares "fishable/swimmable" as a minimal goal for the nation's waters, EPA, in its oversight of state standards, rarely endorses use designations that do not at least provide for "protection and propagation" of aquatic life. Therefore, criteria that are expressly designed to protect the biota are also the most commonly used endpoints for assessing potential impacts (risks) to designated uses.

EPA criteria are developed as national recommendations to assist states in developing their standards. The endpoints most commonly used in risk assessments are chemical-specific criteria and whole-effluent toxicity criteria (5). Both types of criteria have three components, the first serving as the risk assessment endpoint and the latter two being applied in assessing the exposure:

- magnitude—what concentration of a pollutant (or a pollutant parameter such as toxicity) is allowable;
- duration—the period of time over which the predicted in-stream concentration is averaged for comparison with the criteria concentration (this specification limits the duration of concentrations above the criteria); and

- frequency—how often criteria can be exceeded without unacceptably affecting the community.

Hazard assessments for specific criteria chemicals are conducted in accordance with EPA's National Guidelines (6). Concentrations of these chemicals from individual sources are usually translated into ambient levels using conservative exposure models. The models predict steady-state environmental concentrations that persist for a critical duration and recur at a given frequency. Predicted exposure concentrations are then compared to the criteria—the endpoints of concern—using the quotient method. If the model predicts concentrations that exceed the criteria, the source is considered to pose a significant risk to aquatic life.

Risk assessments for point sources of whole-effluent toxicity are conducted following guidance provided in the Technical Support Document (7). This procedure differs somewhat from that used for specific chemicals. Because a unique battery of toxicity tests may be needed to characterize the hazard posed by each effluent, a tiered approach is used to tailor hazard assessment requirements to the site-specific exposure situation.

Test results from a lower tier (acute tests, few species) are first weighted with uncertainty factors to account for potential variations in species sensitivity, acute to chronic ratios, and temporal fluctuations in effluent quality. Estimated effects thresholds are then compared with expected environmental concentrations using the quotient method. An indication of ambient toxicity can either trigger further testing at a higher tier or implementation of regulatory controls.

The risk assessment procedure outlined above illustrates several of the major improvements that have been incorporated into water quality-based control processes in the last few years. Most notably, whole-effluent toxicity, in addition to chemical-specific criteria, has become a legitimate, enforceable parameter for controlling complex discharges. Exposure duration and frequency, in addition to ambient concentrations, have been acknowledged as important attributes of criteria.

The above example also illustrates several of the approach's shortcomings, many of which have been identified by EPA's Science Advisory Board (8, 9). The primary criticism leveled at this type of risk assessment is that the endpoints, although derived in a rigorous and standardized manner, lack realism (10). Furthermore, they may not relate to ecological endpoints that can be directly measured in the field. It is difficult, therefore, to demonstrate that

source controls, essentially derived from single-species response criteria, do in fact produce the desired ecosystem level results.

New directions

Agency-wide. Ecological risk assessment is becoming increasingly important at EPA. The public has learned that chemicals not toxic to humans can have adverse effects on resources we value, including a resource as vital as the global climate. First DDT, which is only slightly toxic to mammals, was shown to jeopardize eagles, other birds, and many species of game fish. Then it became apparent that acid deposition, which has little direct effect on human health, could destroy populations of fish and other aquatic organisms in poorly buffered lakes and might be contributing to the die-back of forests. Most recently, we have learned that compounds as safe as CO_2 and CH_4 can cause global warming with potentially adverse effects on entire regions of the earth. Similarly chlorofluorocarbons (CFCs), used partly because of their stability and low toxicity, have contributed to depletion of stratospheric ozone, increasing chances of skin cancer and vegetation damage.

Responding to such concerns, EPA's Risk Assessment Council (senior managers with significant responsibilities for assessment and reduction of risks) established the Ecotoxicity Subcommittee in 1987, giving it responsibility for development of ecological risk assessment guidelines. The subcommittee has looked at the diversity of EPA's ecological assessment activities and found that

they included not only prediction of risks from chemicals but also prediction of impacts from projects, retrospective assessment of site-specific impacts, and monitoring of ecological changes.

The subcommittee has developed an ecological assessment framework based on levels of biological organization from an individual organism to an entire ecosystem. This framework could be used both for "top-down" assessments based on field studies and "bottom-up" assessments based on laboratory bioassays. For example, chemical effects on aquatic communities can be measured by comparing uncontaminated and contaminated streams or predicted by extrapolating from effects on aquatic organisms measured in the laboratory. In 1990, guidelines drafted by the subcommittee for ecological assessments of aquatic populations and communities and terrestrial populations should be released for review (11).

The EPA Water Program. Recent initiatives in the water quality-based approach have been targeted at enhancing its overall ecological relevance. Guidelines have been developed on assessing the ecological potential of a given body of water to support aquatic life, and procedures have been defined for modifying the national criteria for specific sites (12).

Furthermore, it has been shown that better exposure assessments of both specific chemicals and whole effluent toxicity are possible (13) and that sediment (14) and wildlife (15) criteria are needed for more comprehensive and realistic risk assessments. Perhaps most importantly, "biocriteria" have been developed (16) that quantitatively express water quality standards in terms of the resident aquatic community's structure and function (17). Biocriteria are measures of "biological integrity" that can be used to assess cumulative ecological impacts from multiple sources and stress agents (18). Biocriteria thus provide a means of evaluating whether regulatory actions based on predictive risk assessments are actually protective enough of aquatic ecosystems.

Pesticides and Toxics Programs. Building on a quotient method, the Office of Pesticides and Toxic Substances is actively investigating other methods to improve ecological risk assessments. OTS is exploring population and ecosystem modeling techniques, and an expansion of Quantitative Structure Activity Relationships (QSARs) capability is envisioned as a logical next step in the ecological assessment process. [OTS has recently published a manual on the use of QSAR (19)]. A collection of life histories will be compiled to as-

sist in the use of surrogate species data. Improved capability to assess the effects of multiple toxicants is needed, as these chemicals are seldom discharged into the environment in isolation.

OPP has published standard evaluation procedures for many of the laboratory studies of indicator organisms such as invertebrates, fish, and birds required by the pesticide assessment guidelines. OPP has moved to strengthen its risk assessment capabilities in the terrestrial area by issuing a guidance document on terrestrial field studies *(20)*; in the aquatic area it has published a guidance document on aquatic mesocosm tests *(21)*.

Most recently OPP has proposed cancellation of all uses of granular carbofuran, which has been found to kill birds—including bald eagles and other raptors—in excessive numbers when used on corn according to label directions. At this writing, the agency's risk assessment findings were affirmed after public review by a panel of experts.

Hazardous-waste policy studies and technical guidance. EPA's Office of Policy Analysis has completed a study of the scope and nature of ecological problems at hazardous-waste sites. The study identified key areas for improving technical analysis, policy guidance, and ecological risk management for the programs of the Office of Solid Waste and the Office of Emergency and Remedial Response *(22)*.

Abandoned hazardous-waste sites qualify for remedial actions by inclusion on the National Priorities List (NPL) through a series of progressively more detailed assessments. Sites are scored by the Hazard Ranking System (HRS), which currently includes limited ecological factors (essentially the HRS scores the distance from a site to the nearest "sensitive" environment). EPA has proposed revisions to the HRS *(23)* that expand the list of sensitive environments and incorporate scores that better reflect potential ecological hazards.

Also, EPA has recently issued new guidance on ecological assessment at hazardous-waste sites. Detailed guidance on performing the Remedial Investigation/Feasibility Study (RI/FS), used to characterize the risks posed by the site and to investigate appropriate remedies, requires new information for a "baseline" ecological investigation *(24)*.

This RI/FS guidance refers remedial project managers to a new environmental evaluation manual *(25)*, which provides a science policy framework for performing the ecological effects portions of the baseline risk assessment. From an ecotoxicological perspective, perhaps its most important mandate is

that ecological factors are to be considered "up-front" in the assessment process.

Test methods and protocol references can be found in a new compendium of ecotoxicological methods published by EPA's Corvallis Environmental Research Laboratory (CERL) *(26)* as a companion volume to the Superfund ecological assessment guidance. The CERL document outlines specific laboratory and field tests to be employed during ecological investigations of CERCLA and RCRA sites.

Looking ahead

Despite many demands on limited resources, EPA has developed the capability to assess ecological risks and impacts. Contributions to this capability have been made by programs such as the Water, Toxics, Pesticides, Superfund, and other programs, with the support of the Office of Research and Development. Now there is increasing public interest in, and concern about, ecological effects. Therefore, EPA's programs will continue to expand their efforts to identify, quantify, and reduce adverse impacts on populations, communities, and ecosystems.

Acknowledgments

References

(1) "Estimating Concern Levels for Concentrations of Chemical Substances in the Environment"; U.S. Environmental Protection Agency: Washington, DC, 1984.
(2) Urban, D. J.; Cook, N. J. "Hazard Evaluation Division, Standard Evaluation Procedure, Ecological Risk Assessment"; U.S. Environmental Protection Agency: Washington, DC 1986; EPA-504/9-85-001; NTIS PD 86-247-657.
(3) *Fed. Regist.* **1989**, *54*, 1300.
(4) *Fed. Regist.* **1983**, *48*, 51400.
(5) *Fed. Regist.* **1984**, *49*, 9016.
(6) "Guidelines for Deriving Numerical Water Quality Criteria for the Protection of Aquatic Organisms and Their Uses"; U.S. Environmental Protection Agency: Washington, DC, 1986; NTIS PB 85-227049.
(7) "Technical Support Document for Water Quality-Based Toxics Control"; U.S. Environmental Protection Agency: Washington, DC, 1985; NTIS PB 86-150067.
(8) "Water Quality Criteria: A Report of the Water Quality Subcommittee"; Science Advisory Board; Washington, DC, 1985.
(9) "A Report of the Water Quality Based Approach Research Review Subcommittee"; Science Advisory Board: Washington, DC, 1986; EC-87-011.
(10) Levin, S. A. et al. *Environ. Manag.* **1984**, *8*, 375.
(11) Thomas, L. M. *Environ. Toxicol. Chem.* **1989**, *8*, 275.
(12) "Water Quality Standards Handbook"; U.S. Environmental Protection Agency. Office of Water Regulations and Standards: Washington, DC, 1983.
(13) DiToro, D. M.; Hallden, J. A.; Plafkin, J. L. In *Toxic Contaminants and Ecosystem Health: A Great Lakes Focus*; Evans, M. S., Ed.; Wiley: New York, 1988; pp. 403-425.
(14) Shea, D. *Environ. Sci. Technol.* **1988**, *22*, 1256.
(15) Clark, T. *Environ. Sci. Technol.* **1988**, *22*, 120.
(16) "Biological Criteria for the Protection of Aquatic Life: I-III"; Ohio EPA, Division of Water Monitoring and Assessment: Columbus, OH, 1987.
(17) "Proceedings of the First National Workshop on Biological Criteria"; U.S. Environmental Protection Agency, Region 5: Chicago, IL, 1988; EPA-905/9-89/003.
(18) Hughes, R. M.; Larsen, D. P. *J. Water Pollut. Control Fed.* **1988**, *60*, 486.
(19) "Estimating Toxicity of Industrial Chemicals to Aquatic Organisms Using Structure-Activity Relationships"; U.S. Environmental Protection Agency. Office of Toxic Substances: Washington, DC, 1988; EPA-560/6-88/001.
(20) "Guidance Document for Conducting Terrestrial Field Studies"; U.S. Environmental Protection Agency. Hazard Evaluation Division. Office of Pesticide Programs: Washington, DC, 1988; EPA 540/09-88-109. NTIS PD 89-124-580.
(21) Touart, L. "Aquatic Mesocosm Tests to Support Pesticide Registrations Office of Pesticides Programs"; Hazard Evaluation Division Technical Guidance Document; U.S. Environmental Protection Agency: Washington, DC, 1988; EPA 540/09-88-035.
(22) "Summary of Ecological Risks, Assessment Methods, and Risk Management Decisions in Superfund and RCRA"; U.S. Environmental Protection Agency: Washington, DC, 1989; EPA 230/03-89-048.
(23) *Fed. Regist.* **1988**, *53*, 51962.
(24) "Guidance for Conducting Remedial Investigations and Feasibility Studies under CERCLA (Interim Final)"; OSWER Directive 9355.3-01. Office of Emergency and Remedial Response. U.S. Environ-

mental Protection Agency: Washington, DC, 1988.

(25) "Risk Assessment Guidance for Superfund: Environmental Evaluation Manual (Interim Final)". U.S. Environmental Protection Agency. Office of Solid Waste and Emergency Responses: Washington, DC, 1989; EPA-540/1-89/001A.

(26) "Ecological Assessment of Hazardous Waste Sites"; Office of Research and Development. U.S. Environmental Protection Agency: Corvallis, OR, 1989; EPA 600/3-89/013.

John Bascietto (l) spent 10 years as a wildlife biologist at EPA, serving in the pesticides, Superfund, and policy offices. His biology B.A. and M.S. degrees are from New York University. Currently he is with the U.S. Department of Energy directing cleanups at DOE's hazardous-waste facilities.

Dexter Hinckley (r) is the senior ecologist in the Science-Policy Integration Branch of the Office of Policy, Planning, and Evaluation at EPA headquarters in Washington, DC. He is responsible for overview of ecological assessment activities throughout EPA. He received an A.B. in biology from Harvard and entomology M.S. and Ph.D. degrees from the University of Hawaii.

James Plafkin (l), since joining EPA in 1980, has worked on the development of national policy and guidance regarding the use of biological assessment techniques in evaluating water pollution. He received his B.S. and M.S. degrees from the University of Michigan and his Ph.D. in aquatic ecology from Virginia Polytechnic Institute and State University.

Michael Slimak (r) is deputy director of the Office of Environmental Processes and Effects Research in the Office of Research and Development at EPA. He has been involved with EPA's risk assessment programs since 1976. He has a B.S. degree in biology from Bethany Nazarene College and an M.S. degree in wildlife ecology from Oklahoma State University.

Banning trichloroethylene: Responsible reaction or overkill?

Frank D. Schaumburg
Oregon State University
Corvallis, OR 97331-2302

Trichloroethylene (TCE) has been used since the 1940s. Since the late 1970s TCE has been the subject of environmental and public health concern and controversy. Common methods used by industry and government facilities for the disposal of chlorinated solvents prior to 1980 have resulted in widespread groundwater contamination. This paper provides background information on the use, disposal, fate, and impact of TCE from the 1940s to the present.

From useful to hazardous substance

TCE has been used in the United States for many years as an excellent degreasing agent, a popular dry cleaning solvent, an extraction agent in decaffeinating coffee, a general anesthetic in medicine and dentistry, and in numerous other ways (1). Its uses were severely curtailed in 1976, however, when a study by the National Cancer Institute provided evidence that TCE, in very high experimental dosages, caused tumor growths in a sensitive species of mouse (2). It is interesting to note that subsequent studies by other researchers have failed to reproduce the carcinogenic response to TCE from any species of test animal (3, 4). Recent epidemiological studies in Michigan and California have failed to implicate TCE as a cause of cancer in humans (5, 6).

Although no direct evidence existed in the past, or even now, that the ingestion of small amounts of TCE elicits a carcinogenic response in humans, the scientific community and environmental regulatory agencies concluded in 1976 that TCE was a "suspected carcinogen" and should be banned. In 1976, TCE was included on the ever-expanding EPA list of hazardous substances.

In recent years, TCE has been dis-covered in groundwater used for human consumption throughout the United States. It has become the subject of extensive governmental regulation and a target chemical in perhaps hundreds of environmental litigations. However, little has been presented in the technical literature regarding the origin and development of the environmental and public health problems created by this once-beneficial substance.
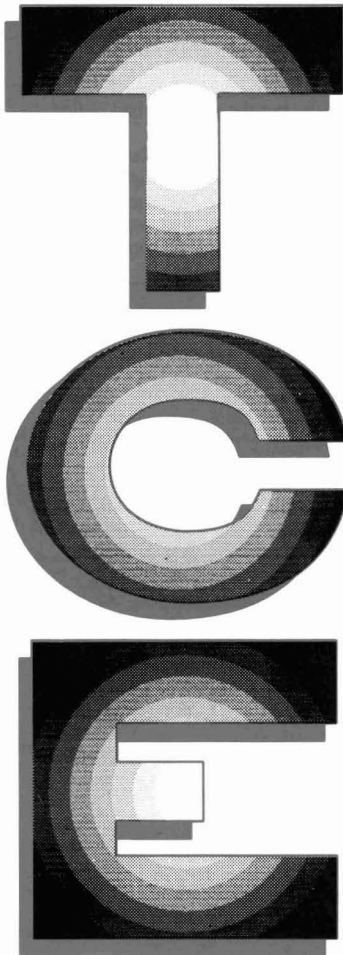
Properties of TCE

An understanding of the origin and fate of TCE in the environment requires some background knowledge of the properties and characteristics of this controversial substance. Trichloroethylene ($Cl_2C{=}CHCl$) is a synthetic, chlorinated organic chemical that fulfills all requirements for the ideal degreasing solvent (1, 7; see box).

TCE is only slightly soluble in water (about 1100 ppm at 77 °F) and forms an azeotrope with water, resulting in a mixture with a lower boiling point and vapor density. It is considered to be a "highly volatile" compound and favors environmental partitioning to the air rather than water (8). TCE is destroyed by photooxidation in the atmosphere, with a half-life of about one day.

TCE, like other chloroethenes, transforms through reductive dehalogenation very slowly in the soil or groundwater environment. Bouwer and McCarty noted that TCE can be transformed slowly under methanogenic conditions at low concentration (9) and also very slowly under denitrification conditions (10). They noted that no degradation occurs under aerobic conditions. These observations indicate why TCE persists in soil and groundwater for a considerable time.

Some other chlorinated organic solvents of current concern are perchlorethylene (PCE), trichloroethane (TCA), carbon tetrachloride, and methylene chloride.

Sources of TCE contamination

Over the years, TCE has been discharged to the nation's surface waters and groundwaters by industry, commerce, and individual consumers. About 90% of the TCE produced in 1974 was used in industrial degreasing. EPA estimates that in 1974 approximately 310,200 tons of waste solvents were produced by degreasing opera-

0013-936X/89/0924-0017$02.50/0 © 1989 American Chemical Society

Environ. Sci. Technol., Vol. 24, No. 1, 1990 **17**

tions *(11)*. Meanwhile, lesser amounts of TCE were being used and discarded by dry cleaners, septic tank cleaners, and other operators of cleaning establishments that used chlorinated solvents.

Until recently, many commonly used consumer products included TCE. Some of these made their way into the environment by way of septic tanks, the sewer, or municipal landfills. Among these products were drain and pipe cleaners, shoe polish, spot removers, paint removers, upholstery cleaners, adhesives, and septic tank cleaners *(12, 13)*.

Discovery of TCE in groundwater

TCE was discovered in the fall of 1979 in a groundwater aquifer in the vicinity of Sacramento, California *(14)*. Although this was one of the earliest reported discoveries of TCE contamination of groundwater, it does not mean that the contamination there, or elsewhere, had just occurred. In fact, it was subsequently found that this aquifer had been contaminated with TCE for sev-

---

TCE: The ideal degreasing solvent and why

- TCE has high solvency for oils, greases, waxes, tars, resins, lubricants, and coolants generally found in the metal-processing industry.
- TCE will not attack steel, copper, zinc, or other metals used in industry.
- TCE was considered to have low toxicity; until the mid-1970s, the air standard for environmental exposure ranged from 100 to 200 ppm.
- TCE is nonflammable and nonexplosive at ordinary temperatures.
- TCE has a high vapor density (4.5 times that of air); this results in maintenance of a distinct vapor level near condensing coils in degreasing tanks and prevents excessive vapor losses to the surrounding atmosphere.
- TCE is highly stable in the presence of common chemical stabilizers.
- TCE has a low boiling point (87.1 °C); this permits low heat input and facilitates handling of work following degreasing operations.

---

eral years, perhaps since as early as the 1950s, but the problem had defied discovery.

Four different, but related, historical reasons for this lag in discovery of the TCE problem in the Sacramento area are identified and discussed below.

- The environmental consciousness of

U.S. citizens was not awakened until the mid-1960s.

- A general knowledge of the fate of TCE in the environment and its potential deleterious effects on human health was absent until the late 1970s.
- The capability to reliably measure

FIGURE 1
Impact of development on environment paralleled by social and governmental response
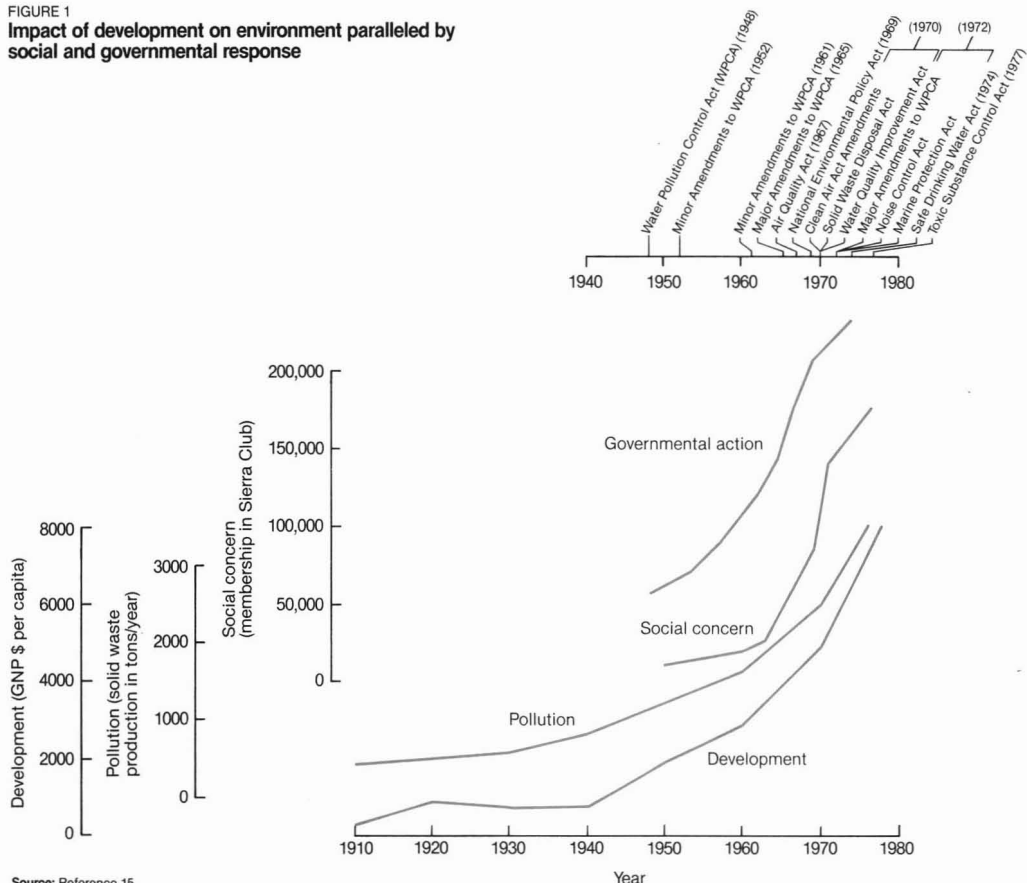
Source: Reference 15.

trace concentrations of TCE in aqueous samples was not developed until the mid-1970s.

• Specific laws and regulations for TCE were not promulgated until the late 1970s to early 1980s.

Environmental consciousness

Immediately following World War II and through the mid-1960s, the prevailing interest in the United States was economic recovery and prosperity. Little attention was paid to the rapidly degrading and abused environment. The graph in Figure 1 (15) shows how environmental contamination paralleled resource development in the United States during the 1950s and 1960s. Few people at the time were aware that economic growth, based on the exploitation of natural resources, would produce enormous quantities of residues that had to come to rest somewhere in the environment. And this phenomenon, which could have been predicted from the basic laws of thermodynamics, resulted in serious water, air, and land pollution nationwide (16).

By the mid-1960s, in the absence of effective regulations and enforcement, environmental degradation had become severe and was no longer tolerated by the citizenry as an acceptable trade-off for economic gain. This change in attitude toward environmental quality marked the beginning of the environmental movement in the United States. This change is quantified in Figure 1 by the growth in membership in the Sierra Club, a national environmental organization. This change is also demonstrated in Figure 2 by the increase in environment-related articles in the press during the late 1960s.

As public concern about the environment intensified, the Congress became responsive to public demands and enacted an increasing number of rigorous environmental laws. Some of the major legislation is shown in Figure 1.

TCE viewed as a hazard

During the past 50 years, several trends in environmental focus or interest can be identified, as shown in Figure 3. The chart plots the number of articles that were indexed in the *Journal of the Water Pollution Control Federation* about selected categories of chemical contaminants. (Each year the *JWPCF* publishes an index of the world literature that relates in some way to the field of water quality.) The articles are contributions from university researchers, governmental regulators, waste treatment facility operators, equipment representatives, and, on occasion, concerned citizens. The numbers of articles about detergents, pesticides, and heavy metals plotted in Figure 3 are

close approximations because duplications of listings were not determined and because the selection of articles was based solely on the abstracted descriptions in the literature review.

It is my contention that an increase in the number of publications about a subject area represents an increase in societal awareness or concern about that subject. The number of articles published and the areas of emphasis also reflect the availability of research funding from government and other sources. It is interesting to note that each of the four trends identified in Figure 3 was initiated by societal concern and action rather than by farsighted leadership by universities. Universities have generally only responded to problems and have focused research primarily where funding is available.

Figure 3 shows that the middle to late 1960s might be termed the "era of detergents" in environmental history. Detergents provoked public ire when foam and scum were visible on rivers, lakes, and harbors. The problem was essentially solved by the replacement of nonbiodegradable detergents with biodegradable formulations that had

FIGURE 2
Environment-related articles in The New York Times

Number of articles
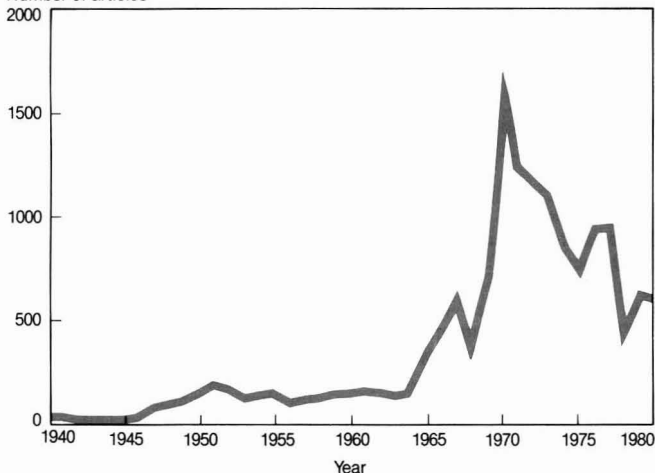
FIGURE 3
Number of articles in the world literature on chemical contaminants[a]

Number of articles
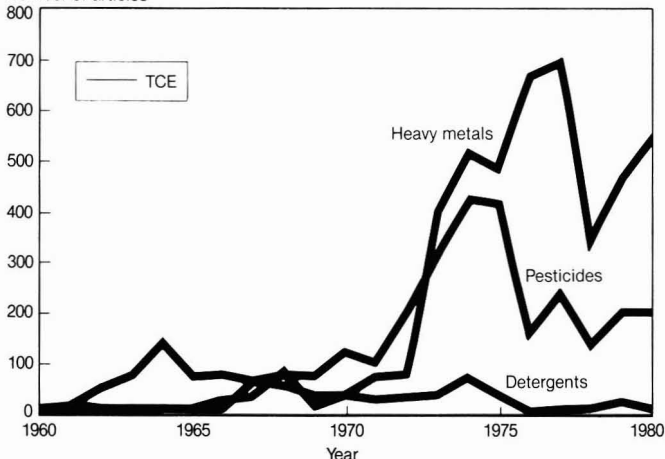
[a]As indexed by the Journal of the Water Pollution Control Federation.

FIGURE 4
Articles on TCE in the world literature[a]

Number of articles

Year
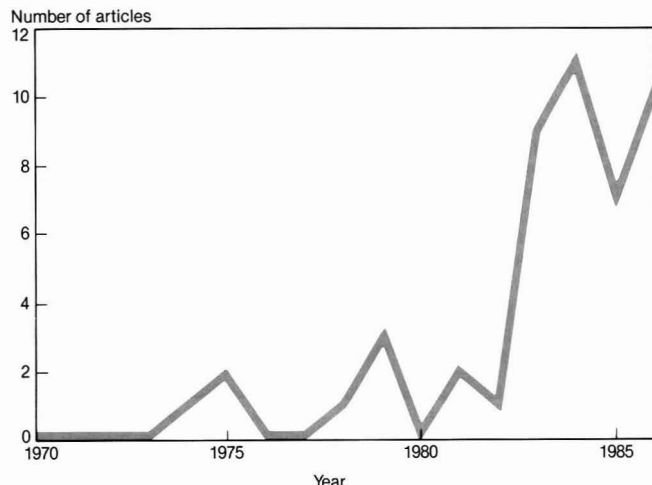
[a]As indexed by the *Journal of the Water Pollution Control Federation.*

comparable cleaning properties. Societal interest then declined significantly, as did the number of publications on the subject.

The "era of pesticides" began in the late 1960s and was prompted, in large measure, by the popular book *Silent Spring* by Rachel Carson *(17)*. The era of pesticides has continued to the present because these chemicals remain in common use and are considered to be toxic, hazardous substances.

The "era of heavy metals" is shown in Figure 3 to have begun in the early 1970s. In 1969 fewer than 50 articles about heavy metals appeared in the literature. By contrast, nearly 700 articles were published on this subject in 1977. Early concerns about chromium from tanning and dyeing intensified as the metal plating industry developed. Plating wastes included chromium, zinc, cyanide, and other highly toxic chemicals. Later concerns focused on lead in gasoline and paint products, cadmium, mercury (causing Mikimoto disease), and other heavy metals. Heavy metals continue to be used extensively by industry and in homes, and serious problems of environmental contamination are prevalent throughout the country.

The final era identified in the chart in Figure 3, and shown in expanded scale in Figure 4, might be referred to as the "era of chlorinated solvents," which began in the late 1970s in response to the infamous Love Canal situation. Prior to the 1980s, the paucity of technical literature about this category of chemicals suggests that there was little concern about chlorinated solvents in

university research programs, regulatory agencies, industry, or the general public. Recently however, considerably more interest in these chemicals has been generated, as many have now been identified as hazardous substances that have been, and continue to be, used in industry (as solvents), in commerce (in dry cleaning), and in homes (in cleaners, cosmetics, and other common household products) *(13)*.

Availability of analytical methods

The analytical capability for detecting and measuring environmental contaminants has expanded greatly in recent years in both precision and sophistication. This has resulted in the discovery of environmental contamination which has heretofore existed but which could not have been detected by less sensitive analytical techniques and devices. Such is the case with TCE.

Prior to the mid-1970s, there were no analytical methods available to environmental analysts to measure, or even detect, specific chlorinated solvents such as TCE in water. The Fujiwara colorimetric method of TCE determination was commonly used, but had many shortcomings—most notably its inability to distinguish TCE from other chlorinated solvents *(18)*. Other limitations included the need to keep all reagents absolutely dry, the need for precise volumetric measurement, and the rapid decay of color density—the basis for measurement. Then in 1974, Bellar and Lichtenberg *(19)* described a gas chromatographic method that could separate and detect chlorinated solvents in water

in the parts-per-billion range. As a consequence of this and other developments in analytical capability, environmental regulators were able to test water samples for TCE. They found the substance in groundwater aquifers nationwide.

The evolution of techniques for the measurement of chlorinated substances in aqueous samples is illustrated in the semiquantitative plot in Figure 5. The plot reflects the methodology generally available to the environmental profession as evidenced in the bible of water analysis, *Standard Methods for the Examination of Water and Wastewater.* (*Standard Methods* is published jointly by the American Public Health Association, the American Water Works Association, and the Water Pollution Control Federation and is edited and updated approximately every five years. New methods of analysis that are proposed for inclusion in the publication must first be thoroughly evaluated by qualified environmental chemists in selected laboratories.)

Figure 5 shows that *Standard Methods* did not include any methods for the analysis of chlorinated pesticides or chlorinated solvents prior to the 12th edition in 1965 *(20)*. This edition made a brief reference to gas-liquid chromatography as a "potential" method of pesticide analysis. It was not until the 13th edition in 1971 *(21)*, however, that even a "tentative" method was adopted; and this method was only for pesticides. A method for chlorinated solvents did not appear in *Standard Methods* until the 15th edition published in 1980 *(22)*.

There is little doubt that the significant improvements in analytical sophistication and detection sensitivity have profoundly affected our ability to evaluate and manage environmental quality. It is highly likely, however, that our ability to detect and measure contaminants far exceeds our ability to properly and responsibly evaluate the impacts of those concentrations on human health, on other biological life, and on overall environmental quality.

Industrial standards of practice

Environmental management in the United States has long featured problem identification by society; legal mandate by Congress; detailed regulation by appropriate governmental pollution control agencies; response to regulation by industry, municipalities, and other dischargers of waste; and conflict resolution in the courts. This management approach, by default or by design, has placed the responsibility for environmental problem evaluation and resolution on government. It is regrettable that our universities and technical,

professional, and scientific societies have not assumed a stronger leadership role in environmental protection.

Over the years, industries that produced wastes generally sought to dispose of them by the most readily available and economical methods consistent with environmental regulations in effect at that time. That practice continues to this day. The methods of treatment and disposal that were commonly used throughout an industry or segment of an industry are referred to as "industry standards of practice." History has shown that as environmental laws and regulations became more rigorous, and as new and better methods for treatment and disposal were developed, the standard of practice for industry (and municipalities) increased in sophistication and rigor.

In retrospect, it is very tempting to criticize industries for standards of practice for handling hazardous substances that were adopted in the 1940s, 1950s, 1960s, and even into the 1970s, because as a result of those practices we now find contaminated groundwater throughout the country. But to judge fairly, one must determine whether the methods used for waste management in the past were "reasonable" for the level of knowledge at that time.

A good example is the handling and disposal of TCE. It continued to be used for several reasons in addition to its solvent properties.

- TCE was considered to be safe for human contact because it was being used by the health profession through the 1970s as an anesthetic. It was also approved for extensive use in food production by the Food and Drug Administration through the late 1970s.
- There were no federal, state, or local laws or regulations that restricted or banned TCE in liquid effluents until the late 1970s.
- There were no analytical methods available to test for this substance in low concentrations until the mid to late 1970s, so detection in groundwater would have been impossible had it been suspected.
- It was not until the mid-1970s that TCE was determined to be a "suspected carcinogen."
- TCE was disposed of directly onto the land at military installations through the 1970s (Figure 6), yet the military had the same responsibilities for environmental protection as industry or municipalities.
- The nation's universities did not provide educational opportunities in hazardous-waste management until the 1980s, so few people in government and industry were trained to identify and effectively react to hazardous-

FIGURE 5
Development of analysis methods for chlorinated pesticides and TCE[a]
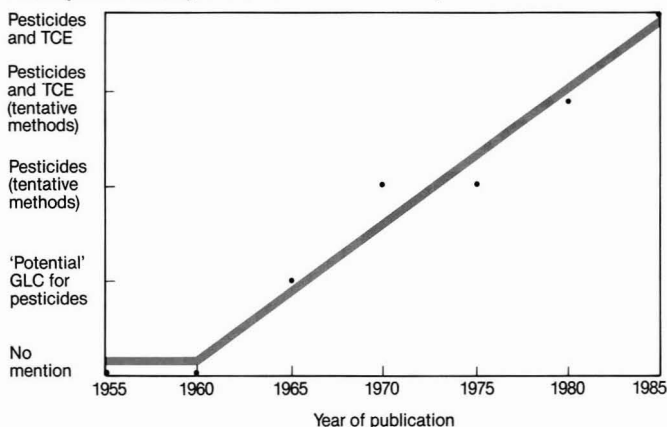
[a]As published in References 20, 21, and 22.

FIGURE 6
Land disposal of TCE at military installations
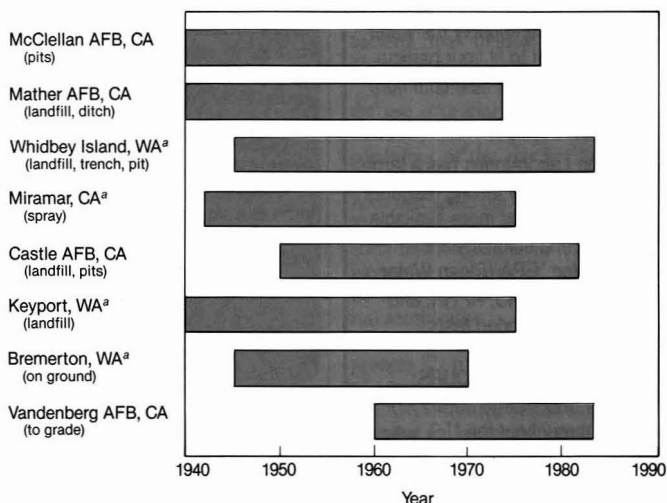
[a]Naval bases

waste problems. Figure 7 shows the increase in availability of hazardous-waste courses at U.S. universities.

Summary

The case against the use of TCE in the work place and its disposal in small quantities in the environment is shaky at best. However, the current environmental regulatory posture of our society apparently is: "If we err, err on the side of conservatism." But this conservatism is not without huge societal costs.

Toxic tort litigations involving TCE are running in the billions of dollars;
remedial actions involving groundwater and soil cleanup to essentially nondetectable levels are costing billions of dollars; and, perhaps most importantly, the populace has been unduly traumatized by overreactive publicity and allegations regarding the deleterious health effects of TCE. It is interesting to note that some "accepted" alternatives to TCE for degreasing since the mid-1970s have been trichloroethane (TCA) and freon. TCA is now on the EPA list of suspected carcinogens, and freon is implicated in the destruction of the ozone layer.

Although Figure 4 shows an increas-

FIGURE 7
Increase in hazardous-waste courses at U.S. universities
Number of universities
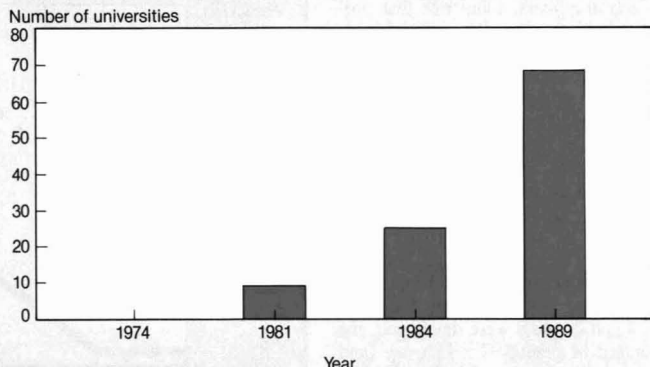
Source: *AEEP Register*, Vol. III–VI.

ing number of publications relating to chlorinated solvents during the 1980s, the absolute numbers remain quite small in comparison to those that reflect other chemicals of environmental concern (Figure 3). This suggests that the level of interest in and concern about chlorinated solvents remains relatively low; and low government priority has meant a low funding level for basic and applied research.

Another factor affecting a rise in interest in chlorinated solvents is the lack of compelling evidence of significant harm to human health or environmental quality. Only in the courts has this substance taken on dimensions of enormous significance.

References

(1) "Status Assessment of Toxic Chemicals: Trichloroethylene" U.S. Environmental Protection Agency. U.S. Government Printing Office: Washington, DC, 1979; EPA-600/2-79-210m.
(2) "Carcinogenesis Bioassay of Trichloroethylene"; National Cancer Institute; Washington, DC, 1976; CAS No. 79-01-6, NCI-CG-TR-2,
(3) Henschler, D., et al. *J. Cancer Res. Clin. Oncol.* **1984**, *104*, 149.
(4) Van Duuren, B. L. et al. *J. Natl. Cancer Inst.* **1979**, *63*, 1433–39.
(5) Freni, S. C.; Bloomer, A. *Report on the Battle Creek Health Study;* Michigan Department of Public Health, Lansing, MI, 1988.
(6) Baker, D. B. et al. *Arch. of Env. Health* **1988**, *43*, 325–34.
(7) Leroy, J.M. *Modern Metal Degreasing*; Dow Chemical of Canada: Sarna, Ontario, Canada, 1952.
(8) "An Exposure and Risk Assessment for Trichloroethylene"; U.S. Environmental Protection Agency. U.S. Government Printing Office: Washington, DC, 1981; EPA-440/4-85-019.
(9) Bouwer, E. J.; Rittmann, B. E.; McCarty, P. L. *Environ. Sci. Technol.* **1981**, *15*, 595–99.
(10) Bouwer, E. J.; McCarty, P. L. *Appl. Env. Microbiology* **1983**, *45*, 1295–99.
(11) "Organic Solvent Cleaners: Background Information for Proposed Standards";
U.S. Environmental Protection Agency. U.S. Government Printing Office: Washington, DC, 1979; NTIS #PB80-137912.
(12) Fishbein, L. *The Science of the Total Environment* **1979**, *11*, 111–61.
(13) "Sources of Toxic Compounds in Household Wastewater"; U.S. Environmental Protection Agency. U.S. Government Printing Office: Washington, DC, 1980; EPA-600/2,80-128.
(14) Munter, J. E.; DeVries, S. P. *Toxics Law Reporter* Jan. 14, **1987**, 874.
(15) Schaumburg, F. D. *J. Environmental Systems* **1979**, *9*, 89–98.
(16) Schaumburg, F. D. *Prog. Water Technol.* **1975**, *7*, 121–26.
(17) Carson, R. *Silent Spring;* Riverside Press: Cambridge, MA, 1962.
(18) Camisa, A. G. *J. Water Pollut. Control Fed.* **1975**, *47*, 1021–31.
(19) Bellar, T. A.; Lichtenberg, J. J. *J. Am. Water Works Assoc.* **1974**, *66*, 739–44.
(20) *Standard Methods for the Examination of Water and Wastewater, 12th ed.;* American Public Health Association: Washington, DC, 1965.
(21) *Standard Methods for the Examination of Water and Wastewater, 13th ed.;* American Public Health Association: Washington, DC, 1971.
(22) *Standard Methods for the Examination of Water and Wastewater, 15th ed.;* American Public Health Association: Washington, DC, 1980.

Frank D. Schaumburg is professor of environmental engineering and head of the Civil Engineering Department at Oregon State University. He earned a Ph.D. in environmental engineering from Purdue University in 1966. His interests include the legal and political implications of hazardous-waste management and the human dimension of engineering.

The role of genes in biological processes

Part 1 of a two-part article

Bruce E. Rittmann
Barth F. Smets
David A. Stahl
University of Illinois
at Urbana-Champaign
Urbana, IL 61801

Applications that require biological processes to meet more stringent treatment goals, such as removal of hazardous compounds, are becoming increasingly important. These new applications challenge the research community to develop a deeper understanding of the genetic capabilities of biological processes, the subject of this two-part article.

The first part introduces the role of genes in biological treatment. It describes the components of microbial genetic systems that may play key roles in biological-process engineering. This paper emphasizes plasmids, which are small, circular DNA strands that can be transferred among cells. It also introduces a structured framework for assessing the roles of plasmids in biological-treatment processes.

Processes currently in use

A biological process is an engineered system designed to accumulate a mass of microorganisms that is great enough to perform a desired reaction *(1)*. The system must be large enough to hold the desired biomass, must have an accumulation or retention mechanism for the biomass, and must be supplied with adequate amounts of substrates and nutrients. To accumulate the desired microorganisms, environmental conditions inside the process are controlled to favor these microorganisms and wash out other microorganisms. This usually is accomplished by controls on
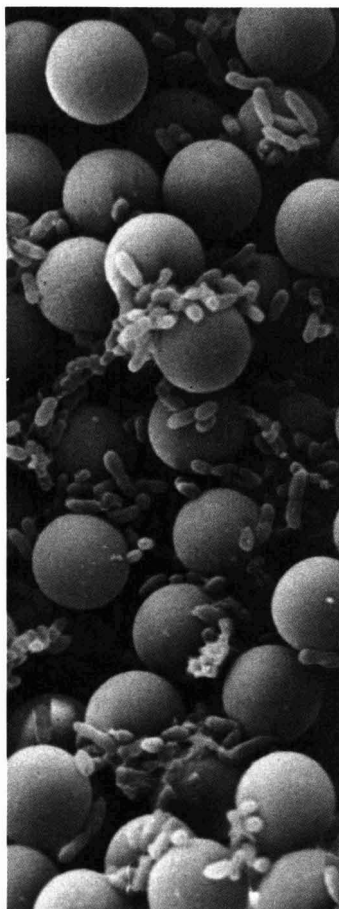
Magnetized polystyrene beads are used to capture bacteria from fresh water.

substrate availability and cell retention.

The activated sludge process offers a good example of controls on substrate supply and cell retention. Wastewater usually contains organic material, which serves as an electron donor, and adequate amounts of nitrogen and phosphorus. The substrate supply is controlled by aeration, which supplies the electron acceptor, oxygen. When enough oxygen is supplied, aerobic bacteria that oxidize organic matter grow and accumulate.

Cell retention is controlled through the use of a clarifier that follows the aeration tank. The quiescent settling conditions of the clarifier favor retention of bacteria that aggregate into large flocs that settle out of the effluent flow. The settled flocs are recycled to the aeration tank, resulting in the buildup of increasing amounts of rapidly settling bacteria that oxidize the organic material aerobically.

The methanogenic fluidized-bed process *(2)* offers a second illustration of a type of process control currently in use. Again, the wastewater typically contains an organic electron donor and sufficient N and P. In the methanogenic process, the supply of standard electron acceptors—mainly O_2, NO_3^-, and SO_4^{2-}—is minimized. Without these electron acceptors, only fermenting and CO_2-reducing microorganisms can thrive. Included among those microorganisms are the methane-producing archaebacteria, the methanogens. Retention control is achieved by providing a very large surface area on fluidized particles of materials such as sand, coal, or granular activated carbon. Cells able to attach firmly to the small fluidized particles are retained and accumulated.

The controls on substrate supply and cell retention are a form of applied ecology. The composition and capabilities of the mixed population of microorganisms are regulated by controlling the availability of the substrate and the

retention of cells in the process *(3)*. Cells with the proper attributes fill the "niche" defined by the controls.

Applied ecology is a powerful tool that has been used effectively. Its power is greatest when the treatment goal is closely allied to the control techniques. One reason current control techniques are so powerful is that most of the traditional pollutants removed by biological processes are electron donors or acceptors.

The changing regulatory emphasis

The regulatory strategy gradually is shifting to emphasize the removal of specific compounds, such as trichloroethene, instead of focusing solely on broad-category pollutants, such as biological oxygen demand. Often, individual compounds comprise only a tiny fraction of the total organic matter in the influent wastewater, and they must be removed to concentrations detectable only by sophisticated analytical techniques, such as gas chromatography.

Ecological selection based on substrate supply and cell retention may not be effective for accumulating enough cells to remove trace concentrations of individual compounds. This is especially true when the compounds are xenobiotic materials, which are produced by the chemical industry and generally are regarded as resistant to biodegradation. Little is known about how very low concentrations of xenobiotic compounds affect the selection of microorganisms in biological processes or the degradative capability of those microorganisms.

When the treatment goal is reliable removal of individual compounds, especially xenobiotic compounds, process analysis must include information about the microorganisms' genetic capabilities to degrade the specific compounds. Genetic capability can be viewed as the information, in the form of genes, that the cell uses to construct and maintain itself, that is, to attain the mass and energy flows needed for construction, maintenance, and reproduction. Genetic capability includes the ability to metabolize or degrade specific compounds. A process goal could be to control, or at least influence, the genetic information of the cells, instead of simply determining whether the process works naturally.

Two facets of genetic information are important for analyzing a biological process. The first facet is the total pool of genes within the population. The total pool of information determines what reactions are possible. Another way to regard the pool of information is as genetic potential, the ability to respond to opportunities, such as a new substrate, when they present themselves. The second facet is how the bits of information, the individual genes, are parceled out among the individual cells in the biological process. Thus, the community has greater genetic information than do individual strains, because each cell need not contain every gene present in the community.

Although the total pool of information determines the potential for reactions, its parceling is critical for determining whether possible reactions actually occur at a measurable rate. For example, if there are 10^{13} bacteria per liter, but only 1 bacterium per liter contains a gene needed for biodegradation of a xenobiotic compound, then it is highly unlikely that noticeable degradation of the xenobiotic compound will proceed. On the other hand, if one-half of the bacteria contain the gene, degradation probably will be significant. Likewise, the parceling of genes determines whether one bacterium can completely mineralize a compound or whether a consortium of different bacteria is required to perform all the steps in mineralization.

In addition to traditional ecological selection, a direct means to control the genetic information of a population is *bioaugmentation*. Bioaugmentation involves adding nonindigenous bacteria to a bioreactor, usually to induce or maintain specific biodegradative reactions within the population. The mechanisms by which bioaugmentation might enhance the performance of a biological process are not well understood; it is known, however, that the key component of successful bioaugmentation is to supply genetic information that the bacterial population can adopt and use but that is not naturally present in the population. Hence, bioaugmentation is a tool to control genetic content. It can be used to enhance the effectiveness of the traditional tools, supply of substrates and cell retention.

Glossary

Accessory DNA—Mobile and nonessential DNA that is not associated with the chromosome.

Chromosomal DNA—Immobile and essential DNA present in every cell and determinative of the cell's basic traits.

Complementary base pairing—Hydrogen bonding between two strands of DNA or a strand of DNA and a strand of RNA, such that the G on one strand pairs with the C on the other and the A on one strand pairs with the T or U on the other strand.

Conjugation—The transfer of a plasmid between two bacterial cells that are in direct contact.

DNA—A linear polymer made up of deoxyribonucleotide repeating units (composed of the sugar 2-deoxyribose, phosphate, and a purine or pyrimidine base) linked by the phosphate groups joining at the 3' position of one sugar and the 5' position of the next sugar; DNA contains the genetic code.

Donor—A bacterium that contains a plasmid that it can transfer by conjugation.

Enzyme—A polymer of amino acids (i.e., a protein) that catalyzes reactions.

Gene—A segment of DNA that codes for the production of a protein or stable RNA (e.g., rRNA).

Mobilization—A form of conjugation in which a plasmid that does not contain a complete set of transfer genes is transferred along with a conjugative plasmid.

Pilus—A fine, hairlike structure that is active in conjugation and attachment; also more accurately called a sex pilus.

Plasmid—A circular strand of DNA that is independent of the chromosome and is self-replicating.

Recipient—A bacterium that receives a plasmid by conjugation.

Repression—Inhibition of the transcription (or translation) of a gene by the binding of a repressor protein to a specific site on the DNA (or mRNA).

Ribosome—Macromolecular complexes of proteins and three molecules of ribosomal RNA (23S, 16S, and 5S) that synthesize proteins from messenger RNA.

RNA—A linear polymer made up of ribonucleotide repeating units (composed of the sugar ribose, phosphate, and one of four heterocyclic bases); RNA is used in several ways to convert the genetic code to protein products.

Segregation—The loss of plasmid during cell division by a daughter cell because one daughter did not receive a plasmid copy.

Strain—A population of genetically identical cells.

Transconjugant—A recipient cell that has gained a plasmid via conjugation.

Transcription—Synthesis of messenger RNA complementary to one of the two strands of DNA.

Translation—The process by which the information in messenger RNA is converted to form proteins; translation is performed by the ribosome.

Xenobiotic—Not naturally occurring; produced by human industry.

FIGURE 1
How genes form proteins

(a) Complementary bonding of DNA and the double helix

Strand 1: ····—G—C—A—C—C—T—····
Strand 2: ····—C—G—T—G—G—A—····

Sugarphosphate backbone
Hydrogen bond
Base
3'ᵃ 5'ᵃ
3'ᵃ 5'ᵃ

(b) The translation of genetic information into proteins

DNA
5' 3'
RNA polymerase

1. RNA polymerase separates DNA strands.

2. Polymerase forms a complementary mRNA strand from one DNA strand.

Amino acid
tRNA
Enzyme

mRNA strand
Ribosomes

3. Ribosome forms enzyme chain from code on mRNA and with amino acids brought to it by complementary tRNA.

ᵃDenotes 3' and 5' positions on sugar portion of DNA molecule.

Using genetic information

All genetic information is contained on strands of DNA (deoxyribonucleic acid). One strand of DNA is made up of a chain of deoxyribonucleotides. Each deoxyribonucleotide contains one of the four bases: adenine (A), guanine (G), cytosine (C), or thymine (T). Each base is connected to a sugar (a ribose), and the sugars are linked to other sugars by phospho-diester bonds to form a chain. The order of the bases in the chain (e.g., CGTCAGTC...) encodes all the information the cell uses to manufacture proteins. The average bacterium requires $3 \times 10^6 - 6 \times 10^6$ bases to encode its genetic information.

DNA strands almost always come in complementary pairs. Complementary means that the C of one strand is hydrogen bonded to the G of the other, while the T of one strand is bonded to the A of the other strand. Figure 1a illustrates the complementary bonding of a segment of a double-stranded DNA molecule and how the complementary strands form a shape called the double helix. The use of complementary strands enables the cells to reproduce their genetic information precisely from generation to generation.

Much of the genetic information contained in DNA specifies the structure of enzymes, which are polymers of amino acids (i.e., proteins) that catalyze the reactions performed by the bacteria. The translation of the information contained in the DNA to form enzymes is a three-step process that involves another cellular polymer, RNA. RNA, or ribonucleic acid, is similar in structure to DNA. The main differences are that the pentose-sugar unit of the nucleotide contains an additional OH group (recall that the D in DNA stands for *deoxy*) and that the base uracil (U) replaces thymine (T).

Figure 1b illustrates the three steps for translation of the information in DNA to form enzymes. RNA plays three roles in information transfer. First, an enzyme, RNA polymerase, moves along the DNA molecule and separates the strands over part of the molecule. Then, the polymerase forms a strand of RNA complementary to one of the DNA strands. Complementary has the same meaning as when it describes DNA pairs, except that U for the RNA has the same role as T for the DNA; thus, C on the DNA complements G on RNA, G complements C, T complements A, and A complements U. The base pairing between DNA and RNA is transient. The complementary pairs of the DNA strands quickly reform, yielding an unpaired single strand of RNA. The complementary strand is called messenger RNA, or mRNA, because it carries the information encoded in the DNA to the site of protein synthesis.

The site of protein synthesis is the ribosome, a complex macromolecular structure composed of about two-thirds RNA and one-third protein. As the mRNA strand exits the polymerase enzyme, it engages the ribosome (Fig. 1b). The active core of the ribosome is ribosomal RNA, or rRNA. Although rRNA is made up of the same ribonucleic acid building blocks as mRNA, its purpose is to translate the information encoded by the mRNA strand into an amino acid chain. It does so by "reading" the mRNA code in sequences of three bases, each of which signifies one amino acid making up the enzyme. For example, GCC means attach an alanine amino acid; CGU means attach an arginine amino acid. The proper amino acids are brought to the ribosome (for incorporation into the growing amino acid chain) by still another form of RNA, transfer RNA (or tRNA).

The key aspect of the genetic content of cells is that it is faithfully stored, replicated, and translated into proteins. The ultimate source of and repository for the information is the DNA, but RNA is a necessary intermediate system for turning the information into working molecules, the proteins.

Characterization of DNA

Although all DNA has the same basic structure and role, cells contain DNA molecules that differ in terms of being essential or accessory and in terms of being mobile or immobile. The differences among the types of DNA are critical for assessing the genetic information in a biological-process population.

Genetic information within a bacterial cell can be characterized as essential to or accessory to the normal cell functions. Essential functions mainly include the generation of energy; the synthesis and maintenance of cell constituents, such as cell walls, membranes, enzymes, and nucleic-acid polymers; and the regulation of transport of materials into and out of the cell. The essential genetic information is contained on the chromosome, one of which resides permanently inside each cell. The chromosome is replicated when the cell divides to form two daughter cells.

Accessory genetic information often is contained on smaller elements, including plasmids, transposons, and viral DNA. These elements share a common characteristic: They can replicate autonomously from the host chromosome. In other words, accessory DNA can be replicated whether or not the cells are dividing. In general, accessory DNA encodes functions that are not essential, at least for the routine operation of the cell.

Although all accessory elements contribute to the pool of genetic information, this review focuses on plasmids, which apparently make up the bulk of accessory elements in bacteria. Plas-

mids are covalently closed strands of DNA that generally exist independently from the chromosome. Plasmids vary in size from a few thousand to several hundred thousand bases; they are much smaller than chromosomes, which typically are about 4 million bases long. The small plasmids (e.g., 10 kilobases) frequently are found in many copies within a single cell, whereas the large plasmids (e.g., larger than 30 kilobases) usually have only one or a few copies.

Whether certain genes are contained on chromosomal or accessory DNA is critical for assessing the genetic capabilities of populations in biological reactors. Information on the chromosome determines traits such as the range of energy-generating substrates the cells use, the rate of growth of the cells, and, in some cases, whether cells are good at being retained through flocculation or attachment. Thus, most traditional process-control strategies address capabilities that are contained on the chromosome.

Plasmid DNA also can be important in biological processes, especially because genes coding for many interesting reactions are contained on plasmids (4). Environmentally important reactions known to be encoded on plasmids include resistance to antibiotics and other toxic substances, oxidation of and resistance to heavy metals, and degradation of halogenated and other xenobiotic organic compounds (5–13). Other potentially important reactions found on plasmids are production of toxins, transfer of genes, degradation of hydrocarbons, and nitrogen fixation (6, 13, 14).

Genetic information within a cell also can be characterized as being mobile or immobile. Mobility means that the DNA can cross cell boundaries and be transferred among different bacteria. Although the cell's chromosome normally is immobile (at least between species), accessory DNA is mobile and can move to other cells.

The mobility of plasmids is an important factor in biological processes. Recent work has shown that the transfer of plasmids among bacteria found in the environment is common and can confer an advantage to the recipient bacteria. For example, Genthner et al. (15) demonstrated that 38% of 68 environmental strains, including species of *Pseudomonas*, *Acinetobacter*, and *Alcaligenes*, can receive a resistance plasmid from laboratory donor strains. Pucci et al. (16) showed that some species of *Leuconostoc* can receive plasmids from several *Streptococcus* species. Krockel and Focht (17) transferred a plasmid for dechlorination of chlorobenzene from an *Alcaligenes*

FIGURE 2
Plasmid transfer and replication during conjugation

a) Nick and transfer of heavy strand

b) Complementary (*) strand synthesis in donor and recipient

[a]Denotes 3′ and 5′ positions on sugar portion of DNA molecule.
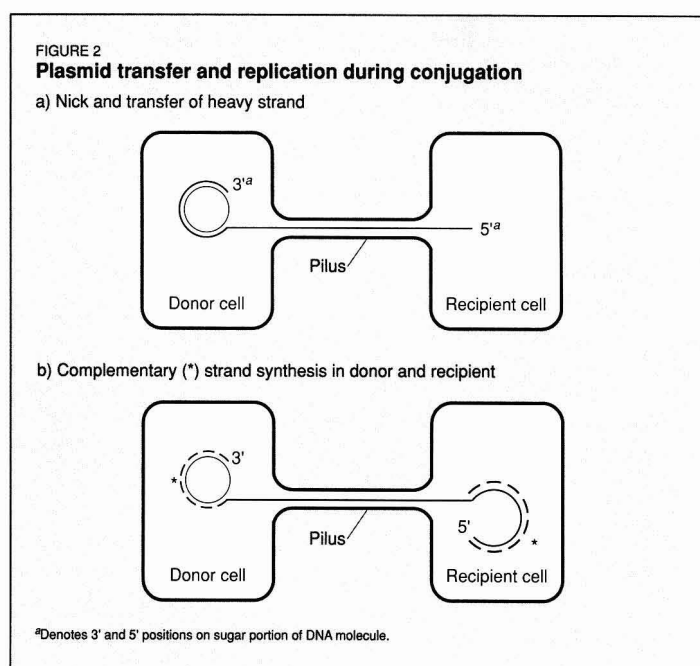
species to a *Pseudomonas putida* strain, thereby allowing the *P. putida* strain to catabolize the chlorinated benzenes. Finally, Rusansky et al. (14) showed that the transfer of plasmid pSR4 to *Acinetobacter calcoaceticus* allowed the species to grow on oil droplets.

Plasmids and conjugation

The focus of this article and the next one in this series is on plasmids. Because they are accessory, they may encode information for the degradation of unusual substrates and resistance to toxic materials. Because they are accessory and mobile, they can replicate and proliferate within a bacterial population independently of the replication of chromosomal DNA and cell division. Hence, the genetic capability of a population can be changed rapidly by plasmid transfer, even though the total biomass and its species composition do not change. (Note that plasmids also generally are replicated within the cells and transmitted to daughter cells during cell division.) This section provides more information on plasmids and their main transfer mechanism, conjugation.

Plasmids discovered since 1976 are given a unique designation of the form pXY1234. Plasmids discovered before 1976, however, have less formal names derived from the dominant characteristic imparted by the plasmid. For example, plasmids whose designation begins with R confer antibiotic resistance. Another common designation is Inc, which stands for incompatibility; plasmids within the same incompatibility group (e.g., Inc Q) cannot coexist stably within the same cell.

The transfer of DNA from one bacterium to another can occur by at least three distinct mechanisms (6, 12, 13). Two of the mechanisms appear to be minor for situations such as those in biological processes: One minor mechanism, transformation, is the direct uptake of DNA from solution, and the second, transduction, is the transfer of DNA during infection by a virus that infects bacteria.

The primary mechanism, conjugation, requires direct cell-to-cell contact for transfer of plasmids from a donor cell to a recipient cell. During conjugation the DNA strands of the donor plasmid separate, and one strand (the heavy strand) is transferred to the recipient (Figure 2). Complementary strands to both original strands are synthesized to give double-stranded plasmid in both cells. Thus, the number of plasmid copies increases relative to the number of cells. Conjugation generally is mediated by filaments, called sex pili, on the cell surface (see photomicrograph). Contact between the pili and specific receptors on the outer membrane of the recipient triggers conjugation.

Conjugative plasmids have genes that control transfer (18, 19). The transfer genes, called the tra genes, code for products that form the pili and mediate transfer of one DNA strand to the recipient (Figure 2). Because conjugative plasmids must contain the transfer
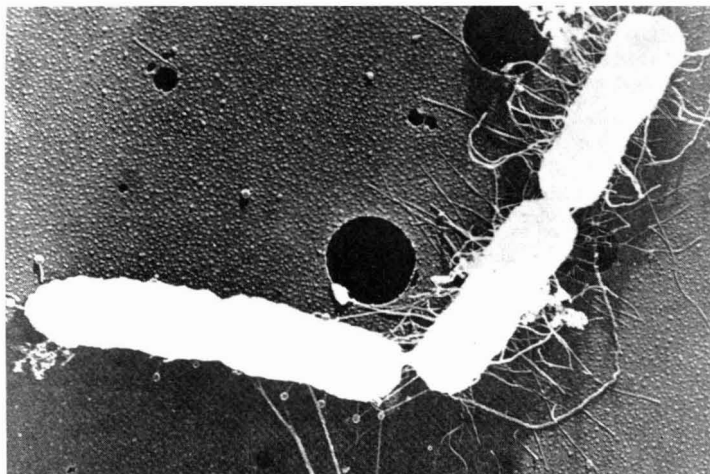
Photomicrograph of conjugating cells connected by a sex pilus.

genes, they usually are large (i.e., larger than 50,000 bases) *(4, 9, 19)*. Most of the time, the tra genes are repressed, which means that they are not producing proteins. Some stimulus, not yet fully understood, is needed to activate the tra genes and begin the process of plasmid transfer. On the other hand, evidence indicates that repression of the tra genes does not occur immediately upon entry of a new plasmid into a recipient cell. Thus, newly acquired plasmids may be able to retransfer themselves at a high rate, until a low rate of transfer is established through tra repression.

A variation on conjugation is called mobilization, which occurs when a plasmid does not have all the transfer genes but can be cotransferred with, or assisted by, a conjugative plasmid *(4, 6, 9, 20)*. Many small plasmids have mobility determinants that promote cointegration with a conjugative plasmid; thus, the deficient plasmid transfers together with a conjugated plasmid. Alternatively, the conjugative plasmid supplies the gene products missing from the deficient plasmid. According to one report, genes coding for degradation of halogenated alkanoic acids were transferred by mobilization *(7)*.

Research has shown clearly that plasmid transfer can occur among bacteria found in biological processes. Several authors *(11, 21–30)* reported the transfer of plasmid-encoded characteristics, such as degradation of chlorinated compounds and resistance to metals or antibiotics, in well-controlled laboratory or field studies. The key issue is whether plasmid transfer has any major control over the genetic capabilities of biological processes and, hence, over process performance. Currently, no definitive data exist to prove the importance of plasmid transfer. Several items of evidence, however, suggest that plasmid transfer may be significant.

First, several research reports *(12, 31–33)* describe acclimatization periods of several days to several months before degradation of xenobiotic chemicals occurs in mixed cultures. Once acclimatization begins, nearly complete degradation quickly follows. The great length of the acclimatization period, coupled with an almost immediate onset of rapid degradation, is difficult to explain by growth of a specialized strain or by ecological selection. An appealing explanation is that the genes for the degradation reaction were rapidly disseminated by plasmid replication and transfer within the well-established indigenous population. Perhaps the initiation of dissemination is the result of a random event, such as a mutation, that requires a long time to occur. On the other hand, the rapid spread of the new capability could have been brought about by conjugation.

Second, several researchers created bacteria that attain novel biodegradative capacities by the conjugative exchange of genetic information. Plasmid transfer was used to construct strains capable of fully degrading new chlorinated aromatic compounds *(34–36)*. Also, cocultivation of strains harboring plasmid genes for different biodegradative functions on plasmids resulted in the formation of new strains able to degrade compounds that the parent strains could not catabolize. Moreover, novel strains degrading chlorobenzoates *(37)*, 2,4,5-T *(10)*, chlorinated alkanoic acids *(23)*, chloroanilines *(38)*, and chlorobenzenes *(17)* were obtained by plasmid transfer procedures.

Finally, research *(39)* that detected a plasmid-encoded gene for naphthalene degradation in activated sludge showed that the ability of the activated sludge to degrade naphthalene is correlated with the number of cells harboring the plasmid. Although not proving that plasmid transfer is the cause of changes in the number of plasmid-containing cells, this research emphasized the need for a significant fraction of the cells to have the gene if noticeable removal of naphthalene was to occur.

Rates of plasmid transfer

Whether or not plasmid transfer is or can be a significant determinant of the genetic capability within biological processes depends on the rates of plasmid transfer. A critical evaluation of the literature reveals a small but important body of information that demonstrates that the kinetics of plasmid transfer can be described in a structured and useful manner. This section synthesizes information from several groups *(40–45)* into a self-consistent model that has parameters and units compatible with those used in environmental engineering.

Three types of bacteria must be represented. The first type is the plasmid donor, or the cells that originally contain the plasmid. The concentration of the donor is called D and has units of g_D/L. The second type is the recipient, whose concentration is R (g_R/L.) Recipients do not contain the plasmid. The third type is the former recipient cell that has gained the plasmid by conjugation. Its concentration is given by T, which denotes transconjugant, and has units of g_T/L.

The most efficient way to formulate transfer kinetics is to write rate expressions in terms of the transconjugant, or T. Previous work has shown that conventional "mass action" expressions can be used to describe the three types of plasmid transfer.

The first mechanism of transfer is from the donor to the recipient. It can be described successfully by the mixed second-order rate equation,

$$r_{DR} = k_{t1}DR \qquad (1)$$

in which r_{DR} is the rate of creation of transconjugants by plasmid transfer from donors to recipients (g_T/L-day), and k_{t1} is the donor-to-recipient transfer coefficient ($L \cdot g_T/g_Dg_R$-day).

The second transfer mechanism is from a transconjugant to a recipient. The rate expression is

$$r_{TR} = k_{t2}TR \qquad (2)$$

in which r_{TR} is the rate of creation of transconjugants from transfer of a plasmid from transconjugants to recipients (g_T/L-day), and k_{t2} is the transconjugant-to-recipient transfer coefficient (L/g_R-day).

Finally, the transconjugants can lose their plasmids by incorrect replication of the plasmid *(46)* or by segregation, which is the division of the cell into two daughter cells when only one plasmid is present. A simple model of plasmid loss is

$$r_L = -b_p T \qquad (3)$$

in which r_L is the rate of loss of transconjugants due to plasmid loss (g_T/L-day), and b_p is the rate of loss of the first-order plasmid from transconjugants (day^{-1}).

Kinetic approaches to plasmid transfers are summarized in the box. The kinetics of the first two mechanisms have been studied and modeled much more extensively than the kinetics of plasmid loss. In general, constant values of k_{t1} are satisfactory for batch and chemostat (i.e., continuously fed) systems. In some cases, k_{t1} and k_{t2} are assumed to be equal, but their equality cannot always be taken for granted.

Although plasmid loss usually is attributed to segregation, its mathematical treatment varies considerably. In some cases it is ignored *(43, 45)*, in one case *(40)* it is expressed directly as a constant b_p, and in two cases *(41, 42, 44)* plasmid loss is described with a decrease in the specific growth rate. The last approach for loss gives a similar result as a constant b_p in that both approaches cause a decrease in the net accumulation rate of transconjugants.

The model of Freter et al. *(44)* groups plasmid segregation with other plasmid-related effects that decrease the net growth rate of cells that contain a plasmid. In general, cells that contain plasmids—especially plasmids for which the transfer genes are activated to allow transfer—have a competitive disadvantage, which usually is represented by a decreased specific growth rate, μ *(12, 40, 44, 47–49)*. If the plasmid-encoded functions provide no advantage, these cells can be washed out of systems in which they must compete with plasmidless cells. Thus, gaining a plasmid can alter the kinetic characteristics of the transconjugant, compared with the recipient.

More work is needed to elucidate the type and magnitude of the effect on kinetic parameters, such as μ, because observed effects have varied. Although many researchers showed that having a plasmid decreases a cell's specific growth rate, some researchers reported no effects *(24, 29, 50)*, and still others observed increased competitiveness by plasmid-containing cells in the absence of selective pressure *(23)*.

If containing a plasmid is a "drain" on the cell's resources, then it seems reasonable that cells would lose their plasmids when the plasmids are confer-

---

Kinetic approaches to plasmid transfers, losses, and other effects

Features of approach	Reference
T ⟶ R transfer included with constant k_{t2}. Plasmid loss assumed by segregation with a constant b_p. Plasmid content affects growth parameter, μ. Applied to chemostats.	*(40)*
D ⟶ R transfer not included. T ⟶ R transfer included, but $k_{t2} \cdot$ R is considered constant for R > 10^7/mL. Retransfer from a new transconjugant is delayed by about 90 min. Segregation loss included indirectly as a reduction in the net transfer rate. Plasmid content does not affect other growth parameters. Applied to batch exponential growth.	*(41, 42)*
D ⟶ R transfer included with contant k_{t1}. T ⟶ R transfer included with constant $k_{t2} = k_{t1}$. Plasmid loss by segregation is considered negligible. Plasmid content does not affect other growth parameters. Applied to chemostats and batch growth.	*(43)*
D ⟶ R transfer included with constant k_{t1}. T ⟶ R transfer included with constant k_{t2}. Segregation loss and a decrease in specific growth rate due to plasmid content are considered together. Applied to chemostats.	*(44)*
D ⟶ R transfer included with constant k_{t1}. Plasmid loss not included. Plasmid content does not affect other growth parameters. Applied to batch microcosms.	*(45)*

---

ring no advantage. In practical terms, b_p might vary as environmental conditions change. Studies of several species and plasmid types *(7, 51)* revealed rapid losses of plasmid when the selective advantage was removed. On the other hand, Jain and Sayler *(52)* found that the TOL and RK2 plasmids are stably maintained in *Pseudomonas putida* in the presence or absence of selective pressure. Similar stable plasmid maintenance in *E. coli* cultures was observed by Tolentino and San *(53)* and Wang et al. *(54)*.

Growth conditions also can affect the rate of plasmid loss. Several researchers *(48, 55, 56)* found that segregation is greater when the cells receive limited amounts of nutrients, such as occurs at low specific growth rates. Because most biological processes operate with very low specific growth rates (e.g., 0.01–0.5 per day), plasmid loss might be accentuated by the normal operating conditions. Again, systematic research is needed to evaluate b_p under conditions that prevail in biological treatment systems.

Effects of plasmid transfer

The presence of a strong selective pressure, such as high concentrations of an antibiotic or toxic heavy metal, gives a major competitive advantage to cells containing a plasmid that codes for a resistance function *(24)*. There also is evidence that degradative plasmids are stably maintained in the presence of a

significant concentration of their substrate *(7)*. An important and unresolved question is, How does the presence of low concentrations of xenobiotic substrates affect plasmid content and cell selection?

When the concentration of a xenobiotic substrate is low, its biodegradation probably contributes little or nothing to the energy, electron, and nutrient flows needed to grow and maintain the bacteria *(1, 57, 58)*. Indeed, the biodegradation of the low-concentration xenobiotic compound may provide no direct advantage to the cells containing the plasmid. Indeed, maintaining the plasmid might confer a competitive disadvantage to a cell. On the other hand, a plasmid-encoded reaction could remove subacute toxicity from a trace-level xenobiotic contaminant. In such a case, the plasmid may be maintained for the purpose of toxicity reduction, which gives the plasmid-containing cell an advantage.

When plasmids are important in maintaining degradative capabilities in microbial populations, even when the advantages to a single cell are minimal or negative, their transfer among different cells may be an important way to keep the plasmids always present in the bacterial population. In effect, the cells share the responsibility and cost of maintaining the plasmid in the population, and they have kinetic characteristics that may be regarded as averaged over the plasmid-containing and plas-

midless parts during the time they remain in the system. Thus, no one cell bears all the costs of plasmid retention when the advantages of having a plasmid are small or negative for any cell.

Sharing the benefits and costs of plasmid content affects the ecology and evolution of bacterial populations. The differences among bacterial species become less distinct if the cells are sharing information that contributes to the long-term benefit of the entire population. Bacterial evolution must be understood in terms of information exchanges among different cell types, as well as in terms of intracellular modifications within an isolated chromosomal lineage *(59)*. Similarly, evolution of accessory DNA must have a population or community component, because new genes that arise from mutation or from input of exogenous DNA are made part of the population's information storehouse, even if it never becomes part of the chromosome of a particular species. By means of plasmid transfer and "population storage," weak environmental pressures, such as low concentrations of a xenobiotic substrate, may be able to affect the genetic capabilities of microbial populations.

Looking ahead

This article described how genetic information is stored, used, replicated, and transferred in bacterial populations such as those that occur in biological processes. Emphasis was given to plasmid transfers among donor, recipient, and transconjugant cells. A structure for kinetic modeling of plasmid transfers was presented.

In the second part of this two-part article, we will analyze transfer parameters critically and quantitatively. We will use the information from our analysis to assess the importance of plasmid transfer in controlling genetic capability, which is the basis for evaluating the performance of biological processes. Finally, we will identify key research needs and directions.

References

(1) Rittmann, B. E. *Environ. Sci. Technol.* **1987,** *21,* 128–36.
(2) Jewell, W. R. *Environ. Sci. Technol.* **1987,** *21,* 14–21.
(3) Pretorius, W. A. *Water Res.* **1987,** *21,* 891–94.
(4) Sherratt, D. *Symp. Soc. Gen. Microbiol.* **1986,** *39,* 239–50.
(5) Shields, M. et al. *J. Bacteriol.* **1985,** *163,* 882–87.
(6) Trevors, J. T. et al. *Can. J. Microbiol.* **1986,** *33,* 191–98.
(7) Hardman, D. J. et al. *Appl. Environ.* **1986,** *51,* 44–51.
(8) Tam, A. C. et al. *Appl. Environ. Microbiol.* **1987,** *53,* 1088–93.
(9) Haas, D. *Experentia* **1983,** *39,* 1199–1213.
(10) Kellog, S. T. et al. *Science* **1981,** *214,* 1133–35.
(11) Hansen, C. L. et al. *Biotechnol. Bioeng.* **1984,** *26,* 1330–33.
(12) Reanney, D. C. et al. *Symp. Soc. Gen. Microbiol.* **1983,** *34,* 379–421.
(13) Beringer, J. E.; Hirsch, P. R. In *Current Perspectives in Microbial Ecology;* Klug, M. J.; Reddy, C. A., Eds.; American Society of Microbiology: Washington, DC, 1984; 63–70.
(14) Rusansky, S. et al. *Appl. Environ. Microbiol.* **1987,** *53,* 1918–23.
(15) Genthner, F. J. et al. *Appl. Environ. Microbiol.* **1988,** *54,* 115–17.
(16) Pucci, M. J. et al. *Appl. Environ. Microbiol.* **1988,** *54,* 281–87.
(17) Krockel, L.; Focht, D. D. *Appl. Environ. Microbiol.* **1987,** *53,* 2470–75.
(18) Hardy, K. *Bacterial Plasmids Aspects of Microbiology,* No. 4, 2nd ed.; American Society of Microbiology: Washington, DC, 1986; 7–54.
(19) Willets, N.; Wilkens, B. *Microb. Rev.* **1984,** *48,* 24–41.
(20) Willets, N. In *Pathogenicity and Ecology of Bacterial Plasmids;* Levy, S. B. et al., Eds.; Plenum Press: New York, 1981; 207–15.
(21) Mach, P. A.; Grimes, D. J. *Appl. Environ. Microbiol.* **1982,** *44,* 1395–1403.
(22) Gealt, M. A. et al. *Appl. Environ. Microbiol.* **1985,** *49,* 836–41.
(23) Slater, J. H. *Current Perspectives in Microbiology;* Klug, M. J.; Reddy, Eds.; American Society of Microbiology: Washington, DC, 1984; 87–93.
(24) Grabow, W.O.K. et al. *Water Res.* **1975,** *9,* 777–82.
(25) Mancini, P. et al. *Appl. Environ. Microbiol.* **1987,** *53,* 665–71.
(26) McPherson, P.; Gealt, M. A. *Appl. Environ. Microbiol.* **1986,** *51,* 904–9.
(27) Bale, M. J. et al. *Appl. Environ. Microbiol.* **1988,** *54,* 2756–58.
(28) Bale, M. J. et al. *Appl. Environ. Microbiol.* **1988,** *54,* 972–78.
(29) Cruz-Cruz, N. E. et al. *Appl. Environ. Microbiol.* **1988,** *54,* 2574–77.
(30) O'Morchoe, S. B. et al. *Appl. Environ. Microbiol.* **1988,** *54,* 1923–29.
(31) Aelion, C. M. et al. *Appl. Environ. Microbiol.* **1987,** *53,* 2212–17.
(32) Bouwer, E. J.; McCarty, P. L. *Appl. Environ. Microbiol.* **1983,** *45,* 1286–94.
(33) Horowitz, A. et al. *Appl. Environ. Microbiol.* **1983,** *45,* 1459–65.
(34) Reineke, W.; Knackmuss, H. J. *Nature* **1979,** *277,* 385–86.
(35) Reineke, W.; Knackmuss, H. J. *J. Bacteriol.* **1980,** *142,* 467–73.
(36) Schwien, U.; Schmidt, E. *Appl. Environ. Microbiol.* **1982,** *44,* 33–39.
(37) Hartmann, J. et al. *Appl. Environ. Microbiol.* **1979,** *37,* 421–28.
(38) Latorre, J. et al. *Arch. Microbiol.* **1984,** *140,* 159–65.
(39) Blackburn, J. W. et al. *Environ. Sci. Technol.* **1987,** *21,* 884–90.
(40) Stewart, F. M.; Levin, B. R. *Genetics* **1977,** *87,* 209–28.
(41) Cullum, J. et al. *Plasmid* **1978,** *1,* 536–44.
(42) Cullum, J. et al. *Plasmid* **1978,** *1,* 545–56.
(43) Levin, B. R. et al. *Plasmid* **1979,** *2,* 247–60.
(44) Freter, R. et al. *Infect. Immun.* **1983,** *39,* 60–84.
(45) Knudsen, G. R. et al. *Appl. Environ. Microbiol.* **1988,** *54,* 343–47.
(46) Bassett, C. L.; Kushners, S. R. *J. Bacteriol.* **1984,** *157,* 661–64.
(47) Godwin, D.; Slater, J. H. *J. Gen. Microbiol.* **1979,** *111,* 201–10.
(48) Wouters, J. T. et al. *Antonie van Leeuwenhoek* **1980,** *46,* 353–62.
(49) Zünd, P.; Lebek, G. *Plasmid* **1980,** *3,* 65–69.
(50) Walter, M. V. et al. *Curr. Microbiol.* **1987,** *15,* 193–97.
(51) Jones, S. A.; Melling, J. *FEMS Microbiol. Lett.* **1984,** *22,* 239–43.
(52) Jain, R. K.; Sayler, G. S. *Microbiol. Sci.* **1987,** *4,* 59–63.
(53) Tolentino, G. J.; San, K. Y. *Biotechnol. Lett.* **1988,** *10,* 373–76.
(54) Wang, P. C. et al. *J. Ferment. Technol.* **1988,** *66,* 63–70.
(55) Jones, I. M. et al. *Mol. Gen. Genet.* **1980,** *180,* 579–84.
(56) Noack, D. et al. *Mol. Gen. Genet.* **1981,** *184,* 121–24.
(57) Namkung, E. et al. *J. Water Pollut. Contr. Fed.* **1983,** *55,* 1366–72.
(58) Namkung, E.; Rittmann, B. E. *J. Water Pollut. Contr. Fed.* **1987,** *59,* 670–78.
(59) Shapiro, J. A. In *Engineered Organisms in the Environment: Scientific Issues;* Halverson, H. O. et al., Eds.; American Society of Microbiology: Washington, DC, 1985; 63–69.
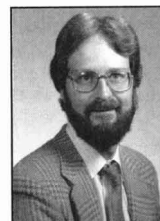
***Bruce E. Rittmann** is professor of environmental engineering at the University of Illinois at Urbana-Champaign. His research focuses on the biodegradation of low-concentration organic compounds, biofilm processes, and interdisciplinary research in environmental biotechnology.*
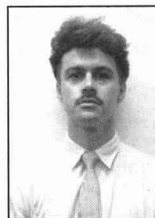
***Barth F. Smets** (l) is a research assistant in environmental engineering at the University of Illinois. He is pursuing a Ph.D. degree in environmental engineering and science. He obtained his M.S. degree in agricultural engineering at the State University of Ghent (Belgium).*

***David A. Stahl** (r) is assistant professor of veterinary pathobiology and is affiliated with the Department of Microbiology at the University of Illinois at Urbana-Champaign. His research concerns the application of molecular ecology and phylogeny to the characterization of natural microbial communities.*

The carcinogenicity of radon

By Rhonda S. Berger

Numerous studies of underground miners exposed to radon daughters (elements that result from the disintegration of radon) in the air of mines have shown an increased risk of lung cancer in comparison with nonexposed populations. Laboratory animals exposed to radon daughters also develop lung cancer. The abundant epidemiological and experimental data have established the carcinogenicity of radon progeny. These observations are of considerable importance because uranium, from which radon and its progeny arise, is ubiquitous in the Earth's crust, and radon in indoor environments can reach relatively high concentrations.

Although the carcinogenicity of radon daughters is established, and the hazards of exposure during mining are well recognized, the hazards of exposure in other environments have not yet been adequately quantified. Risk estimates of the health effects of long-term exposures at relatively low levels are required to address the potential health effects of radon and radon daughters in homes and to refine estimates of the risk in work places.

Two approaches are currently being used to characterize the lung cancer risks associated with radon daughter exposure: mathematical representations of the respiratory tract that model radiation doses to target cells and epidemiological investigation of exposed populations, mainly underground miners.

Radon daughter exposure

Of the several isotopes of radon, radon-222 has the most important impact on human health. An inert gas at temperatures above -61.8 °C, radon-222 is a naturally occurring decay product of radium-226, the fifth daughter of uranium-238 (see Figure 1). Both uranium-238 and radium-226 are present in most soils and rocks in widely varied concentrations. As radon forms from the decay of radium-226, it can leave the soil or rock and enter the surrounding air or water. Radon gas thus becomes ubiquitous, and its concentration is increased by the presence of a rich source and by low ventilation in the vicinity of the source.
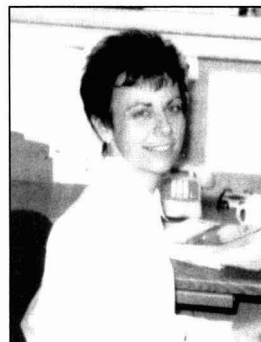
Radon decays with a half-life of 3.82 days into a series of solid, short-lived radioisotopes collectively referred to as radon daughters or progeny. The first four short half-life radioactive decay products of radon are the most important sources of cancer risk. These are polonium-218, lead-214, bismuth-214, and polonium-214. Polonium-218, the first decay product, has a half-life of just over three minutes. This is long enough for most of the electrically charged polonium atoms to attach themselves to microscopic airborne dust particles. When inhaled, these small particles have a good chance of sticking to the moist epithelial lining of the bronchi.

Most inhaled particles are eventually cleared from the bronchi by mucus, but not quickly enough to keep the bronchial epithelium from being exposed to alpha particles from the decay of polonium-218 and polonium-214. This highly ionizing radiation passes through and delivers radiation doses to several types of lung cells. When alpha

Rhonda Berger

FIGURE 1
Radioactive decay of uranium-238
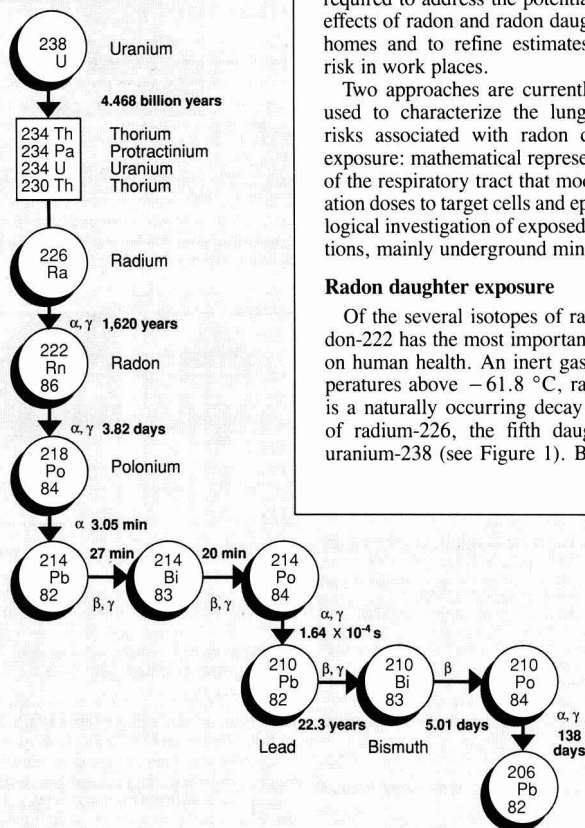
TABLE 1
Radon risk evaluation chart

Exposure level (pCi/L)	No. of excess lung cancer deaths (per 1000)	Comparable risk
200.0	440–770	4 pack/day smoker
100.0	270–630	>60 × non-smoker risk
40.0	120–380	20,000 chest X-rays/year
20.0	60–100	2 pack/day smoker
10.0	30–120	5 × non-smoker risk
4.0	13–50	200 chest X-rays/year
2.0	7–30	
1.0	3–13	Non-smoker risk of lung cancer
0.2	1–3	20 chest X-rays/year

Source: *A Citizens' Guide to Radon;* U.S. Environmental Protection Agency and U.S. Center for Disease Control: Washington, DC. 1986; OPA-86-004.

particle emissions occur, these cells lining the airways can be damaged. The resulting biological changes can ultimately lead to lung cancer.

Underground mining was the first occupation associated with an increased risk of lung cancer. Uranium ores contain particularly high concentrations of radium, and radon daughter exposure has been associated with lung cancer in uranium miners. Miners of other types of ore can also be placed at risk by the combination of a sufficiently strong source of radon and inadequate ventilation.

Radon progeny are also present in the air of dwellings. The source is predominantly the underlying soil. Building materials, groundwater used routinely in the building, and utility natural gas can be contaminated with radon gas as well. The concentration of radon progeny in dwellings is highly variable and depends mainly on the air pressure and ventilation in the home.

Because of their wide distribution, radon daughters are a major source of exposure to radioactivity for the general public as well as for special occupational groups. The estimated dose to the bronchial epithelium from radon daughters far exceeds that to any other organ from natural background radiation. The recent recognition that some homes have high concentrations of radon has focused concern on the potential lung cancer risk associated with environmental radon.

Indoor radon and risk

The radiation dose from inhaled daughters of radon-222 constitutes about half of the total effective dose equivalent that the general population receives from natural radiation. A variety of study results in the United States suggest that radon-222 concentrations in residences average about 1 pCi/L (a picocurie, pCi, is the amount of any radionuclide that undergoes exactly 3.7 × 10^{-2} radioactive disintegrations per second). Estimation of the incidence of lung cancer due to the daughters associated with this quantity of radon-222 yields thousands of cases per year among the U.S. population.

Indoor levels are sometimes an order of magnitude or more higher than the average; it is the common experience of communities that survey homes to find concentrations in the range of 10 to 100 pCi/L. Whereas the risk associated with even 1 pCi/L is very large compared with many environmental insults, exposure to these higher concentrations for prolonged periods leads to estimated individual lifetime risks of lung cancer that exceed 1%. For the extreme concentrations that have been reported, the risk appears to approach that from cigarette smoking. Table 1 is an excess risk evaluation chart based upon exposure to radon for individuals who spend 75% of their time in the home for 70 years.

Recommended exposure levels

There is currently no federal legislation that might be invoked as the statutory basis for a generalized program regulating the radon level in homes. The thrust of the Clean Air Act is toward prevention of atmospheric pollution and the maintenance of ambient air quality. The Toxic Substances Control Act (TSCA) is aimed at chemical substances or mixtures subsequent to manufacture. Therefore, only recommended guideline exposure levels have been issued by EPA at 4 pCi/L and by the National Council on Radiation Protection at 8 pCi/L. These agencies suggest implementation of remedial actions for exposures above these levels.

Rhonda S. Berger is an environmental control engineer in the Engine Division of the Ford Motor Company in Dearborn, MI. She received her B.S. degree in environmental sciences from Michigan State University and her M.S. degree in toxicology from Wayne State University in Detroit.

Regulation of carbon monoxide: Are current standards safe?

By Wendell P. Greek and
Vernon P. Dorweiler

Carbon monoxide regulation as mandated under the National Ambient Air Quality Standards (NAAQS) has not effectively protected the health of this country's citizens. The direct cause-and-effect relationships between carbon monoxide and cardiac dysfunction indicate a clear and urgent need for the re-evaluation of carbon monoxide standards in order to protect the health of urban Americans.

The CO situation

The onset of health problems occurs at far lower CO concentrations than currently mandated under the NAAQS and enforced by EPA. Ranging from the long-term effect of cardiomegaly to the immediate consequences of angina, CO pollution has a lengthy history of serious health implications, particularly for those who live and work in urban areas (1).

In basic terms, breathing CO limits the red blood cells' ability to carry oxygen. Physiologically, the mechanism for adverse CO effects is a fall in capillary oxygen partial pressure (pO_2) due to CO binding to hemoglobin (carboxyhemoglobin, COHb) (2), thus producing the pathological condition known as carboxyhemoglobinemia. Higher CO concentrations result in less oxygen being delivered to the body, resulting in continuous impairment of mental and physical functions; hearing can be damaged by the restriction of the flow of oxygen to nerve cells in the cochlea of the inner ear (3). Although this reaction is reversible over time, some urban concentrations may remain so high that reversal does not occur.

Human tolerance to CO is quite high, considering the lethal effects of pro-
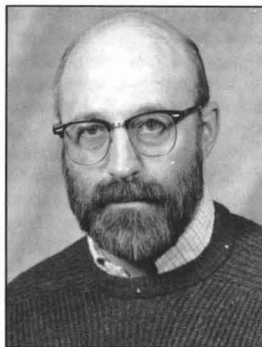
Wendell Greek
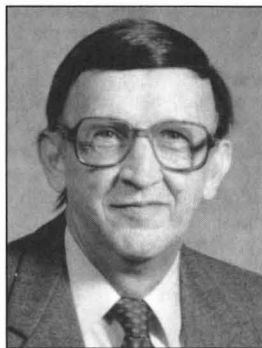
Vernon Dorweiler

longed exposure. Studies have shown that a healthy person could survive episodes of acute exposure with moderately high levels of blood COHb (20–40%); however, a CO "threshold" below which there is no adverse health effect has not been found (2). For the urban American, the adverse health effects of chronic CO exposure represent a significant threat to personal well-being.

Clean Air Act objectives

The Clean Air Act of 1970 serves as the starting point for the regulation of CO emissions. The act's standard is defined as "ambient air quality sufficient

to protect the health of persons whenever there is an absence of adverse effect on the health of a statistically related sample of persons in sensitive groups from exposure to ambient air" (CAA Sec. 109, 42 USCA 7409).

Emphasis is on "an absence of adverse effects" and "sensitive groups"; implicit is the concept of health effect thresholds where benign physiological changes are replaced by adverse health effects.

In practice, determining the point at which to declare that ambient CO concentrations meet the criteria for acceptable risk is predicated on the approximate data parameters achievable with current technology. While the scientific community continues research into the "physical" effects of each pollutant, EPA has retained the (broad) "health-only" threshold approach to standard setting, which is seriously flawed. EPA's own unique interpretation of scientific evidence, based on arbitrary policy decisions, has resulted in federal court intervention. The health and economic considerations inherent in air quality standards have become so politically significant that the entire process of standard setting is largely controlled by congressional, not administrative, action. This has led to pollutant control standards not based primarily on scientific fact.

Establishing standards

In the search for a health effects threshold, a determination must be made of the level at which pollutants cease to be an acceptable risk and become a recognizable threat to human health. Melnick (4) posited four factors to be weighed in defining an acceptable risk level:
- What criteria establish the standard for each pollutant?

- What constitutes an adverse health effect?
- What defines the sensitive group?
- What other factors contribute to the effect of the pollutant in question?

These questions define acceptable risk and also identify current EPA attitudes toward enforcement of CO emission standards.

Ascertainable standards. The linkage of CO exposure and health effects and risk is ascertainable. Pathophysiological effects of CO exposure have been documented since the late 1800s. Recently research has shown, at a cellular level, the biochemical response generated by healthy tissue exposed to CO (5).

Abnormally high COHb levels affect smokers (approximately one-fourth of all Americans) and an additional 10% of nonsmokers with preexisting health problems. Urban concentrations averaging 30 ppm or more for eight consecutive hours are a matter of public record. Thus, adverse health effects of CO exposure will be a certainty, given the NAAQS of 9 ppm for CO, based on the threshold concept.

Ascertainable CO levels. The Congressional Research Service recently stated that more monitors are needed to provide an accurate picture of air quality, noting that 5400 monitors at half-mile intervals would be needed in an urban area of 30 by 45 miles to obtain an accurate profile.

In most epidemiologic studies of air pollution, exposure has been measured by stationary air pollution monitors put into place for public health and regulatory purposes, not research. Data gathered by these monitors have provided the base for decisions regarding CO control levels.

Ascertainable sensitive groups. The EPA has included within its interpretation of the sensitive population those persons suffering from heart disease and respiratory disorders. There has not been acknowledgment of adverse health effects of *chronic exposure* to low concentrations of CO.

In a national survey of 18 metropolitan and rural areas, COHb saturations greater than 1.5% were recorded in 45% of nonsmoking blood donors tested, indicating that exposure to CO in excess of that permitted by the quality standards of the Clean Air Act was widespread and occurring regularly (1). The most sensitive population is males over 45. Approximately 25% of this high-risk group have preexisting coronary disease that may be severe and are unaware of it (6).

The prestigious Health Effects Institute, in its recent work, *Air Pollution, the Automobile, and Public Health,* reports that neither the statute nor the legislative history adequately describes the concept of susceptible populations. The courts and policy makers are left to their own devices in interpreting the term (5).

Conclusion

As noted, ambient CO levels are intended to be regulated to the point "sufficient to protect the health of. . . persons in sensitive groups from exposure to ambient air." If, however, ambient CO is raising the COHb concentration of the average person by 1%, then EPA's current CO emission standards are inadequate, in terms of both "ample margin of safety" and source emission control.

Failure to take effective action now will result in the severe impairment of individuals who are compromised by pathological conditions limiting their ability to live safely amidst rising CO levels. The NAAQS should be revised to ensure that CO emission source levels reflect a realistic margin of safety for individuals whose preexisting health conditions place them within the defined sensitive population.

References

(1) Stewart, R. *Ann. Rev. of Pharmacol.;* Annual Reviews: Palo Alto, CA, 1975.
(2) Dubois, A. et al. *Effects of Chronic Exposure to Low Levels of CO on Human Health, Behavior, and Performance;* National Academy of Sciences: Washington, DC, 1969.
(3) Knox, C. *Science News* **1988,** *134,* 327.
(4) Melnick, R. *Regulation and the Courts: The Case of the Clean Air Act;* The Brookings Institution: Washington, DC, 1983.
(5) Watson, A. et al. *Air Pollution, the Automobile and Public Health;* National Academy Press: Washington, DC, 1988.
(6) Calabrese, E. *Pollutants and High-Risk Groups;* Wiley: New York, 1978.

Wendell P. Greek is a graduate student in wildlife biology in the Forestry Department at Michigan Technological University. He received a B.S. degree in liberal arts and interdisciplinary studies at MTU. His research interests are biological indicators and Arctic ecology.

Vernon P. Dorweiler is associate professor of management and law at Michigan Technological University, Houghton, MI. He holds graduate degrees in engineering business and law, from Iowa State University, University of Chicago, and De Paul University. His interests include management of integrated business functions, regulation of business, and environmental law.

ENVIRONMENTAL INDEX

Time it takes the world to use the amount of fossil fuel produced in one million years: 1 year

Number of major world geocenters that consume 90% of the world's energy: 12

Number of accidental releases of acutely toxic substances to the air
in the United States between 1980 and 1985: more than 6,900

Total number of sites on EPA's National Priorities List (a list of hazardous waste sites potentially
posing the greatest risk to health and the environment) as of October 25: 1,219

Percentage of world oil production OPEC controlled in 1980: 59

Percentage of world oil production OPEC now controls: 47

Number of dollars American industry spends annually to meet environmental requirements: $35 billion

Number of states that have no responsibility under Title III of the Superfund Amendments and
Reauthorization Act, the community right-to-know provisions: 26

Number of states having specific legislation that requires an air toxics program: 6

Number of states relying on general air pollution control legislation
as underlying authority to control air toxics: 44

Number of news, magazine, and wire service stories
on environmental issues during the past five years: 80,980

Most frequently covered topic in these news stories: pesticides (23,261 stories)

Second most frequently covered topic in these stories: toxic waste

Third most frequently covered topic in these stories: acid rain

Fourth most frequently covered topic in these stories: nuclear waste

Fifth most frequent topic: oil spills

Sixth most frequent topic: ozone layer

Sources are listed on p. 37.

Technology: Villain turned hero

Alvin L. Alm

When concern about the environment was awakened in the early 1970s, technology was considered a rapacious force that needed taming. Nuclear power, supersonic transport, and new chemical products were all thought to be inimical to a good quality environment. Some environmentalists yearned for a more pastoral, simple life style.

Attitudes have changed over the past 20 years. Most environmentalists do not expect major life style changes from others, nor are they willing to make major sacrifices themselves. Most environmentally conscious citizens are willing to take wastes to recycling centers and to eschew certain products, but they still prize their mobility, their personal computers, and their compact disc players. These personal preferences are not hypocritical. They are emblematic of an understanding of the compatibility between environmental improvement, technology, and rising standards of living.

Technological change is the key to achieving, simultaneously, an improvement in worldwide standards of living and a reduction of environmental threats. There is certainly no serious movement in the industrialized democracies to eliminate economic growth, and the developing countries look to new technology to pull them out of poverty and backwardness. The desire for a better economic future exists worldwide. Increasingly, however, both developed and developing countries realize that a healthy environment is necessary to achieve politically sustainable growth and public health. Because substantial population growth and economic growth are inevitable (even with strong efforts to reduce the rate of the former), new technologies must reduce the generation of residuals in developed countries and minimize their increase in developing countries. The development and deployment of less polluting technology is the single most important determinant of the future environmental health of the planet.

Two categories of technological development are particularly critical: energy and manufacturing. Energy extraction, transportation, production, and use represent major sources of environmental contamination, whether from strip mining, oil spills, utility emissions, or automobile exhaust. Environmental contaminants from manufacturing are also major sources of air, water, and land pollution. In both cases, environmental damage can be substantially limited by new technology.

Ironically, there is no end-use demand for energy as a commodity. The end-use demand is for energy services such as heat, light, and mechanical power. These services can be provided with substantially less primary energy by substituting other technology for BTUs. More efficient buildings, lighting fixtures, automobiles, and appliances are all technically possible; in most cases, they are also less costly.

Besides being more efficient, less-polluting energy technologies such as solar and renewable technologies are generally less damaging to the environment.

Pollution prevention has become a new rallying cry for the environmental movement. Although in some cases pollution will be prevented by life style changes and abstention, in most cases new technology will provide solutions. Most of the best examples of waste minimization result from process changes or substitution—both highly technological processes.

Technological change has already benefited the environment. New, more energy-efficient technologies have allowed the U.S. economy to grow by 40% over the past 15 years with roughly the same level of energy use. New manufacturing processes use less hazardous substances as inputs and generate fewer residuals.

Despite these gains, the potential for technology innovation to support environmental goals is far from realized. Cheap energy prices fail to account for environmental damages and security concerns. Our end-of-pipe environmental regulatory system fails to optimize waste minimization potential and in some cases inhibits pollution prevention efforts.

Public policy influences the pace of technological innovation significantly. Government research and development programs affect the variety of technological options available. Tax policy affects the deployment of technology and the relative substitution of capital for other inputs. Certain regulatory programs freeze technological progress. Utility rate regulation favors the production of energy rather than the improvement of end-use efficiency.

The U.S. government needs to emphasize technological innovation as a critical component of its environmental protection activities. Terms such as "pollution prevention" or "sustainable development" have little meaning unless we can more effectively adapt technology to needs. Serious attention to technology innovation could remove roadblocks to improving technology beyond "best demonstrated." Research, development, and technology transfer activities could speed technological innovation. And, most important, different tax policies and use of other market incentives could result in substantial improvements in energy efficiency and reduction of residuals.

Alvin L. Alm is a director and senior vice-president for energy and the environment for Science Applications International, Corp., a supplier of high-technology products and services related to the environment, energy, health, and national security.

0013-936X/89/0924-0035$02.50/0 © 1989 American Chemical Society

Environ. Sci. Technol., Vol. 24, No. 1, 1990 **35**

ES&T
BOOKS

Global Warming: Are We Entering The Greenhouse Century? Stephen H. Schneider. Sierra Club Books, San Francisco. 1989. xii + 317 pages. $18.95. hard back.

Reviewed by Stanton S. Miller, Managing Editor of Environmental Science & Technology.

If you read only one book on global warming, this one is heartily endorsed. The author received his Ph.D. in plasma physics and chose to study climate change when the field was first forming in 1971. He has reported on these developments at scientific meetings and political hearings since then. He presents an overview of 60 million years of global climate history in this book and explains the mechanisms that regulate climate.

In 1971 he went to a meeting in Stockholm to help report on a conference on the new field of inadvertent climate modification. There he met Mikhail Budyko, then director of the Main Geophysical Observatory in Leningrad. Schneider writes, "He was the first person to point out to me the importance of social assumptions in studying the greenhouse effect, referring to the need to forecast future fossil-energy consumption as 'people problems'." Schneider didn't meet Budyko again until September 1987 when the field was heating up.

The fact that increases in atmospheric carbon dioxide are correlated with global temperature increase is acknowledged. Budyko's 1987 book pointed this out. Schneider says that computer models are saying the same thing. In his book, Schneider presents the scientific discussion and overview, along with 21 pages of references. He continues, "As Budyko said in 1971, this (climate change) is a question of social science, not natural science. It depends on projection of human population, the per capita consumption of fossil fuel, deforestation rates, forestation activities, and perhaps, even countermeasures to deal with extra carbon dioxide in the air (for instance, planting more trees)."

Schneider writes, "We know that specific scenarios of climate change are plausible, but at present it is very difficult to assign a probability to any of them." In 1987 *global warming* (the greenhouse effect) was not a household word. But with the hot, dry summer of 1988, "nature did more for the notoriety of global warming in 15 weeks than any of us or the sympathetic journalists and politicians were able to do in the previous 15 years."

Schneider wrote this book about climate change rather "than expect the media to carry my message about this complex, uncertainty-riddled topic to the public." Schneider, a climatologist with the National Center for Atmospheric Research, answers his question posed in the subtitle of the book with Yes: "It should be clear by now that I believe we've been in [the greenhouse century] for a while already," but admits that "it will take a decade or so more of record heat, forest fires, intense hurricanes or droughts to convince the substantial number of skeptics that still abound."

Calculating and Reporting Toxic Chemical Releases. Paul N. Cheremisinoff. Scitech Publishers, Inc., P.O. Box 987, Matawan, NJ 07747. 1989. 587 pages. $59.95, paper.

This book examines the basic principles involved in calculating and reporting toxic chemical releases and presents a practical, comprehensive review of computational methods. It discusses Section 313 of the Superfund amendments of 1986 (right-to-know). In addition, the book explains how to estimate releases to the environment and presents pertinent case studies. Appendices contain such information as EPA information sources, instructions for reporting Form R, and a table of uncontrolled fugitive emission sources at synthetic organic manufacturing plants.

State Environmental Law. Kenneth A. Manaster and Daniel P. Selmi. Clark Boardman Company, Ltd., 435 Hudson St., New York, NY 10014. 1989. 810 pages. $125.

State Environmental Law is the first unified work that surveys environmental laws in all 50 states. The book examines common law and state environmental legislation, impact assessment, and litigation. Appendix materials contain state-by-state reference guides to applicable statutes and environmental agencies.

Aerosol Sampling: Science and Practice. James H. Vincent. John Wiley & Sons Inc., 605 Third Ave., New York, NY 10016. 1989. xxi + 390 pages. $180, cloth.

Aerosol Sampling begins by defining and explaining aerosols and particle size. The book then examines fluid and aerosol mechanics, samplers, the nature of air flow near samplers, aspiration efficiencies, methods for sampling, and problems in sampling and samplers.

ENVIRONMENTAL INDEX SOURCE BOX

(1, 2) Goldmark, P., Rockefeller Foundation president, speech at the Town Hall of California, Sept. 26, 1989. *(3)* Baram, M. *Corporate Risk Management;* Report to the Commission of the European Communities Joint Research Center Ispra.; University of Boston, Boston, MA, 1987, p. 82. *(4)* EPA Press Release, R-208, Oct. 25, 1989. *(5, 6)* Moore, W. H., U.S. Deputy Secretary of Energy, speech before the Oil & Money Conference, London, Oct. 20, 1989. *(7)* Moore, W. H., U.S. Deputy Secretary of Energy, speech before the Governing Board and Management Committee of the International Energy Agency, Paris, Oct. 18, 1989. *(8)* *Toxic Air Pollutants: State and Local Regulatory Strategies—1989;* State and Territorial Air Pollution Program Administrators and the Association of Local Air Pollution Control Officials; Washington, DC, Sept. 1989, p. I-6. *(9, 10)* Ibid., pp. 3–5. *(11–17)* Mead Data Central's NEXIS information service, in *Chemecology,* 1989, *18*(8), 6.

ES&T
PRODUCTS

AIR POLLUTION CONTROL

Indoor air cleaner. UltraPure 2000 Indoor Air Cleaners are designed to filter out particles of 0.3 μ diameter with an efficiency of 99.9%. American Filtrona **108**

CFC reclamation. IG-LO/DRAF Field Refrigerant Saver/Model 710 is designed to reclaim and recycle chlorofluorocarbons. CFC refrigerants are drawn into a bag in which they are sealed for shipment to a recycling center. Igloo Products **109**

Acid flue gas cleaning. System is engineered to remove SO_2 and HCl from flue gases from waste incineration and cogeneration plants and coal- and oil-fired boilers. AirPol **110**

Exhaust biological safety cabinet. SterilchemGARD Class II is manufactured to control airborne particulate matter, including microorganisms and potentially harmful chemicals. Baker **111**

HAZARDOUS WASTE

Microbial cleanup. Live bacteria are offered that reduce or neutralize the toxicity of hazardous wastes such as benzene, phenol, toluene, and trichloroethylene. Micro-Bac International **112**

INSTRUMENTATION

Hazardous compound extraction. Model 3740-24-BRE rotary agitator is made to be used in sample extractions for EPA Methods 1310 (toxicity), 1311 (toxic characteristic leaching procedure), and 500 series (pesticide contamination of water). Associated Design and Manufacturing **113**

Flue gas analysis. LANCOM Model 3400 flue gas analyzer is designed to carry out measurements over several hours or days, as well as on-the-spot measurements. Automatic calibration is available. Land Combustion **114**

Need more information about any items? If so, just circle the appropriate numbers on one of the reader service cards bound into this issue and mail in the card. No stamp is necessary.

Hydrogen leak detector. The TG-1500KA hydrogen leak detector uses a patented gas membrane galvanic cell sensor that is designed to detect levels as low as 10 ppm. Range is 0–1990 ppm. Instrument has rechargeable battery that can operate as long as 24 h. CEA Instruments **115**

Food and agricultural analysis. Waters 470 Scanning Fluorescence Detector is used to analyze carbamates (including pesticides) and aflatoxins, as well as vitamins and polycyclic aromatic hydrocarbons. Programmable wavelengths are 200–700 nm. Millipore **116**

DO meter. YSI Model 59 dissolved oxygen (DO) meter is designed to detect DO with accuracies ± 0.03 mg/L, with $\pm 0.2\%$ air saturation. Instrument can be used with a personal computer. YSI **117**

Toxic gas data system. MAI system is designed to supervise eight or more toxic gas sensors, monitor up to 1000 channels, and record the date, time, location, and gas concentration whenever a toxic gas alarm occurs. System works with a personal computer. ENMET **118**

CO monitor. Model 9000 carbon monoxide monitor is intended for use with large industrial boilers and is microprocessor-based. Flue gas CO is continuously monitored by an infrared absorption technique. Land Combustion **119**

Mercury analyzer. Jerome 431 mercury vapor analysis system measures mercury vapor concentrations in the workplace as required by OSHA regulations. Its range is 0–0.999 mg/m^3 mercury. Readouts are digital. Arizona Instrument **120**

Gas chromatograph. Model 8700 gas chromatograph is designed to accomplish selective transfer with columns of different selectivity. Unwanted sections of sample can be foreflushed or backflushed. Perkin-Elmer **121**

H$_2$S$_2$ monitor and alarm. Model ISA-86H$_2$S monitor displays concentrations of 0–50 ppm. Sensor design is explosion-proof and is engineered to provide

high- and low-temperature stability. ENMET **122**

Soil hydrocarbon monitor. MIRAN 1FF infrared spectrometer is designed to quantify petroleum hydrocarbons in soil by gauging the intensity of infrared absorption by a $C-H$ stretch band. Foxboro **123**

Drinking-water analysis method. Method B1011 determines nitrate in water by single column ion chromatography that uses ultraviolet/visible light detection. Company announces that method has been approved by EPA. Millipore **124**

Elemental analyzer. Carlo Erba Model 1108 elemental analyzer is designed to determine carbon, hydrogen, nitrogen, and sulfur in less than 12 min. It can test samples of 0.1–100 mg, depending on type of sample. Fisons Instruments **125**
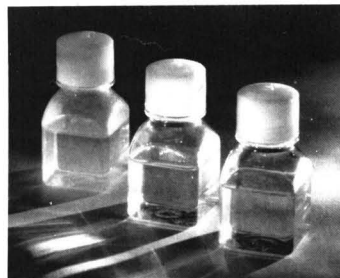
Test kit for coliform bacteria

Coliform testing. Colilert test kit is designed to determine *Escherichia coli* in less than 24 h, with a single inoculation, and with less than 2 min hands-on time. Kit was developed at Yale University with support from the American Water Works Association Research Foundation. Access Analytical Systems **129**

Benchtop GC/MS. Saturn gas chromatograph/mass spectrometer is a benchtop system designed to scan spectra to levels as low as picograms. Sys-

tem is controlled by personal computer. Varian **126**

HPLC replacement parts. Replacement parts for high-performance liquid chromatographs of several makes such as Beckman, Waters/Millipore, Gilson, Shimadzu, and Kratos are available. Able Technologies **127**

Environmental analyzer. DR/2000 microprocessor-controlled spectrophotometer is used for water quality, water conditioning, aquaculture water, and soils analysis. It is designed to eliminate the need for manual calibration curve construction. Hach **128**

PUBLICATIONS

Wastewater Treatment (*ES&T* article series) reports on the processes for the treatment of wastewater, including removing particles and dissolved organic and inorganic contaminants, as well as aerobic treatment. ACS **130**

Computer Usage in Engineering (*ES&T* article series) discusses trends and applications of computers, including artificial intelligence and the impact of computer use in environmental engineering. The report tells how personal computers will change the practice of environmental engineering in the future. ACS **131**

Cancer Risk Assessment (*ES&T* article series) explores scientific topics of public concern regarding regulation of chemicals in the environment. Series reports on managing risk and communicating the results of risk assessment; also covered are exposure assessment and realism about chemical carcinogenesis. ACS **132**

SERVICES

In situ bioremediation. Company offers line of services and group of experts to consult on in situ bioremediation of contaminated sites. Services and technology aim at preventing wastes from migrating. Groundwater Technology **133**

PCB transformer retrofilling. Company drains and replaces polychlorinated biphenyls in transformers and guarantees that the transformers will not fail for 10 years. UNISON **134**

SOFTWARE

Risk assessment data base. The EPA risk assessment data base IRIS (Integrated Risk Information System), which currently covers 375 substances, has become available on The CIS. Chemical Information Systems **135**

UNIX-based analysis software. LAB/UX laboratory information manage-
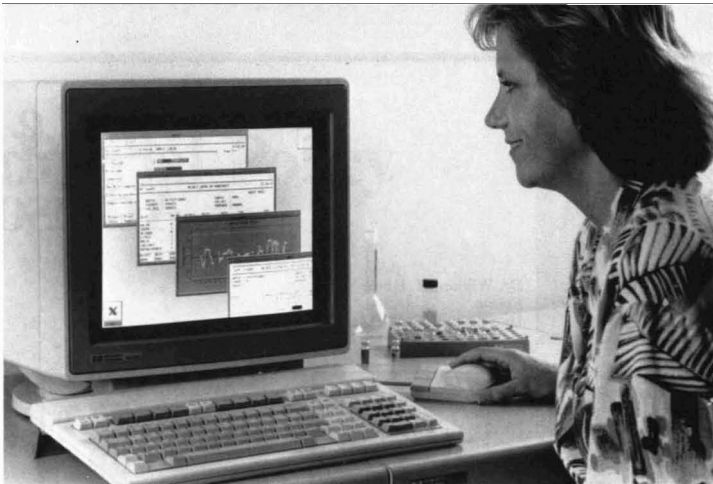
UNIX-based laboratory information management software

ment system is designed to increase analytical productivity and accountability and is supported by AT&T UNIX software. Data can be used with networks and electronically mailed. Hewlett-Packard **136**

Hazardous material data. The IBM mainframe-based system HAZMAT will allow industrial, utility, and medical firms to compile and maintain hazardous material data in keeping with EPA and OSHA regulations. EPI Consulting **137**

Data on 1-2-3 and Symphony. Measure 2.2 software and Lab-PC computer plug-in card allow acquisition and storage of analytical data with *Lotus 1-2-3* and *Symphony*. Applications include engine monitoring and automated titration. National Instruments **138**

Groundwater data bases. Data bases on groundwater services contractors, hazardous waste, Superfund, and sampling device selection now are available. National Ground Water Information Center **139**

AA analysis software. DP1000 Version 4.00 is IBM-compatible software that processes data from flame and graphite atomic absorption (AA) analysis. Results can be displayed in ASCII, a spreadsheet, or printed copy. Labtronics **140**

WATER TREATMENT

Biodegradation. Groundwater contaminated with petroleum hydrocarbons up to 3000 ppb is treated aerobically; effluent contaminants can be reduced to 1–2 ppb. Hydro Group **141**

Sodium percarbonate. Company spokespersons say that sodium percarbonate offers a safe treatment alternative for dechlorination, oil and gas

treatment, and treating ponds and lagoons. Interox America **142**

VOC removal. Air stripping is an efficient means of removing volatile organic contaminants, according to company. Dexter Water Management Systems **143**

Membrane process. Membrane process developed in Israel is designed to reduce impurities and organic wastes in water "to barest minimum" and reduce the need to transport hazardous materials to disposal sites. Membrane Products Kiryat Weizmann **144**

Sludge dewatering. Passavant plate and frame filter press is designed to dewater sludges and slurries and cut disposal costs. Zimpro Passavant **145**

Dewatering. Applications of filter presses include sludge and hazardous-waste dewatering, clarification, and mining and reclamation of precious metals. JWI **146**

Oxidation technologies. Company is marketing a whole line of oxidation technologies for wastewater treatment, including chlorine dioxide, hydrogen peroxide, and potassium permanganate. Carus Chemical **147**

Wastewater treatment improvement. West German product "dosfolat," based on folic acid, is reported to improve wastewater treatment operating parameters. Bioprime **148**

Solar-powered pump. French THR solar-powered submersible pump can provide water needs for a village or small town, according to company. Motor is of brushless design. TOTAL ÉNERGIE **149**

Groundwater decontamination. Process of air stripping and countercurrent flow removes volatile organic compounds from groundwater, according to company. Crane **150**

ES&T's 1990 Advisory Board
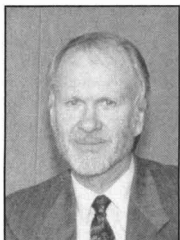
Dr. William H. Glaze
Editor
University of
North Carolina
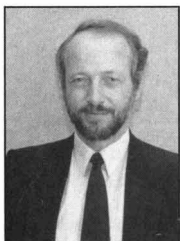
Dr. Walter Giger
Associate Editor
(Europe)
EAWAG
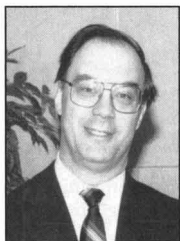
Dr. Ronald A. Hites
Associate Editor
Indiana University
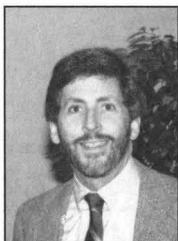
Dr. John H. Seinfeld
Associate Editor (air)
California Institute of
Technology
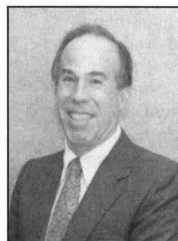
Dr. Philip C. Singer
Associate Editor (water)
University of
North Carolina
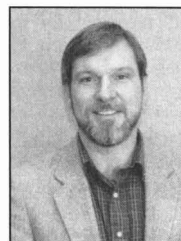
Dr. Joseph Suflita
Associate Editor
University of
Oklahoma

William H. Glaze, Editor, has announced the appointment of two new members to the *ES&T* advisory board. **Joseph M. Norbeck** is manager of the chemistry department research staff at the Scientific Research Laboratory of Ford Motor Company. He oversees research in experimental atmospheric chemistry and modeling, and health effects of vehicle emissions. **Jerald L. Schnoor** is a professor of civil and environmental engineering at the University of Iowa. His research concerns water quality modeling and aquatic chemistry, especially the effects of acid deposition, ground-water toxics and pesticides, and global climatic change.

Board members serve three-year terms. The last year of each member's term is noted in parentheses.

In addition, Dr. Glaze has expanded the roster of Associate Editors from two to five. The new Associate Editors are **Walter Giger** of the Swiss Federal Institute for Water Resources and Water Pollution Control (EAWAG), **Ronald A. Hites** of the School of Public and Environmental Affairs, Indiana University, and **Joseph Suflita** of the Department of Botany and Microbiology, University of Oklahoma.
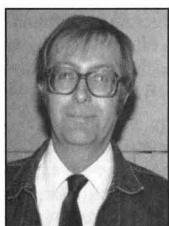
Dr. Roger Atkinson
University of
California, Riverside
(1990)

Dr. Joan M. Daisey
Lawrence Berkeley
Laboratory
(1991)

Dr. Fritz H. Frimmel
Technical University
of Munich
(1992)
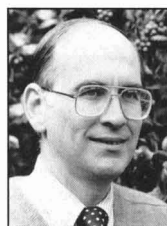
Dr. George Helz
University of
Maryland
(1992)

Dr. Ralph Mitchell
Harvard University
(1991)
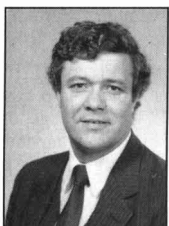
Dr. Joseph M. Norbeck
Ford Motor Company
(1992)
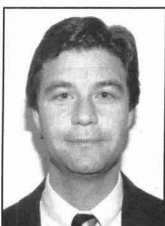
Dr. Jerald L. Schnoor
University of Iowa
(1992)
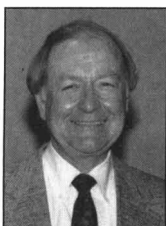
Dr. Walter J. Weber, Jr.
University of
Michigan
(1991)

**Dr. Alexander J. B.
Zehnder**
Agricultural University
of Wageningen
(1991)
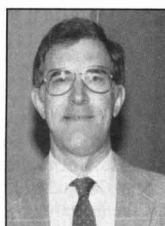
Dr. Richard G. Zepp
EPA
(1991)

Editorial Policy

Environmental Science & Technology reports on aspects of the environment and its control by scientific, engineering, and political means. Contributed materials may appear as feature articles, critical reviews, current research papers, research communications, and correspondence. Central to the evaluation of all contributions is a commitment to provide the readers of *ES&T* with scientific information and critical judgments of the highest quality. For the convenience of authors, the specific nature of each type of contribution is outlined below.

Feature articles. A manuscript submitted for publication as a feature article should present useful discussion and opinion on important research directions in environmental science; developing technology; environmental processes; and social, political, or economic aspects of environmental issues. Each manuscript undergoes review by qualified peers as well as by the editors for the purpose of balance and elimination of inappropriate bias. Review criteria include significance of the scientific issue or process described, quality and succinctness of the text, and identification of potential research needs. Strict requirements for documentation of results, completeness of data, and originality, such as those applicable to research manuscripts, are not included in the review criteria for feature articles. Four copies are required.

Views. A manuscript submitted for publication as a view should be objective, not an advertisement for a product or method, and should comment on a timely event or development. Views are *not* news items, but insightful commentaries on timely environmental topics. The manuscript should be about 1000 words long. The manuscript will be reviewed by members of the *ES&T* advisory board or reviewers to judge the suitability of its publication in *ES&T*.

Critical reviews. Critical reviews are thoroughly documented, peer-reviewed assessments of selected areas of the environmental science research literature for the purpose of identifying critical research needs. Criteria for acceptability include current importance of the field under review, thoroughness of the literature coverage, clarity of text, and adequacy of research need identification.

Current research papers. The research pages of *ES&T* are devoted to the publication of critically reviewed papers concerned with the fields of water, air, and waste chemistry, and with other scientific and technical fields that are relevant to the understanding and management of the water, air, and land environments. Contributed research papers, in general, describe complete and fully interpreted results of original research.

Environmental Science & Technology seeks to publish papers of an original and significant nature. Originality should be evidenced by new experimental data, new interpretations of existing data, or new theoretical analysis of environmental phenomena. Significance will be interpreted with respect to the breadth of impact of the reported findings. Manuscripts reporting data of a routine nature that do not offer heretofore unavailable important information or do not substantially augment already available data will be declined publication in *ES&T*. The scope of the reported data in ambient monitoring studies should be such that broad conclusions applicable to more than the particular local scale are possible.

All research articles emphasizing analytical methodology for air or water analysis must include substantial application to environmental samples. *ES&T* faces some overlap with other journals in this area, and articles that do not contain, in the editors' judgment, a significant emphasis on environmental analysis will be returned to the authors for submission elsewhere.

Manuscripts should be prepared with strict attention to brevity. The vast majority of articles are expected to be fewer than four published pages. Processing time will be shortened if the editors do not have to return manuscripts to be condensed.

Research Communications. Research Communications are short research reports describing results of unusual significance. The subject of the communication should be of such importance and the report of such quality that rapid publication is warranted. Communications are expected to be preliminary reports that will be followed by a more detailed publication. The communication should be no longer than two printed pages including figures, tables, and references. Every effort should be made to keep the length substantially below this maximum, such as by avoiding a lengthy introductory section. The Experimental Section should be as brief as possible, giving only essential details. An abstract should be sent with the communication for publication in *Chemical Abstracts* but it will not be published in *ES&T*. See Current Research Author's Guide for directions for preparation of Abstract. Communications will be reviewed expeditiously and published as rapidly as possible. To ensure prompt attention to their manuscript, authors should consider sending Communications by FAX to the ACS manuscript office (FAX# 202-872-6325) or sending it by express courier. A FAX number for return communications should be included, if available. If minor revisions are required, manuscripts will be returned to authors as expeditiously as possible and should be returned to ACS headquarters within two weeks. The need for major revision is just cause for rejection of the Communication.

Correspondence is a significant comment on work published in the research section of *ES&T*. Comments should be received within six months of date of publication of the original article. The authors of the original article ordinarily will be allowed to reply.

Send manuscripts to: *Environmental Science & Technology*, 1155 16th St., N.W., Washington, DC 20036. Address feature manuscripts to: Managing Editor; research manuscripts to Manager, Manuscript Office. Include a signed copyright transfer form, a copy of which appears in the January issue.

Peer review in *ES&T*

Characteristics of *ES&T*

ES&T stands out among American Chemical Society journals in that it combines both a magazine and a journal. Only one other ACS publication contains this combination—our sister publication, ANALYTICAL CHEMISTRY. Because of the hybrid nature of our publication, it serves a large and diverse audience.

Central to the evaluation of all contributions to *ES&T* is a commitment to provide our readers with scientific information of the highest quality. The publication seeks the most significant, original, and broadly applicable types of articles for its current research section. A vast number of persons review original manuscript contributions and indicate in their evaluations the originality and scientific validity of the work, as well as the appropriateness of the material for our publication.

The Editor and Associate Editors, who are located at the University of North Carolina, the California Institute of Technology, EAWAG, and Indiana University are fully responsible for all material published in *ES&T*. This policy is a general one applicable to all editors of American Chemical Society publications. The 10 members of the Advisory Board are chosen by the editor to provide input to *ES&T*'s operation. The members are chosen to represent various constituent groups in the research and reader communities and serve three-year terms. Although the editors seek advice and help from individuals in the scientific community and from advisory groups, it is ultimately the editors' responsibility to provide editorial direction, set editorial policies, and make individual publication decisions.

The Washington editorial staff handling the current research section is responsible for the day-to-day operation of the peer review system. All editorial staff members have chemistry or related science degrees.

General guidelines and overall editorial policies set by the editor form the basis for evaluating reviewers' comments on research articles submitted for the current research section.

A look at peer review

Each manuscript submitted to the current research section is reviewed by a staff editor and, on the basis of its content, assigned to one of the associate editors or to the editor (hereafter called technical editor). The subject matter of the manuscript determines which editor will receive the file. The technical editor is responsible for the manuscript—including choosing reviewers; evaluating the content of the paper; taking into account the comments of reviewers; and communicating ultimate acceptance or rejection to the corresponding author. The staff editor in Washington assists in this process by screening papers initially to determine whether papers may fall outside of *ES&T*'s scope, by monitoring the progress of the review process, and by carrying out a final check of accepted manuscripts for appropriate format and style.

Beginning in January 1990, reviewers are picked by the technical editors. Three reviewers are carefully selected for each paper, based on the subject matter of the paper, the experts available in a given area, and the editorial staff member's knowledge of the habits of proposed reviewers. Thus, known slow reviewers are avoided when possible. Potential reviewers for each paper are identified through various means, one of which involves a computer search of subjects that reviewers have indicated are their areas of expertise.

Reviewers are normally asked to respond within three weeks, and if they are late, reminders are sent. Late review notifications are generated and dispatched as mailgrams on a weekly basis.

Also beginning in January 1990, reviews will be sent directly to the technical editor to whom the paper has been assigned. If the reviewers do not agree on the disposition of the paper, or if the technical and scientific strengths or shortcomings of the work have not been adequately addressed, an additional reviewer may be selected. The reviews (usually at least two) are used by the technical editor in making the final decision about the disposition of the manuscript. Letters communicating the decision proceed directly from the office of the technical editor to the corresponding author.

If the technical editor has recommended revision of the manuscript, the staff editor goes over the paper carefully in a "pre-edit" check to aid the author in revising the manuscript.

Tips for authors of papers submitted to *ES&T*

- Prepare your paper with the audience of the publication in mind. Papers prepared for other journals are likely to need some revision to make them suitable for *ES&T*.
- Clearly state in the introduction the purpose of the work and put the work in perspective with earlier work in the area. This may appear obvious, but authors often fail to clearly state the purpose and significance of their work.
- Write concisely. The vast majority of articles are expected to be fewer than five published pages. Long manuscripts are looked at much more closely and critically both by reviewers and editors. Do not repeat information or figures or tables that have appeared elsewhere. Use illustrative data rather than complete data where appropriate.
- Suggest names of possible reviewers for your paper. You may also suggest the names of persons whom you do not want to review the paper. The editors try to use at least one reviewer who has been suggested by authors. This cannot be assured, however, since specific reviewers may not be available for reviewing or may already be overloaded.
- Follow the Current research author's guide, published in every January issue.

If your manuscript is rejected

- Read the reviews carefully. If the reviewers have "missed the point," as authors often claim, consider how the presentation can be clarified and improved to make the point clear. If reviewers have not understood, it is unlikely that readers will understand.
- Is the manuscript, after all, more suitable for another journal?
- Is the work sufficiently complete, or do you need to do more work before seeking publication?
- If you feel strongly that the paper has not been judged fairly, then carefully revise the manuscript taking into account the reviewers' criticisms and send the manuscript to the office of the technical editor with a rebuttal letter asking that the manuscript be reconsidered. Provide an itemized list of changes made in the manuscript in response to reviewer comments, as well as objective rebuttals to the criticisms with which you do not agree.

Current research author's guide

This manuscript preparation guide is published to aid authors in writing, and editors and reviewers in expediting the review and publication of research manuscripts in *Environmental Science & Technology*, including full research articles and communications. For a detailed discussion with examples of the major aspects of manuscript preparation, please refer to *The ACS Style Guide* (1986).

Title

Use specific and informative titles. They should be as brief as possible, consistent with the need for defining the subject of the paper. If trade names are used, give generic names in parentheses. Key words in titles assist in effective literature retrieval.

Authorship

List the first name, middle initial, and last name of each author. Omit professional and official titles. Give the complete mailing address where work was performed. If present address of author is different, include the new information in a footnote. In each paper with more than one author, the name of the author to whom inquiries should be addressed carries an asterisk. The explanation appears on the contents page.

Abstracts

An abstract, which will appear at the beginning of each paper, must accompany each manuscript. Authors' abstracts frequently are used directly for *Chemical Abstracts*. Use between 100 and 150 words to give purpose, methods or procedures, significant new results, and conclusions. Write for literature searchers as well as journal readers.

Text

Consult a current issue for general style. Assume your readers to be professionals not necessarily expert in your particular field. Historical summaries are seldom warranted. However, documentation and summary material should be sufficient to establish an adequate background. Divide the article into sections, each with an appropriate heading, but do not oversectionalize. The text should have only enough divisions to make organization effective and comprehensible without destroying the continuity of the text. Keep all information pertinent to a particular section within that section. Avoid repetition. Do not use footnotes; include the information in the text.

Introduction. Discuss relationship of your work to previously published work, but do not repeat. If a recent article has summarized work on the subject, cite the summarizing article without repeating its individual citations.

Experimental. Apparatus: List devices only if of specialized nature. Reagents: List and describe preparation of special reagents only. Procedure: Omit details of procedures that are common knowledge to those in the field. Brief highlights of published procedures may be included, but details must be left to literature cited. Describe pertinent and critical factors involved in reactions so that the method can be reproduced, but avoid excessive description.

Results and discussion. Be complete but concise. Avoid nonpertinent comparisons or contrasts.

Manuscript requirements

Five complete legible copies of the manuscript are required. They should be typed double or triple spaced on 22 × 28 cm paper, with text, tables, and illustrations of a size that can be mailed to reviewers under one cover. Duplicated copies will be accepted only if very clear.

If pertinent references are unpublished, furnish copies of the work or sufficient information to enable reviewers to evaluate the manuscript.

In general, graphs are preferable to tables if precise data are not required. When tables are submitted, however, they should be furnished with appropriate titles and should be numbered consecutively in Roman numeral style in order of reference in the text. Double space with wide margins, and prepare tables in a consistent form, each on a separate 22 × 28 cm sheet.

Submit original drawings (or sharp glossy prints) of graphs, charts, and diagrams prepared on high-quality inking paper. All lines, lettering, and numbering should be sharp and unbroken. If coordinate paper is used, use blue cross-hatch lines because no other color will "screen out."

Typed lettering does not reproduce well: Use black India ink and a lettering set for all letters, numbers, and symbols. On 20 × 25 cm copy, lettering should be at least 0.32 cm high. Lettering on copy of other sizes should be in proportion. Label ordinates and abscissas of graphs along the axes and outside the graph proper. Do not use pressed wax for numbering or lettering.

Photographs should be supplied in glossy print form, as large as possible, but preferably within the frame of 20 × 25 cm. Sharp contrast is essential.

Number all illustrations consecutively using Arabic numerals in the order of reference in the text. Include a typed list of captions and legends for all illustrations on a separate sheet. If drawings are mailed under separate cover, identify by name of author and title of manuscript. Advise editor if drawings or photographs should be returned to the author. Color reproduction is possible provided the author bear all incremental charges. An estimate of these charges will be given upon request. A letter acknowledging the author's willingness to defray the cost of color reproduction should accompany.

Nomenclature

Nomenclature should conform with current American usage. Insofar as possible, authors should use systematic names similar to those used by Chemical Abstracts Service or IUPAC. *Chemical Abstracts* nomenclature rules are contained in Appendix IV of the current *Chemical Abstracts Index Guide*. A list of ring systems, including names and numbering systems, is found in the *Ring Systems Handbook*, American Chemical Society: Columbus, OH, 1988.

Use consistent units of measure (preferably SI).

If nomenclature is specialized, include a "Nomenclature" section at the end of the paper, giving definitions and dimensions for all terms. Write out names of Greek letters and special symbols in margin of manuscript at point of first use. If subscripts and superscripts are necessary, place them accurately. Avoid trivial names. Trade names should be defined at point of first use (registered trade names should begin with a capital letter). Identify typed letters and numbers that could be misinterpreted, for example, one and the letter "l," zero and the letter "O."

Formulas and equations

Chemical formulas should correspond to the style of ACS publications. Chemical equations should be balanced and numbered consecutively along with mathematical equations. The mathematical portions of the paper should be as brief as possible, particularly where standard derivations and techniques are commonly available in standard works.

Safety

Authors are requested to call special attention—both in their manuscripts and in their correspondence with the editors—to safety considerations such as explosive tendencies, precautionary handling procedures, and toxicity.

Acknowledgment

Include essential credits in an "Acknowledgment" section at the end of the text, but hold to an absolute minimum. Give meeting presentation data or other information regarding the work reported (for example, financial support) in a note following Literature Cited.

References

Literature references should be numbered and listed in order of reference in text. They should be listed by author, patentee, or equivalent. In the text, just the number should be used, or the name should be followed by the number. "Anonymous" is not acceptable for authorship. If the author is unknown, list the reference by company, agency, or journal source. Do not list references as "in press" unless they have been formally accepted for publication. Give complete information, using abbreviations for titles of periodicals as in the *Chemical Abstracts Service Source Index, 1907–84*.

For periodical references to be considered complete, they must contain authors' surnames with initials, journal source, year of issue, volume number, and the first and last page numbers of the article. Consult *The ACS Style Guide* for reference style.

Supplementary material

Extensive tables, graphs, spectra, calculations, or other material auxiliary to the printed article will be included in the microfilm edition of the journal. Identify supplementary material as to content, manuscript title, and authors. Three copies of the supplementary material, one in a form suitable for photoreproduction, should accompany the manuscript for consideration by the editor and reviewers. The material should be typed on white paper with black typewriter ribbon or printed on high quality (300 dpi) laser printer. If individual characters for any of the material, computer or otherwise, are broken or disconnected, the material is definitely unacceptable.

Figures and illustrative material should preferably be original high-contrast drawings or good prints of originals. Optimum size is 22×28 cm. Minimum acceptable character size is 1.5 mm. The caption for each figure should appear on the same piece of copy with the figure. Be sure to refer to supplementary material in text where appropriate.

Supplementary material may be obtained in photocopy or microfiche form at nominal cost. Material of more than 20 pages is available in microfiche only. Photocopy or microfiche must be stated clearly in the order. Prepayment is required. See instructions at the end of individual papers.

The supplementary material is abstracted and indexed by Chemical Abstracts Service.

Subscribers to microfilm editions receive, free, the supplementary material in microfiche form from individual papers in any particular issue. For information, contact Microforms Program at the ACS in Washington, DC, or call (202) 872-4554.

Research Communications. Please refer to Editorial Policy for guidelines on research communications.

ENVIRONMENTAL SCIENTISTS/CHEMISTS

The Environmental Assessment and Information Sciences Division of Argonne National Laboratory is involved in a comprehensive effort to support federal agencies in their environmental programs. Efforts include site characterization and RCRA and CERCLA/SARA regulatory compliance activities for a number of DOS and DOD facilities throughout the U.S. Presently there are openings in the Geochemical Analysis Section.

Considerable knowledge and technical skills are required which are relevant to the environmental and chemical aspects of hazardous waste management and to hazardous waste site remedial action techniques. The position requires a M.S. or Ph.D. or equivalent in Environmental Science, Chemistry, Chemical Engineering or some other chemistry related science. At least one year of relevant experience is required which is relevant to hazardous waste site investigations including CERCLA/SARA remedial investigations and feasibility studies and RCRA facility assessments and remedial designs at hazardous waste sites. Some knowledge of waste management laws and regulations and contaminant migration in surface water and groundwater is desirable. The position offers challenges in the assessment of environmental contamination at sites located in geologically diverse areas across the U.S.

If you are interested in cleaning up the environment and have expertise in chemical aspects of waste management we would like to hear from you. We offer an excellent salary commensurate with your background, as well as a comprehensive benefits plan. For prompt consideration, send a detailed resume to: **Nancy L. Griparis, Box J-EID-35576/40053-28, Employment and Placement, ARGONNE NATIONAL LABORATORY, 9700 South Cass Avenue, Argonne, IL 60439.** Argonne is an equal opportunity/affirmative action employer.

ENVIRONMENTAL SCIENTIST

Technology Applications, Inc., an on-site contractor to the USEPA, has an opening for an environmental scientist to provide quality assurance support for a new national environmental monitoring program. The successful candidate will be responsible for development of data quality objectives, development and review of QA program plans and project plans, laboratory performance evaluations, field and laboratory audits, and data quality assessment. MS in environmental science, biology, or chemistry. Prefer prior experience with quality assurance, statistics, PC's. Extensive travel required. Salary commensurate with qualifications. Confidential resume to: **Technology Applications, Inc., c/o USEPA-EMSL, 26 W Martin Luther King Drive, Cincinnati, OH 45268.** AN EQUAL OPPORTUNITY EMPLOYER.

Graduate Studies

M.S. and Ph.D. programs in environmental and water resources engineering offered by the Department of Civil Engineering at the University of Connecticut. Research areas: surface water quality and modeling; groundwater and subsurface contaminant transport and remediation; physicochemical water and wastewater treatment processes; environmental chemistry; air quality modeling and control strategy analysis. Research and teaching assistantships available for fall 1990. For more information, contact **Dr. Jana Milford, Environmental Research Institute, U-210, University of Connecticut, Storrs, CT, 06269, (203) 486-4015.**

CLASSIFIED SECTION

RESEARCH ASSISTANTSHIPS

Utah Water Research Laboratory, Utah State University, offers research assistantships for outstanding students with backgrounds in Engineering, as well as in the Mathematical, Physical, Biological, and Social Sciences, seeking graduate degrees in Civil and Environmental Engineering. Assistantships will be awarded in the following areas:

Bioengineering and microbiology
Drought and climate change
Economic and social aspects of water resources planning
Groundwater management and protection
Hazardous wastes
Hydraulic transients, hydraulic structures, and cavitation
Hydrology of hillslopes, mountainous terrain, and landslides
Natural and environmental or hydraulic systems modeling
Remote sensing • Risk assessment • River salinity
Soil-water-waste chemistry/physics
Spatially distributed hydrology
Systems optimization • Water and waste treatment

Assistantships are awarded on a competitive basis. Applicants should send a letter of interest, transcripts, and resume to Head, Department of Civil and Environmental Engineering, Utah State University, Logan, UT 84322-4110, Telephone (801) 750-2932. Initial awards for each year will be made in March. In keeping with AFFIRMATIVE ACTION/EQUAL OPPORTUNITY guidelines, minorities, the physically disadvantaged and women are particularly encouraged to apply.

Statements of qualifications are requested from firms capable of providing the California State Coastal Conservancy with hazardous waste assessments of wetland, agricultural, and public access sites. Contact Lisa Ames at (415) 464-1015, 1330 Broadway, Suite 1100, Oakland, CA 94612. Bid closing date is January 12, 1990.

INDUSTRIAL HYGIENE tenure track faculty position available beginning Fall, 1990, at Assistant Professor level in undergraduate Environmental Health Program. Position involves teaching and research. Ph.D. in Industrial Hygiene or closely related discipline required (individuals in final stages of degree completion considered). Application review will begin January 2, 1990. Send vita, three letters of reference, and statement of interest including salary requirements to **Dr. Gary Silverman, 102 Health Center, Bowling Green State University, Bowling Green, OH 43403. EOE**

GRADUATE STUDY in ENVIRONMENTAL SCIENCE AND ENGINEERING at the Oregon Graduate Center. Highly qualified, strongly motivated students sought for exciting research programs in transport and fate of organic and inorganic contaminants, atmospheric chemistry and physics, aquifer remediation, microbial ecology and physiology, biodegradation, biogeochemistry, analytical environmental chemistry, numerical modeling, estuarine and coastal studies, elemental cycling in terrestrial ecosystems. Intensive research experience, state-of-the-art instrumentation, maximal student-faculty interaction. Research assistantships with tuition remission available to qualified Ph.D. applicants. Write: **Carl D. Palmer, Department of Environmental Science and Engineering, 19600 N.W. von Neumann Dr., Beaverton, OR 97006, (503) 690-1196.** (Closing date 4/1/90). Affirmative Action/Equal Opportunity Employer.

Postdoctoral Fellowship
Coupled Microbial and Transport Processes in the Subsurface

Lawrence Livermore National Laboratory, one of the nation's leading research and development organizations, has an immediate opportunity for a two-year Postdoctoral Fellowship in our Earth Sciences Department.

The successful applicant will investigate the interaction of microbial processes, fluid flow and chemical transport in subsurface hazardous waste remediation activities.

Requirements include experience in quantitative analysis of subsurface microbial processes; interaction with staff members experienced in modeling subsurface flow and transport in reactive porous and fractured media is encouraged. PhD required.

LLNL's Earth Sciences Department offers a dynamic environment with easy access to both state-of-the-art computational facilities and experimental resources. The Department encourages integration of theory, computations, experiments and field work and is characterized by a strong tradition of multidisciplinary collaboration.

LLNL offers a competitive salary and excellent benefits. For immediate consideration forward your resume to: **Phil Harding, Professional Staffing, Lawrence Livermore National Laboratory, P.O. Box 5510, L-725, Dept. KEV11003C, Livermore, CA 94550.** U.S. citizenship required. Equal Opportunity Employer.

University of California

Lawrence Livermore National Laboratory

HEALTH, SAFETY & ENVIRONMENTAL PROFESSIONALS

Los Alamos National Laboratory, an international leader in technological and scientific research and development, has challenging positions for Health, Safety and Environmental professionals. As a leading R&D institution, we provide a challenging work environment and an attractive salary/benefits package. Los Alamos, a community surrounded by scenic mountain ranges, is close to the artistic and cultural centers of Santa Fe and Taos.

Professional and technician positions are available for entry and experienced personnel in the following discipline areas:

Health Physics
Operational health physics, radiation monitoring, instrumentation and calibration, radiation dosimetry and measurements, accelerator health physics, ALARA engineering, plutonium health physics, and accident/safety analysis.

Clinical Psychology
Demonstrated experience in field of substance abuse counseling and education. Several years postdoctoral experience in setting requirements for independent use of diagnostic and therapeutic techniques with adults, including neurological screening.

Risk/Safety Analysis
Application of risk analysis techniques to a wide range of new and existing operations and facilities; preparation and review of safety analysis reports; development of new analysis tools and techniques; and development of risk assessment policy and guidance.

Industrial Hygiene
Operational industrial hygiene with experience in recognition, evaluation and control of health hazards; experience in working with engineering documents to identify potential health, safety, environmental hazards; workplace monitoring for a wide variety of health hazards; present training to operational organizations; and accident/safety analysis.

Waste Management
Chemical and low-level radioactive waste management; waste minimization and transportation requirements; chemical process design; chemical treating and handling; radioactive and nonradioactive chemical and PCB waste management; development and implementation of technical and administrative programs that comply with federal regulations; chemical process design; project management; incinerator operation; and radioactive and nonradioactive waste management.

Environmental Sciences
Environmental regulations; assessment and interpretation of environmental issues; assessment of environmental impacts; environmental toxicology assessments; translating regulatory mandates in compliance efforts; wastewater management and regulations pertaining to wastewater and toxic substance control; broad hazardous waste programs background; knowledge of RCRA regulations and requirements; accidents/safety analysis.

Criticality Safety
Experience in nuclear criticality safety desirable; knowledge of neutron transport theory and calculations and commonly used computer codes such as KENO and ONETRAN/ANISN; accident/safety analysis.

Environmental, Safety & Health Appraisals
Experienced environmental scientists, waste management scientists, health physicists, industrial hygienists, fire protection engineers, quality assurance specialists, maintenance specialists and safety engineers with extensive knowledge of ES&H regulations are needed as members of ES&H appraisal teams. Teams evaluate ES&H programs, identify ES&H management and noncompliance issues, recommend program improvements, and evaluate corrective actions.

All staff member positions require a Bachelor's, Master's or PhD in appropriate field of interest or the equivalent combination of education and professional-level experience. Technician positions require college-level courses or the equivalent combination of education and experience.

To formally apply for the above areas, you must reference Job Number **G0002** on your resume. Please send resume to Leona Thorpe (MS P280), Personnel Services Division **G0002-EX,** Los Alamos National Laboratory, Los Alamos, NM 87545.

Affirmative Action/Equal Opportunity Employer. Must be able to obtain a Department of Energy Security Clearance.

University of California

Los Alamos

CLASSIFIED SECTION

ES&T   JANUARY, 1990   VALID THROUGH JULY 1990

Please circle appropriate numbers to receive additional information

READER SERVICE

1	2	3	4	5	6	7	8	9	10	11	12	13	14	15
16	17	18	19	20	21	22	23	24	25	26	27	28	29	30
31	32	33	34	35	36	37	38	39	40	41	42	43	44	45
46	47	48	49	50	51	52	53	54	55	56	57	58	59	60
61	62	63	64	65	66	67	68	69	70	71	72	73	74	75
76	77	78	79	80	81	82	83	84	85	86	87	88	89	90
91	92	93	94	95	96	97	98	99	100	101	102	103	104	105
106	107	108	109	110	111	112	113	114	115	116	117	118	119	120
121	122	123	124	125	126	127	128	129	130	131	132	133	134	135
136	137	138	139	140	141	142	143	144	145	146	147	148	149	150

Principal product to which my work relates:

- [ ] A. Oil/Gas/Petroleum
- [ ] B. Plastics/Resins
- [ ] C. Rubber
- [ ] D. Drugs/Cosmetics
- [ ] E. Food/Beverages
- [ ] F. Textile/Fiber
- [ ] G. Pulp/Paper/Wood
- [ ] H. Soaps/Cleaners
- [ ] I. Paint/Coating/Ink
- [ ] J. Agrichemicals
- [ ] K. Stone/Glass/Cement
- [ ] L. Metals/Mining
- [ ] M. Machinery
- [ ] N. Auto/Aircraft
- [ ] O. Instrument/Controls
- [ ] P. Inorganic Chemicals
- [ ] Q. Organic Chemicals
- [ ] R. Other Manufacturing
- [ ] S. Design/Construction
- [ ] T. Utilities
- [ ] U. Consulting Services
- [ ] V. Federal Government
- [ ] W. State Government
- [ ] X. Municipal Government
- [ ] Y. Education

NAME: _____

POSITION: _____

ORGANIZATION: _____

STREET: _____

CITY: _____

STATE: _____ ZIP: _____

TELEPHONE: (___ ___ ___) - ___ ___ ___ - ___ ___ ___ ___
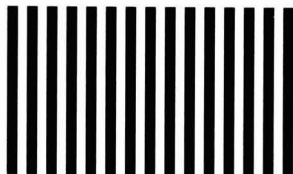
ES&T
**Reader
Service
Reply Card**

**It's computer
processed
for fast
response
to your
inquiries
AND, IT'S
FREE**

INDEX TO THE ADVERTISERS IN THIS ISSUE

Alkylammonium Montmorillonites as Adsorbents for Organic Vapors from Air

Martin Harper* and Colin J. Purnell

Department of Occupational Health, London School of Hygiene and Tropical Medicine, Keppel Street, London WC1E 7HT, U.K.

■ Montmorillonite clays may be modified by the exchange of the inorganic interlayer cations with alkylammonium ions, resulting in a fixed internal porosity. The pore size and shape depend on the nature of the alkylammonium ion. A number of different ions were used to prepare adsorbents with varying properties, and these were examined for their potential application to sampling organic vapors in air. Characterization involved determination of nitrogen and water contents, surface area, interlayer spacing, thermal stability, and breakthrough volumes of organic vapors. The adsorbent that showed the most promise [tetramethylammonium montmorillonite (TMA)] was further evaluated for use as an adsorbent in both thermal- and solvent-desorbable sampling systems.

Introduction

Montmorillonite clay minerals consist of a planar three-layer aluminosilicate lattice, stacked vertically (1). Through the isomorphic replacement of aluminum for silicon and magnesium for aluminum there is an excess net negative charge on the lattice, which is satisfied by the presence of inorganic cations (Ca, Na, K, etc.) situated within the layers, together with water molecules, which form a hydration sphere around the cations.

It is well-known that these cations are readily exchangeable and that exchange is also possible with organic cations such as alkylammonium ions (2). Previous work on the resulting materials by Barrer and co-workers (3–6) was originally concentrated on their application as packings for gas chromatographic columns. Although a few such compounds are still available (Bentones), interest has largely shifted toward porous polymers and molecular sieves. However, sampling of organic vapors in air for occupational hygiene applications requires a wide range of adsorbents, in order to be able to choose the most appropriate for each situation (7). Sampling of gases in the workplace is now a legislated requirement in many countries, and the sensitivity, accuracy, and precision of these methods is under continual review. In general, sampling is normally by adsorption of the contaminants onto an inert medium with subsequent desorption and analysis in the laboratory. Air may be drawn through the adsorbent by a pump, or the contaminant may simply be allowed to migrate to the adsorbent by diffusion (8). Desorption of the collected material may be by solvent displacement or thermal desorption (9). In any case, it is necessary to choose the sorbent taking into consideration the sampling

and analytical method, the concentration of the contaminant and duration of exposure, the environmental conditions, and the presence of interfering species. Available data on many such sorbents are summarized in Table I.

Porous polymers are very useful for thermal desorption systems as the van der Waals forces binding the analyte to the adsorbent are sufficiently weak that the analyte can be driven off by an input of thermal energy. However, such weak binding may result in a substantial vapor pressure of a low-boiling analyte above the adsorbent surface, and this may lead to problems with the sampling efficiency (10). Because of the enhanced adsorption potential in micropores, active carbons may sample more efficiently (11), but they require solvent desorption, which involves toxic chemicals (e.g., CS_2), and the continual determination of desorption efficiencies. The aim of this study was to examine other adsorbents that might fill the gap between these two extremes.

Methods and Materials

From previous studies it was thought likely that tetramethylammonium and tetraethylammonium montmorillonite would have good potential as adsorbents, but it was also thought necessary to examine other possible compounds of this type. The *tert*-octyl-(2,4,4-trimethylpentyl-)ammonium ions are a rather different shape from normal straight-chain molecules. It was thought that this molecule, in pushing further out from the interlayer surface, might confer an increased adsorption volume on the montmorillonite structure. From the available evidence (2), myristyltrimethylammonium should form a double-layer complex, although there could still be large gaps between the molecules. As the methyl groups would surround these gaps, the adsorption volume would be highly hydrophobic.

A number of montmorillonite clays are available (12). Wyoming bentonite (a sodium montmorillonite) is frequently used for experimental purposes. It has a high cation-exchange capacity (CEC) and forms a stable thixotropic gel in water. The high CEC was thought to be a possible disadvantage, since the more cations adsorbed the smaller the remaining volume for adsorption of other species. Fuller's earth (a calcium montmorillonite) has a rather lower CEC, and this can be further reduced by acid activation with dilute hydrochloric acid (producing a hydrogen montmorillonite). The X-ray diffraction picture of the acid-washed material is not significantly different from that of the precurser material, but both have substantially broader peaks than the sodium clay.

There are many analytical methods available whose results would aid in elucidating the structure and properties of these materials. Surface area measurements and

*SKC Ltd., Sunrise Park, Higher Shaftesbury Rd., Blandford Forum, Dorset DT11 8STr, U.K.

Table I. Properties of Some Solid Adsorbents Used in Organic Vapor Sampling[a]

adsorbent	specific surface area, m²/g	upper limit T, °C	pore type[b]	polymer type[c]
active charcoals				
coconut shell	800–1000		I	
	1100–1400		I	
Carbosieve B	1000		I	
silica gels	300–800		I–II	
	340–670		I–II	
alumina				
Actal A	275		II	
U.G.1	175		II	
molecular sieves	600–700		I	
GC packings				
Carbopack C-HT	14	500	I	
Tenax GC	19	375	III	DPPPO
Chromosorb				
101	<50	275	III	STY-DVB
102	300–400	250	II	STY-DVB
103	15–25	275	III	STY
104	100–200	250	III	Acrylate
105	600–700	250	II	Aromatic
106	700–800	225	II	STY
107	400–500	225	II	Acrylate
108	100–200	225	III	Acrylate
Porapak				
P	50–100	250	III	STY-EVB
Q	500–600	250	II	EVB-DVB-DVB
R	550–750	250	II	NVP
T	250–350	190	II	EGDMA
N	225–350	190	II–III	CVP
Amberlite				
XAD2	300–400	250	II	STY-DVB
XAD4	498		I–II	STY-DVB
XAD7	326		I–II	Acrylate

[a] Data from: Butler and Burke (*16*), Namiesnik et al. (*17*), Vidal-Madjar et al. (*18*), Gunderson and Fernandez (*19*), Matsumara (*20*), and manufacturer's data. [b] Pore type I, microporous (<2 nm); II, transitional pores (2–50 nm); III, macroporous (>50 nm). [c] DPPPO, diphenyl-*p*-phenylene oxide; CVP, *C*-vinylpyrrolidone; STY, styrene; DVB, divinylbenzene; EVB, ethylvinylbenzene; EGDMA, ethyleneglycoldimethacrylate; NVP, *N*-vinylpyrrolidone.

$d(001)$ spacings provide information on the size and shape of the pores. Nitrogen determinations may be used as a direct measure of the quantity of cation actually exchanged. Thermal analysis gives the water content and temperature at which breakdown of the complex begins. From breakthrough volume determinations the safe sampling volume can be derived, which is an important measure of the performance of the adsorbent. Indirectly, these determinations provide information about the sorption isotherm. The selection of the most appropriate adsorbent was based on these results. Desorption efficiency determinations were used to validate the chosen adsorbent for use in thermal desorbable sampling systems for certain organic vapors in air.

Preparation of Alkylammonium Montmorillonites. Tetramethylammonium bromide (GPR, BDH), tetraethylammonium bromide (GPR, BDH), and myristyltrimethylammonium bromide (99%, Aldrich) are readily available. *tert*-Octylamine (2,4,4-trimethylpentylamine) (95%, Aldrich) was reacted with gaseous hydrogen chloride (BOC grade N2.6) by bubbling the HCl slowly into an alcoholic amine solution (the reaction is exothermic) for ~30 min. Upon cooling, the amine salt crystallized. The crystals were washed several times with ethanol and recrystallized from hot water solution. The identity of the crystals was checked by melting point determination.

The following alkylammonium salts were prepared in accord with the method of Barrer and MacLeod (*3*) and are designated in the text by the accompanying abbreviations: tetramethylammonium montmorillonite, TMA; tetraethylammonium montmorillonite, TEA; *tert*-octylammonium montmorillonite, TOA; myrystyltrimethylammonium montmorillonite, MTMA. (The designation

Ca-mont or Na-mont is added where applicable; otherwise, H-mont was the precursor clay). AWM represents H-mont, the acid-washed calcium montmorillonite.

Determination of Total Nitrogen. Samples of the various adsorbents were analyzed for total organic nitrogen. Samples (500 mg) were digested in a mixture of 3 cm³ of 30% hydrogen peroxide and 5 cm³ of concentrated sulfuric acid to oxidize the organic matter and to convert the nitrogen to ammonium sulfate. This reaction was assisted by the presence of two tablets, each containing 1.5 g of potassium sulfate and 75 mg of selenium as a catalyst. The digestion tubes were heated to 200 °C for 1 h and then to 450 °C until the sample became colorless.

After being allowed to cool, and after addition of a few milliliters of water, the tubes were placed in a Tecator Kjeltec 1030 autoanalyzer, operated according to manufacturers instructions. The recorder was calibrated (minus a blank determination) in percent nitrogen. A high- and a low-concentration standard were run on each batch for quality control purposes.

X-ray Diffraction. X-ray diffraction was employed to determine the relative distances [$d(001)$ spacings] between the aluminosilicate layers of the montmorillonite when separated by the different alkylammonium cations. A Siemens K710 X-ray generator produced Cu Kα radiation, and a monochromated beam irradiated the powdered sample mounted on a silicon crystal sample holder coated with a thin film of silicon grease. The X-ray generator was used in conjunction with a standard Siemens D500 goniometer. The sample was rotated in steps of 0.05° and counts were for 2 min at each step. As the determination was made at very low angles, there was some leakage from the main beam and a Fit program using split Pearson
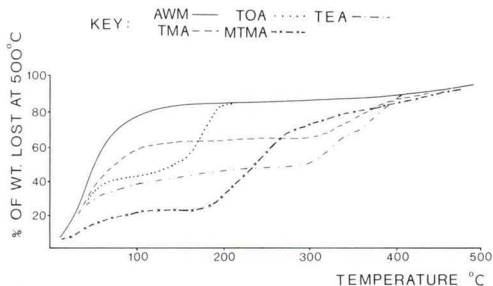
Figure 1. Results of thermal analysis: cumulative weight loss on heating expressed as a percentage of the total weight lost at 500 °C. (Key as per text.)

correlation coefficients was used to determine the exact 2θ reflection angle from the curve produced. This program forms part of the Siemens Diffrac 11 Fortran software system.

Adsorption of vapors by these materials normally results in some slight expansion of the lattice. Under the conditions used (room temperature and ambient relative humidity), it was not possible to exclude water vapor from these samples and the results must be interpreted accordingly. However, it was possible to run some of the samples under a vacuum of $\sim 10^{-4}$ Torr in a specially constructed environmental chamber.

Thermogravimetry. Thermogravimetric analysis was carried out on a selection of the adsorbent samples on a Stanton Redcroft TG-750 thermobalance. A nitrogen flow was used to remove any decomposition products. The crucible was lowered into the furnace and the heating rate set at 10 °C/min to 1000 °C. The results are given in Figure 1 as graphs of percentage weight loss against temperature. Since it was observed on the first few samples that after 500 °C no further abrupt weight changes occurred, only a slow loss thought to be due to the decomposition of structural (hydroxyl) water, the succeeding samples were only taken to between 500 and 600 °C.

Surface Area Measurements. The Brunauer–Emmet–Teller (BET) gas adsorption method has become the most widely used standard procedure for the determination of the surface area of finely divided and porous materials (13). The samples were weighed into the special sample buret provided for use in the Carlo Erba Sorptomatic 1800 and outgassed at 120 °C overnight with the pressure reduced to 3×10^{-4} Torr. The sample tubes were then reweighed to give the final mass for the surface area calculations. Each sample was then placed in the Sorptomatic at a temperature of 77 K, and the BET isotherm was constructed point by point by the admission of successive charges of nitrogen gas to the sample according to the manufacturers directions.

A graph of $P/(P_0 - P)v$ on the y axis against P/P_0 on the x axis gives V_m as the reciprocal of the intercept plus slope. The BET surface areas were calculated assuming the surface area of the nitrogen molecule to be 0.162 nm^2.

Breakthrough Volumes. A critical discussion of the use of breakthrough volumes as a means of characterizing sorbents will be described elsewhere (7). Breakthrough can be defined as the point at which an adsorbate first appears in the outlet stream of an atmosphere flowing through a bed of adsorbent. As this depends on the depth of the bed, which is related to the quantity of adsorbent, then, provided a standard method is used for the evaluation, it is normal to quote the breakthrough volume (V_b) in liters of contaminated atmosphere per gram of adsorbent.

Provided the number of adsorbent theoretical plates (N) is ~ 30 (14), it is possible to calculate a safe sampling volume (15) based on the equation

$$V_s = V_b(1 - 2/N^{1/2}) \tag{1}$$

where V_s is the safe sampling volume and V_b is the breakthrough volume. The breakthrough volume at room temperature is simply derived from a set of results obtained at higher temperatures extrapolated ($\log_{10} V_b$ versus $1/T$) to the required value (16). N is given by the equation

$$N = 16(R/w)^2 \tag{2}$$

where R is the chromatographic retention volume (to the center of the peak) and w the basal peak width.

A consideration of breakthrough volumes can give important insights into the probable behavior of the adsorbent during sampling. It is not possible to ensure efficient sampling of an adsorbent when the breakthrough volume is less than 10 L/g (21), and a value greater than 10^6 L/g could lead to difficulties when employing thermal desorption, since adsorption would be very strong. The method of determining breakthrough volumes was that of Brown and Purnell (22). In this method the adsorbate is introduced as an aliquot of vapor of known concentration. Previously (23), a screening method using direct liquid injections had indicated the usefulness of TMA as an adsorbent for compounds as volatile as carbon disulfide.

Atmosphere Generation System. A large (28-L) flat-bottomed, bell-shaped borosilicate glass vessel was used as a mixing chamber for the generation of static vapor atmospheres. It contained two openings, one at the top and one at the bottom fitted with short lengths of glass tube, connected by lengths of PTFE tubing to a recirculatory pump, the inlet tube passing also through a gas sampling valve attached to a Perkin-Elmer F11 gas chromatograph. An injection port fitted with a septum enabled liquid organic reagents to be injected and evaporated in the air flow. For calibration purposes a Miran infrared spectrometer was inserted in the outlet line.

A calibrated 20-μL syringe was used for sample injection. Eight different organic vapors at various concentrations were used to check that the expected concentration of the atmosphere by calculation was not significantly different from that measured with the Miran. Breakthrough volumes were determined for cyclohexane by this method, over a concentration range of 40–1400 mg/m^3. No significant difference was observed and for this reason it was felt that breakthrough was reasonably independent of concentration over this range. Therefore, the same 20-μL syringe was used to generate all the atmospheres under investigation.

In this procedure, sample injection onto the column took place via the gas sampling valve. Once generated, the atmosphere was used to flush the 5-μL volume of the valve. Turning the valve introduces this volume into the nitrogen carrier gas line and then into the GC column of the F-11. The column consisted of 500 mg of adsorbent packed into a Perkin-Elmer ATD tube, connected via copper tubing and swagelock fittings with a flame ionization detector (FID). The nitrogen flow rate was measured by bubble flowmeter after the tube and the flow adjusted to between 25 and 30 mL/min. Breakthrough times were determined for a range of vapors on each of the prepared adsorbents, by taking a tangent to the output peak and extrapolating this back to the base line. The breakthrough volume is simply obtained by multiplying by the flow rate.

Preparation of Packing Material for Thermal Desorption Studies. It was necessary to convert TMA into

a granular form as a powder is not an ideal medium for back-flushing into a gas chromatograph. Montmorillonite is often used as a binder for other materials, especially when sintered at high temperatures. TMA was therefore mixed with a small quantity of water to form a slurry, which was poured onto a notched aluminum plate. The plate was heated at 250 °C for 8 h. This is well below the temperature of breakdown, and analysis after 2, 4, and 6 h showed no loss of organic nitrogen. After cooling, the TMA was scraped off the plate and sieved. The 500–700-μm fraction was retained for use. This material was checked by matching breakthrough volume determinations with results from the powdered TMA. The granular material has now been subjected to many cycles of adsorption and desorption, and conditioning and sampling at high flow rates (up to 2.5 L/min), without any significant structural degradation.

Thermal Desorption Efficiencies. The automated thermal desorption system represents a major advance in the technology of vapor sample analysis. Up to 50 adsorption tubes per run, containing environmental or other samples, can be processed for gas-phase analysis, in this case by gas chromatography. The Perkin-Elmer automated thermal desorption (ATD 50) system has already been described (9).

Primary desorption from the sample tube was achieved with a 0.5 mL/min He flow for 10 min at 250 °C. Analysis was by GC-FID using the standard CONCAWE conditions for hydrocarbon analysis.

Sample Tube Spiking. Sample tubes were packed with either 50 or 100 mg of granular TMA. Together with three tubes containing 150 mg of Tenax GC (the recommended standard quantity), the filled tubes were conditioned prior to use by passing dry nitrogen at ~200 °C overnight, to remove any remaining contamination. The tubes were spiked with a solution of hexane of such a concentration that a 5-μL aliquot would be equivalent to the amount collected diffusively by a sample tube operating for an 8-h period at the U.K. occupational exposure limit (OEL). The solution for the TMA tubes was made in carbon disulfide, but that for the Tenax tubes had to be made up in methanol. Dry nitrogen was passed through an injection port and then through an adsorbent tube at a flow rate of 100 mL/min. A 5-μL aliquot of the stock solution was then injected into the port to evaporate in the passing gas stream. Under these conditions the majority of the solvent would break through the bed long before the adsorbate of interest. Calculations based on the results from the breakthrough volume experiments can be used to ensure that none of the adsorbate is also lost.

Each sample was run twice through the desorption and analysis cycle. Desorption efficiencies (Table VII) are expressed as the amount recovered on the first run as a percentage of the total recovered on both runs, whereas absolute recovery is expressed as the amount recovered on the first run (since in practice the sample would not be run twice) as a percentage of the amount recovered from the reference tubes. At least four tubes containing 50 mg and four tubes containing 100 mg of TMA were used in each experiment, with at least two Tenax GC or Chromosorb 106 standards. The solutions of analyte were made as previously detailed for hexane (ethylbenzene, 1,1,1-trichloroethane, trichloroethylene, and tetrachloroethylene) or containing the amount expected after diffusively monitoring twice the OEL for 8 h (benzene and toluene). Each 5-μL injection therefore contained either 14.6 μg of hexane, 2.1 μg of benzene, 20.3 μg of toluene, 9.5 μg of ethylbenzene, 54.8 μg of 1,1,1-trichloroethane, 12.9 μg of tri-

Table II. Nitrogen Contents of Various Montmorillonite Adsorbents

adsorbent[a]	wt % N (undried)	wt % H$_2$O	wt % N (dried)
AWM	0.08	11.31	0.09
TMA (H-mont)	0.77	7.40	0.83
TMA (Ca-mont)	0.80	6.80	0.85
TMA (Na-mont)	1.12	6.30	1.19
TEA	0.72	3.94	0.75
TOA (1) July 1986	0.62	10.98	0.70
TOA (2) Jan 1987	0.77	7.85	0.84
TOA (3) Aug 1987	0.97	5.16	1.02
MTMA	0.81	2.17	0.83

[a] Key as per text. TOA samples analyzed August 1987.

chloroethylene, or 25.3 μg of perchloroethylene.

Results and Discussion

Nitrogen Determinations and Thermogravimetry. It is well-known that there is no perfect method of measuring the cation-exchange capacity (CEC) of a claylike material. There are many methods available, all giving different values and all requiring skilled operation (1). If the total organic nitrogen is expressed as a dry weight percentage and this figure is divided by the atomic weight of nitrogen, the result is the number of equivalents of the alkylammonium cation per 100 g. This is probably a more useful and relevant measure since it represents the total quantity of cations exchanged rather than that potentially available. The results are presented in Table II together with water contents derived from thermogravimetric studies.

The results from TMA prepared from acid-washed (H-mont) and untreated (Ca-mont) material are not significantly different, indicating that the acid treatment has had little effect on the cation-exchange capacity. However, the figure of 71 mequiv/100 g provided by BDH for the acid-washed material is equivalent to a nitrogen content of 0.99% assuming full exchange, while the figure obtained (0.85% nitrogen) is equivalent to a CEC of 61 mequiv/100 g. TMA prepared from Wyoming bentonite (Na-mont) has a higher nitrogen content, which is a reflection of the higher CEC of this material. The figure of 1.19% nitrogen is equivalent to 85 mequiv/100 g. BDH gives a wide range of 65–75 mequiv/100 g, while 85 mequiv/100 g is within the range expected from the standard clay SWy-1 (Clay Mineral Society). Exchange of organic cations for calcium ions may not have taken place up to the theoretical maximum. The X-ray data may not necessarily be able to distinguish this, but a single peak close to that expected from the literature (3) is evidence that exchange is almost complete, and that there may be some error in the organic nitrogen results. Any remaining inorganic cations are likely to be arranged in a mixed sandwich of organic- and inorganic-rich layers.

The amount of water adsorbed by Ca-mont TMA was 6.8%, which is approximately that expected from three water molecules adsorbed per unit cell, or six molecules per hexagonal site in the silicate lattice. This should be compared with six molecules per unit cell for the unexchanged clay. Since the ratio of internal to external adsorption sites is not known for certain and the external surface area may vary from 8 to 90 m^2/g depending on the material (Barrer, R. M., personal communication), it is almost impossible to determine how much of this water is within the layers and how much is external. An approximate figure of one external to two internal is only a very rough guide, based on the water content of MTMA
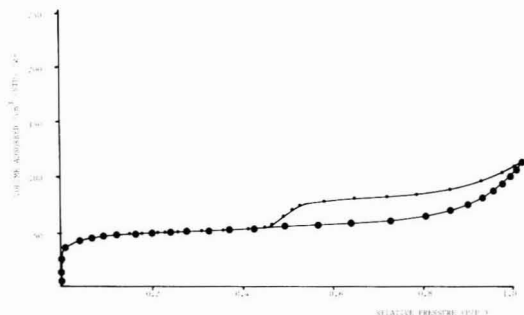
Figure 2. Typical adsorption isotherm: nitrogen on TMA.

Table III. BET Surface Areas and *d* Spacings by XRD[a]

sample	area, m^2/g	d, nm
AWM	82.8	1.56
TMA	177.2	1.42
TEA	121.7	1.42
TOA	149.0	1.51
MTMA	12.0	1.83

[a] Key as per text. Note: *d* spacings determined in ambient air.

(2.17%) and TMA from heat-treated montmorillonites (2.56%) (24), neither of which would be considered to contain much interlayer water. As expected, the larger and more hydrophobic tetraethylammonium molecule results in a lower water content of TEA (approximately two molecules per unit cell), whereas TOA appears to adsorb more than expected.

There is an interesting relationship between the age of the three samples of TOA prepared at different times and their respective water and nitrogen contents. It appears that there is a progressive loss in the amount of alkyl-ammonium ion with storage and this loss is accompanied by a gain in adsorbed water as the adsorbent becomes less hydrophobic. This effect was not noticed with TMA, even after 3-years storage. Furthermore, the temperature at which breakdown of the alkylammonium clay complex takes place can be derived from the thermal analysis data (see Figure 2). As expected from the results of Barrer and Reay (4), TMA was the most stable, with the onset of breakdown not occurring until a temperature of 290–300 °C. TEA is also stable to about the same temperature. TOA and MTMA, however, both experienced breakdown at much lower temperatures, 170–180 °C for the former and 180–190 °C for the latter. This greater instability may be the reason for the noticeable changes in TOA with time mentioned above, in which case the same effect may also occur with MTMA. However, during the breakthrough volume studies TOA was also found to have a very high flame ionization detector background, and the nitrogen content of the most recently produced sample is greater than expected. Cations lost from TOA during heating or storage are not strongly bound and this indicates adsorption within the interlayer space, possibly as the amine. The low basicity of *tert*-octylammonium may be the reason for this, especially as an acid clay was used. MTMA does not behave in a similar fashion.

Surface Areas. The BET surface areas are given in Table III, and a typical isotherm (TMA) is given in Figure 2. The nitrogen adsorption isotherm is of type II with H4 hysteresis, characteristic of platey materials with slitlike micropores (13). Such an isotherm can be thought of as exhibiting Langmuirian (type I) behavior at low relative pressures of the adsorbate during the filling of the mi-
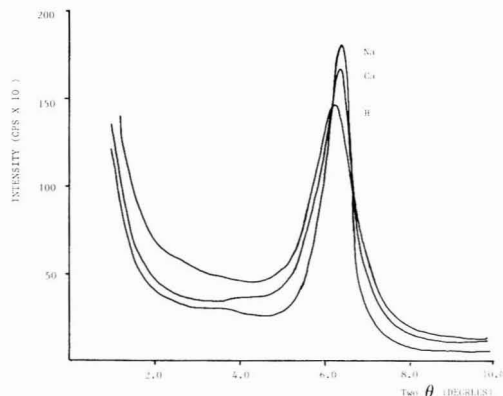
Figure 3. Comparison of the major X-ray diffraction peak of TMA prepared from Wyoming bentonite (Na), fuller's earth (Ca), and acid-washed fuller's earth (H). Results obtained under vacuum.

croporous volume. At much higher relative pressures, the microporous volume is filled and the remainder of the isotherm relates to capillary condensation on the external surface of the molecules.

The surface area of the original acid-washed clay is very close to quoted values for similar montmorillonites. The surface area of MTMA is very small. It is likely that the whole of the internal volume is taken up with a forest of hydrocarbon "tails". The values for the other adsorbents are all higher than that of the precursor material, with TMA giving the highest value. That of TEA is less, reflecting a greater coverage of the internal surface by the larger cation. TOA also has a high surface area, and until the results of the thermal analysis, it was thought likely to be as useful as TMA. The hysteresis loop on the isotherms exhibited closure, suggesting no structural changes accompanying the adsorption/desorption process.

X-ray Diffraction. X-ray diffraction was employed to check the homogeneity of the samples as well as to provide further information relevant to an understanding of the internal structure. All of the $d(001)$ peaks were reasonably sharp and Gaussian as expected from pure materials. This is especially important as a check for structural damage of the acid-washed montmorillonite since any defects would have caused peak broadening. The manufacturers of the acid-washed clay also employ this parameter as a check. The $d(001)$ spacings are given in Table III.

The value of 1.56 nm for the acid-washed clay is close to that expected from the formation of a double-layer hydrate, that is the normal $d(001)$ spacing (0.96 nm) plus twice the van der Waals radius of a water molecule (0.28 nm). The results for TMA and TEA (1.42 nm) are close to those expected from the literature (1.35 and 1.39 nm) (3) if a further slight expansion from the presence of water molecules is postulated. Under vacuum $d(001)$ spaces fell from 1.42 to 1.40 nm (TMA-H), 1.40 to 1.38 (TMA-Ca), and 1.38 to 1.38 (TMA-Na), as shown in Figure 3.

It can be assumed that the nitrogen of the *tert*-octyl-ammonium group also keys into the ditrigonal hole and the N–C bond rises perpendicular from this. Consideration of the shape of this molecule and the requirement (due to pressure of the silicate layers) to adopt the flattest lying configuration leads to a situation where the limiting dimension is increased by slightly more than the van der Waals radius of two methyl groups (2 × 2.4 nm). The spacing of MTMA (1.83 nm) is almost exactly that expected for a double layer of long-chain-length interlayer cations as predicted by Jordan (25). The absence of any

Table IV. Breakthrough Volumes on Alkylammonium Montmorillonite Clays

	adsorbent[a,b]						
	TMA	TEA	TOA	MTMA	106	PPK	Tenax
pentane	2.38	0.15	0.77	<0.0	1.38	0.92	<0.0
hexane	3.98	0.79	1.66	<0.0	2.13	1.66	0.63
heptane	4.94	2.24	2.69	<0.0	2.96	2.60	1.36
octane	6.06	3.04	3.38	<0.0	3.53	3.53	2.00
nonane	···	3.78	···	0.62	ND	ND	ND
decane	···	4.79	···	0.99	ND	ND	ND
undecane	···	5.63	···	1.81	ND	ND	ND
dodecane	···	···	···	2.67	ND	ND	ND
cyclohexane	2.09	0.62	1.25	<0.0	2.11	1.89	ND
benzene	3.94	1.51	1.61	0.46	1.96	1.93	0.90
toluene	4.97	3.46	3.02	1.36	3.00	2.35	1.70
ethylbenzene	···	4.53	···	1.62	3.56	3.24	ND
cumene	···	5.53	···	2.16	4.15	3.34	2.78
mesitylene	···	···	···	2.71	4.33	4.34	3.26
styrene	···	4.57	···	2.09	3.62	3.41	2.60
CH_3CCl_3	1.86	0.75	0.88	ND	1.72	1.73	0.75
$CHCl_2CHCl_2$	3.73	1.97	···	ND	3.48	3.25	2.34
$CHClCCl_2$	2.92	1.31	1.90	<0.0	2.04	1.96	1.30
CCl_2CCl_2	3.04	2.03	2.71	<0.0	2.63	2.43	2.03

[a] 106, Chromosorb 106; PPK, Porapak Q; ···, too high to be determined at the working temperature of the adsorbent; ND, not determined. Tenax data from Brown and Purnell (22). [b] Data given as $\log_{10}$ liters per gram of adsorbent.

extra increase due to water adsorption suggests that all of the water content of this material is adsorbed either around the organic molecule or on external surfaces. The extremely low internal surface is probably due to the occupation of any remaining volume by the three methyl groups and suggests that the water molecules might be external.

Breakthrough Volume Determinations. All the breakthrough volume results are quoted as logarithms, so that comparisons are essentially between orders of magnitude. The safe sampling volumes derived from these figures are intended to be safety guidelines and there is a large safety factor built into their calculation. The bulk of the breakthrough volume determinations are presented in Table IV; the results for the alkylammonium montmorillonites are compared with experimental data on two porous polymers (Chromosorb 106 and Porapak Q) and literature values from Tenax, another polymer adsorbent. Results below 0.00 (< 1 L/g) are irrelevant since the best estimate for a minimum useable breakthrough volume is greater than 1.00 (>10 L/g). Results above 6.00 (>10^6 L/g) are difficult to obtain since they involve working above the thermal stability limit of the adsorbent, and in practice such an adsorbent may prove too strong for thermally desorbable systems. For TOA the maximum values become limited by the lower breakdown temperature of the adsorbent. It is possible to measure the breakthrough times at lower temperatures, but it becomes very time consuming. In practice, low-temperature desorption would not be acceptable in a rapid, automated thermal desorption system. It is not possible to determine breakthrough volumes for aromatic compounds on simple unexchanged montmorillonite. Many attempts have failed and this could well be due to catalytic activity within the adsorbent bed.

The results clearly show that TMA has by far the largest affinity for all of the organic vapors tested, greater than the porous polymers and of the same order as might be expected from active charcoal. Determinations on TMA made from each of the three clays indicated that TMA H-mont gave the highest breakthrough volumes for each adsorbate. TMA Na-mont gave the lowest values; these results are in line with the reasoning given above. The results from the different adsorbents follow the same trend as the results of surface area determinations (Table III).

Table V. Safe Sampling Volumes for Granular TMA

adsorbate	$\log_{10} V_b$	N	safe sampling vol, L/g
pentane	2.56	19	200
hexane	3.43	24	1600
heptane	5.34	25	130000
octane	5.95	25	530000
isooctane	3.02	23	640
cyclohexane	1.85	22	40
benzene	3.37	23	1300
toluene	4.19	20	8800
CH_2Cl_2	2.91	27	500
$CHClCCl_2$	2.08	25	70
CCl_2CCl_2	2.76	25	340

There is also a trend within each adsorbent; the results may be correlated with boiling point of the adsorbate (e.g., for the series pentane to undecane on TEA, r = 0.997), in line with theory. This is not precisely true for the chlorinated compounds, which are less well adsorbed than expected. The reason for this is unclear, but may reflect a size effect.

Since these materials are all of equivalent density, it is appropriate to compare the number of theoretical plates within 500 mg of adsorbent contained in equal-bore tubes. With hexane as the adsorbent, the results (at 160 °C) for TMA, TEA, TOA, and MTMA are 28, 17, 10, and 3, respectively. These figures are related to the strength of adsorption and therefore the adsorption isotherms. It should be noted that only TMA fulfills the criterion necessary to enable calculation of safe sampling volumes, that is N approximately equal to 30. To be sure that this is the case for all adsorbates, values of N were determined and are presented together with the calculated safe sampling volumes in Table V. Note that these values are for granular TMA, the form in which the adsorbent is most likely to be used in practice. A slight reduction in overall porosity is inevitable on microcrystallite aggregation and a small reduction in N compared to the powdered material was observed.

Two vapors did not give symmetrical peak shapes. The value of N for 1,1,2,2-tetrachloroethane was 2, similar to those values obtained from adsorbents with little or no microporous adsorption volume. This is possibly due to

Table VI. Reduction in N with Temperature: 1,1,1-Trichloroethane on Granular TMA

temp, °C	160	150	140	130
N (for 500 mg of TMA)	26	13	8	4

Table VII. Sample Recovery and Desorption Efficiencies[a]

analyte	recovery	desorp effic
(1) 50 mg of TMA/Tube		
hexane	100.7	99.5
benzene	91.7	99.7
toluene	96.5	99.8
ethylbenzene	96.9	97.8
1,1,1-trichloroethane	95.6	100.0
trichloroethylene	89.7	100.0
tetrachloroethylene	99.3	100.0
(2) 100 mg of TMA/Tube		
hexane	104.5	99.9
benzene	104.8	99.5
toluene	117.4	99.9
ethylbenzene	115.8	99.2
1,1,1-trichloroethane	103.2	100.0
trichloroethylene	106.6	100.0
tetrachloroethylene	108.3	100.0

[a] All results expressed in percent; average of at least four determinations.

the size of the organic molecule. The micropores of TMA are slitlike, approximately 0.52 nm high by 0.32 nm (the distance between adjacent alkylammonium groups) wide. It is possible for a single chlorine atom (approximate atomic radius, 0.17 nm) to pass through these slits, and both trichloroethylene and perchloroethylene are adsorbed since their chlorine atoms are held in the same plane by the absence of rotation about the double bond. The preferred orientation of the chlorine atoms in the 1,1,2,2-tetrachloroethane molecule is in two perpendicular planes, and consequently, the molecule may not pass through the pores; any adsorption must take place on external sites. 1,1,1-Trichloroethane presents a slightly different picture. Values of N are found to increase with increasing temperature of the adsorbent (Table VI). This probably represents an energetic increase in the interlamellar spacing with temperature. The preferred arrangement of chlorine atoms would give a molecular diameter only slightly greater than the normal interlayer distance. Since the $d(001)$ spacing is increased slightly by the adsorption of water vapor, it is possible that adsorption of both of these species may occur at ambient temperatures under conditions of high relative humidity.

Desorption Efficiency Determinations. Desorption experiments carried out by spiking under dry nitrogen are presented in Table VII. The desorption efficiency is taken to be the proportion of sample recovered during the first of two desorption sequences. It can be seen that the desorption efficiencies are very good (>99.5%) until the effects of the strength of adsorption become apparent with high molecular weight compounds (e.g., ethylbenzene). There should be no difficulty in applying the technique to even these compounds, considering the carrier gas flow rate through the tube during desorption can easily be increased from 0.5 to 100 mL/min.

The overall recovery is defined as the total amount recovered compared to that recovered from the reference adsorbent. The results appear to be similar to Tenax GC for 50 mg of adsorbent or even better for 100 mg. This could be due to slight losses from the Tenax during spiking, which could be expected from a macroporous adsorbent

with type III isotherms (8). The same effect is seen with Chromosorb as the reference adsorbent, but to a lesser extent.

In order to model more closely actual sampling conditions a series of experiments was attempted using ambient air in place of the nitrogen stream during the tube spiking operation. Subsequent analysis indicated a possible interference on the analytical column from the release of adsorbed water. A number of technical alterations to the desorption parameters should have reduced this quantity to that tolerable by the column. In fact, the apparent loss in sample was reduced but not eliminated, and therefore, it is possible that sampling efficiency may be reduced by the presence of water vapor. This effect may be quantified by exposing the sorbent to a standard atmosphere of known contaminant concentration and relative humidity. Two sets of three SKC diffusive sampling badges (SKC Inc., Eighty Four, PA) were exposed to an atmosphere of trichloroethylene (350 ppm) in dry air. One set was filled with SKC Lot 120 PCB charcoal, the other with TMA. The badges were exposed to the trichloroethylene atmosphere for 4 h in a specially designed apparatus described elsewhere (26). After exposure, the contents of the badges were desorbed with 2 mL of carbon disulfide and analyzed by GC-FID. Under dry conditions the TMA badges gave an average of 81% of the charcoal results, and this small difference may be a result of collection or desorption efficiency differences between the TMA and charcoal. In a repeat experiment at 85% relative humidity, the TMA badges were found to give an average of only 1.5% of the charcoal results. This is undoubtedly due to a large difference in collection efficiency. The amounts recovered on thermal desorption of samples collected from a humidified atmosphere were similarly reduced. It is likely that this effect becomes pronounced when the internal area of the TMA is saturated with water molecules. Experience has shown that this saturation is accomplished very quickly in a humid atmosphere. Obviously, this effect represents a drawback with normal pumped or diffusive sampling applications. However, if the preferred sampling method is by diffusion, a hydrophobic silicone membrane across the face of the sampler would exclude water from the system altogether; such a sampling combination is well-known and is acceptable to the U.K. Health and Safety Executive.

Conclusions

A novel adsorbent system for organic vapor sampling has been described. A number of variations on the basic design of the compound were evaluated for this purpose. As previously reported (23), tetramethylammonium montmorillonite (TMA) appeared the most suitable for application in sampler systems utilizing thermal desorption. It appears that water should be excluded from the system, at least until further evaluation has taken place, which will limit immediate application to diffusive samplers with hydrophobic membranes rather than pumped samplers. Further work is necessary to fully investigate the effect of water vapor and to evaluate the adsorbent under actual sampling conditions both in the laboratory and in the field.

Registry No. CH₃CCl₃, 71-55-6; CHCl₂CHCl₂, 79-00-5; CHClCCl₂, 79-34-5; CCl₂CCl₂, 127-18-4; CH₂Cl₂, 75-09-2; pentane, 109-66-0; hexane, 110-54-3; heptane, 142-82-5; octane, 111-65-9; nonane, 111-84-2; decane, 124-18-5; undecane, 1120-21-4; dodecane, 112-40-3; cyclohexane, 110-82-7; benzene, 71-43-2; toluene, 108-88-3; ethylbenzene, 100-41-4; cumene, 98-82-8; mesitylene, 108-67-8; styrene, 100-42-5; isooctane, 26635-64-3.

Literature Cited

(1) Grim, R. E. *Clay Mineralogy*, 2nd ed.; McGraw-Hill: New York, 1969.
(2) Theng, B. K. G. *The Chemistry of Clay-Organic Reactions*; Hilger: Bristol, U.K., 1974.
(3) Barrer, R. M.; MacLeod, D. M. *Trans. Faraday Soc.* **1955**, *51*, 1290.
(4) Barrer, R. M.; Reay, J. S. S. *Trans. Faraday Soc.* **1957**, *53*, 1253.
(5) Barrer, R. M.; Perry, G. S. *J. Chem. Soc.* **1961**, 850.
(6) Barrer, R. M.; Millington, A. D. *J. Colloid Interface Sci.* **1967**, *25*, 359.
(7) Harper, M. In preparation.
(8) Harper, M.; Purnell, C. J. *Am. Ind. Hyg. Assoc. J.* **1987**, *48*, 214.
(9) Brown, R. H.; Charlton, J.; Saunders, K. J. *Am. Ind. Hyg. Assoc. J.* **1981**, *42*, 865.
(10) Coker, D. T.; Jones, A. L.; Simms, M. C. Practical and Theoretical Assessment of Passive Samplers. British Occupational Hygiene Society Conference, Nottingham, U.K., 1981.
(11) Underhill, D. W. *Am. Ind. Hyg. Assoc. J.* **1984**, *45*, 306.
(12) Grim, R. E.; Güven, N. *Bentonites: Geology, Mineralogy, Properties and Uses*; Elsevier: Amsterdam, 1978.
(13) Sing, K. S. W.; Everett, D. H.; Haul, R. A. W.; Moscou, L.; Pierotti, R. A.; Rouquerol, J.; Siemieniewska, T. *Pure Appl. Chem.* **1985**, *57*, 603.
(14) Senum, G. I. *Environ. Sci. Technol.* **1981**, *15*, 1073.
(15) Cropper, F. R.; Kaminsky, S. *Anal. Chem.* **1963**, *35*, 735.
(16) Butler, L. D.; Burke, M. F. J. *J. Chromatogr. Sci.* **1976**, *14*, 117.
(17) Namiesnik, J.; Torres, L.; Kozlowski, E.; Mathieu, J. *J. Chromatogr.* **1981**, *208*, 239.
(18) Vidal-Madjar, C.; Gonnord, M. F.; Benchah, F.; Guiochon, G. *J. Chromatogr. Sci.* **1978**, *16*, 190.
(19) Gunderson, E. C.; Fernandez, E. L. *ACS Symp. Ser.* **1981**, *No. 149*, 179.
(20) Matsumara, Y. *Ind. Health* **1987**, *25*, 63.
(21) Russell, J. W. *Environ. Sci. Technol.* **1975**, *9*, 1175.
(22) Brown, R. H.; Purnell, C. J. *J. Chromatogr.* **1979**, *178*, 79.
(23) Harper, M.; Purnell, C. J. A Novel Adsorbent for Use in Diffusive Samplers. Comm. Euro. Communities, [Rep] EUR 1987, 10555, 396.
(24) Harper, M. *An Investigation of Novel Methods of Sampling Organic Gases and Vapours*. Ph.D. Thesis, University of London, in preparation.
(25) Jordan, J. W. *J. Phys. Colloid Chem.* **1949**, *53*, 294.
(26) Guild, L. V.; Myrmel, K. H.; Myers, G.; Dietrich, D. Bilevel Passive Monitor Validation—An Effective Way of Assuring Sampling Accuracy for a Larger Number of Related Hazards. American Industrial Hygiene Conference, St. Louis, MO, 1989.

Heterogeneous Polycyclic Aromatic Hydrocarbon Degradation with Ozone on Silica Gel Carrier

Ana Alebić-Juretić,[†] Tomislav Cvitaš,*,[‡] and Leo Klasinc[‡]

Institute of Public Health, Rijeka, Yugoslavia, and The Ruđer Bošković Institute, Zagreb, Yugoslavia

■ Heterogeneous degradation of five polycyclic aromatic hydrocarbons (PAHs), perylene (Pe), pyrene (Py), benzo[a]pyrene (BaP), benz[a]anthracene (BaA), and fluoranthene (Flo), adsorbed on nonactivated (moisture-containing) silica gel with ozone in a fluidized-bed reactor has been studied. The concentrations of ozone employed varied from 0.050 to 0.400 ppm. The results obtained show that, concerning their kinetics, there is a clear difference between reactions with less than and more than monolayer coverage of the particle surface with PAHs, those carrying a submonomolecular layer being faster and indicating the effect of the particle surface. In more highly covered samples, the observed degradation obeys two distinct first-order laws, the slow one changing into the faster at monomolecular coverage; the relative reactivities are as follows: Pe > BaP > BaA > Py ≫ Flo, and BaP > Pe > BaA > Py ≫ Flo, respectively. According to the present results, heterogeneous degradation of PAHs by ozone on particle surfaces is one of important pathways for their removal from the atmosphere.

Introduction

Polynuclear aromatic hydrocarbons (PAHs) formed by fossil or other biomass fuel combustion are present in the atmosphere either as gases (lower molecular weight) or adsorbed on solid particles (1). Experiments in simulated atmospheric conditions have shown that a solid carrier can strongly influence their reactivity toward photooxidation (2, 3) and/or nitration (4–6), though recent results suggest that the lower molecular weight PAHs (naphthalene, fluoranthene, pyrene) undergo nitration more readily in the gaseous phase (7–9).

According to the literature, filter materials used for high-volume sampling can affect the PAH reactivity toward ozonolysis (10), while there are opposite results on the effect of ambient particulates as adsorbants. Thus, Peters and Seifert (11) found that ambient particulates might have little influence on PAH degradation by ozone, which was recently emphasized by Brorström et al. (12).

In this work we have investigated the degradation rates of five PAHs, perylene (Pe), pyrene (Py), benzo[a]pyrene (BaP), benz[a]anthracene (BaA), and fluoranthene (Flo), adsorbed on a nonactivated (moisture-containing) silica gel surface by ozone at ambient concentrations. Silica gel had been chosen as a model solid carrier because SiO₂ forms a significant portion of the tropospheric aerosols. It has to be kept in mind, however, that the presence of other microconstituents can strongly affect the chemical transformation of adsorbate on particle surfaces (13). In addition, the choice of a chemically and physically well-defined carrier facilitates the performance and understanding of chemical reactions on particles and could give

---

[†] Institute of Public Health.
[‡] The Ruđer Bošković Institute.

valuable data to be applied on further investigation with other carriers and experimental systems. However, silica gel may not be representative of many basic air shades like $(NH_4)_2SO_4$ or NH_4HSO_4 and carbonaceous particles, the latter known to stabilize PAHs toward degradation in the atmosphere (3, 14).

Materials and Methods

Solid Carrier. Nonactivated silica gel (70–230 mesh, Kemika) with ca. 10% moisture was selected as the solid carrier. Granulometric analysis gave the average particle diameter as 0.112 mm. The particles were approximated as cubes when calculating specific surface.

PAHs. The following PAHs were used: perylene (GFT Aromaten), pyrene (purified by zone melting), benzo[a]-pyrene (Merck, p.a.), benz[a]anthracene (Fluka A. G., purum), and fluoranthene (Merck, p.a.). Except for pyrene, all the other PAHs were used without further purification.

PAHs were dissolved in distilled acetone at concentrations of ca. 0.02 mg mL^{-1} each. Solutions of lower concentrations were prepared by multiple dilution (1:2, 1:4, 1:8, and 1:16) of these stock solutions. Silica gel (5 g) was added to 50 mL of each solution, and the acetone was evaporated under stirring. The amount of adsorbed PAHs obtained in this way varied from 0.040 to 0.200 mg g^{-1}, forming submonolayer and/or higher than monolayer coverage. Since the moisture present can block the porous structure (15), it was assumed that the PAH molecules were adsorbed only on the silica gel surface. This was confirmed by the quantitative analysis of PAHs adsorbed on particles and those adsorbed on the walls of the flask. The experimental procedure of particle coating is commonly used in the study of chemical reactions under simulated atmospheric conditions (6, 16), though some works suggest coating from the gas phase (17), which certainly better simulates the conditions of coating under ambient conditions (e.g., from hot stacks), but is harder to control.

Ozone Sources. Ozone monitor Dasibi 1008 PC was used as an ozone generator and analyzer. The monitor generates ozone with a UV lamp (photozone). The applied ozone concentrations were 0.050–0.200 ppm for samples with submonomolecular layer and 0.100–0.250 ppm for greater than monolayer surface coverages. Higher concentrations of ozone (0.200–0.400 ppm) were used only in experiments with fluoranthene.

In the early stages of our investigations we also used ozone generated in cold discharge (ozone generator Fischer 501) to follow the reaction kinetics, since according to some sources, it has a different composition than photozone. Under the described experimental conditions with perylene in higher than monolayer coverage, however, no difference in reaction rates was found ($k = 0.233 \pm 0.039$ ppm^{-1} min^{-1}), although photozone has, as reported (18), up to 25% of reactive species like H_2O_2, OH, and singlet oxygen.

Fluidized-Bed Reactor. A fluidized-bed reactor system was used to simulate atmospheric conditions (Figure 1). The advantages of this system are cited elsewhere (6, 16). The gas flow necessary to make a fluidized bed for ca. 1.0 g of solid sample was 5 L min^{-1}, the maximum flow our ozone generator could produce. The ozone analyzer sampled the mixture continuously at the rate of 2 L min^{-1}, which was compensated by adding the same flow of pure nitrogen. A feedback between the analyzer and generator provided control over constant concentrations of ozone under such conditions.

An open system was used in order to avoid instabilities in ozone generation owing to small changes in airflow through the reactor column. A stream of ozonized air
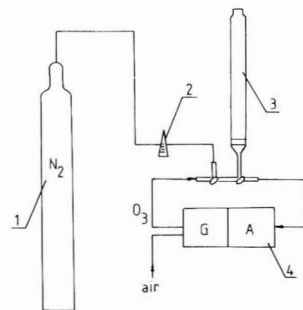
Figure 1. Scheme of the apparatus used to expose PAHs adsorbed on a silica gel surface to ozone: (1) cylinder with pure nitrogen; (2) rotameter; (3) fluidized-bed reactor; (4) generator and ozone analyzer.
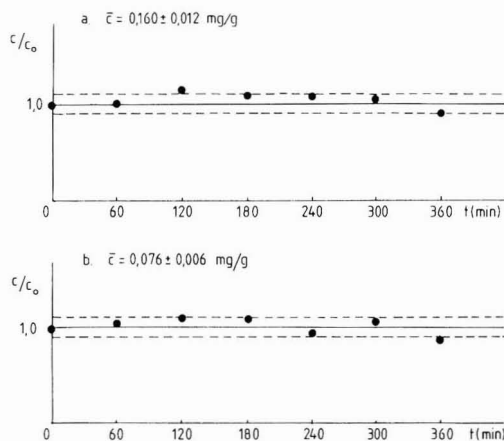
Figure 2. Proof of negligible fluoranthene sublimation from a silica gel surface under flow conditions (5 L min^{-1} pure nitrogen): (a) at more than and (b) at less than monolayer coverage.

(0.100–0.150 ppm) was blown through the column for at least 30 min before each experiment to prevent ozone loss on the column walls (19).

Desorption experiments in streaming nitrogen through a column with samples of PAHs adsorbed on silica gel showed that no losses by sublimation occurred, even in the case of the most volatile compounds (Py and Flo, Figure 2). Thus, we found no evidence of the losses mentioned in the literature (20).

Kinetic Measurements. The reaction kinetics have been followed by determining the amount of unreacted PAHs that remained on the particle surfaces. The PAHs were eluted from the solid samples (20–40 mg) with 10 mL of distilled acetone, and their absorption spectra were recorded on a Cary 19 UV–vis spectrometer. The decrease in absorption of perylene, pyrene, benzo[a]pyrene, benz[a]anthracene, and fluoranthene was monitored at 434 ($\epsilon = 3.46 \times 10^4$ L mol^{-1} cm^{-1}), 334 ($\epsilon = 4.80 \times 10^4$ L mol^{-1} cm^{-1}), 385 ($\epsilon = 2.60 \times 10^4$ L mol^{-1} cm^{-1}), 341 ($\epsilon = 6.70 \times 10^3$ L mol^{-1} cm^{-1}) and 358 nm ($\epsilon = 8.20 \times 10^3$ L mol^{-1} cm^{-1}), respectively. The half-life of the reaction determined from the ln c vs t plot gave the observed kinetic constant k_{obs} directly. Plotting k_{obs} against the concentration of ozone gives a straight line, with a slope equal to the rate constant k, which was determined by the least-squares method.

Results and Discussion

The degradation of PAHs adsorbed on particles at constant concentration of ozone follows first-order kinetics
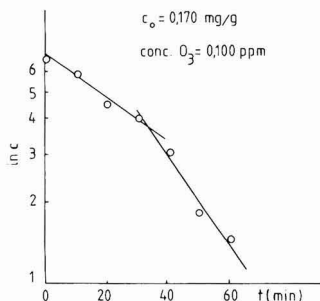
Figure 3. First-order kinetics plot for samples carrying more than a monolayer of BaP showing two distinct processes taking place.

Table I. Kinetic Constants for Degradation of PAHs Adsorbed on Silica Gel Surface with Ozone at Lower ($k_{<1}$) and Higher ($k_{>1}$) Than Monolayer Coverage

PAH	$k_{<1}$, ppm^{-1} min^{-1}	$k_{>1}$, ppm^{-1} min^{-1}	$k_{<1}/k_{>1}$
perylene	0.401 ± 0.016	0.203 ± 0.010	1.98
benzo[a]pyrene	0.449 ± 0.041	0.190 ± 0.002	2.36
benz[a]anthracene	0.228 ± 0.010	0.156 ± 0.009	1.46
pyrene	0.127 ± 0.006	0.068 ± 0.006	1.87
fluoranthene	(9.60 ± 0.56) 10^{-3}	(7.40 ± 0.27) 10^{-3}	1.30

(21). In our early experiments with Pe, Py, and BaP (0.100–0.150 mg g^{-1}), the data plotted as ln c vs t showed two straight lines as if two mechanisms were taking place (Figure 3). This can be interpreted in terms of the effect of the particle surface on the reaction rate. After some reaction time the amount of PAH drops below the value necessary to form a monolayer, freeing the surface to increase the reaction rate. This, of course, is based on the assumption that the primary reaction products are blown off the surface in the air stream. Support for this interpretation was gained in experiments with submonolayer quantities of PAHs coated on the particles. Under otherwise identical experimental conditions, the observed reaction rates were higher for larger than for monolayer quantities of PAHs. The intercept of the two straight lines in the ln c vs t graph can be used to estimate the total particle surface. For this reason, the PAH degradation experiments were carried out with different amounts of adsorbed PAHs: greater or less than required to form a monolayer.

The coverage of particle surfaces by PAH molecules strongly affects the reaction rates, those with partial surface coverage being faster. Similar reaction rate dependences on the amount of PAHs coated have been noticed previously for ozonolysis on fused silica plates (21) and photodegradation on wood soot (22). With higher than monolayer coverage the reaction rate is independent of the initial amount of PAH, as already noticed (23). This means that ozone molecules react only with PAH molecules from the outer layer and the reaction conditions remain practically unchanged until the amount of unreacted PAH falls to/below monolayer and the effect of the supportive surface becomes evident.

The obtained rate constants are given in Table I.

Under these experimental conditions, the resulting relative reactivities for higher coverages were Pe > BaP > BaA > Py ≫ Flo, while for lower coverage the reactivity scale was BaP > Pe > BaA > Py ≫ Flo.

The above reactivities as well as the fact that the acidic silica gel surface enhances the reaction suggest that this is most likely an electrophilic substitution. The most reactive PAHs were BaP and Pe, belonging to group II in
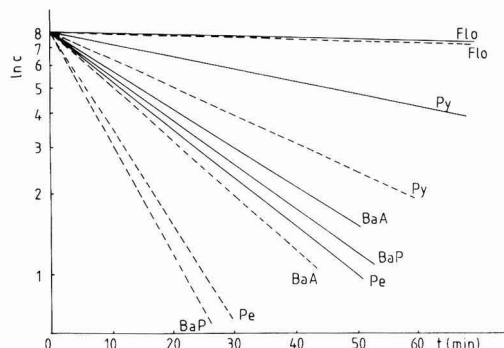
Figure 4. Schematic diagram for the degradation of PAHs adsorbed on a silica gel surface with ozone in the case of higher (—) and lower (- - -) than monolayer coverage. Concentration of ozone, 0.200 ppm.

Nielsen's reactivity scale toward electrophilic substitution (24). Although BaA and Py are within the same group III, under the described experimental conditions, BaA reacted almost twice as fast as Py. The observed increased reactivity of BaA can be explained by the fact that the ozone molecule can attack the most reactive atom (C$_7$) or the most reactive bond (C$_5$–C$_6$) with comparable efficiency, and the total reactivity of BaA is the result of two simultaneous reactions taking place (25), which cannot be differentiated under the present experimental conditions. Flo, classified within the very stable group V, was found also to be the most stable toward ozonolysis. The relative stability of Flo toward reactions under simulated atmospheric conditions is the reason why some authors did not observe any reactions (6, 26), while others did (10). The observed stability of Flo is an additional reason why this PAH is usually one of the most abundant in the atmosphere.

The obtained reactivity scale is in accordance with the results of Katz et al. (27) and Van Vaeck and Van Cauwenberghe (28), but disagrees with the results of Cope and Kalkwarf (20, 23), who found Py more reactive than Pe, and Butković et al. (29), who predicted higher reactivity for Py than for BaP under atmospheric conditions on the basis of kinetic studies of PAH ozonolysis in aqueous solutions.

The increased reactivity in the case of partial surface coverage with PAH molecules is most pronounced in the most reactive Pe and BaP, while it has the least effect for the most stable Flo (Figure 4). Wu et al. (21) explained the slower ozonolysis of PAHs coated on fused silica plates in greater than monolayer coverage with the fact that primary reaction products remained on the surface, thereby preventing ozone from reacting with the inner layer. According to our results, in a fluidized-bed reactor the primary products are obviously blown off the particle surface. The increase in reaction rate appeared after the amount of unreacted PAH had fallen below the value necessary to form a monolayer. We can suggest three possible reasons for such an enhancement:

(i) The rate increase might be due to the increase in electrophilic character of ozone bound at Lewis acid sites on the silica gel surface (30). This assumption requires ozone adsorption on the particle surface, which has been considered earlier (4, 28).

(ii) Another reason might be that moisture desorption in a flow system frees additional sites for ozone adsorption and hence increases the reaction rate by the previously mentioned mechanism. This statement is further supported by the observed retention time at the beginning of the reaction for particles of submonolayer coverage.

Dehydration of particle surfaces in flow systems has already been discussed by Jäger and Hanuš (4).

(iii) The third possibility is that certain aromatic hydrocarbons could undergo changes and/or shifts in electronic states during adsorption owing to interactions with the particle surfaces; such bathochromic shifts could facilitate the reactions by decreasing the activation energy (31, 32).

Although OH radical reaction rates with organics in the gas phase exceed those with ozone by several orders of magnitude (33), we have no experimental evidence that OH radicals play a major role in the case of heterogeneous degradation of PAHs in the adsorbed state. It is unlikely that OH radicals, which are probably formed during the reaction, could be the reason for the observed rate increase because of two facts: first, the half-life of Py under the experimental conditions at 0.050 ppm ($t_{1/2}$ = 130 min) is approximately equal to the one predicted for atmospheric conditions ($t_{1/2}$ = 150 min), on the basis of kinetic data obtained for the ozonation in aqueous solution (29); and second, according to some authors (10), moisture can even slow down the reaction. However, the latter argument has to be taken with reservation since contrary results can also be found in the literature (34).

Conclusion

Several conclusions can be drawn from the obtained results:

1. The degradation of PAHs adsorbed on solid carriers with ozone might be an important sink for such compounds in the atmosphere.

2. The amount of PAHs adsorbed on the particle surface, i.e., partial or complete coverage of adsorbant, strongly influences the reaction rates, thus confirming the importance of the supporting surface on heterogeneous reactions in the atmosphere.

3. The relative reactivities and the fact that the acidic silica gel surface enhances the reaction suggests this reaction to be an electrophilic substitution.

4. Half-lives of PAHs obtained under laboratory conditions can be used to predict their lifetimes in the atmosphere. Thus, at constant concentration of ozone (0.050 ppm) for several hours, the half-lives for BaP and Pe are ~0.5 h, for BaA ~1 h, and for Py ~2 h, while for the most stable Flo it is 24 h under submonolayer coverage of the particle surface, which simulates the real situation in the atmosphere (13). Under such conditions, the lifetimes of PAHs would be from 3.0–3.5 (BaP and Pe) to 12 h (Py), while for the most stable Flo the lifetime would be 6 days. Relatively short lifetimes of these PAHs in the presence of ozone at ambient concentrations are one of the reasons for these PAHs (except Flo) being present only in traces in urban atmospheres during the summer months.

5. The observed half-life of Py adsorbed in submonolayer quantity on nonactivated silica gel ($t_{1/2}$ = 130 min) is similar to that extrapolated on the basis of kinetic data obtained for PAH ozonolysis in water ($t_{1/2}$ = 150 min), thus confirming the assumption that in the case of particles with adsorbed moisture the degradation mechanism is similar to that in aqueous solution.

6. The sudden change in the reaction rate at the amount of PAH that corresponds to monolayer coverage is observed as a pronounced kink in the ln c vs t curve and can be used to determine the specific surface of nonactivated silica gel.

In the real atmosphere, PAHs and ozone can also react with other pollutants, thus affecting their lifetimes. The degradation of primary products from PAH ozonolysis in the atmosphere (quinones, epoxides) can proceed in different ways (photooxidation, nitration) to final mineralization. Possible oxo, hydroxy, nitro, and hydroxynitro intermediates that are formed in these reactions are responsible for the observed mutagenicity of the medium polarity and polar fraction of urban airborne particles.

Literature Cited

(1) Cautreels, W.; Van Cauwenberghe, K. *Atmos. Environ.* **1978**, *12*, 1133.
(2) Žorž, M. Ph.D. Dissertation, University of Zagreb, 1983 (in Croatian).
(3) Korfmacher, W. A.; Wehry, E. L.; Mamantov, G.; Natusch, D. F. S. *Environ. Sci. Technol.* **1980**, *14*, 1094.
(4) Jäger, J.; Hanuš, V. *J. Hyg. Epidemiol. Microbiol. Immunol.* **1980**, *24*, 1.
(5) Hughes, M. M.; Natusch, D. F. S.; Taylor, D. R.; Zeller, M. V. In *Polynuclear Aromatic Hydrocarbons: Chemistry and Biological Effects*; Bjorseth, A., Dennis, A. J., Eds.; Battele Press: Columbus, OH, 1980; pp 1–8.
(6) Ramdahl, T.; Bjorseth, A.; Lokensgard, D. M.; Pitts, J. N., Jr. *Chemosphere* **1984**, *13*, 527.
(7) Pitts, J. N., Jr.; Atkinson, R.; Sweetman, J. A.; Zielinska, B. *Atmos. Environ.* **1985**, *19*, 701.
(8) Sweetman, J. A.; Zielinska, B.; Atkinson, R.; Ramdahl, T.; Winer, A. M.; Pitts, J. N., Jr. *Atmos. Environ.* **1986**, *20*, 235.
(9) Arey, J.; Zielinska, B.; Atkinson, R.; Winer, A. M.; Ramdahl, T.; Pitts, J. N., Jr. *Atmos. Environ.* **1986**, *20*, 2339.
(10) Pitts, J. N., Jr.; Paur, H.-R.; Zielinska, B.; Arey, J.; Winer, A. M.; Ramdahl, T.; Mejia, V. *Chemosphere* **1986**, *15*, 675.
(11) Peters, S.; Seifert, B. *Atmos. Environ.* **1980**, *14*, 117.
(12) Brorström, E.; Greenfelt, P.; Lindskog, A. *Atmos. Environ.* **1983**, *17*, 601.
(13) Güsten, H. In *Chemistry of Multiphase Atmospheric Systems*; Jaeschke, W., Ed.; NATO ASI Series; Springer-Verlag: Berlin, Heidelberg, 1986; Vol. G.6, pp 567–592.
(14) Korfmacher, W. A.; Natusch, D. F. S.; Taylor, R. D.; Mamantov, G.; Wehry, E. L. *Environ. Sci. Technol.* **1980**, *14*, 1094.
(15) Schure, M. R.; Soltys, D. A.; Natusch, D. S. F.; Mauney, T. *Environ. Sci. Technol.* **1985**, *19*, 82.
(16) Daisey, J. M.; Lewandowski, C. G.; Žorž, M. *Environ. Sci. Technol.* **1982**, *16*, 857.
(17) Miguel, A. H.; Korfmacher, W. A.; Wehry, E. L.; Mamantov, G.; Natusch, D. F. S. *Environ. Sci. Technol.* **1979**, *13*, 1229.
(18) Report. Analytical Testing Laboratory. Los Angeles, CA, 1983.
(19) Bergshoeff, G.; Lanting, R. W.; Prop, J. M. G.; Reynders, H. F. R. *Anal. Chem.* **1980**, *52*, 541.
(20) Cope, V. W.; Kalkwarf, D. R. *Environ. Sci. Technol.* **1987**, *21*, 643.
(21) Wu, C.-H.; Salmeen, I.; Niki, H. *Environ. Sci. Technol.* **1984**, *18*, 603.
(22) Kammens, R. M.; Guo, Z.; Fulcher, J. N.; Bell, D. A. *Environ. Sci. Technol.* **1988**, *22*, 103.
(23) Cope, K. W.; Kalkwarf, D. R. Pacific Northwest Laboratory, Annual Report for 1982 to the DOE Office of Energy Research, Part 3: Atmospheric Sciences, 1983.
(24) Nielsen, T. *Environ. Sci. Technol.* **1984**, *18*, 157.
(25) Pryor, W. A.; Gleicher, G. J.; Church, D. F. *J. Org. Chem.* **1983**, *48*, 4198.
(26) Niessner, R.; Klockow, D.; Bruynseels, F.; Van Gricken, R. *Int. J. Environ. Anal. Chem.* **1985**, *22*, 281.
(27) Katz, M.; Chan, C.; Tosine, H.; Sakuma, T. In *Polynuclear Aromatic Hydrocarbons*; Jones, P. W., Leber, P., Eds.; Ann Arbor Science: Ann Arbor, MI, 1979; pp 171–189.
(28) Van Vaeck, L.; Van Cauwenberghe, K. *Atmos. Environ.* **1984**, *18*, 323.
(29) Butković, V.; Klasinc, L.; Orhanović, M.; Güsten, H. *Environ. Sci. Technol.* **1983**, *17*, 546.

(30) Bailey, P. S. *Ozonation in Organic Chemistry*; Academic Press: New York, 1982; Vol. II, Chapter 3.
(31) Robin, M.; Trueblood, K. N. *J. Am. Chem. Soc.* 1957, 79, 5138.
(32) Gäb, S.; Nitz, S.; Parlar, H.; Korte, F. *Chemosphere* 1975, 4, 251.
(33) Davenport, J. E.; Singh, H. B. *Atmos. Environ.* 1987, 21, 1696.
(34) Lindskog, A.; Brorström-Lunden, E.; Sjödin, A. *Environ. Int.* 1985, 11, 125.

Concentration and Fate of Airborne Particles in Museums

William W. Nazaroff,[†] Lynn G. Salmon, and Glen R. Cass*

Environmental Engineering Science, California Institute of Technology, Pasadena, California 91125

■ To investigate the potential soiling hazard to works of art posed by the deposition of airborne particles, time-resolved measurements were made of the size distribution and chemical composition of particles inside and outside of three southern California museums. The measured indoor aerosol characteristics agree well with predictions of a mathematical model of indoor aerosol dynamics based on measured outdoor aerosol characteristics and building parameters. At all three sites, the fraction of particles entering from outdoor air that deposit onto surfaces varies strongly with particle size, ranging from a minimum of 0.1–0.5% for particles having a diameter in the vicinity of 0.15 μm to greater than 90% for particles larger than 20 μm in diameter. Deposition calculations indicate that, at the rates determined for the study days, enough elemental carbon (soot) would accumulate on vertical surfaces in the museums to yield perceptible soiling in as little as 1 year at one site to as long as 10–40 years at the other two sites.

Introduction

Air pollutant exposure may damage objects kept indoors. This hazard is an acute concern among museum curators (*1*). The objects in their charge often are valued entirely for their visual qualities, characteristics that may be particularly susceptibile to air pollution damage. Furthermore, it is desired to preserve these objects for centuries. Even modest rates of deterioration may yield an unacceptable cumulative effect.

Airborne particles constitute a major class of pollutants that are hazardous to works of art. Deposition of particulate matter onto the surface of an object may cause chemical damage and/or soiling. Consequently, activities that generate particles, such as smoking, are restricted in museum galleries. However, regardless of the presence or absence of indoor emissions, particulate matter may enter the building with the outdoor air that is supplied for ventilation. Although some research has been reported on indoor/outdoor relationships for airborne particles (e.g., ref 2 and references therein), little is known about particle concentrations in museums, the factors that affect those concentrations, the fate of particles that enter museum atmospheres, and the magnitude of the soiling hazard posed by deposition of airborne particles (*3*). The present paper addresses these issues.

Over periods of 24 h, at each of three museums in southern California, time-dependent measurements were made of the chemical composition and size distribution of the indoor and outdoor aerosol. Building characteristics that influence aerosol concentrations and fates were measured: ventilation rate, temperature differences be-

Table I. Characteristics of the Study Sites

	Norton Simon	Scott Gallery	Sepulveda House
dimensions			
no. of floors	2	1	2
floor area, m^2	4930	535	330
wall area, m^2	6950	1990	1050
volume, m^3	21540	2530	1200
ventilation[a]			
outdoor air-exchange, h^{-1}	0.37[b]	0.28 ± 0.01	3.6 ± 1.4
recirculation, h^{-1}	5.8	8.2	
monitoring period			
start date	6 April 88[c]	24 April 88	30 March 88
start time	1000 PDT	1800 PDT	2100 PST

[a] Flow rate divided by building volume; mean ± SD of measurements for 24-h period. [b] Based on hot-wire anemometry measurements of outdoor air flow rate into mechanical ventilation system. Tracer gas decay yielded 0.40 h^{-1} with 90% confidence bounds of 0.37–0.44 h^{-1}. [c] Boundary layer flow and temperature differences measured for 24 h commencing at 1200 PDT on 4 April 1988.

tween a wall and the air, fluid velocities adjacent to a wall, and the particle removal efficiency of filters in the mechanical ventilation system. From these data, the concentrations and fates of indoor particles were computed for each site, by use of a mathematical model previously developed for this study (*4*). To evaluate model performance, predicted indoor aerosol properties—based on measured outdoor aerosol data and building characteristics—were compared against the results of the indoor measurements. The fate of particulate matter entering the museums was assessed with the model, emphasizing the deposition of particles—particularly those containing elemental carbon and soil dust—onto indoor surfaces. Results indicate that the rate of deposition of elemental carbon (soot) particles onto museum surfaces is sufficient to produce perceptible soiling over time periods that are short relative to the desired lifetimes of works of art. The results also suggest that the principal soiling hazard to smooth vertical surfaces and to downward facing surfaces results from the deposition of particles with diameters in the vicinity of 0.1 μm. For floors and other upward facing surfaces, both fine and coarse particles contribute significantly to the rate of soiling.

Study Sites

Three sites in southern California were selected for the study: the Norton Simon Museum in Pasadena, the Scott Gallery on the Huntington Library grounds in San Marino, and the Sepulveda House at El Pueblo de Los Angeles State Historic Park in downtown Los Angeles. These were chosen from among five museums in which indoor and outdoor aerosol characteristics were measured on a 24-h-average basis every sixth day during the previous summer and winter seasons (*5*). The range of values for the ratio of indoor to outdoor aerosol mass concentration thus was

[†] Present address: Department of Civil Engineering, University of California, Berkeley, CA 94720.
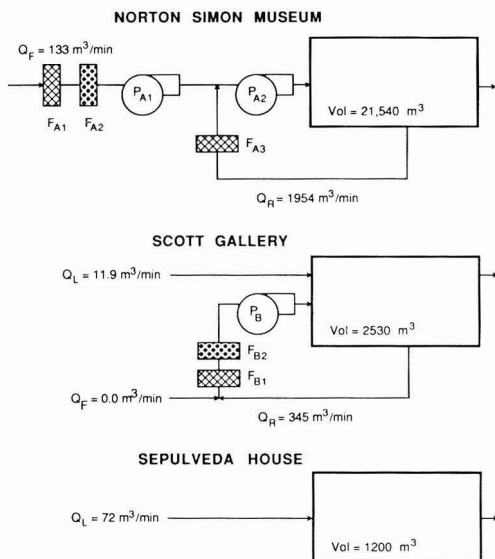
Figure 1. Schematic representation of the ventilation and filtration systems for the three study sites, showing the flow rates (Q), fans (P), and filters (F) in each system. For air flows, subscripts L, F, and R represent leakage (infiltration), forced supply (make-up), and recirculation, respectively. Filters F_{A2} and F_{B2} contain activated carbon for ozone removal; the other filters are mat-fiber type for removing particles.

known in advance, and the three sites were selected to span the range from high to low indoor aerosol concentration. Major characteristics of the buildings are summarized in Table I and in the following discussion.

The Norton Simon Museum and the Scott Gallery are modern buildings with custom-engineered heating, ventilation, and air conditioning (HVAC) systems (see Figure 1). At the Norton Simon Museum, make-up air from outdoors passes through a fibrous mat filter (F_{A1}), and through an activated carbon filter (F_{A2}), before being blended with return air that has been passed through a fibrous mat filter (F_{A3}); the air mixture is then conditioned for proper temperature and humidity and distributed to the building. At the Scott Gallery, the flow rate of make-up air was recently reduced effectively to zero by closing the intake dampers. At the time of the present study, air exchange between indoors and outside occurred entirely due to infiltration through cracks in the building shell and through door openings. Recirculated air is passed through a fibrous mat filter (F_{B1}) and an activated carbon filter that was recently added to the system for ozone removal (cf. ref 6).

The Sepulveda House is an historical museum with no HVAC system. Air exchange is provided by infiltration through relatively large openings in the building shell. When the building is open to the public (1000–1500 daily, except Sunday) and the weather is warm, two downstairs doors are kept open.

At each site, one wall was selected for investigation of boundary-layer air flows and temperature gradients that influence particle deposition rates. Measurements of particle deposition rate, reported elsewhere (7, 8), were made on the same walls. A detailed description of the walls is provided in ref 8. Briefly, an interior wall with a painted dry-wall surface was selected for investigation at the Norton Simon Museum; a painted plywood panel mounted onto an interior wall with furring strips was selected at the Scott Gallery; and an outer brick wall having a painted, irregular plaster surface was chosen at the Sepulveda House.

Because the experiments would have been disruptive to normal museum operation, measurements at the Norton Simon Museum and at the Scott Gallery were conducted while the buildings were closed to the public (museum staff were still present). Consequently, the measurements at these sites do not fully incorporate the effects of occupancy on aerosol properties, including particle generation by occupant activities. The Sepulveda House was open to the public, as usual, from 10 a.m. to 3 p.m. on the day of monitoring.

Experimental Methods

Detailed, time-resolved information on the indoor and outdoor aerosol size distribution and chemical composition was collected at each site for a period of 24 h. To measure the aerosol size distribution, two pairs of optical particle counters were operated, one pair sampling from a central indoor location with the second sampling from an outdoor location on the grounds of the site. One instrument in each pair (Particle Measuring Systems Model ASASP-X, referred to subsequently as the "midrange OPC") is capable of detecting particles over a nominal size range of 0.09–3-μm optical diameter and classifying them, according to the amount of light scattered in the forward direction, into 32 size channels. Sampling flow rates were measured and recorded at least hourly with rotameters that had been calibrated against a bubble flow meter; the flow rate was adjusted whenever it deviated by more than 10% from a nominal rate of 1 cm^3 s^{-1}. The second instrument in each pair (Particle Measuring Systems Model CSASP-100HV, referred to as the "large-particle OPC") detects and classifies light scattered from particles in the size range 0.5–47-μm diameter. All of the optical particle counters were operated continuously, with cumulative counts per channel recorded at 6-min intervals.

Several tests were conducted with the OPCs to investigate instrument performance (9). The performance of the midrange OPCs was good in all of the tests. However, the large-particle OPCs failed to yield satisfactory results in these tests, and consequently, the data from the large-particle OPCs were not used in the analyses reported in this paper.

Indoor and outdoor aerosol mass concentration and chemical composition were determined for total suspended particulate matter (TSP) and for fine particles ($< \sim$2-μm diameter) by using sampling devices and analysis methods similar to those described by Gray et al. (10). Briefly, for indoor and outdoor sampling locations, air was drawn through each of two sets of three 47-mm-diameter filters—one quartz fiber (Pallflex 2500 QAO) and two Teflon membrane filters (Gelman, PTFE, ringed, 2.0-μm pore size). One filter set at each site was deployed in open-faced holders to collect the TSP, while the other set was placed within in-line holders downstream of a cyclone separator (11) to collect the fine particles. The air flow rate through each filter holder was nominally 30 L min^{-1}, and each of the fine particle filter holders was preceded by its own cyclone separator. The sampling interval was typically 4 h; however, because of access restrictions, 8-h intervals were used at night at the Norton Simon Museum. The quartz filters were analyzed for elemental and organic carbon (12, 13). One of the Teflon filters was used to gravimetrically determine aerosol mass concentration and, by X-ray fluorescence, the concentrations of 34 trace metals (14). The second Teflon filter was analyzed for sulfate and nitrate concentrations by ion chromatography

(15) and for ammonium ion by colorimetry (16). For the purpose of this paper, the elemental carbon concentrations are of great interest, as this component governs the blackness of fine particulate matter (17), and therefore a major portion of the soiling hazard. In addition, the aluminum and silicon concentrations are useful markers for soil dust that may contribute to soiling.

Air-exchange rates were measured at each site by the tracer-gas decay technique, with sulfur hexafluoride as the tracer (18). At the Scott Gallery and the Sepulveda House, SF_6 measurements were made continuously throughout the study period, with samples collected at intervals of ~10 min and analyzed with a portable gas chromatograph. At the Norton Simon Museum, because of access restrictions, a single 2-h tracer decay measurement was made during the study period. The air flow rates through the mechanical ventilation system were determined by hot-wire anemometry at the Norton Simon Museum and on the basis of building design specifications at the Scott Gallery.

The air velocity adjacent to surfaces and the temperature difference between the surface and the adjacent air are important factors governing the deposition rate of fine particles (19,20). During the study period, continuous measurements were made of the temperature difference between the air and the surface of one wall by using an array of thermistors (Yellow Springs Instrument, part no. 44202). Two thermistors were used to determine the temperature of the wall surface; one was mounted in a thin (1.5-mm) aluminum plate that was attached to the wall with thermal joint compound, the other was coated with thermal joint compound and set into a small hole drilled in the wall so that the thermistor was flush with the surface. Likewise, two thermistors were used to determine the air temperature at approximately 15 cm from the wall; one was shielded with insulating foam to eliminate radiant heat transfer; the other was unshielded. The wall–air temperature difference was determined as the difference between the mean of the two wall probes and the mean of the two air probes. The probes were individually calibrated and have an intrinsic uncertainty of ~0.02 °C. Differences in paired temperature measurements for the two wall probes and for the two air probes were less than 0.1 °C in 53%, less than 0.2 °C in 83%, and less than 0.3 °C in 94% of the measurements made during the entire study.

Air velocity was measured adjacent to the same wall by use of two omnidirectional sensors (TSI Model 1620), placed at approximately 0.6 and 1.2 cm from the surface of the wall. The temperatures and velocities were sampled with a microcomputer-based data logger at intervals of 2 s, and the mean value was recorded for each minute. At the Norton Simon Museum, again because of access limitations, surface and air temperatures and the air velocities were monitored for 24 h 2 days prior to the aerosol monitoring period. At the other sites, the temperatures and velocities were measured simultaneously with aerosol monitoring.

The particle removal efficiency of the filters found in the buildings' mechanical ventilation systems was measured as a function of particle size for each fiber filter by simultaneously measuring the upstream and downstream particle concentrations with the two sets of optical particle counters. The measurements at the Norton Simon Museum were done in situ. For filter F_{B1} at the Scott Gallery, a section of a used filter panel from the site was obtained. At a Caltech laboratory (located ~1.5 km from the Scott Gallery), outdoor air was drawn through the filter section at the same face velocity as for actual use of the filter, and
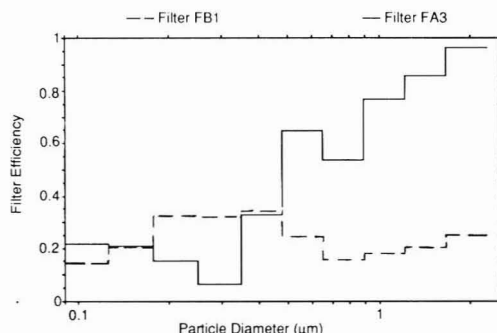
Figure 2. Filtration efficiency of particle filters as a function of particle size. The results are based on 21 and 4.5 h of data for filters F_{A3} and F_{B1}, respectively. The corresponding operating flow velocities across the filter faces are 0.44 and 1.7 m s^{-1}. Filter media: filter F_{A3} is Servodyne type SR-P1L; filter F_{B1} is Servodyne type Mark 80. Filter F_{A1} was found to have less than 5% removal efficiency when new for particles smaller than 2.3 μm in diameter.

the percent removal as a function of particle size was determined.

Measurement and Modeling Results: Aerosol Size Distribution and Chemical Composition

Filter Efficiency. The filtration efficiency as a function of particle size for a single pass through the building ventilation system filters F_{A3} and F_{B1} is shown in Figure 2. The efficiency for particles in size interval i, η_i, was computed as

$$\eta_i = \frac{C_{u_i} - C_{d_i}}{C_{u_i}} \quad (1)$$

where C_{u_i} and C_{d_i} are the measured upstream and downstream particle volume concentration in size range i, respectively.

At the Norton Simon Museum, filter F_{A1} is composed of the same material as filter F_{A3}. However, whereas filter F_{A3} was sufficiently loaded with particulate matter to appear heavily soiled, new filter material had recently been installed for F_{A1}. Very little difference (<5%) between upstream and downstream particle concentrations was observed for all particle sizes measured for filter F_{A1}. (These observations are consistent with the general knowledge that particle filters become more efficient as the loading increases.) Measurements across the charcoal filter, F_{A2}, indicate that it also is ineffective in removing fine particles.

Temperature Differences and Boundary-Layer Flows. The results of monitoring temperature difference and near-surface air velocity at three sites are shown in Figure 3. The prominent features of the temperature difference profiles are readily understood. For example, the largest peak in $T_{wall} - T_{air}$ at the Norton Simon Museum occurs in the late afternoon. At this time, the air temperature in this gallery increases due to solar heating of the roof and the south and west-facing walls. The mechanical ventilation system supplies cool air in an attempt to maintain the set point temperature, thereby increasing $T_{wall} - T_{air}$ (see also ref 8). (During the long-term monitoring reported in ref 8, a west-facing window opposite the monitored wall was covered by foam board and curtains. Before the present study, the foam board was removed. Consequently, during the afternoon, a portion of the wall was in direct sun, which probably contributed to the peak in $T_{wall} - T_{air}$.) The large dip and rise in the profile at the Scott Gallery is associated with an inad-
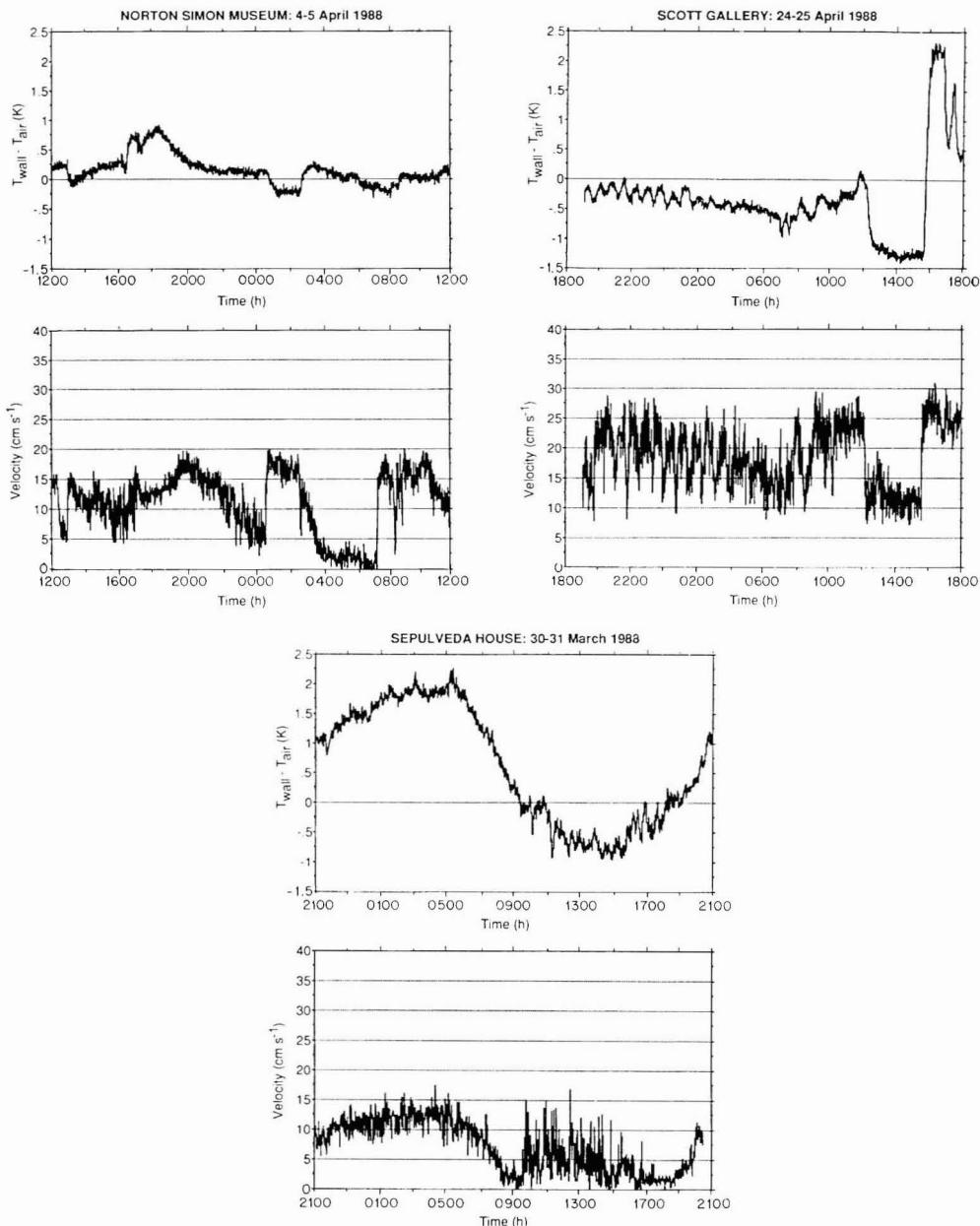
Figure 3. Temperature difference between the surface of a wall and the air, and the air velocity near the same wall vs time, for 24-h periods at each site. The air velocity probe was located at a distance from the wall of 1.05 cm for the Norton Simon Museum, 1.3 cm for the Scott Gallery, and 1.2 cm for the Sepulveda House.

vertent interruption in air conditioning for the building during the period 1200–1545 PDT. (It appears that the fans in the mechanical ventilation system continued to operate during this time, but that the cooling function ceased for almost 4 h.) The indoor air temperature rises rapidly at 1200 PDT and heat is transferred to the (interior) wall. At approximately 1545 PDT, the air-conditioning system resumes operation, rapidly cooling the air, and heat is transferred from the wall back to the air. At the Sepulveda House, without any thermal control, the diurnal cycle is driven by the outdoor air temperature and the delayed thermal response of the brick wall. The

maximum value of $T_{wall} - T_{air}$ occurs just before dawn and the minimum occurs at 1400 PST, corresponding approximately to the peak outdoor air temperature.

At the Sepulveda House the near-wall air velocity is consistent with expectations for natural convection (21,22), driven by the temperature difference between the wall and the air, for the periods 0000–1000 and 1500–2400 PST, i.e., whenever the museum is closed. Note that during these periods, the maximum velocity occurs when the temperature difference is greatest; likewise, when the temperature difference is near zero, the air velocity is very small. When the museum is open, the air flow velocity adjacent to the

wall is highly variable and appears to be driven predominantly by turbulent air movement in the core of the room.

At the Scott Gallery, the near-wall air velocity appears to be strongly dominated by the flow of air within the building due to the operation of the mechanical ventilation system. At this site, the supply and return-air registers are located at the tops of the walls. The lower velocity observed during the period when air cooling failed probably results from the fact that the buoyant warm air entering the room from the ceiling registers would not promote convective mixing in the core of the room. After cooling is restored, peak near-wall air velocities are observed. A similar correlation between the wall–air temperature difference and the near-wall air velocity is observed at other times during the monitoring period, most notably for the first 7 h. During this interval $T_{wall} - T_{air}$ oscillates with an amplitude of ~0.3 K and a period of approximately 45 min; an envelope of the near-wall air velocity can be traced with an amplitude of approximately 5 cm s^{-1} and the same period. Some of the high-frequency fluctuations in the air velocity at the Scott Gallery may be a result of the fact that the sampling location was located near a door that was opened and closed approximately 10 times hourly during monitoring.

At the Norton Simon Museum, air is supplied to the gallery through perforated tiles that cover more than half of the ceiling. Air is returned to the ventilation system through the interior hallways of the building. Given the combination of this circulation pattern with a lower recirculation rate (see Table I), it is not surprising that the measured near-wall air velocities are generally lower at this site than at the Scott Gallery.

Modeling Aerosol Characteristics. The indoor aerosol size distribution and chemical composition were computed from measured outdoor aerosol properties for each site by use of the indoor air quality model previously reported (4). That model tracks the evolution of the indoor aerosol size distribution and chemical composition as it is affected by ventilation, filtration, emission, coagulation, and deposition. For the present study, the aerosol size distribution was represented by 15 sections spanning the diameter range 0.05–40 μm and by three chemical components—elemental carbon, soil dust, and "other".

Measured outdoor concentrations were used as input to the model as follows. Hourly averaged results from the outdoor midrange OPC were used to compute the total mass concentration per section for sections 2–11, assuming the particle density to be 2.0 g cm^{-3} (see ref 9). The total mass concentration for sections 12–15 was determined from filter-based coarse particle concentration measurements, assuming that the mass is distributed uniformly with the log of the particle diameter. Concentrations of elemental carbon and soil dust were determined from analyses of filter samples. The fine elemental carbon concentrations were partitioned into sections 1–11 by using size distribution data reported by Ouimette (23) for the Los Angeles and Pasadena elemental carbon aerosol. The concentration of soil dust was computed from the aluminum and silicon content of the aerosol with the data of Miller et al. (24) on the percent of these elements in suspended samples of local soil dust. The fine soil dust was apportioned into sections 2–11 in proportion to the size distribution of the total 24-h-average aerosol mass in these sections. For coarse particles both elemental carbon and soil dust were allocated to produce a constant value of $dM/d(\log d_p)$ across sections 12–15, where M is the aerosol mass concentration and d_p is the particle diameter. For section 1, spanning particle diameters in the range of 0.05–0.09 μm,

Table II. Deposition and Filtration Conditions Simulated at Study Sites by Using the Indoor Air Quality Model

case	conditions
	Norton Simon Museum
A	deposition: forced laminar flow; filter F_{A1}: ineffective
B	deposition: homogeneous turbulence in the core of the room; filter F_{A1}: ineffective
C	deposition: forced laminar flow; filter F_{A1}: same efficiency as filter F_{A3}
	Scott Gallery
A	deposition: forced laminar flow
B	deposition: homogeneous turbulence in the core of the room
	Sepulveda House
A	deposition: natural convection flow (0000–1000 and 1500–2400 h), homogeneous turbulence in the core of the room (1000–1500 h)

the total aerosol mass of material other than elemental carbon is unknown, and for this paper that other material is neglected. For sections 2–15, the component "other" was determined by difference between the total aerosol mass and the soil dust plus elemental carbon mass.

For the model calculations, each site was represented as a single well-mixed chamber, with building size and ventilation characteristics as indicated in Figure 1 and Table I. A constant ventilation rate was adopted for the Norton Simon Museum, based on the apparent dominance of the constantly operated mechanical ventilation system over infiltration. Likewise, the rate of outdoor air exchange at the Scott Gallery was taken to be constant, based on the small variance in results from tracer gas decay measurements. At the Sepulveda House, tracer decay data were used to obtain hourly averaged air exchange rates, which were then applied in the model calculations.

Particle removal efficiencies for filters F_{A3} and F_{B1} were based on measurements reported in Figure 2 for particles in the diameter range 0.09–2.3 μm. The efficiencies for particles smaller than 0.09 μm and larger than 2.3 μm in diameter were estimated to be the same as the measured efficiencies for the 0.09–0.13 and 1.7–2.3-μm sections, respectively. The charcoal filters, F_{A2} and F_{B2}, were assumed to have no effect on particle concentrations, on the basis of measurements of the penetration efficiency for F_{A2}. To best reflect the prevailing conditions on the monitoring day for this study, the effectiveness in removing particles of the newly replaced filter F_{A1} was taken to be zero, based on measurements showing its effectiveness to be less than 5% at that time. An additional modeling run (case C, see Table II) was carried out with filter F_{A1} having the same effectiveness as filter F_{A3}. The latter case better represents ordinary conditions at the Norton Simon Museum. [The particle filter material is contained in large rolls. Routinely, the filters are advanced a small fraction (<10%) of their exposed length, thereby maintaining a fairly uniform degree of particle loading. Just prior to the day of monitoring in this study, a new roll of material was installed for filter F_{A1}.]

Aerosol deposition rates were computed for idealized flow conditions by using the data on wall–air temperature differences and near-wall air velocities reproduced in Figure 3. These data were used to determine the hourly average temperature difference between the wall and the air. The temperature differences were than assumed to apply to all surfaces of the building. For the Sepulveda House, particle deposition was computed by using the natural convection description of air flow during 0000–1000 and 1500–2400 PST (20). Homogeneous turbulence in the

Table III. Average Mass Concentration (μg m^{-3}) of Aerosol Components for Study Periods from Filter-Based Measurements and Simulations

	fine			coarse[b]		
	EC[a]	soil dust	total	EC	soil dust	total
			Norton Simon Museum			
outdoor, measured	3.9	1.5	50	2.7	30	81
indoor, measured	0.67	0.15	9.3	0.09	0.25	−2.0
indoor, modeled, case A	0.83	0.36	12.5	0.10	1.0	2.9
indoor, modeled, case B	0.82	0.36	12.4	0.10	1.0	2.9
indoor, modeled, case C	0.62	0.30	10.1	0.004	0.04	0.11
			Scott Gallery			
outdoor, measured	1.5	0.75	26	0.95	6.9	37
indoor, measured	0.16	0.09	4.1	0.01	0.13	2.3
indoor, modeled, case A	0.23	0.08	3.7	0.05	0.32	1.8
indoor, modeled, case B	0.22	0.08	3.6	0.05	0.32	1.8
			Sepulveda House			
outdoor, measured	5.0	2.6	34	1.3	41	117
indoor, measured	5.6	0.86	24	0.75	23	57
indoor, modeled, case A	4.9	2.5	22	0.49	14	40

[a] Elemental carbon particles. [b] Coarse component data are obtained by difference between mass concentration determined for filters in open-faced holders and filters downstream of cyclones with ~2.0-μm-diameter cutpoint. The negative measured value at the Norton Simon Museum results from subtraction of two small and nearly identical measurement results.

core of the building was assumed to dominate deposition processes for the remaining period at this site. At the Norton Simon Museum and at the Scott Gallery, deposition calculations were carried out for two representations of near-wall air flows. As shown in Table II, the base case (case A) calculations were made assuming laminar, forced flow, parallel to the surfaces. Case B calculations were made assuming that the near-wall flows were dominated by homogeneous turbulence in the core of the rooms. A comparison of model and measurement results for particle deposition velocity at these two sites suggests that the actual deposition rates lie between the values predicted for case A and case B conditions at the Scott Gallery and closer to the results for case A relative to case B conditions at the Norton Simon Museum (8).

For deposition calculations based on laminar, forced flow, the free-stream air velocity, U_∞, is required to compute the deposition velocity. For laminar flow conditions, the air velocity probes located at ~0.6 and ~1.2 cm from the wall would be within the momentum boundary layer. The hourly averaged free-stream air velocity was estimated from velocity measurements with these probes using the boundary layer velocity profile for an isolated flat plate (25). This free-stream velocity was assumed to apply for all indoor surfaces. The mean hourly averaged value [± one standard deviation (SD)] of the free-stream air velocity so obtained was 0.33 ± 0.11 m s^{-1} for the Norton Simon Museum and 0.29 ± 0.04 m s^{-1} for the Scott Gallery.

For calculations based on the assumption of homogeneous turbulence, the turbulence intensity parameter, K_e, was estimated on an hourly basis from the air velocity, linearly interpolated to a distance of 1 cm from the wall, by use of the relationship proposed by Corner and Pendlebury (26):

$$K_e = k_o^2 \frac{0.073}{\mu} \frac{\rho u^2}{2} \left(\frac{\mu}{\rho u X} \right)^{1/5} \quad (2)$$

where k_o is von Kármán's constant, taken to be 0.4, μ is the dynamic viscosity of air, ρ is the air density, u is the mean air velocity, and X is the length of the surface in the direction of the mean motion. This equation is based on a correlation for the turbulent drag on a flat plate in an infinite fluid moving parallel to the plate. The turbulence intensity parameter so obtained has a mean hourly aver-

aged value (±1 SD) of 0.56 ± 0.34 s^{-1} for the Norton Simon Museum, 1.25 ± 0.45 s^{-1} for the Scott Gallery, and 0.18 ± 0.04 s^{-1} for the period 1000–1500 PST at Sepulveda House. Note that the results of other studies of pollutant deposition velocity based on measurements inside buildings are bounded approximately by predictions based on the assumption of homogenous turbulence with K_e in the range 0.1–10 s^{-1} (20).

For each site, a comparison is presented in Figure 4 of the results of outdoor measurements, indoor measurements, and the indoor model predictions (under case A conditions) for the total fine particle concentration as a function of time and for the 24-h-average aerosol size distribution. At both the Norton Simon Museum and the Scott Gallery, the fine particle mass concentration indoors is reduced to 15–20% of the outdoor value and coarse aerosol mass present indoors is less than 5% of the outdoor value. The agreement between the indoor model and measurement results ranges from excellent to good: the size distribution and total fine aerosol concentration is predicted quite accurately for the Scott Gallery, while at the Norton Simon Museum the agreement is good except that the aerosol mass concentration for particles having a diameter in the range 0.18–0.35 μm is overpredicted by the indoor air quality model.

At the Sepulveda House, there is little difference between the indoor and outdoor fine particle concentrations. The model reflects this fact; however, the high-frequency fluctuations in the indoor concentration, which result from the high air-exchange rate, are smoothed in the model calculations, an artifact of using hourly averages for outdoor concentrations in the model. (Although the model as used here employs outdoor aerosol concentration data on an hourly averaged basis, there is no intrinsic reason in the method of solution that precludes using data with finer time resolution.) One does not need a detailed mathematical model to predict the indoor concentrations of fine particles based on outdoor values if the building has a high air-exchange rate and no filtration. However, the estimates of particle flux to the walls and other surfaces of the Sepulveda House are complex and utilize the indoor air quality model's capabilities.

Table III compares measurements and predictions of the aerosol constituents, sorted according to particle size into coarse and fine modes. Again, the agreement is good,
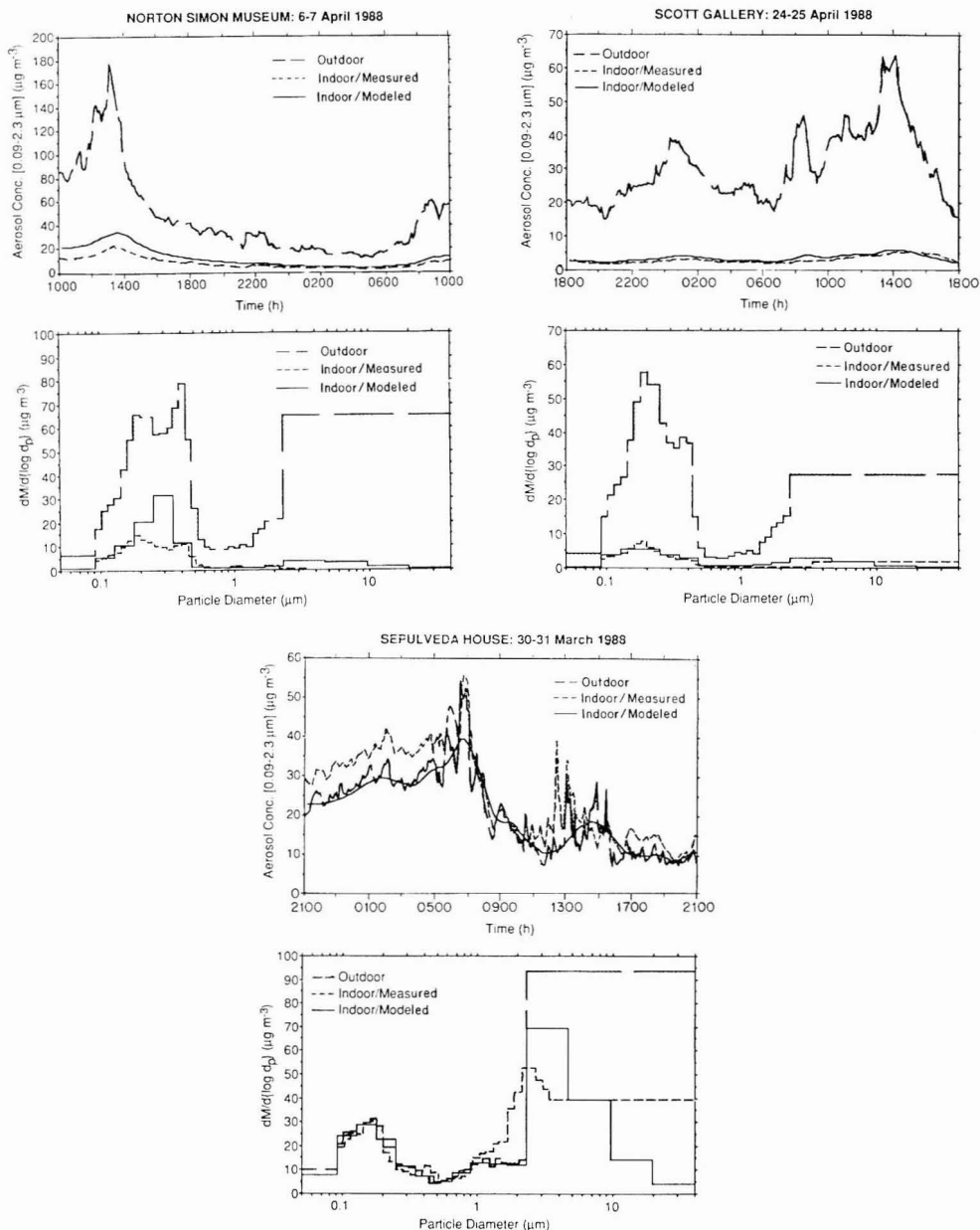
Figure 4. Fine aerosol mass concentration vs time and 24-h-average aerosol size distribution for the three study sites. The figure compares outdoor measurements, indoor measurements, and indoor modeling results. The measured fine particle concentrations are based on the midrange optical particle counters. The coarse component, and the mass in the smallest section of the size distribution, are based on analysis of filter samples. The modeling results for the Norton Simon Museum and the Scott Gallery reflect case A conditions defined in Table II.

particularly for the fine particles for which the input data are more detailed.

Overall, the agreement between model calculations and measurement results justifies confidence in using the model to further consider the dynamics of indoor aerosols. The next two sections explore the fate of particles and the magnitude of the soiling hazard in museums.

Fate of the Particles Entering from Outdoor Air

The design of effective control measures for indoor aerosols can be facilitated by examining the relative

strengths of particle sources and sinks. For the three sites considered in this paper, the overwhelming source of indoor airborne particles during these experiments was due to the entry of outdoor air. The validity of this observation is substantiated by the agreement between measurement and model results. It remains to consider the relative strength of the aerosol sinks: filtration, removal by ventilation, and deposition onto interior surfaces. Coagulation, which serves as a sink for very fine particles, transferring their mass to larger particles, is also considered.

For each simulation and for each particle size section,
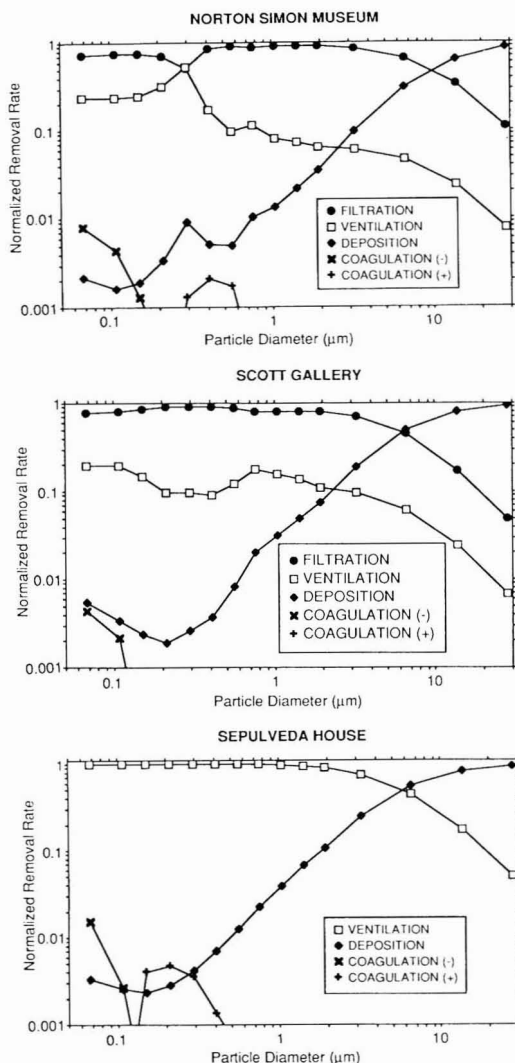
Figure 5. Predicted fate of particles introduced into the buildings from outdoors. The ordinate of each point represents the 24-h-average fraction of the mass in that section brought in from outdoors that is removed by the indicated process. The abscissa reflects the logarithmic midpoint of the range of diameters in the size section. Coagulation (–) indicates a net loss of aerosol mass in the section due to particle coagulation, and Coagulation (+) indicates a net gain. The results shown for the Norton Simon Museum and the Scott Gallery reflect the case A conditions defined in Table II.

the mean rate of removal of aerosol mass by the various sinks was computed and then normalized in each case by the mean rate of supply of aerosol mass in the section from outdoor air. The results for case A, displayed in Figure 5, show that at the Norton Simon Museum and at the Scott Gallery the dominant fate of particles smaller than approximately 10 μm in diameter is removal by the filters. This result is obtained despite the moderately low particle filtration efficiencies, because during its residence time within these museums, air makes a large number of passes through the filters in the recirculating air ducts. At Sepulveda House, particles of this size are predominantly removed by ventilation. Surprisingly, at all three sites the dominant fate of larger particles is deposition onto sur-

faces, essentially entirely by gravitational settling onto the floor and other upward-facing surfaces. This result demonstrates the importance of an effective filter for removing coarse particles from the inlet outdoor air. Under ordinary conditions at the Norton Simon Museum, with filter F_{A1} partially loaded with particles rather than clean, it is expected that 95% or more of coarse particles are removed from the air entering the building.

Deposition constitutes a much smaller sink for fine particles; for example, for particles that are 0.1 μm in diameter, only 0.1–0.5% of those that enter the buildings will ultimately deposit on a surface. This result indicates that detailed calculations of deposition rates are not necessary to obtain accurate predictions of the indoor airborne concentrations of fine particles in these particular buildings.

At all three sites, and for all particle sizes, coagulation is seen to be of little importance. It is not correct to conclude, however, that particle coagulation is never important in indoor air. Conditions at these three sites tend to minimize the rates of coagulation: low particle concentrations at the Norton Simon Museum and at the Scott Gallery imply low particle collision rates, and the high air-exchange rate at Sepulveda House does not allow sufficient time for coagulation to have a significant effect. On the other hand, previous analysis of the fate of cigarette smoke in a room having a low air-exchange rate showed that coagulation was an important sink for particles smaller than 0.2 μm in diameter (4).

Particle Deposition onto Indoor Surfaces

Even though only a small fraction of the fine particles that enter a building deposit onto surfaces, the soiling hazard posed by particle deposition may still be significant. To assess the magnitude of the problem, the rates of particle accumulation onto the floor, walls, and ceiling of each of the three sites were computed by using the indoor air quality model for the 24-h study periods. The results are displayed in Figure 6 in terms of the rate of mass accumulation per unit surface area, J, as a function of particle size and composition. Table IV gives the total rate of accumulation of elemental carbon, soil dust, and the total aerosol onto the walls, floors, and ceilings for each of the three sites. Before considering the significance of the results, it is important to emphasize that the calculations at each site represent predictions for a single day. Thus, extrapolations to longer time periods must be regarded only as indicative estimates. In particular, differences in the deposition rates between sites may reflect differences in the outdoor conditions on the particular days studied, rather than differences in the long-term average rates of soiling. Note, also, that although the calculations are done specifically for the floor, walls, and ceiling, the results are indicative of expected values for other surfaces, such as those of art objects, that have corresponding orientations. Finally, there is preliminary evidence suggesting that particles larger than a few micrometers in diameter deposit onto vertical surfaces at rates that are substantially larger than predicted by the deposition mechanisms included in the indoor air quality model. Thus, deposition rates of aerosol mass to the walls and ceiling probably represent lower bounds, particularly for the soil dust component, which is found primarily in the coarse particle mode.

Given these cautions, the computed total rate of accumulation of elemental carbon particles onto the walls of the three sites is in the range of 0.02–0.7 μg m^{-2} day^{-1}. The corresponding rates for the ceilings are smaller, 0.002–0.5 μg m^{-2} day^{-1}, and are very sensitive to the assumed nature
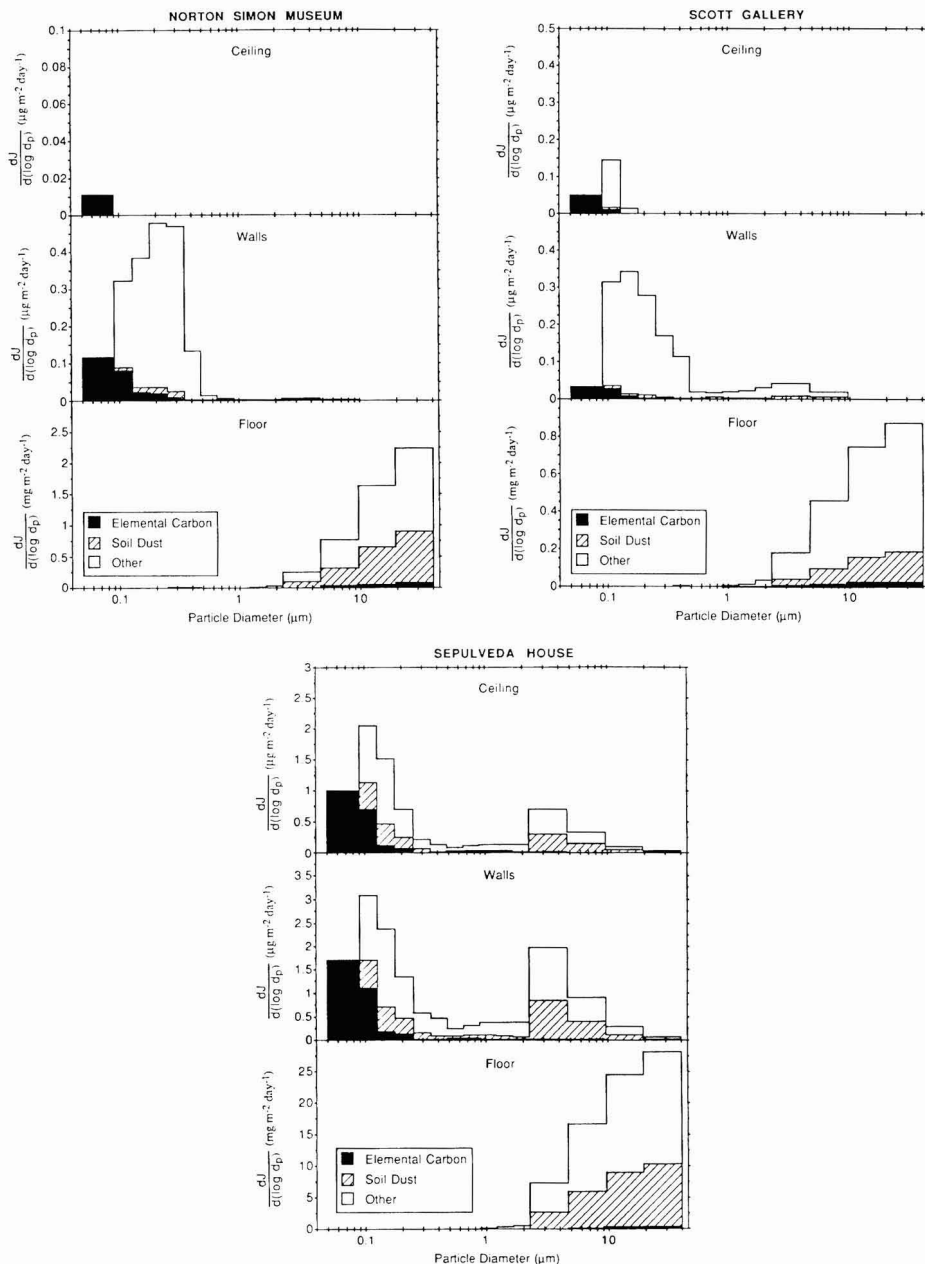
Figure 6. Predicted average rate of accumulation, based on the single study day, of aerosol mass as a function of particle composition and size for three major surface orientations. Note that the vertical axes have different scales; in particular, the mass unit for the floors is milligram, compared with microgram for the other surfaces. The results shown for the Norton Simon Museum and the Scott Gallery reflect the case A conditions defined in Table II.

of near-surface air flow. For forced laminar flow conditions (case A), gravitational settling is effective in reducing deposition of ~0.1-μm particles onto the ceiling. For homogeneous turbulence (case B), however, eddy diffusivity dominates gravitational settling for the very fine elemental carbon particles, and the deposition rate is about the same for the ceiling as for the walls. The rates of accumulation of elemental carbon onto the floors are much larger, 2–50 μg m^{-2} day^{-1} for the Norton Simon Museum, 20 μg m^{-2} day^{-1} for the Scott Gallery, and almost 300 μg

m^{-2} day^{-1} for Sepulveda House. The particle sizes associated with volume-weighted elemental carbon deposition onto these surfaces are quite distinct: predominantly 0.05–0.3 μm for the walls and ceiling, compared with 4–40 μm for the floor. However, considered in terms of the rate of accumulation of projected particle cross-sectional area [probably the appropriate scale for assessing the rate of soiling (27)], the deposition of fine particles onto the floor has a significance comparable with the deposition of coarse particles.

	EC[a]	soil dust[b]	total
	Norton Simon Museum—Case A		
ceiling	0.003	(0.000)	0.003
walls	0.050	(0.010)	0.30
floor	52	560	1540
	Norton Simon Museum—Case B		
ceiling	0.54	(0.10)	3.6
walls	0.64	(0.23)	6.2
floor	53	560	1540
	Norton Simon Museum—Case C		
ceiling	0.002	(0.000)	0.002
walls	0.039	(0.007)	0.24
floor	2.4	23	67
	Scott Gallery—Case A		
ceiling	0.015	(0.001)	0.036
walls	0.017	(0.008)	0.22
floor	19	130	710
	Scott Gallery—Case B		
ceiling	0.26	(0.08)	3.0
walls	0.29	(0.13)	3.9
floor	19	130	710
	Sepulveda House—Case A		
ceiling	0.40	(0.32)	1.4
walls	0.69	(0.70)	2.8
floor	280	8500	24,000

[a] Elemental carbon particles. [b] The soil dust results for walls and ceilings represent lower bounds. Inertial effects, which may be important for coarse particle deposition to these surfaces, are not included in the model predictions of deposition.

Because of its lower rate of accumulation, soil dust appears to pose a smaller soiling hazard than elemental carbon for the ceiling and walls at the Norton Simon Museum and at the Scott Gallery. However, the rates of accumulation of soil dust onto the floor at those two sites are 7–10 times larger than those of soot. These differences are a consequence of the fact that soil dust, being mechanically generated, is found predominantly in the coarse particle mode and settles onto upward facing surfaces under the influence of gravity, whereas elemental carbon, produced in combustion systems, is found primarily in fine particles for which deposition occurs to surfaces of any orientation by a combination of advective diffusion and thermophoresis (20).

The much higher flux density of particle mass to the floor compared with values for the ceiling and walls points to another limitation of the calculations employed here in assessing the soiling hazard for certain surfaces. In these calculations, vertical surfaces are assumed to be smooth; however, many real surfaces are rough. Through gravitational settling, large particles will deposit preferentially on the upward-facing portions of surface roughness elements. Because contrast is readily detected, nonuniform deposition of elemental carbon particles by such a process would probably lead to noticeable visual degradation of the object more rapidly than an equivalent rate of deposition spread uniformly over the surface.

To gain perspective on the significance of these results in the context of protecting museum collections, a characteristic time interval for soiling was computed. Previous studies have shown that a white surface is perceptibly darkened when 0.2% of its area is effectively covered either by black dots that are too small to be distinguished individually (27) or by black particles (28). Since the light-absorbing properties of elemental carbon particles

	ceiling		walls		floor	
case	$\tau_{s;EC}$	$\tau_{s;SD}$	$\tau_{s;EC}$	$\tau_{s;SD}$	$\tau_{s;EC}$	$\tau_{s;SD}$
	Norton Simon Museum					
A	180		12	(170)	1.2	0.2
B	1.2	(12)	1.1	(8.4)	0.6	0.2
C	230		16	(210)	4.7	3.0
	Scott Gallery					
A	35	(720)	40	(240)	2.9	0.6
B	2.5	(19)	2.4	(16)	1.4	0.6
	Sepulveda House					
A	1.5	(6.2)	0.9	(4.1)	0.15	0.01

[a] Based on the predicted deposition rates for the single study day at each site. The characteristic soiling time is computed as the time required for the accumulation of sufficient elemental carbon particles ($\tau_{s;EC}$) or soil dust particles ($\tau_{s;SD}$) onto a smooth surface to effectively cover 0.2% of the surface area. For black particles on a white surface, this degree of coverage has been shown to yield perceptible soiling (27, 28). [b] Predictions of particle deposition rate do not include inertial effects, which may be important for coarse particle sizes, where most of the soil dust is found. Therefore, the characteristic times for perceptible soiling to occur on walls and ceilings due to soil dust deposition represent upper limits. For floors, deposition of coarse particles is dominated by gravitational settling, and so the estimates are believed to be accurate.

differ from those of soil dust, the degree of surface coverage needed to produce perceptible soiling probably differs for the two components. The information needed to combine the accumulation rate of the two components into a single soiling rate is lacking, and so, for the present study, the characteristic times for soiling by elemental carbon particles ($\tau_{s;EC}$) and by soil dust ($\tau_{s;SD}$) were estimated as the time required to achieve 0.2% coverage of a surface by these components independently. These times were computed for each surface orientation and each model case, given the deposition rates as a function of size (as displayed for case A in Figure 6), and assuming that, within each section, the deposited elemental carbon or soil dust can be considered to exist as pure, spherical particles with a diameter equal to the logarithmic mean for the section. Then, the characteristic time for a perceptible deposit of either component to accumulate is given by

$$\tau_{s;c} = 0.002 \left[\sum_i \left(\frac{3}{2d_i} \right) \left(\frac{\Delta J_{i;c}}{\rho} \right) \right]^{-1} \quad (3)$$

where c represents the soiling component (EC or SD), d_i is the particle diameter for section i, $\Delta J_{i;c}$ is the rate of mass deposition of component c for section i, and ρ is the particle density.

The resulting values for $\tau_{s;c}$ are given in Table V for the three sites. For walls and ceilings, deposition of elemental carbon particles appears to constitute a greater soiling hazard than the deposition of soil dust. Characteristic soiling times associated with elemental carbon particle deposition are in the range 1–40 years for walls. For ceilings, the corresponding predictions are in the range 1–35 years except for the Norton Simon Museum under the assumption of forced laminar flow for which the estimated characteristic soiling time is 2 centuries. For floors, predicted characteristic soiling times due to soil dust deposition are shorter than those due to elemental carbon deposition. The values of $\tau_{s;SD}$ range from as short as 3 days at the Sepulveda House to as long as 3 years for the Norton Simon Museum with an effective intake filter (case C). Among the three surface orientations, predictions for the ceilings must be regarded as the least certain, since,

as with the walls, the deposition rates depend critically on near-surface air flows, and no measurements of flows near ceilings were made in this study.

With the exception of the few large values of τ_s for the ceiling of the Norton Simon Museum, these soiling periods are short relative to the time scales over which museum curators wish to preserve their collections. In some respects, however, these estimates are conservative. For example, the degree of effective area coverage by black particles needed to produce perceptible soiling would be a minimum for a purely white surface for which the 0.2% result applies. The surfaces of heavily pigmented paintings could probably accrue a greater deposit before soiling became perceptible.

As expected, the soiling problem is most acute at the Sepulveda House because of its high ventilation rate and lack of particle filtration. Taking the geometric mean of the results for cases A and B as an estimate of the true soiling rates at the Norton Simon Museum and the Scott Gallery, soiling rates due to elemental carbon deposition at these sites are approximately 5–10 times lower than at the Sepulveda House. For soil dust deposition onto upward surfaces, the difference between the characteristic soiling time at the Sepulveda House and those at the other two sites is even greater. It is noteworthy that the effectiveness of the supply air filter at the Norton Simon Museum in lengthening the soiling periods (compare cases A and C) is not large for soiling by elemental carbon particles. This result is obtained because the deposition of fine particles onto the floor contributes significantly to $\tau_{s;EC}$, and the inlet filter is relatively ineffective in removing these particles. On the other hand, an effective supply air filter at the Norton Simon Museum does significantly extend the characteristic soiling time for the floor associated with soil dust deposition.

Discussion

The results of this study serve several purposes. First, they substantially increase the basis for confidence in the ability to predict the size distribution and chemical composition of the indoor aerosol by use of the indoor air quality model previously described (4). Second, they provide considerable information beyond that previously available about the indoor–outdoor aerosol relationship for two types of buildings. (The Norton Simon Museum and the Scott Gallery are representative of modern commercial buildings, apart from their relatively high ratio of recirculated air to outdoor make-up air flow rates and the presence of activated carbon filters. Sepulveda House is representative of many older buildings, at least those in temperate climates.) Third, the results constitute, to our knowledge, the first detailed estimates of the cause-and-effect relationships that lead to soiling of indoor surfaces. The information about the size of particles that contribute to soiling is crucial in designing efficient control measures. Estimates of the rate of soiling will help concerned officials make informed decisions about how much of their limited resources to devote to control measures.

In addition to the progress marked by the results reported here, related papers address associated issues: a direct and sensitive test of the deposition calculations (8), and an evaluation of options available for controlling the soiling of indoor surfaces (29). Because of the nature of the experiments reported here, particle generation due to occupant activities and other indoor sources, to the extent that it occurs, will be underrepresented. Data from long-term studies suggest that the provision of outdoor air for ventilation is the largest source of airborne particles in five southern California museums—including the three

considered here (5). Nevertheless, to protect works of art from soiling, it is important to limit indoor aerosol sources (29).

The other hazard for artwork associated with the deposition of particles—corrosion and other chemical attack—has not been addressed specifically here. The potential for chemical damage caused to the surfaces of art objects from particle deposition should be investigated.

In addition to these topics, there is a need for further investigation of the relationship between the deposition rate of elemental carbon and other particles and the rate of optical degradation of surfaces. Results of such studies are needed to refine estimates of the time periods over which perceptible soiling occurs.

With the capability of testing candidate protection measures and ventilation system designs in advance of their construction by using a model such as the one employed here, the ability to protect artwork from soiling due to the deposition of airborne particles will improve. It may become not only possible but practical to greatly increase the time periods over which artwork can be preserved while retaining the visual qualities given by the artist.

Literature Cited

(1) Thomson, G. *The Museum Environment*; Butterworths: London, 1978.
(2) Yocum, J. E. *J. Air Pollut. Control Assoc.* **1982**, *32*, 500–520.
(3) Baer, N. S.; Banks, P. N. *Int. J. Museum Manage. Curatorship* **1985**, *4*, 9–20.
(4) Nazaroff, W. W.; Cass, G. R. *Environ. Sci. Technol.* **1989**, *23*, 157–166.
(5) Ligocki, M. P.; Salmon, L. G.; Fall, T.; Jones, M. C.; Nazaroff, W. W.; Cass, G. R. Characteristics of airborne particles inside Southern California museums. California Institute of Technology, Pasadena (manuscript in preparation).
(6) Nazaroff, W. W.; Cass, G. R. *Environ. Sci. Technol.* **1986**, *20*, 924–934.
(7) Ligocki, M. P.; Liu, H. I. H.; Cass, G. R.; John, W. Measurements of particle deposition rates inside Southern California museums, submitted for publication in *Aerosol Sci. Technol.*
(8) Nazaroff, W. W.; Ligocki, M. P.; Ma, T.; Cass, G. R. Particle deposition in museums: Comparison of modeling and measurement results, submitted for publication in *Aerosol Sci. Technol.*
(9) Nazaroff, W. W. Ph.D. Thesis, California Institute of Technology, Pasadena, CA, 1989; pp 200–206.
(10) Gray, H. A.; Cass, G. R.; Huntzicker, J. J.; Heyerdahl, E. K.; Rau, J. A. *Environ. Sci. Technol.* **1986**, *20*, 580–589.
(11) John, W.; Reischl, G. *J. Air Pollut. Control Assoc.* **1980**, *30*, 872–876.
(12) Johnson, R. L.; Shah, J. J.; Cary, R. A.; Huntzicker, J. J. In *Atmospheric Aerosol: Source/Air Quality Relationships*; Macias, E. S., Hopke, P. K., Eds.; ACS Symposium Series 167; American Chemical Society: Washington, DC, 1980; pp 223–233.

(13) Cary, R. Presented at the Third International Conference on Carbonaceous Particles in the Atmosphere, Berkeley, CA, October 1987.

(14) Dzubay, T. G. *X-ray Fluorescence Analysis of Environmental Samples*; Ann Arbor Science: Ann Arbor, MI, 1977.

(15) Mulik, J.; Puckett, R.; Williams, D.; Sawicki, E. *Anal. Lett.* 1976, 9, 653–663.

(16) Bolleter, W. T.; Bushman, C. T.; Tidwell, P. W. *Anal. Chem.* 1961, 33, 592–594.

(17) Cass, G. R.; Conklin, M. H.; Shah, J. J.; Huntzicker, J. J.; Macias, E. S. *Atmos. Environ.* 1984, 18, 153–162.

(18) *ASHRAE Handbook: 1985 Fundamentals*; American Society of Heating, Refrigerating, and Air Conditioning Engineers: Atlanta, GA, 1985; Chapter 22.

(19) Nazaroff, W. W.; Cass, G. R. *J. Aerosol Sci.* 1987, 18, 445–454.

(20) Nazaroff, W. W.; Cass, G. R. Mass-transport aspects of pollutant removal at indoor surfaces. *Environ. Int.*, in press.

(21) Schiller, G. E. Ph.D. Thesis, University of California, Berkeley, CA, 1984.

(22) Bejan, A. *Convection Heat Transfer*; Wiley: New York, 1984.

(23) Ouimette, J. Ph.D. Thesis, California Institute of Technology, Pasadena, CA, 1981.

(24) Miller, M. S.; Friedlander, S. K.; Hidy, G. M. *J. Colloid Interface Sci.* 1972, 39, 165–176.

(25) Schlichting, H. *Boundary-Layer Theory*, 7th ed.; McGraw-Hill: New York, 1979; pp 315–321.

(26) Corner, J.; Pendlebury, E. D. *Proc. Phys. Soc., London* 1951, B64, 645–654.

(27) Carey, W. F. *Int. J. Air Pollut.* 1959, 2, 1–26.

(28) Hancock, R. P.; Esmen, N. A.; Furber, C. P. *J. Air Pollut. Control Assoc.* 1976, 26, 54–57.

(29) Nazaroff, W. W.; Cass, G. R. Protecting museum collections from soiling due to the deposition of airborne particles. California Institute of Technology, Pasadena. Manuscript in preparation.

Liquid Chromatography Analysis of Chloride and Nitrate with "Negative" Ultraviolet Detection: Ambient Levels and Relative Abundance of Gas-Phase Inorganic and Organic Acids in Southern California

Daniel Grosjean

DGA, Inc., 4526 Telephone Road, Suite 205, Ventura, California 93003

■ A simple, cost-effective method is described for the determination of chloride and nitrate in environmental samples using conventional liquid chromatography equipment and "negative" photometry detection, i.e., the detection of weakly UV-absorbing analytes in a strongly UV-absorbing eluent. Method performance and validation are described, along with an example of application to the simultaneous measurements of gas-phase inorganic (nitric, hydrogen chloride) and organic (formic, acetic) acids in ambient air. During a 10-day period of intensive measurements at a southern California smog receptor site, ambient levels of nitric acid and hydrogen chloride ranged up to 16.6 and 2.7 ppb, respectively (4-h samples). However, organic acids were more abundant than inorganic acids and accounted for 73.5% (ppb basis) of the total gas-phase acids.

Introduction

The determination of low concentrations of chloride and nitrate in environmental samples is of importance with respect to several issues, including drinking water quality, effluent control, atmospheric aerosols, and acid deposition. Conventional ion chromatography, with aqueous buffer eluent (e.g., carbonate/bicarbonate), suppressor, and conductivity detection, has been generally used for the determination of nitrate, chloride, and other anions in environmental samples (1, 2). However, recent progress in liquid chromatography column technology has made it possible to measure a number of ionic analytes by single-column liquid chromatography (i.e., no suppressor needed) with ultraviolet detection. Desirable features of this approach include the inherent selectivity of UV detection (obviously not possible with conductivity detection) and the possibility of using standard, inexpensive liquid chromatography equipment that is already available for other applications in many environmental laboratories. Thus, ultraviolet detection has been applied recently to the determination of inorganic anions (3), phenols (4, 5), aromatic acids (5, 6) and aliphatic carboxylic acids (6, 7).

The method described here involves ultraviolet detection. However, instead of the usual configuration of direct UV detection of analytes using a non-UV absorbing eluent, we elected to use a strongly absorbing eluent, i.e., an aromatic acid. In this way analytes that absorb only weakly are recorded as "negative" peaks. This detection mode, "negative" photometry (or "indirect" photometry), allows for substantially better detection limits than would be achieved by direct photometric detection of weakly absorbing anions, organic or inorganic. A similar configuration with conductivity detection has been proposed by Okada (8), who took advantage of the high conductivity of aqueous OH^- to measure aromatic acids and phenols as negative peaks in a KOH eluent.

Also described in this paper is an application of our method to the determination of the relative abundance of gas-phase inorganic and organic acids in ambient southern California air, with focus on the most abundant acids in each category, i.e., nitric acid, hydrogen chloride, formic acid, and acetic acid. While these acids have been measured before (ref 6, 9–11, and references therein), simultaneous measurements have seldom been carried out. The relative abundance of inorganic and organic acids in urban air is relevant to population exposure, acid deposition, and other air quality issues.

Experimental Methods

Analytical Protocol. All analyses were carried out with inexpensive, standard liquid chromatography equipment, including a SSI Model 300 pump, a Valco injection valve, a Perkin-Elmer LC 75 UV–visible detector (190–600 nm)

and a Hitachi D-2000 integrator. Analytical conditions for the basic configuration (other conditions were investigated; see Results) were as follows: Hamilton PRP-X-100 low-capacity anion-exchange resin column [poly(styrene–divinylbenzene)–trimethyl ammonium, 10-μm spherical particles, exchange capacity, 0.19 mequiv/g; see ref 12 for details]; eluent, 1.5 mM phthalic acid buffered (pH = 4) with 0.8 mM sodium tetraborate decahydrate; eluent flow rate, 1.0 mL/min; detection wavelength, 248 or 290 nm; absorbance, full-scale setting 0.02; injection volume, 50 μL. Quantitative analysis involved the use of external standards, i.e., dilute eluent solutions of chloride and nitrate (free acids or sodium salts) at concentrations bracketing those of interest for ambient air measurements, i.e., 5–500 ng per injection. In this range of concentrations, negative absorbance (i.e., peak height and peak area) vs concentration was linear for both nitrate and chloride. The corresponding calibration curves had near-zero intercepts, slopes with relative standard deviations of less than 5%, and correlation coefficients of at least 0.99.

Sampling Protocol. Air samples were collected on the Citrus College campus in Glendora, CA, some 40 km ENE of downtown Los Angeles. The samples were collected during the Carbon Species Methods Comparison Study (CSMCS) on August 12–21, 1986, according to a sampling schedule common to all CSMCS participants and involving the collection of consecutive 4- or 8-h samples. Filter packs housed in open-face 47-mm-diameter dual filter holders were used to collect the acids of interest with calibrated flow meters and Barnant Air Cadet dual head sampling pumps. Each filter pack included a Teflon filter upstream (Sartorius, 1.2-μm-diameter pore size, 47-mm diameter) to remove particulate matter, including particulate nitrate, chloride, formate, and acetate, if any. Downstream filters, all 47-mm diameter, were nylon, carbonate-impregnated, and alkaline-impregnated for the collection of gas-phase nitric acid, hydrogen chloride, and organic acids, respectively. Nylon filters (Sartorius, 0.45-μm pore size) were washed with dilute aqueous KOH and rinsed with deionized water prior to use in order to remove impurities, including chloride and nitrate. Carbonate-impregnated and alkaline-impregnated glass fiber filters (Gelman AE) were prepared by using 2% aqueous solutions of sodium carbonate and HPLC-grade methanol solutions of 0.5 N potassium hydroxide, respectively.

Sampling flow rates were in the range 8–15 L/min, depending upon filter pack configuration. Teflon–nylon, Teflon–alkaline, and Teflon–carbonate filter packs were operated side by side in all cases. The collection efficiency of nylon filters for nitric acid, of carbonate-impregnated filters for hydrogen chloride, and of alkaline-impregnated filters for formic acid and acetic acid was established in previous studies (11, 13, 14).

Sample Handling and Storage. Before sampling, all downstream filters were individually stored in the dark at refrigerator temperature in Petri dishes sealed with Parafilm. After sampling, each downstream filter was promptly placed in a glass vial sealed with a Teflon-lined screw cap and containing 10 mL of deionized water and 40 μL of HPLC-grade chloroform added as a biocide. The vials were stored refrigerated in the dark. The addition of a biocide is critical to sample stability (7); chloroform was selected after verifying that its presence does not interfere with the determination of the analytes of interest.

Sample Analysis. After sonication for 20 min in their original vials, sample extracts were injected directly with a syringe equipped with an in-line 0.2-μm filter, which was replaced after each injection. Nylon filter extracts were analyzed directly for nitrate by negative photometry, as is described above. Aqueous extracts of carbonate-impregnated filters, which contained large amounts of carbonate/bicarbonate, were first diluted 10-fold to improve base-line stability and were analyzed for chloride by negative photometry, as is described above. Comparison of aqueous and carbonate-containing chloride standards indicated a lower detector response to chloride in the presence of carbonate. Thus, all chloride calibration curves were prepared with chloride standards containing the same amount of carbonate as that used for preparation of the carbonate-impregnated filters. Formate and acetate were analyzed by liquid chromatography with ultraviolet detection using a different column and conditions described elsewhere (7). Laboratory blanks, field controls, and calibration standards were analyzed along with each batch of samples. Replicate analyses were carried out on 10% of the samples and of the corresponding blanks, controls, and standards.

Results and Discussion

Analytical Performance. With 50-μL injections, analytical detection limits (signal to noise ratio, 5) were 17 ng for nitrate and 6 ng for chloride. Column resolution was not affected by hundreds of consecutive 50-μL injections. Larger samples can be analyzed, e.g., 200–300 μL, but we have not investigated their long-term effect on column performance. Comparison of calibration curves constructed from freshly prepared standards indicated good system stability, with slopes identical within 10% over a 6-month period during which many batches of standard solutions and field samples were injected.

Multiple injections of calibration standards yielded relative standard deviations (RSD) of ±4% for 50–200 ng of analyte injected (n = 10) and ±12% for 20–50 ng of analyte injected (n = 10). The corresponding RSD for multiple injections of field samples were ±15% for ambient air samples (aqueous extracts of filter samples, range 15–200 ng, n = 6) and ±10% for aqueous samples (dew, fog, and rain water samples, n = 6). RSD for colocated ambient air samples were ±17% for chloride (range 15–200 ng, n = 7) and ±14% for nitrate (range 20–300 ng, n = 7). For a typical air sample collected for 4 h at a sampling flow rate of 15 L/min (volume of air sampled, 3.6 m^3), the analytical detection limits correspond to ambient air detection limits of 0.36 parts per billion (ppb) for nitric acid and 0.22 ppb for hydrogen chloride.

We verified that other anions unavoidably present along with nitrate and chloride in aqueous extracts of air samples did not coelute or otherwise interfere under the conditions employed. Anions tested included formate, acetate, oxalate, some 20 other organic acids, both aliphatic and aromatic, sulfate, sulfite, carbonate, bicarbonate, and nitrite. A sensitive method for nitrite determination by liquid chromatography with UV detection is described in ref 6.

Other combinations of columns and eluents were investigated, all in the negative photometry mode with aromatic acids as eluents. A conductivity detector (Waters Associates) was sometimes employed along with the UV detector for comparison. The results are summarized in Table I and may be useful for the determination of chloride, nitrate, or both in environmental samples or other complex sample matrices.

Ambient Levels of Nitric Acid and Hydrogen Chloride. As an example of application, ambient levels of nitric acid and of hydrogen chloride were measured in Glendora, CA, along with those of formic acid and acetic acid. For sampling with Teflon–nylon filter packs, the convention suggested by Grosjean (14) was adopted, i.e.,

Table I. Selected Liquid Chromatography Methods for Negative Photometry Analysis of Chloride and Nitrate

column[a]	eluent	analyte	retentn time, min	detection limit, µg/mL	
				UV (nm)	conductivity
SAX	2 mM phthalic acid	chloride	19	12.5 (247)	
		nitrate	28	12.5 (247)	
SAX	2.6 mM benzoic acid	chloride	6	8.5 (247)	
		nitrate	8	8.0 (247)	
WAX	phthalic acid + sodium tetraborate, pH 4.0	chloride	8	0.5 (248)	0.5
		nitrate	9	0.9 (248)	0.9
PRP-X100	phthalic acid + sodium tetraborate, pH 4.0	chloride	8	0.6 (248)[b]	1.2
		nitrate	12	0.8 (248)[b]	1.4
PRP-X-300	phthalic acid + sodium tetraborate, pH 4.0	chloride	1.8[c]	0.01 (248)	
		nitrate	7.3[d]	0.02 (248)	

[a] SAX, Whatman Partisphere, 5-µm silica-bonded amino anion-exchange cartridge; WAX, Whatman Partisphere cartridge, 5-µm silica; PRP-X-100, Hamilton low-capacity anion-exchange resin, 10-µm poly(styrene–divinylbenzene)–trimethyl ammonium; PRP-X-300, anion-exclusion resin, 7-µm poly(styrene–divinylbenzene) sulfonate. [b] Similar detection limits are also obtained at 290 nm. [c] Would coelute with formate, if any present in sample. [d] Would coelute with benzoate, pyruvate, and oxalate, if any present in sample.

Table II. Ambient Concentrations of Nitric Acid (ppb), Glendora, CA, August 12–21, 1986

	sampling period				
date	8–12	12–16	16–20	20–24	0–8
8/12–13	1.83	1.8	2.5	0.75	0[a]
8/13–14	1.71	6.1	4.2	1.33	0.51
8/14–15	0.63	7.3	5.8	1.34	1.1
8/15–16	0.8	8.7	7.0	1.0	0.5
8/16–17	2.5	16.6	3.8	0[a]	0.16
8/17–18	2.4	6.6	5.9	1.70	0.27
8/18–19	1.0	3.5	1.0	0	0
8/19–20	3.3	2.6	1.45	0.4	0.53
8/20–21	1.3	5.1	2.9	0.9	0.69
av, ppb	1.72	6.48	3.84	0.82	0.42

[a] Below detection.

Table III. Ambient Concentrations of Hydrogen Chloride (ppb), Glendora, CA, August 12–21, 1986

	sampling period				
date	8–12	12–16	16–20	20–24	0–8
8/12–13	1.77	1.93	0.77	1.48	0.71
8/13–14	1.01	0.93	0.98	0.22	0[a]
8/14–15	2.53	1.99	0.91	0.69	0.22
8/15–16	2.45	1.26	0.48	0.53	0.14
8/16–17	0.57	0.32	1.40	0.24	0.85
8/17–18	0.55		1.35	1.27	0.52
8/18–19	2.68	2.65	0.50	1.90	0.61
8/19–20		0.87	1.20	1.46	0.63
8/20–21	0.83	1.15	1.82	1.62	0.79
av, ppb	1.55	1.39	1.04	1.03	0.50

[a] Below detection.

nylon filter collected nitrate is construed to be an upper limit for gas-phase nitric acid. This definition makes allowance for the possible decomposition of particulate nitrate during sampling:

$$NH_4NO_3 \rightleftharpoons NH_3 + HONO_2$$

which would be lost from the upstream Teflon filter, collected on the downstream nylon filter, and thus measured as nitric acid. We adopt here the same convention for hydrogen chloride collected on Teflon-carbonate filter packs, i.e., the carbonate-collected chloride is an upper limit for gas-phase HCl. In this case, allowance is made for the possible decomposition of particulate chloride during sampling:

$$NH_4Cl \rightleftharpoons NH_3 + HCl$$
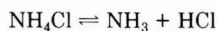
Both equilibria are strongly temperature dependent, with ammonium chloride being even less stable than ammonium nitrate at ambient temperature (equilibrium constants of ~73 and ~27 ppb^2, respectively, at 25 °C; see for example ref 15 and 16). Thus, the positive bias from salt decomposition during sampling may be somewhat higher for hydrogen chloride than for nitric acid. The advantages and limitations of filter packs and other methods for the determination of ambient nitric acid have been discussed by Hering et al. (9). The corresponding analysis of filter pack performance for measuring ambient HCl has yet to be carried out.

With these operational definitions in mind, we have listed in Tables II and III the ambient concentrations of nitric acid and hydrogen chloride, respectively. Four- and eight-hour-averaged nitric acid levels ranged from less than 1 to 16.6 ppb. Nitric acid levels exhibited strong diurnal

Table IV. Literature Data for Ambient Levels of HCl

location	HCl, ppb	ref
over Atlantic Ocean	0.05–0.1	17
rural Ohio	0.4	18
Hampton, VA	0.7–2.1	19
Tucson, AZ	up to 2	20
Tokyo, Japan	0.5–2	13
Claremont, CA	0.1–1.0	21
Los Angeles, CA	0.14–2.9	22
Los Angeles, CA[a]	0.8–1.8[b]	23
Glendora, CA	0.05–2.68	this work
	(mean 1.00, n = 45)	

[a] Nine sites in Los Angeles area. [b] Annual averages.

variations with midafternoon maxima and nighttime minima (Figure 1). These concentrations and their diurnal variations are consistent with those measured at other southern California smog receptor sites (9–11). They reflect photochemical production as well as gas–particle phase partition, the equilibrium being shifted toward particulate nitrate at lower temperature and higher humidity, i.e., at night.

Ambient levels of hydrogen chloride ranged from 0.05 to 2.7 ppb (4- and 8-h-averaged values). Literature data regarding ambient HCl are sparse (13, 17–23) and are summarized in Table IV. It has been suggested (21) that the reaction of nitric acid with sea-salt sodium chloride is a source of HCl in the South Coast Air Basin:

$$NaCl + HONO_2 \rightarrow NaNO_3 + HCl$$
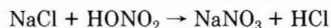
The HCl thus displaced may react with ammonia to form ammonium chloride as indicated above or may react at the surface of coarse alkaline particles. The net result may
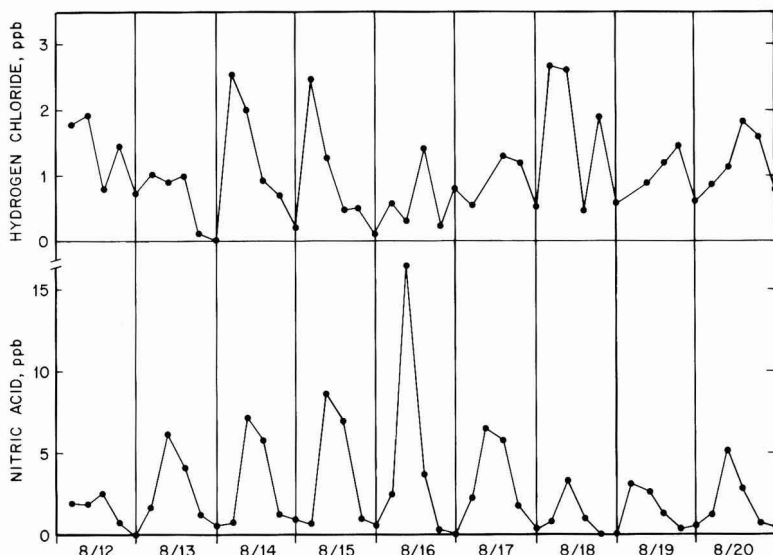
Figure 1. Ambient levels of gas-phase nitric acid and hydrogen chloride, Glendora, CA, August 12–20, 1986.

Table V. Relative Abundance of Inorganic and Organic Acids, Glendora, CA, August 12–21, 1986

	sampling period				
	8–12	12–16	16–20	20–24	0–8
	Volume Basis, ppb				
HCl	1.55	1.39	1.04	1.03	0.50
HONO$_2$	1.72	6.48	3.84	0.82	0.42
HCOOH	5.10	3.43	3.36	3.53	6.34
CH$_3$COOH	4.54	2.84	3.24	3.52	5.55
total	12.9	14.1	11.5	8.9	12.8
organic acids, % of total	74.7	44.3	57.5	79.2	92.8
inorganic acids, % of total	25.3	55.7	42.5	20.8	7.2
	Mass Basis, μg m^{-3}				
HCl	2.25	2.01	1.51	1.49	0.72
HONO$_2$	4.35	16.39	9.71	2.07	1.06
HCOOH	9.59	6.45	6.32	6.64	11.92
CH$_3$COOH	11.13	6.96	7.95	8.63	13.61
total	27.3	31.8	25.5	18.8	27.3
organic acids, % of total	75.8	42.2	56.0	81.1	93.4
inorganic acids, % of total	24.2	57.8	44.0	18.9	6.6

be a shift from coarse chloride (NaCl + Cl$^-$ produced by reaction of HCl with coarse particles) to fine chloride (NH$_4$Cl) plus gaseous hydrogen chloride. However, ambient levels of HCl in Hampton, VA, (19) and Tuscon, AZ, (20) are comparable (~2 ppb) to those measured in southern California and suggest that sources of HCl other than sea salt are likely to exist. More detailed studies of the sources and sinks of urban HCl are obviously needed.

Relative Abundance of Inorganic and Organic Acids. Table V summarizes the relative abundance of inorganic and organic acids in Glendora during the period August 12–21, 1986. During that period, inorganic acids accounted for only a small fraction of the total gas-phase acids in the Basin atmosphere. Formic acid accounted for 24–49% (volume basis, ppb) or 20–44% (mass concentration basis, μg m^{-3}) of the total acids. In the same way, the sum of formic acid and acetic acids accounted for 44–93% (volume basis) and 42–93% (mass basis) of the total acids. The relative contribution of inorganic acids to the total gas-phase acid burden of the atmosphere was highest in the midafternoon (~57%), and lowest at night

(~7%). Formic acid and acetic acid *each* exceeded the sum of the inorganic acids during the 16-h period 8 p.m. to 12 noon and together accounted for 73.5% (ppb basis) of the total gas-phase acids. These results, while limited to a short period at one smog receptor site, underline the importance of including organic acids when assessing the atmospheric acid burden in urban southern California.

Literature Cited

(1) *Ion Chromatographic Analysis of Environmental Pollutants*; Sawicki, E., Mulik, J. D., Wittgenstein, E., Eds.; Ann Arbor Science Publishers: Ann Arbor, MI, 1978.
(2) Grosjean, D.; Nies, J. D. *Anal. Lett.* **1984**, *17*, 89–96.
(3) Williams, R. J. *Anal. Chem.* **1983**, *55*, 851–854.
(4) Naikwadi, K.; Rokushika, S.; Hatano, H. *Anal. Chem.* **1984**, *56*, 1525–1527.
(5) Fung, K.; Grosjean, D. *Anal. Lett.* **1984**, *17*, 475–482.
(6) Grosjean, D.; Van Neste, A.; Parmar, S. *J. Liq. Chromatogr.*, in press.
(7) Grosjean, D. *Environ. Sci. Technol.*, in press.
(8) Okada, T.; Kuwamoto, T. *Anal. Chem.* **1983**, *55*, 1001–1004.
(9) Hering, S. V.; Lawson, D. R. et al. *Atmos. Environ.* **1988**, *22*, 1519–1539.
(10) Grosjean, D. *Environ. Sci. Technol.* **1983**, *17*, 13–19.
(11) Grosjean, D. *Atmos. Environ.* **1988**, *22*, 1637–1648.
(12) Lee, D. P. *J. Chromatogr. Sci.* **1984**, *22*, 327–331.
(13) Okita, T.; Ohta, S. In *Nitrogenous Air Pollutants: Chemical and Biological Implications*; Grosjean, D., Ed.; Ann Arbor Science Publishers: Ann Arbor, MI, 1979; Chapter 17, pp 282–306.
(14) Grosjean, D. *Anal. Lett.* **1982**, *15*, 785–796.
(15) Grosjean, D. *Sci. Total Environ.* **1982**, *25*, 263–275.
(16) Pio, C. A.; Harrison, R. M. *Atmos. Environ.* **1987**, *21*, 1243–1246.
(17) Vierkorn-Rudolph, B.; Bachmann, K.; Schwarz, B.; Meixner, F. X. *J. Atmos. Chem.* **1984**, *2*, 47–63.
(18) Spicer, C. W. *Environ. Int.* **1986**, *12*, 513–518.
(19) Cofer, W. R.; Collins, V. G.; Talbot, R. W. *Environ. Sci. Technol.* **1985**, *19*, 557–560.
(20) Farmer, J. C.; Dawson, G. A. *J. Geophys. Res.* **1982**, *87*, 8931–8942.
(21) Wall, S. M.; John, W.; Ondo, J. L. *Atmos. Environ.* **1988**, *22*, 1649–1656.
(22) Appel, B. R; Tokiwa, Y.; Kothny, E. L.; Wu, R.; Povard, V. *Studies of dry acid deposition in the South Coast Air Basin*. Contract 4-147-32, California Air Resources Board, Sacramento, CA, 1986.
(23) Solomon, P. A.; Fall, T.; Salmon, L. G.; Cass, G. R. *Prepr. Pap. Natl. Meet.—Am. Chem. Soc., Div. Environ. Chem.* **1988**, *28* (No. 2), 72–75.

Chlorination of Cyanoethanoic Acid in Aqueous Medium

Ruud J. B. Peters*

National Institute of Public Health and Environmental Protection, Antonie van Leeuwenhoeklaan 9, 3720 BA Bilthoven, The Netherlands

Ed W. B. de Leer and Leo de Galan

Delft University of Technology, Department of Analytical Chemistry, De Vries van Heystplantsoen 2, 2628 RZ Delft, The Netherlands

■ The reaction of cyanoethanoic acid with chlorine in aqueous medium at different pH values produces dichloroacetic acid, dichloromalonic acid, and trichloroacetic acid as the final products. At pH 4 and 7, dichloroacetonitrile was found as the only intermediate. At pH 10, dichloroacetonitrile, N-chlorodichloroacetamide, N-chlorodichloromalonmonoamide, and N-chlorotrichloroacetamide were detected as the intermediates. The N-chloroamides gave an unexpected reaction with diazomethane producing N-chloroimidates, which were previously erroneously identified as methylated hydroxamoyl chlorides. The identities of the intermediates and final products were confirmed by comparison with synthetic standards.

Introduction

The production of cyano compounds in the aqueous chlorination of amino acids was discovered early this century (*1–3*). The structures of a number of these compounds were confirmed much later by Burleson et al. (*4*) with gas chromatography–mass spectrometry (GC/MS). The presence of chlorinated cyano compounds in drinking water as the result of chlorine disinfection was reported by Trehy and Bieber (*5*, *6*), who identified dihaloacetonitriles (DHAN) and demonstrated that dichloroacetonitrile (DCAN) was produced in the chlorination of as-

partic acid in aqueous medium.

De Leer et al. (*7*) identified 3-cyanopropanoic acid (CPA) and 4-cyanobutanoic acid (CBA) after the aqueous chlorination of terrestrial humic acid (HA). Cyanoethanoic acid (CEA) was not detected in this study, possibly as a result of a rapid conversion to DCAN and dichloroacetic acid (DCA). In a second study (*8*) the production of CPA and CBA was standard confirmed and the amino acids glutamic acid and lysine, respectively, were shown to be potential precursors.

In further chlorination reactions in aqueous medium at different pH values it was shown that CPA and CBA were quite stable. CEA reacted rapidly with chlorine at all pH values producing DCA, dichloromalonic acid (DCMA), and a small amount of trichloroacetic acid (TCA) as the final products. DCAN was detected as the only intermediate at pH 4 and 7. However, at pH 10 several intermediates were detected, which were tentatively identified from their EI and CI mass spectra as the corresponding amides and hydroxamoyl chlorides of DCA, DCMA, and TCA.

The reaction mixture that resulted after chlorination of CEA showed to be mutagenic. Since the hydroxamoyl chlorides are interesting compounds in this respect, we planned to synthesize all the proposed intermediates in the mixture to find out which of them were responsible for the observed mutagenicity. Doing so we would also be able to confirm the identity of the compounds by comparison with the synthetic compounds. During this study we noticed, however, that some of the intermediates had not been correctly identified, partly as the result of an unexpected reaction during the methylation of the reaction

*Corresponding address: Delft University of Technology, Department of Analytical Chemistry, De Vries van Heystplantsoen 2, 2628 RZ Delft, The Netherlands.

products with diazomethane. We report here on a reinvestigation of the reaction of CEA with chlorine in aqueous medium, in which the identification of the intermediates is standard confirmed.

Experimental Section

Chlorination Procedure. The chlorination of CEA was carried out at pH 4.5, 7.2, and 10.0. For pH 4.5 and 7.2, 0.3 M phosphate buffers were used, and for pH 10.0, a 0.3 M carbonate buffer was used.

For the identification studies, a solution (160 mL) of CEA (6.25 mM) and sodium hypochlorite (62.5 mM) was allowed to react in the dark without headspace. After a selected reaction time, the excess of chlorine was destroyed by addition of solid sodium arsenite, 50 g of sodium chloride was added, and the solution was acidified to pH 0.5 with concentrated sulfuric acid. The chlorination products were extracted with three portions of 25 mL of distilled diethyl ether. The extracts were dried with sodium sulfate and methylated by passing a stream of diazomethane gas through the solution. The extracts were analyzed initially on a Varian 3700 gas chromatograph equipped with a flame ionization detector (FID) and a ^{63}Ni electron capture detector (ECD), which were operated simultaneously with an effluent splitter. The GC column used was a 25-m fused-silica capillary CP-SIL-5 column, i.d. 0.22 mm and film thickness 0.12 μm (Chrompack; Middelburg, The Netherlands), while nitrogen was used as the carrier gas. The oven temperature was held at 50 °C for 3 min and then programmed to 280 °C at 8 °C/min. The extracts were further concentrated with a stream of N_2 gas and analyzed by GC/MS with a Hewlett-Packard 5890 gas chromatograph equipped with a 12-m fused-silica capillary HP-1 column, i.d. 0.2 mm and film thickness 0.33 μm, coupled with a Hewlett-Packard 5970B mass selective detector. Temperature was programmed as above, while helium was used as the carrier gas.

For the quantitation of the chlorination products at pH 10, the experiments were conducted on the same scale as above. After reaction times of 2, 5, 15, 30, and 60 min, aliquots (10 mL) were taken for analysis. The excess of chlorine was destroyed; the samples acidified to pH 0.5, extracted with diethyl ether, and methylated with diazomethane. The ether extracts were analyzed by GC/ECD/FID with nonane as the internal standard and GC conditions as before. Retention times and response factors of the chlorination products were determined by injection of standards prepared as described below.

Chemical Standards. DCA and TCA were obtained commercially from J. T. Baker Chemicals B.V.

DCMA was synthesized by addition of 33 mL of sulfuryl chloride to 21 g of malonic acid in 200 mL of ether (9). After all the malonic acid had dissolved, refluxing was continued for 30 min. The solvent was removed at room temperature, first at the rotary evaporator and then at the oil pump, giving a crystalline material, which was recrystallized twice with thionyl chloride yielding 18 g of DCMA, mp 111–112 °C.

Dichloroacetamide (DCAA) was synthesized from chloral hydrate in 65% yield, mp 98–99 °C, as described in ref 10.

Trichloroacetamide (TCAA) was prepared by treating the acid chloride (11) with concentrated ammonia in 72% yield, mp 141–142 °C (12).

Dichloroacetohydroxyamoyl chloride (DAHC) (13) was prepared by slowly adding 30 g of trans-dichloroethylene to a solution of 7 g of AlCl₃ in 30 g of nitrosyl chloride, at −30 °C. After 2 h at −30 °C the mixture was stirred an additional hour at room temperature. Then 50 mL of methylene chloride was added, and the insoluble parts

were removed by filtration. The solvent was removed at the rotary evaporator and the residue distilled under reduced pressure yielding 14 g of the hydroxamoyl chloride, bp 90 °C (20 mmHg).

Trichloroacetohydroxamoyl chloride (TAHC) (14) was synthesized by adding 83 g of chloral hydrate to a cold solution of 35 g of hydroxylamine hydrochloride and 220 g of calcium chloride hexahydrate in 100 mL of water. After 15 min at 60 °C, the mixture was allowed to cool to room temperature. The oily layer was separated and the water layer extracted twice with ether. The combined organic layers were dried (MgSO₄), and the solvent was removed at the rotary evaporator. Distillation under reduced pressure gave 22 g of trichloroacetaldoxime: bp 85 °C (20 mmHg); mp 56 °C. The 22 g of trichloroacetaldoxime was heated to 80 °C and a gentle stream of chlorine gas was passed through the liquid for 3 h. After the mixture cooled to room temperature, 50 mL of methylene chloride was added and the insoluble parts were removed by filtration. The solvent was evaporated at the rotary evaporator and the residue distilled under reduced pressure, giving 9 g of trichloroacetohydroxamoyl chloride: bp 96 °C (15 mmHg); mp 60–62 °C.

Methyl N-chlorodichloroacetimidate dichloroacetonitrile (55 g) was added to a stirred solution of 0.5 g of potassium carbonate in 25 mL of absolute methanol at 0 °C. Water was excluded carefully from the reaction mixture. After 30 min, the mixture was distilled directly, yielding 52 g of methyl dichloroacetimidate, bp 138 °C. Methyl dichloroacetimidate (14.1 g) in 50 mL of benzene was cooled in an ice bath and 12.3 mL of tert-butyl hypochlorite in 12 mL of benzene was added slowly. After stirring for 3 h at room temperature, the solvent was evaporated at room temperature and the residue distilled carefully under reduced pressure, giving 12 g of methyl N-chlorodichloroacetimidate, bp 67 °C (1 mmHg).

Methyl N-chlorotrichloroacetimidate was synthesized in the same way as the dichloro compound; 72 g of trichloroacetonitrile yielded 68 g of methyl trichloroacetimidate, bp 150 °C; 17.5 g of methyl trichloroacetimidate gave 14.4 g of methyl N-chlorotrichloroacetimidate, bp 78 °C (1 mmHg). DCAN and trichloroacetonitrile (TCAN) were synthesized from their amides as described by Fieser (15).

N-chlorodichloroacetamide and N-chlorotrichloroacetamide were prepared as described by Lessard (16).

Results and Discussion

The chlorination of humic materials in aqueous medium produces a number of cyano-substituted compounds. CEA is very interesting in this respect, since it is converted rapidly into DCAN and DCA. At high pH the conversion of DCAN into DCA has been suggested (8) to proceed through dichloroacetohydroxamoyl chloride (DAHC) (eq 1). This intermediate in the reaction of CEA to DCA is interesting from a mutagenicity point of view since the reaction mixture was shown to be mutagenic in the Klebsiella pneumoniae fluctuation test (17).

$$HO_2C\ CH_2-CN \longrightarrow CHCl_2-CN \longrightarrow$$

$$CAZ \qquad\qquad DCAN$$

$$CHCl_2-C\overset{\displaystyle NOH}{\underset{\displaystyle Cl}{\diagdown}} \longrightarrow CHCl_2-CO_2H$$

$$DAHC \qquad\qquad DCA$$

(1)
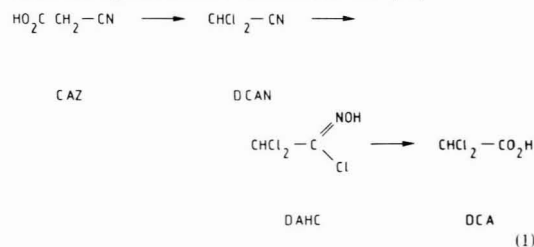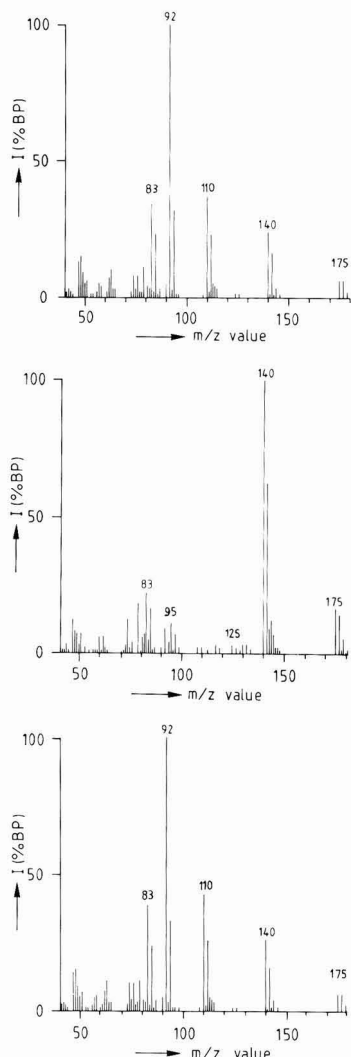
Figure 1. Mass spectra: (a) (top) compound **5/7**, (from ref 8; both isomers showed identical mass spectra); (b) (middle) synthetic methylated dichloroacetohydroxamoyl chloride [m/z 175, 177, 179 (M); 140, 142, 144 (M – Cl); 125, 127, 129 (M – Cl – CH₃); 95, 97, 99 (M – Cl – CH₃ – NO); 83, 85, 87 (CHCl₂)]; (c) (bottom) synthetic methyl *N*-chlorodichloroacetimidate [m/z 175, 177, 179 (M); 140, 142, 144 (M – Cl); 110, 112, 114 (M – Cl – CH₂O); 92, 94 (M – CHCl₂); 83, 85, 87 (CHCl₂)].

Our purpose in this study was to synthesize DAHC together with the hydroxamoyl chlorides of TCA and DCMA, and the corresponding amides, to confirm the earlier structural assignments and to prepare sufficient material for mutagenic testing.

Compounds **5/7**, **9**, and **10/11** (**5/7** and **10/11** are pairs of E/Z isomers) were previously identified as DAHC and the hydroxamoyl chlorides of TCA and DCMA after methylation with diazomethane and interpretation of their EI mass spectra. The mass spectra showed similar fragmentation patterns with an intense fragment at m/z 92/94 (Figure 1a). DAHC and the corresponding trichloro compound were synthesized and compared to compounds **5/7** and **9**, respectively. Trichloroacetohydroxamoyl chloride (TAHC) was synthesized by an addition of hydroxylamine to chloral and subsequent chlorination with

chlorine gas (*14*), while DAHC was prepared by an addition of nitrosyl chloride to *trans*-dichloroethylene (*13*). The synthetic compounds behaved different from the compounds in the reaction mixture since they were only partly methylated by diazomethane. The methylated hydroxamoyl chlorides showed mass spectra (Figure 1b) in which loss of chlorine was the major fragmentation and in which the m/z 92/94 fragments were almost absent. The retention times of the methylated synthetic hydroxamoyl chlorides also differed from compounds **5/7** and **9**. So, we conclude that the compounds **5/7**, **9**, and **10/11** have been erroneously identified as hydroxamoyl chlorides.

The hydroxamoyl chlorides were thought to result from the addition of HOCl to the cyano group of the nitrile (eq 2). Alternatively, addition of HOCl to the cyano group

$$R - C \equiv N \quad + \quad HOCl \longrightarrow$$

E isomer   Z isomer

$$(2)$$
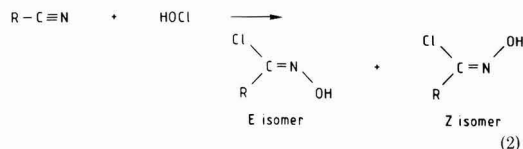
may also result in bonding of chlorine to the nitrogen, producing an imidic acid. Free imidic acids, however, are very instable and have never been detected before (*18*), since they rearrange immediately to the isomeric and more stable *N*-chloroamides (eq 3). On methylation, the hy-

$$R - C \equiv N \ + \ HOCl \longrightarrow R - C{\overset{NCl}{\underset{OH}{}}} \overset{0}{\longrightarrow} R - C{\overset{NHCl}{\underset{0}{}}} \quad (3)$$
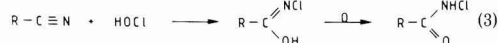
pothetical *N*-chloroimidic acid intermediate would give a methyl *N*-chloroimidate (eq 4), which is more stable than

$$R - C{\overset{NCl}{\underset{OH}{}}} \ + \ CH_2N_2 \longrightarrow R - C{\overset{NCl}{\underset{OCH_3}{}}} \quad (4)$$

the imidic acid itself. We synthesized methyl *N*-chlorodichloroacetimidate and the corresponding trichloro compound to compare them with the compounds **5/7** and **9** in the reaction mixture. The retention times and mass spectra of these synthetic imidates (Figure 1c) were in excellent agreement with those of the compounds **5/7** and **9**, previously identified as hydroxamoyl chlorides. Since **10** and **11** have mass spectra with a fragmentation pattern similar to compounds **5/7** and **9** we expect them to be *N*-chloroimidates as well, and therefore, **10** and **11** are tentatively identified as the E/Z isomers of methyl *N*-chlorodichloromonomalonimidate, although this is not confirmed by synthesis.

The synthesis of the methyl *N*-chloroimidates consists of two steps. In the first step the N-unsubstituted imidates are prepared by a base-catalyzed addition of methanol to the nitriles DCAN and TCAN. In the second step the N-unsubstituted imidates are subsequently chlorinated at the nitrogen by a reaction with *tert*-butyl hypochlorite (eq 5). Comparison of the N-unsubstituted imidates, methyl

$$R - C \equiv N \ + \ CH_3OH \longrightarrow R - C{\overset{NH}{\underset{OCH_3}{}}}$$

$$R - C{\overset{NH}{\underset{OCH_3}{}}} \ + \ (CH_3)_3COCl \longrightarrow R - C{\overset{NCl}{\underset{OCH_3}{}}}$$

$$(5)$$
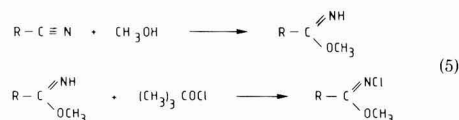
dichloroacetimidate and methyl trichloroacetimidate, with compounds **2** and **4** showed that their retention times and mass spectra were completely identical. Compounds **2** and **4** were previously identified after methylation with diazomethane and were thought to be N-methylated amides (*8*). However, the synthetic amides DCAA and TCAA could not be methylated at all, indicating that **2** and **4** were

Table I. Compounds in the Chlorination Mixture after 1-h Reaction Time at pH 10 before and after Methylation with Diazomethane (the Previous Identifications (8) Are Included)

before methylation	compd no.[a]	after methylation	previous identification[b]
$CHCl_2CO_2H$	1	$CHCl_2CO_2Me$	$CHCl_2CO_2H$
$CHCl_2CONHCl$	2	$CHCl_2COMe=NH$	$CHCl_2CONH_2$
	5/7	$CHCl_2COMe=NCl$	$CHCl_2CCl=NOH$
CCl_3CO_2H	3	CCl_3CO_2Me	CCl_3CO_2H
$CCl_3CONHCl$	4	$CCl_3COMe=NH$	CCl_3CONH_2
	9a	$CCl_3COMe=NCl$	$CCl_3CCl=NOH$
$HO_2CCCl_2CO_2H$	8	$MeO_2CCCl_2CO_2Me$	$HO_2CCCl_2CO_2H$
$HO_2CCCl_2CONHCl$	9b	$MeO_2CCCl_2COMe=NH$	coeluted with 9a
	10/11	$MeO_2CCCl_2COMe=NCl$	$HO_2CCCl_2CCl=NOH$

[a] Compound numbers refer to peak numbers and numbers in the text. [b] Identified after methylation with diazomethane.
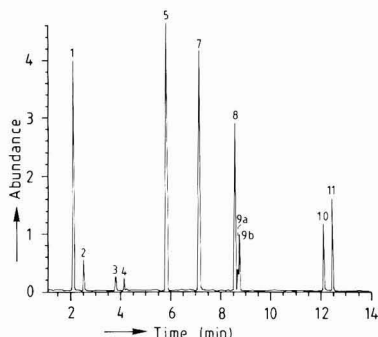
Figure 2. Gas chromatogram of methylated chlorination products of CEA after a reaction time of 1 h at pH 10. Peak numbers refer to numbers in the text and numbers in Table I.

Figure 3. Profiles giving the amounts of intermediates and final products in the reaction mixture during the chlorination of CEA at pH 10 after different reaction times (1, N-chlorodichloroacetamide; 2, dichloroacetonitrile; 3, dichloroacetic acid; 4, other chlorination products).

not amides. Compounds 2 and 4 are now identified as imidates and they are the corresponding N-unsubstituted imidates of compounds 5/7 and 9, respectively.

When we repeated the chlorination experiment at pH 10, we noticed a few differences. Peak 6 in the chromatogram of de Leer (8), identified as an amide, was most of the time absent in our chromatogram while peak 9 (peak = compound number) appeared to consist of two peaks, 9a and 9b (Figure 2). Comparison of the mass spectra showed that 9a was the methyl N-chlorotrichloroacetimidate mentioned before, while 9b showed a fragmentation pattern very similar to compounds 2 and 4. Therefore, we concluded that 9b probably is the corresponding N-unsubstituted imidate of compound 10/11.

Although the methylated compounds 2, 4, 5/7 9a, 9b, and 10/11 are now identified as imidates, it is unlikely that free imidic acids exist in the reaction mixture, and we asked ourselves if the isomeric N-chloroamides could be their precursors. To find out we synthesized N-chlorodichloroacetamide and the corresponding trichloro compound and methylated them with diazomethane. Both N-chloroamides gave a mixture of the N-chloroimidate and the N-unsubstituted imidate (eq 6). This type of reaction

$$R-C{\overset{\text{NHCl}}{\underset{\text{O}}{}}} \xrightarrow{CH_2N_2} R-C{\overset{\text{NCl}}{\underset{\text{OCH}_3}{}}} + R-C{\overset{\text{NH}}{\underset{\text{OCH}_3}{}}} \quad (6)$$
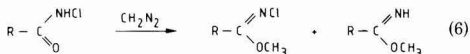
has been reported before by Stieglitz (19) for N-chlorobenzamide, which was converted into methyl N-chlorobenzimidate by the action of diazomethane. A later report (20) showed that two geometrical isomers were formed and that apart from O-methylation some N-methylation occurred, while no reaction took place at the N–Cl bond. In our case, we found that N-chlorodichloroacetamide gave methyl N-chlorodichloroacetimidate (two peaks, E and Z isomers) and also the corresponding N-unsubstituted im-

idate, methyl dichloroacetimidate. N-Chlorotrichloroacetamide gave methyl N-chlorotrichloroacetimidate (one peak only) and the corresponding N-unsubstituted imidate. The ratio between the N-chloroimidate and the N-unsubstituted imidate depended on the excess of diazomethane used and varied between 10:1 and 2:1. All methylation products of both N-chloroamides showed the same retention times and mass spectra as the compounds in the reaction mixture. This indicated that N-chlorodichloroacetamide was responsible for the production of peaks 2 and 5/7, and the corresponding trichloro compound for peaks 4 and 9a. In the same way we expect that the N-chloroimidates 10/11 and the corresponding N-unsubstituted imidate 9b are the methylation products of N-chlorodichloromalonmonoamide. Table I gives a list of the compounds in the reaction mixture, and of the compounds found after methylation of the reaction mixture with diazomethane. The previous identifications are also included in this table. All the compounds, except 10/11 and 9b, are identified by comparison with synthetic standard compounds.
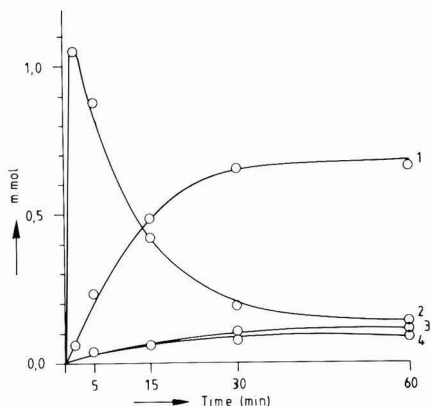
To find out more about the mechanism of the conversion of CEA in DCA and the other products, we stopped the chlorination experiment after selected reaction times and analyzed the products with GC. The results are given in Figure 3.

The first reaction step is a rapid chlorination of CEA due to the electron-withdrawing effect of the substituents (21), producing dichlorocyanoethanoic acid (DCEA), followed by a decarboxylation to DCAN. DCEA was detected
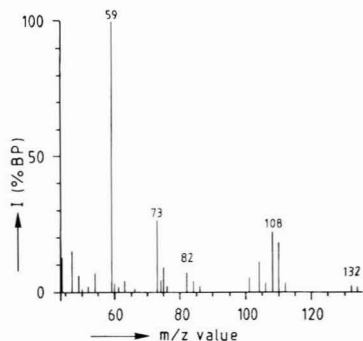
Figure 4. Mass spectrum of methylated dichlorocyanoethanoic acid [m/z 132, 134 (M − Cl); 108, 110, 112 (M − CO_2Me); 82, 84, 86 (CCl_2); 73, 75 (M − Cl − CO_2Me); 59 (CO_2Me)].

Scheme I
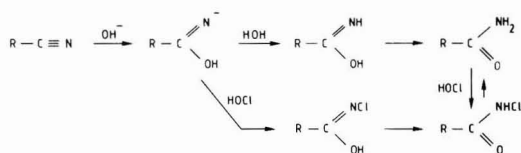
only once when the reaction was stopped after 5 min, and the tentatively identified mass spectrum is given in Figure 4. Trichloroacetonitrile is likely to be produced through a chlorine-induced decarboxylation of DCEA, since chlorination of DCAN under the same conditions as CEA did not give trichloro compounds. After chlorination and decarboxylation the next step is an addition of HOCl to the cyano group, leading to the *N*-chloroamides. This may be a direct addition of HOCl but also a hypochlorite-catalyzed hydrolysis of the cyano group, producing an amide that reacts rapidly with HOCl to give the *N*-chloroamide. Both routes are shown in Scheme I.

Hypochlorite-catalyzed hydrolysis has been shown before in the chloroform formation from trichloroacetone (*22*). Oliver reported that DCAN was quite stable in water for several days, but the presence of chlorine induced a rapid disappearance of DCAN (*23*). We measured the hydrolysis rate of DCAN and found that it was much higher when chlorine was present, as shown in Figure 5a and b.

When DCAA was chlorinated under the conditions used before it reacted rapidly to form the *N*-chloroamide. This may explain peak 6 in the gas chromatogram of de Leer, since peak 6 had the same retention time as DCAA. The mass spectrum of 6, however, can be explained in more than one way.

The last step in the reaction sequence is the hydrolysis of the *N*-chloroamides. In most cases *N*-haloamides will yield amines, which are the products of the Hofmann rearrangement. However, hydrolysis of *N*-chloroamides containing strong electron-withdrawing groups, as an alternative to the Hofmann rearrangement, has been observed (*24*). The *N*-chloroamides showed to be quite stable in water for several days at different pH values. However, when chlorine was present, the *N*-chloroamides were easily hydrolyzed. Especially at lower pH values the hydrolysis was complete within a few minutes, while at pH 10, 50% of the material was hydrolyzed after 8 h. The reaction of CEA with chlorine is visualized in Scheme II. The *N*-chloroamides were not detected as intermediates in the reaction at pH 4 and pH 7 and after a 1-h reaction time; only the acids DCA (**1**), TCA (**3**), and DCMA (**8**), which
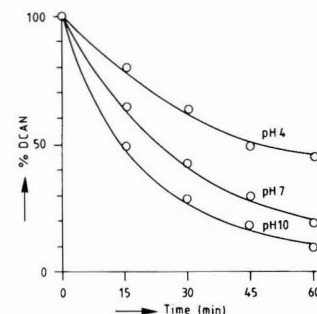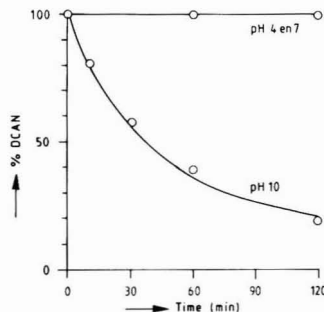
Figure 5. Hydrolysis of DCAN at different pH values in buffered water solutions without (a) (top) and with (b) (bottom) the presence of chlorine.
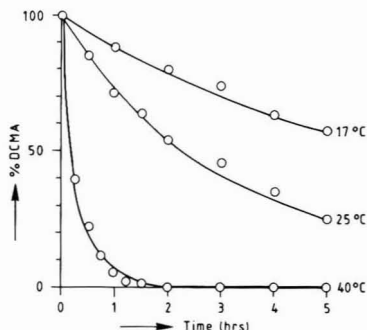
Figure 6. Decarboxylation of dichloromalonic acid (DCMA) at different temperatures.

Scheme II
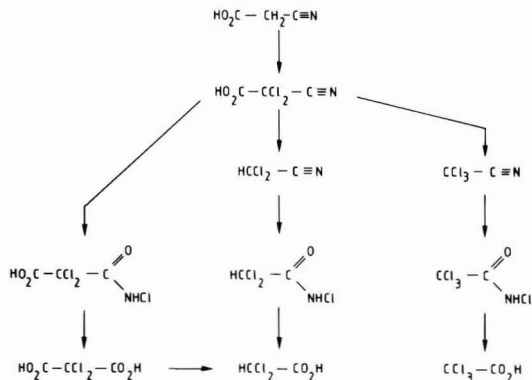
were also standard confirmed, were detected. DCMA showed to be unstable in aqueous medium and decarboxylated almost completely in 12 h at room temperature

(Figure 6) and may thus contribute to the amount of DCA found.

Conclusions

CEA showed to be very reactive under chlorination conditions in aqueous medium, producing DCA, TCA, and DCMA as the final products. At pH 10, N-chloroamides were detected as the intermediates that were previously reported as N-hydroxamoyl chlorides. The first step in the reaction sequence is a rapid chlorination followed by a decarboxylation producing mainly DCAN. DCAN is then converted into an N-chloroamide by an addition of HOCl. Depending on the pH, the N-chloroamides will hydrolyze more or less rapidly to the final products DCA, DCMA, and, to a lesser extent, TCA. The hydrolysis of the N-chloroamides was hypochlorite-catalyzed. On methylation with diazomethane these N-chloroamides gave an unexpected reaction, producing N-chloroimidates and N-unsubstituted imidates by O-methylation and an unexplained reaction at the N–Cl bond.

Registry No. CEA, 372-09-8; DCA, 79-43-6; DCMA, 56857-23-9; TCA, 76-03-9.

Literature Cited

(1) Langheld, K. *Chem. Ber.* **1909**, *42*, 2360–2374.
(2) Dakin, H. D. *Biochem. J.* **1916**, *10*, 319–323.
(3) Dakin, H. D. *Biochem. J.* **1917**, *11*, 79–95.
(4) Burleson, J. L.; Peyton, G. R.; Glaze, W. H. *Environ. Sci. Technol.* **1980**, *14*, 1354–1359.
(5) Trehy, M. L.; Bieber, T. I. In *Advances in the Identification and Analysis of Organic Pollutants in Water*; Keith, L. H., Ed.; Ann Arbor Science: Ann Arbor, MI, 1981; pp 941–975.
(6) Bieber, T. I.; Trehy, M. L. In *Water Chlorination: Environmental Impact and Health Effects*; Jolley, R. L. et al., Eds.; Ann Arbor Science: Ann Arbor, MI, 1983; Vol. 4, pp 85–96.
(7) De Leer, E. W. B.; Sinninghe Damsté, J. S.; Erkelens, C.; de Galan, L. *Environ. Sci. Technol.* **1985**, *19*, 512–522.
(8) De Leer, E. W. B.; Baggerman, T.; van Schaik, P.; Zuydeweg, C. W. S.; de Galan, L. *Environ. Sci. Technol.* **1986**, *20*, 1218–1223.
(9) Conrad, M.; Reinbach, H. *Chem. Ber.* **1902**, *35*, 1813–1821.
(10) Clark, J. R.; Shibe, W. J.; Conner, R. *Organic Syntheses*; Wiley: New York, 1955; Collect. Vol. III, pp 260–261.
(11) Brown, H. C. *J. Am. Chem. Soc.* **1938**, *60*, 1325–1328.
(12) McMaster, L.; Langreck, F. B. *J. Am. Chem. Soc.* **1917**, *39*, 103–109.
(13) Titov, A. I. *Dokl. Akad. Nauk SSSR* **1963**, *149*, 619–622; *Chem. Abstr.* **1963**, *59*, 7361a.
(14) Brintzinger, H.; Titzmann, R. *Chem. Ber.* **1952**, *85*, 344–345.
(15) Steinkopf, W. *Chem. Ber.* **1908**, *41*, 2540–2542.
(16) Bachard, C.; Driquez, H.; Paton, J. M.; Touchard, D.; Lessard, J. *J. Org. Chem.* **1974**, *39*, 3136–3138.
(17) Luria, S. E.; Delbruck, M. *Genetics* **1943**, *28*, 491.
(18) Neilson, D. G. In *The Chemistry of Amidines and Imidates*; Patai, S., Ed.; Interscience Publication: New York, 1975; pp 385–489.
(19) Stieglitz, J. *Chem. Ber.* **1901**, *34*, 1613–1619.
(20) Orazi, O. O.; Corral, R. A.; Schuttenberg, H. *Tetrahedron Lett.* **1969**, *31*, 2639–2642.
(21) Pearson, R. G.; Dillon, R. L. *J. Am. Chem. Soc.* **1953**, *75*, 2439–2443.
(22) Gurol, M. D.; Wowk, A.; Myers, S.; Suffet, I. H. In *Water Chlorination: Environmental Impact and Health Effects*; Jolley, R. L. et al., Eds.; Ann Arbor Science: Ann Arbor, MI, 1983; Vol. 4, pp 269–284.
(23) Oliver, B. G. *Environ. Sci. Technol.* **1983**, *17*, 80–83.
(24) Hauser, C. R.; Renfrow, W. B. *J. Am. Chem. Soc.* **1937**, *59*, 121–125.

Biodegradation Experiments of Linear Alkylbenzenes (LABs): Isomeric Composition of C$_{12}$ LABs as an Indicator of the Degree of LAB Degradation in the Aquatic Environment

Hideshige Takada* and Ryoshi Ishiwatari

Department of Chemistry, Faculty of Science, Tokyo Metropolitan University, Fukasawa, Setagaya-ku, Tokyo 158, Japan

■ Laboratory incubations of linear alkylbenzenes (LABs), potential molecular tracers of domestic waste, were conducted to obtain experimental evidence of systematic microbial alteration of their isomeric composition. The results showed that external LAB isomers (E) are more rapidly biodegraded than internal LAB isomers (I). The degree of LAB degradation was found to be quantitatively related to the change in their isomeric composition. The isomeric composition, represented by I/E ratio, is proposed as an indicator of LAB degradation. The I/E ratio was applied to estimate the persistence of LABs around Tokyo. The results indicate that the degree of LAB degradation in estuarine and bay sediments is ~45%.

Introduction

Today, linear alkylbenzenes (LABs) with alkyl carbon numbers of 10–14 are manufactured as raw materials of linear alkylbenzenesulfonate (LAS) surfactants. LASs are synthesized by sulfonation of alkylbenzene with H$_2$SO$_4$ or SO$_3$. The yield of the sulfonation is generally high, but some residual unsulfonated LABs persist and are carried with LASs into detergents. Recently, we found LAB pollution in sediments of Tokyo Bay (*1*, *2*). Our subsequent study showed that LABs occur as ubiquitous constituents in riverine environments (treated and untreated domestic wastewater, river water, and sediments) in Tokyo (*3*). Eganhouse et al. (*4*) also showed that LABs are present in municipal wastes of southern California and in nearby coastal sediments. Albaigés et al. (*5*) also found LABs in sediments and tissues of fishes in the western Mediterranean.

It has been suggested that LAB pollution results from incomplete sulfonation of the linear alkylbenzenes and their discharge with LAS detergents into the aquatic environment. The following facts, which have reported in previous papers (*1–4*, *6*), support the above statements: (1) LABs are present in LAS detergents in minute amounts and their molecular composition closely resembles LAB

*Present address: Department of Environmental Science & Conservation, Faculty of Agriculture, Tokyo University of Agriculture & Technology, Fuchu, Tokyo 183, Japan.
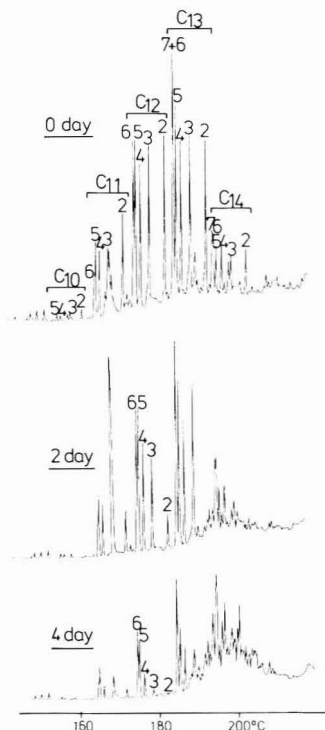
Figure 1. Gas chromatograms of LABs in suspended form from incubation experiment I. C_n:n indicates the number of alkyl carbons. Superscript on each peak indicates the position of the phenyl group on the alkyl chain. GC conditions: 25 m × 0.3 mm i.d. fused-silica capillary column coated with SE-54; 0.7 atm helium as carrier gas; flame ionization detector; splitless mode; column temperature, 50 °C for initial 2 min, and then programmed to 120 °C at a rate of 30 °C/min to 220 °C at a rate of 3 °C/min.

compositions in untreated domestic wastewater. The amounts of LABs in detergents are sufficient to account for the amounts of LABs in wastewaters; (2) heavy LAB pollution occurs in urban areas (river, bay, and coastal sediments); (3) in sediment cores, LAB pollution starts from the depth corresponding to the time when LAS detergents began to be used in the catchment. The wide distribution of LABs in riverine environments (3), estuarine sediments (1, 2, 4, 7, 8), and pelagic fishes (5) shows their high persistency. In this context, LABs have been proposed as a useful indicator of domestic waste derived pollutants (3, 4, 9). The potential of LABs as molecular tracers of domestic wastes was reviewed by Vivian (10).

LABs consist of isomers that differ in the position of the phenyl group on the alkyl side chain, as shown in Figure 1. Systematic changes in the isomeric composition of LABs in the aquatic environment have been observed (3–5). For detergents and untreated domestic wastes, the relative abundance of isomers with a given alkyl chain length is nearly equal. For river and coastal sediments, however, internal isomers (those having the phenyl attachment toward the middle of the alkyl chain; e.g., 6-C_{12}) dominate over external isomers (those having the phenyl attachment near the end of the alkyl chain; e.g., 2-C_{12}; n-C_m:n indicates the position of substitution of benzene to the alkyl chain and m indicates the number of carbons in the alkyl chain). This difference in isomeric composition has been considered to be caused by selective biodegradation of external isomers relative to internal isomers (3–5).

If this is true, the isomeric composition of LABs may provide information on the degree of LAB biodegradation.

In this study, untreated domestic waste was incubated to obtain experimental evidence of selective biodegradation of LAB isomers and to investigate quantitative relationships between the degree of LAB degradation and the changes in their isomeric composition. Furthermore, the isomeric compositions of LABs were used to estimate the degree of degradation of LABs in the aquatic environment around Tokyo.

Experimental Section

Incubation Experiment. Untreated domestic wastes were chosen for incubation. The untreated domestic wastewater was collected from treatment plant A, a representative sewage treatment plant in Tokyo receiving domestic waste from 1.3×10^6 persons (11). The wastewaters contain 100–200 mg/L suspended solids, ~60 mg/L organic carbon, ~5 mg/L LAS, and ~10 µg/L LABs (3).

Three sets of incubation experiments were conducted for the purpose of examining the reproducibility of selective LAB degradation. The first experiment (experiment I) was conducted at 25–28 °C for 6 days, the second (experiment II) at 26–28 °C for 6 days, and the third (experiment III) at 13–19 °C for 32 days.

In each experiment, a wastewater sample (300 L) was taken in a large plastic bottle without filtration and incubated under aerobic conditions with stirring and continuous aeration. At appropriate intervals (0, 1, 2, 3, 4, 5, and 6 days for experiments I and II; 0, 1, 3, 7, 15, and 31 day for experiment III) a 20-L water sample was taken and filtered through a prebaked glass fiber filter (Toyo Roshi GB100R; nominal pore size, 0.6 µm). Both filtrates and suspended particles were analyzed for LABs and LASs.

Also, an anaerobic incubation was conducted in experiment I. In the anaerobic experiment, 20 L of the same fresh wastewater sample as the aerobic incubation was taken in a plastic bottle. The bottle was sealed after removing dissolved oxygen by bubbling nitrogen gas and incubated for 6 days. Since no considerable change of LABs and LASs was expected to occur under anaerobic conditions, the 20-L sample was filtered and analyzed for these compounds after only 6 days of incubation.

Alkylbenzenes. The analytical procedure used for determination of alkylbenzenes was essentially the same as reported previously (12). LABs in suspended particles were Soxhlet-extracted from freeze-dried glass fiber filters containing suspended particles with 1.5 L of benzene–methanol (6:4) for 18 h. The cycling rates for the extractions were 45 min/cycle. To each of the extracts was added 100 µL of a 25.0 ng/µL solution of 1-C_{11} as a recovery standard. Dissolved LABs were liquid/liquid extracted from 8 L of the filtrates with 600 × 3 mL of benzene. Before the liquid/liquid extraction, 100 µL of a 25.0 ng/µL solution of the recovery standard (1-C_{11}) was added to each of the filtrates.

The organic solvent extracts from suspended particles and filtrates, respectively, were concentrated to dryness and taken up in 5 mL of benzene. The extract was then applied to a Florisil column (1.0 cm i.d. × 8 cm) for removal of polar materials (pigments). The first 30 mL of benzene eluate was collected and evaporated to dryness. The eluate was then taken up in 0.3 mL of n-hexane and subjected to silica gel column chromatography (Mallinckrodt, 100 mesh, 0.5 cm i.d. × 18 cm). n-Hexane was used as an eluent to give three fractions: 0–5, 5–18, and 18–60 mL. The second n-hexane fraction, containing LABs, was evaporated to just dryness and taken up in 50 µL of iso-

octane. A 2-μL sample was then injected into a Hewlett-Packard 5880A gas chromatograph equipped with a flame ionization detector (FID) and a 25 m × 0.3 mm i.d. SE-54 fused-silica capillary column in the splitless mode at 50 °C. The column was maintained at 50 °C for 2 min, followed by heating to 120 °C at 30 °C/min and then temperature programmed from 120 to 220 °C at 3 °C/min with He as the carrier gas. The FID was maintained at 310 °C and the injection port at 300 °C.

Peak identification was performed by use of retention indexes and/or the coinjection with a standard mixture of linear alkylbenzenes supplied by Mitsubishi Petrochemical Co. The details of the identification have been described by Takada and Ishiwatari (12), in which GC/MS confirmation was performed. Alkylbenzene (AB) concentrations reported here were computed by using response factors of 1-C_{10}, 1-C_{11}, 1-C_{12}, 1-C_{13}, and 1-C_{14} AB that were determined from a gas chromatographic run on the same day, assuming that the response factor of n-C_m AB is the same as that of 1-C_m AB. All LAB concentrations were corrected for recovery by using the recovery efficiency of 1-C_{11} AB (recovery standard), assuming that all LABs are recovered at the same rate as 1-C_{11} AB. The agreement of recovery for each homologue is tested as follows. A 2.5-μg sample each of 1-C_{10}, 1-C_{11}, 1-C_{12}, and 1-C_{13} AB was added to the organic solvent extract from 5 g of a sediment sample from the Tamagawa River (Tokyo, Japan) and analyzed by GC after taking all the steps of the analytical procedure. The percent recoveries calculated by the external standard method were 94 ± 4, 84 ± 5, 89 ± 3, and 81 ± 2% (duplicate analyses) for 1-C_{10}, 1-C_{11}, 1-C_{12}, and 1-C_{13} AB, respectively. This result indicates that the recoveries of 1-C_{10}, 1-C_{12}, and 1-C_{13} AB agree with that of 1-C_{11} AB to within 12%. Thus, the fluctuation of percent recovery among LAB homologues (C_{10}–C_{13}) is thought to be small (less than 12%). Also, agreement of percent recovery for each isomer was checked by using a mixture consisting of 2-C_{12}, 3-C_{12}, 4-C_{12}, 5-C_{12}, and 6-C_{12} AB supplied from the Mitsubishi Petrochemical Co. A 10-μg aliquot of this mixture was subjected to all the steps of the analytical procedure. Triplicate analyses using the external standard method showed that the percent recoveries were 83 ± 1, 80 ± 1, 77 ± 1, 77 ± 1, and 78 ± 1% for 2-C_{12}, 3-C_{12}, 4-C_{12}, 5-C_{12}, and 6-C_{12} AB, respectively. This result indicates that differences of recovery among LAB isomers are less than 5%. Consequently, these small deviations (less than 12%) of percent recovery among both homologues and isomers afford the justification for making the recovery correction by use of 1-C_{11} AB. 1-C_{10}, 1-C_{12}, and 1-C_{13}, and 1-C_{14} AB were unsuitable for recovery standards because these were interfered with by coeluting substances on gas chromatograms of these wastewater samples.

The reproducibility was determined by triplicate analyses of a wastewater sample (0-day sample on experiment I). The relative standard deviation of LABs concentration was below 8%.

Linear Alkylbenzenesulfonates (LASs). Dissolved LASs were extracted from 100 mL of filtrate with chloroform after formation of a LAS–methylene blue complex by adding a few milliliters of 0.025% methylene blue solution. Suspended LASs were Soxhlet-extracted from the freeze-dried glass fiber filters with benzene–methanol (6:4), after which the extracts were evaporated to dryness under reduced pressure. The residue was dissolved in ~20 mL of distilled water, and LAS was extracted as the LAS–methylene blue complex. The chloroform extract from filtrates and suspended particles, respectively, was evaporated to dryness under reduced pressure, dissolved in a small amount of ethanol and passed through a cation-exchange column (Dowex 50W-X8, 50–100 mesh, 1.0 cm i.d. × 5 cm) for removal of methylene blue. The first 10 mL of ethanol eluate (containing LAS) was then evaporated, and the residue was dissolved in ~20 mL of water. The aqueous solution was washed with chloroform and concentrated to a small volume (below 1 mL).

LAS was quantified by an HPLC method. The HPLC analytical conditions were essentially the same as reported by Nakae et al. (13, 14). Briefly, LAS was analyzed on a Hitachi 655 high-performance liquid chromatograph with a fluorometric detector (excitation at 225 nm and emission at 295 nm). A 10-μL aliquot of an aqueous solution was injected via a Rheodyne 7125 syringe loading injector fitted with a 20-μL sample loop and separated on a 15 cm × 4.6 mm i.d. Hitachi Gel 3053 ODS (5-μm particle) reversed-phase column at a flow rate of 1.0 mL/min. Sodium perchlorate (0.1 M) in acetonitrile–water (45:55) was employed to separate LASs. LASs were identified by coinjection with a standard mixture of LASs supplied by Kao Corporation Ltd. and/or the comparison of retention times with those reported by Nakae et al. (14).

LAS concentrations were computed by using the response factors of C_{12} LAS authentic standard (a mixture of 6-C_{12} LAS + 5-C_{12} LAS + 4-C_{12} LAS + 3-C_{12} LAS + 2-C_{12} LAS) that was determined from a run on the same day. The C_{12} LAS standard was purchased from WAKO chemical Ltd.

In order to test LAS recovery from suspended materials, 50 μg of the C_{12} LAS standard was added to the organic solvent extract from a sediment sample (the Tamagawa river) and analyzed. The recovery was 100 ± 11%. In the case of recovery of dissolved LAS, 100 μg of the C_{12} LAS standard was added to filtrates from a Tamagawa river water and analyzed. The recovery was 81.2 ± 4.5%. LAS concentrations were not corrected for recovery, because 1-C_n LASs were not available.

Results and Discussion

LABs derived from LAS detergent consist of 26 isomers, as shown in Figure 1. "$\sum$LAB" represents the sum of the concentration of these 26 isomers. Similarly, sum of the 26 isomers of LASs is referred to as "$\sum$LAS".

Biodegradation of LAB Isomers. Table I gives the result of incubation experiment I. At the start, $\sum$LAB in dissolved plus suspended forms ("D+S" is used hereafter to indicate these forms) was 9.3 μg/L. Under aerobic conditions $\sum$LAB (D+S) gradually decreased from 9.3 to 4.9 μg/L on 3 days and 2.1 μg/L on 6 days after the start, corresponding to 53% and 22% of the initial $\sum$LAB (D+S), respectively. In contrast, $\sum$LAS (D+S) rapidly decreased from 4.4 to 0.26 mg/L on 2 days and 0.002 mg/L on 6 days after the start, corresponding to 6% and 0.1% of the initial $\sum$LAS (D+S), respectively. The degradation rate of LASs is apparently much more rapid than that of LABs, as shown in Figure 2. The ratio of $\sum$LAS (D+S) to $\sum$LAB (D+S) decreases from 467 at day 0 to 1.0 at day 6. In our previous paper (3), it was shown that LASs/LABs ratios decreased from 550 for the suspended particles in wastewater influents to 22 for the river sediments to 1 for the Tokyo Bay sediment. The causes for this decreasing trend in LAS/LAB ratios were thought to be the higher water solubility and biodegradability of LASs compared to LABs. The result in the present incubation gives experimental evidence that greater biodegradability of LASs relative to LABs is responsible for the decreasing LAS/LAB ratios observed in the aquatic environments.

As can be seen in Figure 1, the isomeric composition of the LABs changes with increasing incubation time. Ex-

Table I. Results of Incubation Experiment I

duration, day	∑LABs concn, μg/L suspen	dissolv	total	% remain.	I/E ratio[a] suspen	dissolv	total	∑LASs total concn, μg/L	% remain.
0	5.0	4.3	9.3	100	0.71	0.81	0.75	4369	100
oxic									
1	6.0	2.8	8.8	95	0.95	1.00	0.95	3460	79
2	5.0	1.8	6.8	74	1.15	1.27	1.18	256	6
3	3.7	1.2	4.9	53	2.10	2.13	2.10	6	0.1
4	3.5	0.7	4.2	44	3.19	2.77	3.13	6	0.1
5	2.3	0.1	2.4	26	4.70	5.65	4.75	2	0.05
6	2.0	0.1	2.1	22	5.87	nd[b]	5.87	2	0.05
anoxic									
6	4.7	3.9	8.6	92	0.75	0.78	0.76	3889	89

[a] I/E ratio: ratio of [6-C_{12} AB + 5-C_{12} AB] relative to [4-C_{12} AB + 3-C_{12} AB + 2-C_{12} AB]. [b] Not determined.
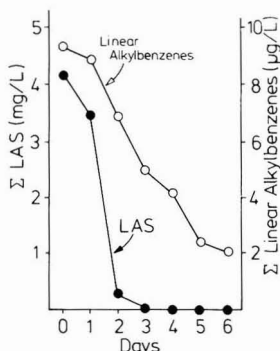
Figure 2. Time course of ∑LAB (D+S) and ∑LAS (D+S) concentrations from incubation experiment I.

Figure 3. Time course of isomeric composition of C_{12} LABs in suspended form from incubation experiment I.

ternal isomers disappeared more rapidly than internal isomers during incubation. C_{12} isomers were selected as representative to show the changes in isomeric composition of LABs, because C_{12} isomers are most abundant, their gas chromatographic peaks are well differentiated and no interferences occurred for these isomers, as shown in Figure 1. It is obvious from Figure 3 that the relative abundance of external isomers of C_{12} LABs decreases with time. A ratio of [6-C_{12} AB + 5-C_{12} AB] relative to [4-C_{12} AB + 3-C_{12} AB + 2-C_{12} AB], which we call the I/E ratio hereafter, was calculated to express the change of the isomeric composition quantitatively. As shown in Table I, the I/E ratio monotonously increases from 0.71 on day 0 to 5.87 on day 6 from the start of incubation. Also, in experiments II and III (Table II), the I/E ratio monotonously increased throughout the incubation periods, indicating progress in the selective LAB degradation. In our previous paper (3), the progressive relative enhancement of the internal isomers at the expense of external ones was seen on going from untreated domestic waste to river sediments and to Tokyo Bay sediments. The similar systematic isomer alteration was noted in Los Angeles on going from effluent to suspended particles to sediments (4). These systematic isomer alterations were thought to be caused by selective microbial degradation of external isomers. The results in the present incubation experiments afford experimental evidence of the selective biodegradation of external isomers. Also, Bayona et al. (15) conducted an aerobic degradation experiment of LABs using pure cultures of bacterial strains (Pseudomonas sp) and showed that external isomers degraded more rapidly than internal ones.

Physicochemical partitioning is another possible cause for the isomeric change of LABs. In this study, however,
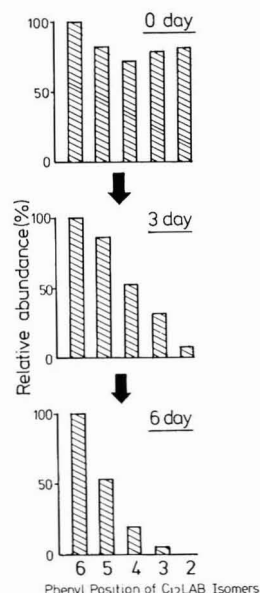
Table II. Results of Incubation Experiments II and III

day	∑LAB concn, μg/L	% remain.	I/E ratio[a]
	Experiment II		
0	9.3	100	0.74
1	7.4	80	0.93
2	6.4	69	1.18
3	5.5	59	2.10
4	3.5	38	3.67
5	2.5	27	6.13
6	2.1	23	7.20
	Experiment III		
0	11.6	100	0.87
1	10.3	89	0.99
3	9.3	80	1.32
7	5.0	43	3.93
15	2.6	22	5.69
31	2.0	17	5.97

[a] I/E ratio: ratio of [6-C_{12} AB + 5-C_{12} AB] relative to [4-C_{12} AB + 3-C_{12} AB + 2-C_{12} AB].

the systematic changes in the isomeric composition were observed for total LABs (i.e., suspended LABs plus dis-

Table III. I/E Ratios[a] and Estimated Degree of Degradation of LABs

	no. of samples	I/E ratio		degree of degradation, %	
		average	range	average	range
synthetic detergents[b]	12	0.81 ± 0.15	0.63–1.08		
suspended particles from untreated wastewater[b]	11	0.69 ± 0.05	0.62–0.81		
suspended particles from river water[b]	5	1.66 ± 0.50	1.09–2.67	30	20–50
river sediments[b]	18	1.48 ± 0.20	1.09–1.85	30	20–40
estuarine sediments[c]	32	2.00 ± 0.50	1.13–3.54	45	20–60
Tokyo Bay sediments[d]	24	2.02 ± 0.50	1.26–3.09	45	30–55

[a] I/E ratio: ratio of $[6\text{-}C_{12} \text{ AB} + 5\text{-}C_{12} \text{ AB}]$ relative to $[4\text{-}C_{12} \text{ AB} + 3\text{-}C_{12} \text{ AB} + 2\text{-}C_{12} \text{ AB}]$. [b] Sample descriptions were detailed in ref 3. [c] Collected from the Tamagawa, Arakawa, and Sumidagawa rivers, which flow into Tokyo Bay. [d] Surface (0–2.5 cm) sediments collected from all over the bay.

solved LABs; Table I). Even if, therefore, differential physicochemical partitioning of LAB isomers occurred between suspended and dissolved phases, the isomer changes for total LABs during incubations would not be explained by the differential partitioning but by selective degradation. Furthermore, no practical differences in isomeric compositions were observed between dissolved LABs and suspended ones throughout the incubation experiment (Table I). This indicates that adsorption/desorption of LABs between dissolved and suspended phases does not differentiate their isomeric compositions. Consequently, it is reasonable to conclude that the isomeric changes of LABs in the aquatic environments are caused by selective microbial degradation.

Table I shows also the result of the anaerobic incubation. In contrast to the aerobic incubation, LAB concentration and I/E ratio did not show a considerable change even after 6 days of anaerobic incubation. This may explain the ubiquitous distribution of LABs in the sediments around Tokyo (3), where anaerobic conditions are prevailing. Also, this finding may give experimental support to the observation of the lower rate of isomer degradation after burial in coastal sediments off Los Angeles than during sedimentation of waste particles under aerobic conditions (4).

I/E–Degradation Diagram for LABs. From the results of incubation experiment I (Table I), we have drawn a I/E–degradation diagram that gives a relationship between I/E ratios of C_{12} LABs and the extent of degradation of LABs. As shown in Figure 4, there exists a good correlation between the I/E ratio and the extent of degradation of $\sum$LABs (D+S). The excellent reproducibility of this correlation was confirmed by incubation experiments II and III (Figure 4).

Using the I/E–degradation diagram, we have tried estimating the degree of LAB degradation in environmental samples, on the assumption that the results of the incubation experiments are valid for the natural environment. This assumption would be reasonable because the medium used for our incubation experiments is actual wastewater, which contains various nutrients, organic matter, and biota similar to that in the natural environment. Therefore, the biological processes occurring in incubation experiments are probably similar to those in the natural environment. Of course, water temperature, redox potential, and nutrient concentration may affect the microbial activities on LAB degradation. Consequently, the rate of LAB degradation in natural environments may differ from that in these incubation experiments. But the differences in the microbial activity do not affect the relative relationship of degradation among LAB isomers (i.e., I/E–degradation diagram). As shown in Table II, for example, LABs were degraded more slowly in experiment III than in experiments I and II, probably because lower water temperatures
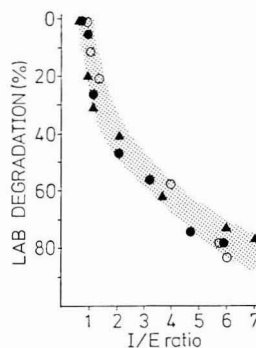
Figure 4. I/E–degradation diagram of LABs. I/E ratio: ratio of $[6\text{-}C_{12} \text{ AB} +5\text{-}C_{12} \text{ AB}]$ relative to $[4\text{-}C_{12} \text{ AB} + 3\text{-}C_{12} \text{ AB} +2\text{-}C_{12} \text{ AB}]$. LAB degradation (%): weight percent of $\sum$LAB (D+S) remaining after incubation relative to those initially. Closed circle, experiment I; closed triangle, experiment II; open circle, experiment III.

in experiment III made the microbial activities lower. Nonetheless, the relationship between LAB degradation and I/E ratio in experiment III coincides well with those in experiments I and II (Figure 4). This result supports the suggestion that the difference in the microbial activities does not significantly affect the relationship between LAB degradation and I/E ratio. Thus, the I/E–degradation diagram for the incubation experiments may be valid for the natural environment.

Table III lists the degree of degradation of LABs in environmental samples estimated from the I/E–degradation diagram (Figure 4). The I/E ratio of suspended river particles is 1.7 ± 0.5 corresponding to 30 ± 20% degradation of $\sum$LAB. Similarly, the degree of degradation of $\sum$LAB in Tokyo Bay sediments is estimated to be 45 ± 10%. During incubation experiment I, 30% of the initial $\sum$LAB was degraded after 2 days of aerobic incubations and 45% after 3 days. Therefore, the isomer change from suspended river particles to Tokyo Bay sediment requires only 1 day of aerobic incubation (26–29 °C; continuous aeration). Actually, however, LABs in the surface (0–2.5 cm) sediments of Tokyo Bay have been present in the bay for more than 1 year since carried from the river, because the sedimentation rate for Tokyo Bay is approximately 1 cm/year (16). This indicates that LABs degrade extremely slowly in Tokyo Bay sediments. Probably LAB degradation is suppressed in Tokyo Bay sediments by various conditions such as water temperature, redox potential, and bacterial number. Anaerobic conditions in the sediments may be largely responsible for the suppression of LAB degradation. As mentioned above (Table I), few LABs degraded under anaerobic conditions. Because Tokyo Bay sediments are likely to be anaerobic (16), LABs may be

hardly degraded once incorporated into the sediments.

Conclusion

Incubation experiments of untreated domestic waste showed that the isomeric composition of LABs changes systematically due to microbial degradation. An I/E–degradation diagram (I/E ratio versus the extent of degradation of LABs) is proposed as an indicator of the degree of LAB degradation. By use of the I/E-degradation diagram, it was estimated that 55% of LABs entering the aquatic environment of Tokyo remain in the sediments without biodegradation.

Literature Cited

(1) Ishiwatari, R.; Takada, H.; Yun, S.-J.; Matsumoto, E. *Nature (London)* **1983**, *301*, 599–600.

(2) Takada, H.; Ishiwatari, R.; Yun, S.-J. *Jpn. J. Water Pollut. Res.* **1984**, *7*, 172–181.

(3) Takada, H.; Ishiwatari, R. *Environ. Sci. Technol.* **1987**, *21*, 875–883.

(4) Eganhouse, R. P.; Blumfield, D. L.; Kaplan, I. R. *Environ. Sci. Technol.* **1983**, *17*, 523–530.

(5) Albaigés, J.; Farrán, A.; Soler, M.; Gallifa, A.; Martin, P. *Mar. Environ. Res.* **1987**, *22*, 1–18.

(6) Eganhouse, R. P.; Ruth, E. C.; Kaplan, I. R. *Anal. Chem.* **1983**, *55*, 2120–2126.

(7) Eganhouse, R. P.; Kaplan, I. R. *Mar. Chem.* **1988**, *24*, 163–191.

(8) Valls, M.; Bayona, J. M.; Albaigés, J. *Nature* **1989**, *337*, 722–724.

(9) Eganhouse, R. P.; Olaguer, D. P.; Gould, B. R.; Phinney, C. S. *Mar. Environ. Res.* **1988**, *25*, 1–22.

(10) Vivian, C. M. G. *Sci. Total Environ.* **1986**, *53*, 5–40.

(11) *Sewerage in Tokyo*; Sewerage Bureau of Tokyo Metropolitan Government: Tokyo, Japan, 1985.

(12) Takada, H.; Ishiwatari, R. *J. Chromatogr.* **1985**, *346*, 281–290.

(13) Nakae, A.; Tsuji, K.; Yamanaka, M. *Anal. Chem.* **1980**, *52*, 2275–2277.

(14) Nakae, A.; Tsuji, K.; Yamanaka, M. *Anal. Chem.* **1981**, *53*, 1818–1821.

(15) Bayona, J. M.; Albaigés, J.; Solanas, A. M.; Grifoll, M. *Chemosphere* **1986**, *15*, 595–598.

(16) Matsumoto, E. *Chikyu Kagaku (Nippon Chikyu Kagakkai)* **1983**, *17*, 27–32.

Transformations of Selenium As Affected by Sediment Oxidation–Reduction Potential and pH

Patrick H. Masscheleyn,* **Ronald D. Delaune, and William H. Patrick, Jr.**

Laboratory for Wetland Soils and Sediments, Center for Wetland Resources, Louisiana State University, Baton Rouge, Louisiana 70803-7511

■ The influence of E_h and pH on selenium solubility, speciation, and volatilization was studied. Kesterson Reservoir sediments contaminated with selenium were incubated under controlled redox (−200, 0, 200, and 450 mV) and pH (6.5, natural, 8.5, and 9) conditions. Under reduced conditions selenium solubility was low and controlled by an iron selenide phase. Se(−II,0) comprised 80–100% of the total soluble selenium. Upon oxidation dissolved selenium concentrations increased. The oxidation of Se(−II,0) to selenite was rapid and occurred immediately after the oxidation of iron. Above 200 mV selenite slowly oxidized to selenate. Under oxidized conditions (450 mV) selenium solubility reached a maximum. Selenate was the predominant dissolved species present, constituting 95% at higher pH's (8.9, 9) to 75% at lower pH's (7.5, 6.5) of the total soluble selenium at 450 mV. Biomethylation of selenium occurred only under oxidized conditions. Redox potential and pH are key factors in the biogeochemistry of selenium.

Introduction

The discovery of toxic concentrations of selenium in evaporation ponds of the Kesterson National Wildlife Refuge, located in the Western part of California's San Joaquin Valley, has led to an increasing interest in the biogeochemistry of selenium in recent years.

The chemistry of selenium is complicated since it can exist in four different oxidation states, selenide (Se(−II)), elemental Se (Se(0)), selenite (Se(IV)), and selenate (Se(VI)), and as a variety of organic compounds. The major features of selenium biogeochemistry affecting its movement and toxicity are associated with changes in its oxi-

dation state and the resulting differences in chemical properties of these various chemical forms. Adsorption and mobility of the selenite and selenate species have been studied extensively during the past few years (1–7). Briefly, conditions that favor the mobility of selenium with respect to adsorption are alkaline pH, oxidizing conditions, and high concentrations of additional anions.

Although the importance of the redox status in the study of selenium biogeochemistry is evident, few studies have investigated the effects of changes in oxidation–reduction potential on the transformations of selenium species in soils and sediments. Geering et al. (8) constructed an E_h–pH diagram and theoretically investigated selenium transformations as affected by pH and E_h. In a more recent paper, Elrashidi et al. (9) used thermodynamic data to develop equilibria reactions and constants for selenium minerals and solution species that relate to soils. Based upon thermodynamics, they reported metal–selenite and in particular metal–selenate minerals to be too soluble to persist in soils. At low redox potentials, however, elemental Se or a metal–selenide could control Se solubility.

We developed a laboratory experiment that allowed us to study selenium transformations under controlled redox and pH conditions. In this paper we describe the critical redox levels at which selenium transformations in contaminated Kesterson Reservoir sediments occurred and report the influence of redox and pH on selenium speciation, solubility, and volatilization.

Experimental Section

Sediments. Selenium-contaminated soils (further called sediments) of the Kesterson Reservoir in California were
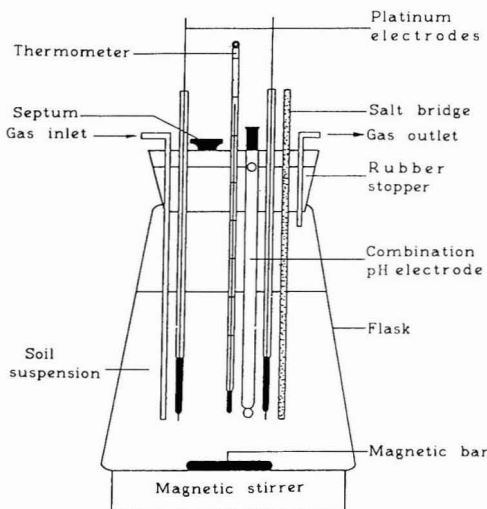
Figure 1. Schematic of experimental setup used for pH and redox control of the sediment suspensions.

collected at the northeast side of pond no. 2, approximately 30 m from the levee. The sediment was transported to the laboratory in tightly closed plastic containers. Upon arrival, the sediments were homogenized under an argon atmosphere and stored in closed 4-L polyethylene flasks until use.

Incubation Apparatus. The sediments were incubated in laboratory microcosms at various redox–pH conditions by using a modification of the redox control system developed by Patrick et al. (*10*) (Figure 1). In this system, the suspension pH is continuously measured and manually adjusted by additions of 4 M HCl or NaOH, daily, or as required to bring the pH to the desired value. The redox potential was maintained at a preselected potential automatically. Platinum electrodes in the suspension were connected to a millivolt meter to give continuous measurement of the redox potential of the sediment–water suspension. The recorder output of the millivolt meter was in turn connected to a meter relay that activated an air pump. Whenever the redox potential dropped below the desired potential, a small amount of air was pumped into the system to maintian the desired redox potential. This system of regulating redox potential with air input works because, in the absence of oxygen, chemical and especially microbial processes cause the redox potential to decrease. The flasks were continuously purged with oxygen-free argon gas. Argon gas was effective in purging excess air at the end of the aeration cycle and in preventing a buildup of gaseous decomposition products such as carbon dioxide and hydrogen sulfide. Using this system, we could maintain the desired redox potential within ±20 mV. The outflow gas passed out the incubation apparatus into a 10-mL concentrated HNO_3 solution followed by a water trap. Nitric acid has been reported to retain volatile selenium compounds from soils (*11*).

Experiments. In experiment one, the critical redox levels where selenium transformations occur were determined. Suspensions of the strongly reduced sediments were incubated (at 28 ± 2 °C) in the microcosms for 6 h before adjusting redox levels. Suspensions were prepared by mixing an amount of sediment equivalent to 200 g of dry weight with distilled water so that the final sediment water ratio was 1 to 7. Four incubations were performed each at a different E_h: –200, 0, 200, and 450 mV. The

experiment was run in duplicate. The microcosms were sampled at a 5-day interval over a 3-week period. The pH was monitored and recorded.

In experiment two, similar sediment suspensions were equilibrated under controlled redox and pH conditions. The following redox–pH combinations were used: redox –200, 0, 200, and 450 mV; pH 6.5, natural, 8.5, and 9. Natural (uncontrolled) pH values after a 28-day incubation period were 7.5 for 450 mV, 7.8 for 200 mV, 7.9 for 0 mV, and 8.1 for –200 mV. Microcosms were sampled after 28 days of incubation. Incubations were run in duplicate.

A sediment suspension aliquot was withdrawn, centrifuged [20 min at 7000 rpm ($31g$), Sorvall GSA-400 rotor, Du Pont CO., Wilmington, DE] and filtered through a 0.45-μM micropore filter, under an inert argon atmosphere for reduced treatments (*12*). Five dissolved selenium species were identified in the water extract.

In order to better validate E_h measurements in the systems we also measured the NO_3/NH_4, soluble Mn (Mn(II)), soluble Fe (Fe(II)), and the SO_4/S redox species. Other major cations (Ca, Mg, K, Na, Al), metals (Cu, Zn, Cd, Pb, Ni), and chlorides were also determined.

Analysis. Selenium species (Se(IV), Se(VI), Se(–II,0), dimethyl selenide (DMSe), and oxidized methylated Se compounds (Ox·MSe) in the water extracts were determined with a hydride generation/trapping/detection apparatus. The system was similar to that described by Cooke and Bruland (*13*). It included a helium-purged glass stripping vessel, a glass U tube immersed in an isopropyl alcohol–ice bath, a glass U tube immersed in liquid nitrogen, and an atomic absorption spectrophotometer (Perkin-Elmer 360) fitted with a flame in tube burner. A slightly longer hydride trap (40 cm) was used. Column packing material was found not necessary to separate methylated selenium compounds from selenium hydride. The output was recorded on a strip chart recorder and peak heights were used to calculate concentrations. Absorbance was found to be linear over the range 0–150 ng of selenium (amount placed in the hydride generator) with a sensitivity of 0.0045 absorbance units ng^{-1} of Se and a detection limit of 5 ng of Se.

Extracts were analyzed for selenium species within 10 h after sampling. A 10-mL aliquot of the extract was purged with He for the determination of volatile dimethyl selenide. Aliquots that had been previously stripped of volatile methylated compounds were then analyzed for selenite and dissolved oxidized methylated selenium compounds (*13*). Other aliquots were analyzed for (selenate + selenite), after reduction of Se(VI) to Se(IV) in 6 M HCl (*14*), and for total selenium by a modification (*15*) of the method described by Presser and Barnes (*16*). Sulfanilamide was used to eliminate possible nitrite interference in the determination of selenium (*17*). The selenate was calculated as the difference between the (selenate + selenite) and the selenite analysis. The difference between the total Se content and the (selenate + selenite) fraction is the Se(–II,0) fraction. The maximum sample volume analyzed for inorganic selenium species was 5 mL, which gave a detection limit of 1 μg of Se L^{-1} or 7 μg of Se kg^{-1} of dry sediment. Due to the small sample volume analyzed (normally between 0.5 and 2 mL), no interferences in the analysis of selenium species by dissolved organic carbon (*15*, *18*) were found. Several samples were analyzed by the standard addition technique. The relative precision of the technique was the same as reported by Cooke and Bruland (*13*): 5% for selenium species that were determined directly and ~10% for the species determined by difference. For the quantification of the volatilized selenium com-

Table I. Concentration of Soluble Redox Species and Ca during a 20-Day Incubation Period at −200 mV

day	concn, mg kg⁻¹ of dry sediment							concn, μg kg⁻¹	
	NH_4 N	NO_3 N	Mn	Fe	S(−II)	SO_4 S	Ca	Se(−II,0)	Se(IV)
2	212[a]	<2.00[c]	5.74	7.73	65	2905	934	21	<7[c]
	±11[b]		±0.20	±0.67	±9	±770	±229	±7	
7	241	<2.00	4.22	7.90	74	2919	903	56	<7
	±3		±1.48	±1.68	±20	±679	±168	±28	
12	264	<2.00	5.47	7.95	64	3052	931	42	<7
	±12		±0.56	±1.72	±20	±546	±204	±23	
20	259	<2.00	4.55	7.85	70	3395	1091	84	<7
	±6		±1.32	±0.76	±22	±1021	±165	±15	

[a] Mean of duplicate incubations. [b] Standard deviations. [c] Detection limit.

Table II. Concentration of Soluble Redox Species and Ca during a 20-Day Incubation Period at 0 mV

day	concn, mg kg⁻¹ of dry sediment							concn, μg kg⁻¹	
	NH_4 N	NO_3 N	Mn	Fe	S(−II)	SO_4 S	Ca	Se(−II,0)	Se(IV)
2	258[a]	<2.00[c]	4.22	7.95	50	3402	1068	44	<7[c]
	±8[b]		±0.37	±1.01	±3	±98	±230	±10	
7	229	<2.00	4.23	6.90	42	3556	1165	42	<7
	±9		±1.34	±1.71	±15	±826	±285	±2	
12	246	<2.00	5.18	8.00	45	3801	1400	72	<7
	±12		±1.57	±1.90	±15	±714	±290	±14	
20	259	<2.00	7.21	0.55	3	5056	2305	35	259
	±26		±0.82	±0.25	±3	±1174	±475	±7	±103

[a] Mean of duplicate incubations. [b] Standard deviation. [c] Detection limit.

pounds, the HNO_3 solutions were carefully taken to near dryness, 40 mL of 4 M HCl was added, and the solutions were treated as for (selenite + selenate) analysis.

Ammonium and nitrate were determined by the Kjeldahl distillation technique. Metals and major cations in solution were analyzed with a Jarrel Ash ICP, and a Dionex Ion Chromatograph was used for chloride and sulfate analysis. EPA reference standards were analyzed to check the preformance of the ICP. Sulfide was measured by an ion-specific Ag/S electrode in an anoxic buffer solution (sulfide electrode operating instruments; Lazar Research Laboratories, Los Angeles, CA). Due to the limited sensitivity of the electrodes, these analyses are probably less accurate.

Total Se in the sediment was determined by the prewetting digestion procedure as described by Fujii et al. (15).

The loss on ignition method (19) was used to estimate the organic matter content of the sediment.

X-ray diffraction (Cu Kα radiation) of bulk powder samples was used to study the mineralogy of reduced and oxidized sediment.

Results and Discussion

Critical Redox Potentials for Selenium Transformations. The sediments from the Kesterson Reservoir were extensively anaerobic and characterized by a high pH (8.1), an organic matter content of 5.2%, and a dark grayish color due to the large concentration of iron monosulfides. Presser and Barnes (16) reported the presence of thenardite (Na_2SO_4) in Kesterson reservoir sediments. Our X-ray diffraction patterns showed the presence of a large amount of calcite and some pyrite in the reduced sediments. The sediment had a total Se content of 9.06 ± 2.40 mg kg⁻¹ (n = 8) of dry sediment.

The critical redox potentials at which selenium transformations occurred were determined (experiment one). Results for a 3-week incubation study at −200 (PE = E_h/59.16) and 0 mV are given in Tables I and II. When incubated at −200 mV (pH 8.1), the solubility of selenium was very low and Se(−II,0) was the only detectable form

(Table I). At −200 mV nitrogen, manganese, and iron were present in a reduced form. Sulfide concentrations up to 74 mg kg⁻¹ of dry sediment were measured. High chloride, sodium, and sulfate concentrations (approximately 4200, 3750, and 3400 mg kg⁻¹ of dry sediment, respectively) were due to the solubility of salts like Na_2SO_4 and NaCl. As the incubation time progressed, concentrations of dissolved Na and Cl remained constant in both reduced and oxidized experiments, suggesting the independence of their solubility from oxidation–reduction reactions. Soluble Cu, Zn, Cd, Pb, and Ni were less than 1 mg kg⁻¹ of dry sediment.

Oxidation of Se(−II,0) to Se(IV) occurred at an E_h of approximately 0 mV (Table II). For the first 14 days total soluble selenium concentrations and forms at 0 mV (pH 7.9) were comparable with those reported for the incubation at −200 mV. However, after approximately 2 weeks the color of the suspension changed gradually from dark grayish to light brown due to the formation of iron oxides. Levels of dissolved iron and sulfides decreased and the sulfate concentration increased sharply, illustrating the oxidation of the iron sulfides. The concurrent increase of the calcium concentration (Table II) is somewhat ambiguous. It could result from the dissolution of gypsum ($CaSO_4\cdot2H_2O$) or anhydrite ($CaSO_4$)

$$CaSO_4\cdot2H_2O = Ca^{2+} + SO_4^{2-} + 2H_2O \quad (1)$$
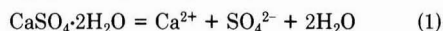
or it could result from the oxidation of an iron sulfide (pyrite or an iron monosulfide) and reaction with calcite:

$$FeS_2 + 3.75O_2 + 3.5H_2O = Fe(OH)_3 + 4H^+ + 2SO_4^{2-} \quad (2)$$

$$4H^+ + 2CaCO_3 = 2Ca^{2+} + 2H_2CO_3 \quad (3)$$
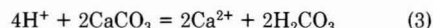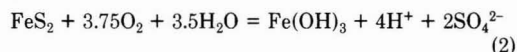
It is very difficult to distinguish [except perhaps by study of sulfur isotopes (20)] between these alternatives without investigation of the solid phases involved. Mineral identification by X-ray diffraction clearly showed the absence of gypsum and the presence of large amounts of both iron sulfides and calcite in the reduced sediments. Therefore the reactions described in eq 2 and 3 are responsible for
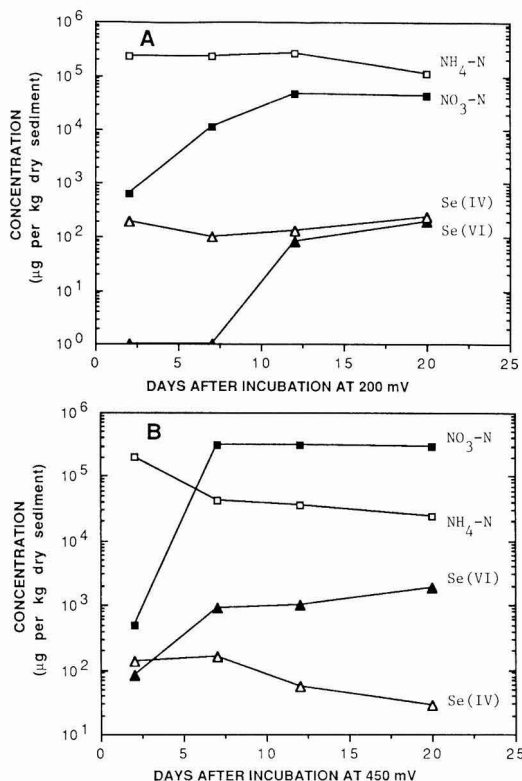
Figure 2. Ammonium/nitrate and selenite/selenate transformations during a 20-day incubation period. (A) at 200 mV. (B) at 450 mV.

Figure 3. Sequential oxidation of several redox systems in Kesterson Reservoir Sediments.

Table III. Solubility Products at 25 °C and 10^5 Pa

mineral	reaction products	$-\log K_{sp}$	ref
α-$Fe_{0.95}S$ (pyrrhotite)	$0.85Fe^{2+}$ + $0.10Fe^{3+}$ + S^{2-}	18.74	23
α-FeS (troilite)	Fe^{2+} + S^{2-}	16.21	23
FeS_2 (pyrite)	Fe^{2+} + S_2^{2-}	26.93	23
FeS_2 (markasite)	Fe^{2+} + S_2^{2-}	26.23	23
FeSe (achavalite)	Fe^{2+} + Se^{2-}	26.00	9

the increase of Ca concentration in our experiments. A large part of the alkalinity formed is lost to the atmosphere as CO_2.

Analysis of variance [PROC GLM procedure of the Statistical Analysis System (21)], comparing the solubility of redox species and calcium at −200 vs 0 mV, supports the interpretations made above. Concentrations of soluble redox species and Ca were not significantly different between the two redox levels studied. However, significant ($P < 0.05$) differences were found for the dissolved concentrations of Fe, S(−II), Ca, and Se(IV) between the different sampling times. There also was a significant interaction ($P < 0.05$) between the days after incubation and the E_h for these elements. As can be implied from Tables I and II, the interaction (day 20, −200 vs 0 mV) can be interpreted as the oxidation of iron sulfides, the consequent release and oxidation of Se(−II,0) to selenite, and the reactions described in eq 2 and 3.

The dominant selenium species found at 200 and 450 mV are shown in Figure 2. The transformation of selenite to selenate began at a redox potential of approximately 200 mV (pH was 7.7 at end of incubation) and occurred at values corresponding with nitrification and denitrification. Low concentrations of dissolved Mn (0.17 ± 0.08 mg kg⁻¹), Fe (0.87 ± 0.36 mg kg⁻¹), and S(−II) (<0.02 mg kg⁻¹) were typical for the oxidized sediment. Concentrations of Ca and SO_4 S at the end of the incubation period were 2710 ± 212 and 4780 ± 590 mg kg⁻¹ of dry sediment, respectively. When incubated at 450 mV, the oxidation of ammonium to nitrate and selenite to selenate was evident after 2 days of incubation (Figure 2B). Over time almost all selenite was oxidized and selenate became the

dominant selenium species in solution. At the end of the incubation the dissolved concentrations of the other redox species (mg kg⁻¹ of dry sediment) were as follows: Mn, 0.08 ± 0.05; Fe, 0.61 ± 0.48; S(−II), <0.02. During the incubation the pH dropped from 8.1 to 7.5 and soluble SO_4 S and Ca concentrations rose to 5159 ± 903 and 3160 ± 480 mg kg⁻¹, respectively.

Figure 3 summarizes the order of various inorganic oxidation−reduction reactions for the Kesterson Reservoir sediments. The same sequence was found in preliminary studies (results not shown), where transformations of added selenite were determined in Mississippi River sediments under controlled redox conditions. Data presented indicate that the oxidation and chemical weathering of iron sulfides leads to increases in soluble selenium species. The released Se(−II,0) is quickly oxidized to selenite. We also found that the oxidation of selenite to selenate occurred at a considerable higher E_h than the sulfide to sulfate oxidation. The oxidation rate of selenite to selenate is rather slow and is a function of the redox potential. Selenate was detected only when nitrate was present. From our experiments, it is difficult to calculate exact transformation rates because adsorption−desorption reactions occur simultaneously with the oxidation reactions.

From our study it is clear that selenium solubility increases with increased redox potential. It also seems that the chemistry of selenium under reduced conditions is closely related to that of iron. Recently Elrashidi et al. (9), using thermodynamic data to develop chemical equilibria reactions and constants of selenium in soils, also reported very low solubilities of selenides under reduced conditions. When an iron sulfide mineral forms in natural waters or sediments, the first phase to precipitate is usually an unstable monosulfide (22). Solubility products of iron monoselenide and sulfides are given in Table III. If we assume that selenide can substitute for sulfide in a solid solution phase, for example, troilite (Fe(S,Se)), then from the equilibrium reaction

$$FeS + Se^{2-} = FeSe + S^{2-} \quad (4)$$
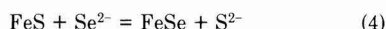
with $\log K = \log (a_{FeSe}/a_{FeS}) + \log (a_{S^{2-}}/a_{Se^{2-}}) = 9.79$, it can be seen that even in the presence of high sulfide concen-
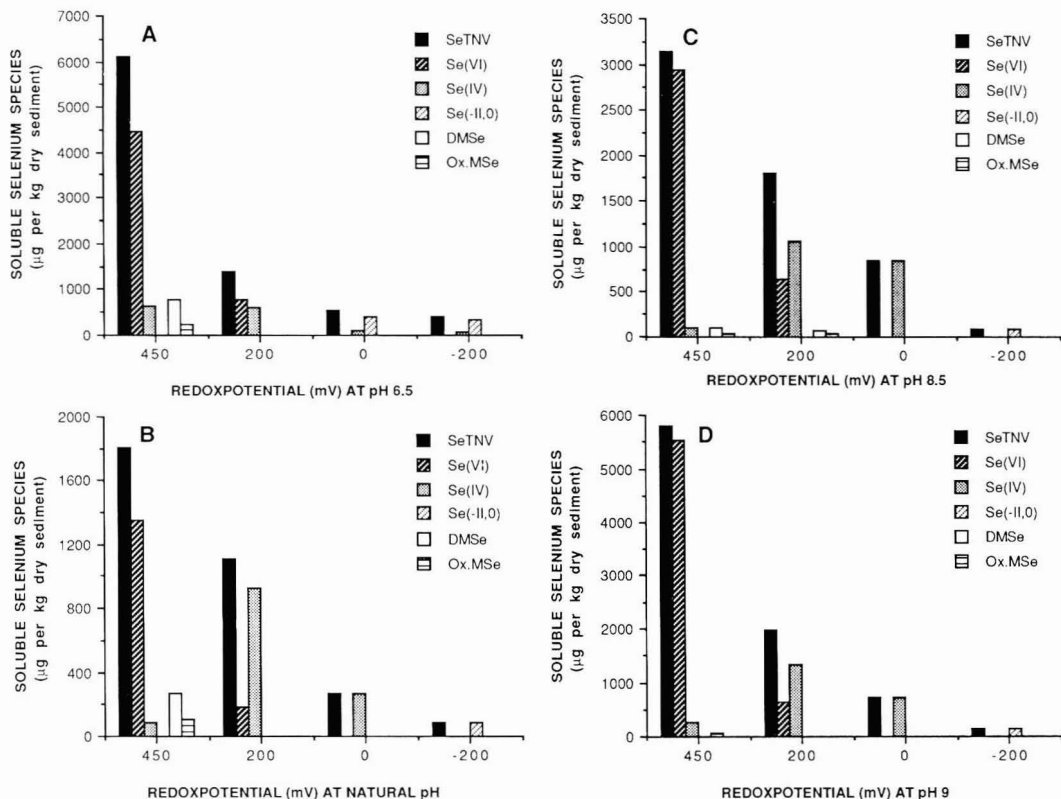
Figure 4. Distribution of soluble selenium species after a 28-day incubation period under controlled redox and pH conditions. (A) incubations at pH 6.5. (B) incubations at natural pH (7.5 for 450 mV, 7.8 for 200 mV, 7.9 for 0 mV, and 8.1 for −200 mV). (C) incubations at pH 8.5. (D) incubations at pH 9.

trations only a very small amount of selenide is needed in order to get supersaturation with respect to the iron selenide component in the solid solution. Over time monosulfides are generally oxidized to pyrite (FeS + S⁰ = FeS₂) (22), and it is very likely that in the presence of elemental sulfur the reaction $FeSe + S^0 = FeSeS$ exists. Although the existence of such a compound has not been proven yet, it undoubtedly may exist in nature. Howard (24) summarized selenium geochemistry on an E_h–pH diagram and included a stability field for the mineral ferroselite ($FeSe_2$). The redox–pH conditions of the reduced Kesterson Reservoir sediments are in accordance with this stability field. In the presence of an excess elemental sulfur, ferroselite was found to be unstable with respect to pyrite. The released elemental selenium was thought to be incorporated in pyrite (24).

Influence of Redox Potential and pH on Selenium Solubility, Speciation, and Volatilization. The redox–pH chemistry of indigenous selenium in Kesterson Reservoir sediments in relation to its solubility and its distribution among the various chemical species was determined (experiment two). Figure 4 shows the species distribution of total soluble selenium after 4 weeks of incubation at four different redox levels (−200, 0, 200, and 450 mV) ranging from strongly reduced to well oxidized. Four suspension pH levels (6.5, natural, 8.5, and 9) were selected and maintained during the incubation period. Incubations at pH values lower than 6.5 led to a massive dissolution of $CaCO_3$ and the precipitation of $CaSO_4 \cdot 2H_2O$ and were therefore not included in this study. Total nonvolatile selenium (SeTNV) represents the sum of the

inorganic (Se(−II,0), Se(IV), Se(VI)), and organic (DMSe and Ox·MSe) selenium compounds that was in solution at the time of sampling.

The selenium solubility strongly increased with increasing redox potential for all pH treatments. The pH had a major effect upon both the levels and chemical forms of dissolved selenium. In general, the selenium solubility was lowest in the incubations at natural pH. Both an increase or decrease in pH led to a higher amount of total soluble selenium. The highest total soluble selenium concentrations were found at a pH of 6.5. Up to 67% of the total Se present in the sediment was found to be soluble at the high redox level (450 mV). This was due to the higher solubility of the iron sulfides and the concurrent release of selenium into solution. The precipitation of Ca^{2+} and SO_4^{2-} as gypsum maintained the reactions in eq 2 and 3. Presser and Barnes (16) reported a small substitution of SeO_4^{2-} for SO_4^{2-} in gypsum precipitated from water samples of the Kesterson Reservoir. In our experiment we did not find evidence of precipitation of a $CaSeO_4$ or $CaSeO_3$ phase, although the formation of such highly soluble compounds is probably possible in conditions of a dry and hot climate. The increase in soluble selenium at pH values greater than 7.5 was significant only at 450 mV. Under the oxidized conditions (450 mV), 20–63% of the total Se present in the sediment was solubilized, depending on the pH. This increase can be explained by the decrease in adsorptive capacity of the soil, especially from the oxidized iron forms for selenite with increasing pH. The adsorption processes of selenite and selenate have been extensively studied in recent years

(4–8). It is generally accepted that selenite adsorption decreases with increasing pH in the range 4–9 and that selenate adsorption is minimal under most pH conditions. The oxidation of iron sulfides resulted in the formation of hydroxylated ferric oxides whose surfaces can adsorb selenite and to a much lesser extent selenate.

The species distribution of selenium identified in the present study is consistent with the stability field of Se species in theoretically derived E_h–pH diagrams (6, 24, 25). Selenate was the major dissolved species under highly oxidized conditions, constituting 95% at higher pH's (8.5, 9) to 75% at lower pH's (7.5, 6.5) of the SeTNV. The Se(−II,0) concentrations were below the detection limit at the high redox levels and the Se(IV) only became detectable at the lower pH levels. At 200 mV, the major part of the SeTNV (60–78%) was in the selenite form. When incubated at 0 mV, there seems to be a rapid oxidation of the Se(−II,0) to selenite since no Se(−II,0) could be detected. No oxidation of selenite to selenate occurred at 0 mV during the 4-week incubation period. In the reduced (−200 mV) treatment, Se(−II,0) comprised 80–100% of the SeTNV. Selenite was detected only at pH 6.5.

Dissolved DMSe and oxidized methylated selenium compounds were detected only in the aerobic incubations. DMSe comprised 15% of the SeTNV, while the Ox·MSe fraction made up 5% of the SeTNV. Assimilation of selenite and reductive methylation have been proposed as first steps in the methylation pathway of selenium (25, 26). Cooke and Bruland (13) showed outgassing of selenium in the biologically active Kesterson Reservoir to be substantial. They suggested that the production of DMSe occurred by intra- and/or extracellular transformation of biogenically derived Se-methylselenomethionine. Although we found dissolved methylated selenium compounds only under aerobic conditions, selenium volatilization under anaerobic conditions has also been reported (26–28). It is important to note that in these studies very high selenium concentrations were added to the soil. In the experiment reported here, solubility of indigenous selenium was very low under the reduced conditions (Tables I and II). Contamination of the analytical-grade HNO_3 with selenium (up to 20 ng mL^{-1}), used to trap evolved selenium species, made it difficult to determine the exact amount of selenium volatilized. However, after making the appropriate corrections, we found selenium volatilization to be significant only at 200 and 450 mV. No evidence was found for selenium volatilization under reduced conditions in our experiments.

Conclusions

Sediment redox potential and pH were shown to control the speciation and solubility of selenium. At low redox levels selenium solubility was low and controlled by an iron selenide phase. Total soluble selenium concentrations substantially increased upon oxidation or increase in sediment redox potential. Under highly oxidized conditions, selenate became the major species in solution and soluble selenium concentrations reached a maximum. Dimethyl selenide and other dissolved methylated selenium compounds were detected only under oxidized conditions. Redox potential and pH exhibit a major impact on selenium speciation, solubility, and volatilization and are therefore of paramount importance in the study of selenium biogeochemistry.

Literature Cited

(1) Ahlrichs, J. S.; Hossner, L. R. *J. Environ. Qual.* **1987**, *16*, 95–98.
(2) Alemi, M. H.; Goldhamer, D. A.; Grismer, M. E.; Nielsen, D. R. *J. Environ. Qual.* **1988**, *17*, 613–618.
(3) Alemi, M. H.; Goldhamer, D. A.; Nielsen, D. R. *J. Environ. Qual.* **1988**, *17*, 603–613.
(4) Balistrieri, L. S.; Chao, T. T. *Soil Sci. Soc. Am. J.* **1987**, *51*, 1145–1151.
(5) Bar-Yosef, B.; Meek, D. *Soil Sci.* **1987**, *144*, 11–19.
(6) Neal, R. H.; Sposito, G.; Holtzclaw, K. M.; Traina, S. J. *Soil Sci. Soc. Am. J.* **1987**, *51*, 1161–1165.
(7) Neal, R. H.; Sposito, G.; Holtzclaw, K. M.; Traina, S. J. *Soil Sci. Soc. Am. J.* **1987**, *51*, 1165–1169.
(8) Geering, H. R.; Cary, E. E.; Jones, L. H.; Allaway, W. H. *Soil Sci. Soc. Am. J.* **1968**, *32*, 35–40.
(9) Elrashidi, M. A.; Adriano, D. C.; Workman, S. M.; Lindsay, W. L. *Soil Sci.* **1987**, *144*, 141–152.
(10) Patrick, W. H., Jr.; Williams, B. G.; Moraghan, J. T. *Soil Sci. Soc. Am. J.* **1981**, *37*, 331–332.
(11) Abu-Erreish, G. M.; Whitehead, E. I.; Olson, O. E. *Soil Sci. Soc. Am. J.* **1968**, *106*, 415–420.
(12) Patrick, W. H., Jr.; Henderson, R. E. *Soil Sci. Soc. Am. J.* **1981**, *45*, 855–859.
(13) Cooke, T. D.; Bruland, K. W. *Environ. Sci. Technol.* **1987**, *21*, 1214–1219.
(14) Brimmer, S. P.; Fawcett, R. W.; Kulhavy, K. A. *Anal. Chem.* **1987**, *59*, 1470–1471.
(15) Fujii, R.; Deverel, S. J.; Hatfield, D. B. *Soil Sci. Soc. Am. J.* **1988**, *52*, 1274–1283.
(16) Presser, T. S.; Barnes, I. *Water Res. Invest. Rep. (U.S. Geol. Surv.)* **1984**, *84*–4122.
(17) Cutter, G. A. *Anal. Chim. Acta* **1983**, *149*, 391–394.
(18) Roden, R. D.; Tallman, D. E. *Anal. Chem.* **1982**, *54*, 307–309.
(19) Davies, B. A. *Soil Sci. Soc. Am. J.* **1974**, *38*, 150–151.
(20) Drever, J. I. *The Geochemistry of Natural Waters*, 2nd ed.; Prentice Hall: Englewood Cliffs, NJ, 1988; Chapter 11.
(21) SAS Institute, Inc. *SAS User's Guide*; SAS Institute, Inc.: Cary, NC, 1985.
(22) Berner, R. A. *Am. J. Sci.* **1970**, *268*, 1–23.
(23) Lindsay, W. L. *Chemical Equilibria in Soils*; Wiley: New York, 1979; Chapter 17.
(24) Howard, J. H., III, *Geochim. Cosmochim. Acta* **1977**, *41*, 1665–1678.
(25) Coleman, R. G.; Delevaux, M. *Econ. Geol.* **1957**, *52*, 499–501.
(26) Doran, J. W.; Alexander, M. *Soil Sci. Soc. Am. J.* **1976**, *40*, 687–690.
(27) Challenger, F. *Adv. Enzymol.* **1951**, *12*, 432–486.
(28) Reamer, D. C.; Zoller, W. H. *Science (Washington, D.C.)* **1980**, *208*, 500–502.

Temperature Dependence of the Aqueous Solubilities of Highly Chlorinated Dibenzo-p-Dioxins

Kenneth J. Friesen* and G. R. Barrie Webster

Pesticide Research Laboratory, Department of Soil Science, University of Manitoba, Winnipeg, Manitoba, Canada R3T 2N2

■ The aqueous solubilities of a series of highly chlorinated dibenzo-p-dioxins (PCDDs) are reported over an environmentally significant temperature range of 7–41 °C. We have demonstrated that aqueous solubilities may be determined by the dynamic coupled-column liquid chromatography or generator column method with a column loading as low as 0.0002% by weight. The enthalpies of solution of the solid solutes (1,2,3,7-tetra-, 1,2,3,4,7-penta-, 1,2,3,4,7,8-hexa-, and 1,2,3,4,6,7,8-heptachlorodibenzo-p-dioxin) ranged from 39.8 to 47.5 kJ/mol, in good agreement with literature data for lower chlorinated dioxins. A brief thermodynamic analysis of the results indicated that entropy changes may be more important than enthalpy changes in limiting the aqueous solubilities of these solutes over the temperature range under consideration. The total surface areas (TSAs) and total molecular volumes (TMVs) of these solutes show a linear relationship with the logarithm of the aqueous activity coefficients.

Introduction

Polychlorinated dibenzo-p-dioxins (PCDDs) are a group of essentially planar, aromatic compounds (1) characterized by extremely low water solubilities (2, 3), high octanol–water partition coefficients (3), and low vapor pressures (4). Although PCDD congeners have been shown to undergo aqueous photolysis when exposed to light of environmentally significant wavelengths (5, 6), the more highly chlorinated PCDDs are persistent organic chemicals, generally resisting chemical and biological degradation. A number of the 75 PCDDs are extremely toxic (7, 8), particularly those with four to six chlorine atoms and the lateral (2, 3, 7, and 8) positions chlorinated (9). The combination of persistence and toxicity has increased the necessity of understanding the environmental behavior of these chemicals.

Incineration of municipal and industrial wastes, the use of chlorophenols in wood treatment, and chlorine kraft bleaching in pulp and paper mills are considered major sources of PCDD emission into the environment (10). A wide range of PCDDs, including tetra-, penta-, hexa-, hepta-, and octachlorinated congeners have been found in a variety of samples including human adipose tissue and breast milk, fish and sediments from the Great Lakes, and air particulate matter (11–13).

Accurate physical constants of these compounds are necessary in order to better understand and predict the behavior of PCDDs in the environment. The aqueous solubility is of particular importance since the fate and distribution of persistent, hydrophobic chemicals in the environment is largely controlled by this parameter. The availability of the chemical for uptake by biota and the availability for aqueous photolysis are two processes that are directly related to the freely dissolved water concentration and hence the aqueous solubilities of the chemical.

The dynamic coupled-column liquid chromatography or generator column method developed by May et al. (14, 15)

has become a widely accepted method for the accurate determination of aqueous solubilities of highly hydrophobic compounds. In their initial development of the technique, May et al. (14) reported the water solubilities of several polynuclear aromatic hydrocarbons (PAHs). More recently, the generator column method or a slight modification of the technique has been used to determine the aqueous solubilities of polychlorinated dioxins (PCDDs) (2, 3) and polychlorinated biphenyls (PCBs) (16, 17).

In this investigation the water solubilities of four highly chlorinated PCDD congeners are reported over the environmentally significant temperature range of 7–41 °C. Except for octachlorodibenzo-p-dioxin (O_8CDD) (3), the temperature dependence of the aqueous solubilities of PCDD congeners with more than four chlorines has not previously been reported in the literature. The results are used for a brief evaluation of the thermodynamics of dissolution of these solid solutes. Correlation of the water solubilities or aqueous activity coefficients of these congeners with two molecular descriptors, total surface area and total molecular volume, is also presented.

Experimental Section

Chemicals. The PCDDs, purchased from Pathfinder Laboratories Inc. (St. Louis, MO), were each universally carbon-14 ring labeled with a specific activity of 24.16 mCi/mmol. Solvents used to purify the dioxins were distilled-in-glass quality purchased from Caledon Laboratories Inc. (Georgetown, ON). Water for the solubility determinations was laboratory distilled water further distilled from $KMnO_4$ and then from $K_2Cr_2O_7$ to destroy organic impurities and finally filtered through a 0.22-μm Durapore filter (Waters Scientific, Mississauga, ON) prior to use. Liquid scintillation cocktail, Scintiverse I, was purchased from Fisher Scientific (Winnipeg, MB).

Analysis of individual PCDD congeners by HPLC with 85% CH_3OH (15% H_2O) as the mobile phase, collecting fractions for liquid scintillation counting using 10 mL of Scintiverse I as scintillation cocktail, showed that all congeners required purification prior to use in solubility measurements. All PCDDs were, therefore, purified by preparative HPLC on a C_{18} column with 85% CH_3OH as the mobile phase at a flow rate of 1.0 mL/min, collecting each dioxin in a window centered at its retention time. The water in each of these fractions was then removed by a series of azeotropic distillations (81% $CHCl_3$–15% CH_3OH–4% H_2O; bp 52.6 °C) followed by careful rotary evaporation as previously described (2). The process was repeated until addition of $CHCl_3$ no longer caused formation of either a second layer or cloudiness, indicating that all of the water had been removed. $CHCl_3$ was then removed as a binary azeotrope (87% $CHCl_3$–13% CH_3OH; bp 53.5 °C) followed by removal of CH_3OH also as a binary azeotrope (88% acetone–12% CH_3OH; bp 55.7 °C), leaving the dioxin in a relatively volatile solvent. Radiopurity of all congeners was determined by HPLC/LSC to be >99%.

Apparatus. All high-pressure liquid chromatography (HPLC) was performed with a system consisting of a Waters Model 6000A solvent delivery system, a Waters Model 440 UV detector operated at 254 nm, and a 3.9 mm

*Current address: Department of Chemistry, University of Winnipeg, 515 Portage Ave., Winnipeg, Manitoba, Canada R3B 2E9.

0013-936X/89/0924-0097$02.50/0 © 1989 American Chemical Society

Environ. Sci. Technol., Vol. 24, No. 1, 1990 **97**

i.d. × 30 cm Waters μBondapak C_{18} analytical column. The system included a Rheodyne sample injection valve and a Valco eight-port switching valve to place the generator column in or out of line with the C_{18} column. A Waters Model III column oven and temperature control unit were used to maintain the temperature of the generator column to better than ±0.5 °C.

A Beckman LS 7500 liquid scintillation counter was used for liquid scintillation counting. The H# method, with automatic quench compensation, was used for quench monitoring of all samples. A 10-min count time was preset with samples counted to a 2σ error of 2%. β-Emissions from carbon-14 were monitored in the 397–655 counting channel, providing an energy window of 18–160 keV. A set of Amersham sealed quenched standards containing ^{14}C-labeled toluene were used to prepare the quench curve for the analyses.

Water Solubility Determinations. The generator column (3.9 mm i.d. × 30 cm) was prepared as previously described (2) by coating 60/80 mesh glass beads with 0.0002–0.0003% by weight ($\sim$20–30 μg/10 g of beads) of the PCDD.

The generator column was placed into the column oven, which was set into a Styrofoam cooling chamber maintained at temperatures just below 5 °C for the low-temperature determinations. The generator column was plumbed into the HPLC system forming a loop on the eight-port Valco switching valve. With each change in temperature the column and the tubing from the generator column to the switching valve were conditioned with 300 mL of water at 1.0 mL/min prior to connecting it at the switching valve.

Saturated solutions of the PCDDs were prepared by pumping the purified water through the system at 1.0 or 2.0 mL/min and extracting the PCDD onto the C_{18} analytical column. After a measured volume of water had been collected, the generator column was taken out of line with a turn of the switching valve. The analytical column was eluted with 85% CH_3OH at a flow rate of 1.0 mL/min. Fractions were collected at regular intervals, 10 mL of Scintiverse I was added to each, and analyses were carried out by liquid scintillation counting. Water solubilities were calculated after correcting for background activity.

Results and Discussion

Aqueous Solubilities. Solubilities of four congeners, 1,2,3,7-tetrachlorodibenzo-p-dioxin (T_4CDD), 1,2,3,4,7-pentachlorodibenzo-p-dioxin (P_5CDD), 1,2,3,4,7,8-hexachlorodibenzo-p-dioxin (H_6CDD), and 1,2,3,4,6,7,8-heptachlorodibenzo-p-dioxin (H_7CDD), were each measured at six temperatures as summarized in Table I. In most cases precisions for replicate analyses ranged from 0.2 to 4.4%. However, when the entire procedure including PCDD purification and generator column preparation was repeated, overall variations ranged from 2.3% for P_5CDD to 9.6, 14.3, and 14.1% for H_6CDD, H_7CDD, and T_4CDD, respectively, based on the 21 °C solubilities. The variations for H_6CDD and H_7CDD are believed to indicate the difficulty in determination of solubilities of the more hydrophobic congeners. The variability in the determinations of the T_4CDD congener, however, was attributed to difficulties in reproducibly purifying the parent dioxin from a closely related isomer.

Solubilities were generally determined at several flow rates, usually 1.0 and 2.0 mL/min, to verify that saturated solutions were in fact prepared. Except for H_7CDD at 40 °C, no statistically significant differences in solubility (at the 95% confidence level) could be attributed to flow rate changes. Solubilities at 1.0 mL/min varied within

Table I. Water Solubilities of Four PCDD Congeners at Different Temperatures

congener	temp,[a] °C	S_w, mol/L
T_4CDD	7.0	$(7.56 \pm 0.20) \times 10^{-10}$
	11.5	$(8.12 \pm 0.11) \times 10^{-10}$
	17.0	$(12.5 \pm 3.6) \times 10^{-10}$
	21.0	$(14.9 \pm 2.1) \times 10^{-10}$
	26.0	$(22.6 \pm 1.0) \times 10^{-10}$
	41.0	$(43.3 \pm 5.4) \times 10^{-10}$
P_5CDD	7.0	$(1.42 \pm 0.01) \times 10^{-10}$
	11.5	$(1.88 \pm 0.01) \times 10^{-10}$
	17.0	$(2.44 \pm 0.01) \times 10^{-10}$
	21.0	$(3.45 \pm 0.08) \times 10^{-10}$
	26.0	$(4.63 \pm 0.03) \times 10^{-10}$
	41.0	$(12.8 \pm 0.1) \times 10^{-10}$
H_6CDD	7.0	$(5.91 \pm 0.05) \times 10^{-12}$
	11.5	$(7.98 \pm 0.15) \times 10^{-12}$
	17.0	$(10.7 \pm 0.4) \times 10^{-12}$
	21.0	$(12.5 \pm 1.2) \times 10^{-12}$
	26.0	$(20.2 \pm 0.4) \times 10^{-12}$
	41.0	$(48.6 \pm 1.4) \times 10^{-12}$
H_7CDD	7.0	$(2.20 \pm 0.09) \times 10^{-12}$
	11.5	$(2.69 \pm 0.01) \times 10^{-12}$
	17.0	$(3.04 \pm 0.06) \times 10^{-12}$
	21.0	$(5.40 \pm 0.77) \times 10^{-12}$
	26.0	$(6.03 \pm 0.18) \times 10^{-12}$
	41.0	$(14.9 \pm 0.5) \times 10^{-12}$

[a] Generator column oven temperature calibrated with an iron–constantan thermocouple (Omega Engineering Model 199 J).

95.3–106.3% of the values at 2.0 mL/min for all other determinations. These variations fell within the range of all the determinations at 1.0 mL/min, indicating that saturation conditions were established even at 2.0 mL/min. For H_7CDD at 40 °C, solubilities at 1.0 mL/min were 25% greater than those measured at 2.0 mL/min. Since this suggested that saturation was not achieved at 2.0 mL/min, only the data at 1.0 mL/min were considered valid.

In several experiments, the volume of water used in the determination was varied in order to ensure that a systematic error was not left undetected. Volumes of 50, 100, 500, and 1000 mL were used for most solubility determinations for T_4CDD, P_5CDD, H_6CDD, and H_7CDD, respectively. Doubling the volume of water collected in a number of trials resulted in solubility changes ranging from −1.7 to +6.0%, well within the precision of the method. Changes in the volume of water, therefore, did not produce statistically significant differences in the measured aqueous solubilities of the chlorinated dioxins under investigation. The relative error in the analysis, however, was expected to increase as smaller amounts of material were collected. Increasing the volume of water used was designed to compensate for this phenomenon.

Differences in melting points of the congeners studied have a noticeable correlation with observed solubilities. For example, T_4CDD (mp 175 °C) and P_5CDD (mp 188 °C) have similar melting points, with P_5CDD exhibiting a 4.3-fold decrease in S_w at 26 °C. A large melting point change occurs between P_5CDD and H_6CDD (mp 261 °C), with a corresponding 27-fold decrease in solubility. The melting point of H_7CDD (mp 265 °C) is virtually identical with that of H_6CDD, with only a 2.3-fold decrease in S_w observed at 26 °C.

The aqueous solubilities determined in this study are in reasonable agreement with those available in the literature. Shiu et al. (3), using a column loading of 0.1–0.5%, reported a water solubility of 630 ng/L for 1,2,3,4-T_4CDD at 25 °C with an enthalpy of solution of 33.36 kJ/mol. Doucette and Andren (18) reported 470 ng/L as the solubility for the same congener using 0.1% column loading.
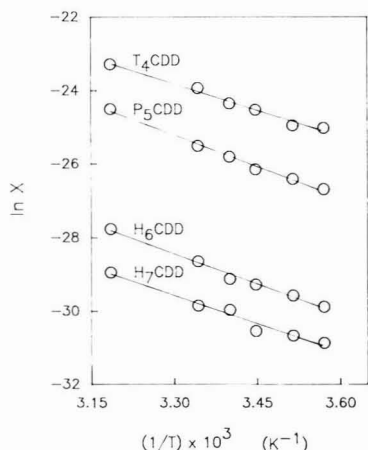
Figure 1. Temperature dependence of the aqueous solubilities of four polychlorinated dibenzo-p-dioxins.

Table II. Enthalpies of Solution of PCDD Congeners

congener	ΔH_s, kJ/mol	r^2
1,2,3,7-T$_4$CDD	39.8 ± 2.4	0.985
1,2,3,4,7-P$_5$CDD	47.5 ± 1.9	0.993
1,2,3,4,7,8-H$_6$CDD	45.5 ± 2.2	0.991
1,2,3,4,6,7,8-H$_7$CDD	42.2 ± 3.6	0.971

With a column loading of 0.0017%, Lodge (19) obtained an aqueous solubility for 2,3,7,8-T$_4$CDD of 483 ng/L at 17 °C. Our data for 1,2,3,7-T$_4$CDD, with a water solubility of 727 ng/L at 26 °C and an enthalpy of solution of 39.8 kJ/mol, determined with 0.0002% (w/w) column loading, are consistent with the data for other tetrachlorinated PCDDs and illustrates that low column loadings may be used in solubility determinations of this type. The excellent correlation of subcooled liquid solubilities of PCDDs with chlorine number and molar volume presented in Shiu et al. (3), which includes our 21 °C data, further supports the use of the low column loadings used in this study.

Thermodynamics of Dissolution. Assuming that the enthalpy of solution of the solid solutes (ΔH_s) is constant over the fairly small temperature range used in this study (7–41 °C), the temperature dependence of the aqueous solubility may be expressed by the integrated form of the van't Hoff equation (20)

$$\ln X = -\Delta H_s/RT + C \tag{1}$$

where X is the mole fraction aqueous solubility, T is the absolute temperature, and R is the gas constant. This equation, which applies to solutes below their melting point, has previously been used to determine the enthalpies of solution of a series of polychlorinated biphenyls (16). Therefore, plotting $\ln X$ vs $1/T \times 10^3$ (Figure 1) provided ΔH_s from the slope of a linear regression of each set of data, as summarized in Table II. A linear relationship of $\ln X$ with inverse absolute temperature is a valid treatment, since no obvious curvature is evident in the plot. Hence the assumption of a constant enthalpy of solution over the temperature range under investigation is appropriate.

The enthalpies of solution for the PCDDs studied fall within a fairly narrow range of 39.8–47.5 kJ/mol. These values are in good agreement with the data of Shiu et al. (3), who reported enthalpies of solution ranging from 33.4 to 53.6 kJ/mol for a series of chlorinated dioxins, ranging
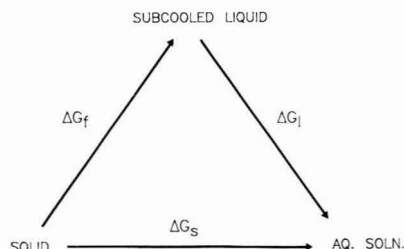
Figure 2. Thermodynamic cycle for the dissolution process, involving the solid, the hypothetical subcooled liquid, and the aqueous solution.

from the parent nonchlorinated dioxin to 1,2,3,4-T$_4$CDD. There is no obvious correlation between enthalpy of solution and either chlorine number or melting point. However, by comparison with reported enthalpies of solution for PCBs and PAHs, it appears that the range of enthalpies may have some relation to the structure of the class of chemicals under investigation. Previous studies have reported a range in ΔH_s for PCBs from 28.5 to 66.6 kJ/mol (16) and for PAHs from 28.7 to 56.9 kJ/mol (15). The smaller variation in ΔH_s for the PCDDs and PAHs above may reflect the greater degree of rigidity of these compounds since they are not subject to rotation about a C–C bond as are most PCBs (21). If the PCB and PAH data for structurally similar compounds are compared, the variation is not nearly as great. For example, ΔH_s for the three members of the anthracene group range from 42.3 to 44.8 kJ/mol, whereas ΔH_s for hexa-, octa-, nona-, and decachlorobiphenyl, with similar Cl substitution patterns, range from 45.6 to 66.6 kJ/mol. However, the observed range is greater for the PCBs than for the PAHs and PCDDs.

The dissolution of a solid solute may be treated thermodynamically as a stepwise process (Figure 2) as recently discussed by Opperhuizen et al. (22). The Walden rule (23), that the entropy of fusion (ΔS_f) for rigid organic solids may be approximated by the value 56.5 J/mol K, is normally assumed to apply to rigid structures such as the PCDDs (3). We have used this value in the following treatment, although somewhat higher entropies of fusion have been estimated for a series of PCDDs by Rordorf (24, 25) using a vapor pressure correlation method. The free energy change for the dissolution of the solid (ΔG_s) may be broken down into contributions for the solid → subcooled liquid process (ΔG_f), essentially a melting point correction term, and the subcooled liquid → aqueous solution process (ΔG_l).

For the overall solid → aqueous solution process, the free energy change (ΔG_s) is calculated from the mole fraction solubility at 26 °C (299 K) according to

$$\Delta G_s = -RT \ln X \tag{2}$$

The entropy contribution is calculated from the relation between these three thermodynamic parameters

$$\Delta G_s = \Delta H_s - T\Delta S_s \tag{3}$$

For the solid → subcooled liquid step, assuming $\Delta S_f = 56.5$ J/mol K, the enthalpy of fusion may be calculated as

$$\Delta H_f = T_m\Delta S_f \tag{4}$$

This calculation further assumes that ΔH_f at the system temperature of 299 K is the same as that at the melting point (T_m). The free energy change associated with this process is calculated from

$$\Delta G_f = \Delta S_f(T_m - T) \tag{5}$$

Table III. Free Energy, Enthalpy, and Entropy Changes Accompanying the Dissolution of PCDDs at 299 K (All Values in kJ/mol)[a]

congener	ΔG_s	ΔG_f	ΔG_l	ΔH_s	ΔH_f	ΔH_l	$-T\Delta S_s$	$-T\Delta S_f$	$-T\Delta S_l$
T_4CDD	59.5	8.4	51.1	39.8	25.3	14.5	19.7	−16.9	36.6
P_5CDD	63.4	9.2	54.2	47.5	26.0	21.5	15.9	−16.9	32.7
H_6CDD	71.2	13.3	57.9	45.5	30.2	15.3	25.7	−16.9	42.6
H_7CDD	74.2	13.5	60.7	42.2	30.4	11.8	32.0	−16.9	48.9

[a] ΔG, ΔH, and ΔS represent free energy, enthalpy, and entropy changes, and subscripts s, f, and l refer to the solid → aqueous solution, solid → subcooled liquid, and subcooled liquid → aqueous solution steps, respectively (see Figure 2).

The thermodynamics of the subcooled liquid → aqueous solution stage are simply determined from a summation, since the overall dissolution is viewed as a two-step process.

The thermodynamic parameters for each of these steps calculated for each PCDD congener are summarized in Table III. The fact that $\Delta G_l \gg \Delta G_f$ suggests that the subcooled liquid → aqueous solution step is a critical step in determining the solubilities of these solutes. A similar observation has recently been reported for PCBs (16). For the solid → subcooled liquid step, the unfavorable enthalpy of fusion is somewhat offset by a favorable entropy change. However, for the subcooled liquid → aqueous solution step, both enthalpy and entropy changes are thermodynamically unfavorable. However, the large negative entropy change that accompanies the dissolution of the subcooled liquid appears to be more important than the corresponding enthalpy of solution in controlling the solubility of these solutes in water. This is consistent with the observations recently discussed regarding the solubility process for PCBs (16, 22). The solute–solvent interactions that accompany the formation of a cavity in the solvent (26) followed by placement of the hydrophobic solute into the cavity are thus important interactions determining the solubilities of these compounds as they are for PCBs.

When the entropies of fusion estimated for the PCDDs by Rordorf (25), (82, 90, 88, and 100 J/mol K for 1,2,3,7-T_4CDD, 1,2,3,4,7-P_5CDD, 1,2,3,4,7,8-H_6CDD, and 1,2,3,4,6,7,8-H_7CDD, respectively) are used, the enthalpy changes become less unfavorable whereas the entropy changes become more unfavorable for the subcooled liquid → aqueous solution step. The net result is that the greater entropies of fusion predicted for these compounds by Rordorf's vapor pressure correlation method strengthen the conclusion that entropy changes in the subcooled liquid → aqueous solution step limit the solubility of these PCDDs in water.

Correlation of Solubility with Structure. A number of molecular descriptors have been correlated with aqueous solubility to provide expressions that may be used to estimate solubilities based on structural information. For example, chlorine number and molar volumes of PCDDs have been correlated with subcooled liquid solubilities (3) and aqueous activity coefficients of PCBs have been correlated with total surface areas (22, 27) and with total molecular volumes (22). For the PCDDs used in this study, the correlations of both total surface area (TSA) and total molecular volume (TMV) with the aqueous activity coefficient of the solute, γ_W, are examined. For solutes that are solids at the system temperature, γ_W may be calculated according to the equation (27)

$$-\ln X = \ln \gamma_W + \frac{\Delta S_f}{R}\left(\frac{T_m - T}{T}\right) \quad (6)$$

This calculation assumes that the differential heat capacity between the solid and subcooled liquid, $\Delta C_P = 0$. By use of $\Delta S_f = 56.5$ J/mol K, the activity coefficients are calculated for the system temperature, $T = 26$ °C or 299 K.

Table IV. Aqueous Solubility and Structural Parameters of Several PCDD Congeners at 299 K

congener	T_m,[a] °C	$-\ln X$	$\ln \gamma_w$	TSA, Å²	TMV, Å³
T_4CDD	175	23.93	20.54	297	210
P_5CDD	188	25.51	21.83	309	224
H_6CDD	261	28.64	23.30	321	239
H_7CDD	265	29.85	24.42	338	253

[a] Melting points provided by Pathfinder Laboratories, Inc.
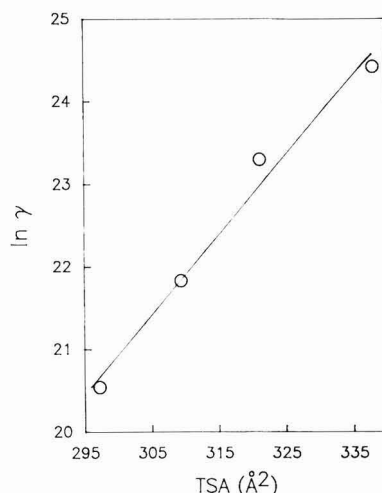
Figure 3. Correlation of total surface area with the aqueous activity coefficient for four PCDD congeners.

TSAs were calculated by Gobas (28) using a previously described shorthand method (29), whereas TMVs were calculated by the method proposed by Edward (30) using volume increments for each type of atom or group in the molecule. The results, along with the calculated γ_W values, are summarized in Table IV.

Plots showing the correlation of γ_W with TSA and TMV are presented in Figures 3 and 4, respectively. The relationship of these structural parameters to the aqueous activity coefficient is determined by first-order linear regression as

$$\ln \gamma_W = 0.0966(TSA) - 8.041 \quad r^2 = 0.984 \quad (7)$$

$$\ln \gamma_W = 0.0904(TMV) + 1.569 \quad r^2 = 0.998 \quad (8)$$

The fact that TMV provides a somewhat better correlation with solubility than TSA may relate to the importance of entropy in the dissolution process. During the dissolution of the solute, a cavity of a particular volume must be created in the aqueous medium to accommodate placement of the solute. This structuring process in the solvent becomes more unfavorable as the volume of the solute molecule increases. Hence, the increased order or unfavorable entropy plays a significant role in limiting the
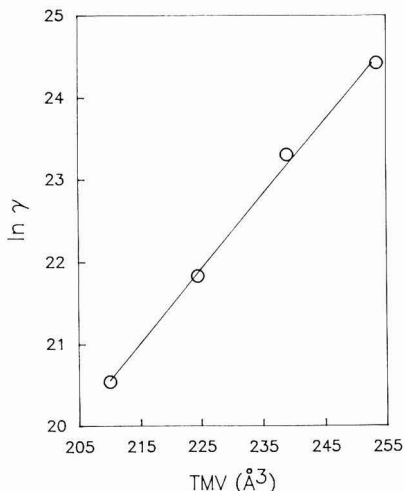
Figure 4. Correlation of total molecular volumes with the aqueous activity coefficient for four PCDD congeners.

solubility of these highly hydrophobic PCDDs, as was the case for PCBs (22).

Conclusions

The generator column method has been used, with ^{14}C-labeled chemicals, to determine aqueous solubilities of polychlorinated dibenzo-p-dioxins down to the nanogram per liter range. Column loading of $\sim$0.0002% by weight produced data that were consistent with literature in which 0.1–1.0% column loading is commonly used for generator column work. This has important safety considerations since considerably less chemical is required for preparation of the column (we used $\sim$20 μg/column), reducing the exposure and disposal problems with hazardous chemicals such as PCDDs.

The enthalpies of solution of these solid solutes, ranging from 39.8 to 47.5 kJ/mol, are comparable to those reported in the literature for other PCDD congeners. Losses in entropy appear to be important in limiting the solubility of PCDDs in water as has been reported for PCBs. For the homologous series of chlorinated dioxins used in this study, linear relationships are demonstrated between both total molecular volumes (TMVs) and total surface areas (TSAs) with the aqueous activity coefficient.

Registry No. 1,2,3,7-T$_4$CDD, 67028-18-6; 1,2,3,4,7-P$_5$CDD, 39227-61-7; 1,2,3,4,7,8-H$_6$CDD, 39227-28-6; 1,2,3,4,6,7,8-H$_7$CDD, 35822-46-9.

Literature Cited

(1) Boer, F. P.; van Remoortere, F. P.; North, P. P.; Neuman, M. A. *Acta Crystallogr.* **1972**, *B28*, 1023–1029.

(2) Friesen, K. J.; Sarna, L. P.; Webster, G. R. B. *Chemosphere* **1985**, *14*, 1267–1274.

(3) Shiu, W. Y.; Doucette, W.; Gobas, F. A. P. C.; Andren, A.; Mackay, D. *Environ. Sci. Technol.* **1988**, *22*, 651–658.

(4) Rordorf, B. F. *Thermochim. Acta* **1985**, *85*, 435–439.

(5) Choudhry, G. G.; Webster, G. R. B. *Chemosphere* **1985**, *14*, 893–896.

(6) Dulin, D.; Drossman, H.; Mill, T. *Environ. Sci. Technol.* **1986**, *20*, 72–77.

(7) Kociba, R. J.; Cabey, O. *Chemosphere* **1985**, *14*, 649–660.

(8) Barnes, D. G.; Bellin, J.; Cleverly, D. *Chemosphere* **1986**, *15*, 1895–1903.

(9) Rappe, C. *Environ. Sci. Technol.* **1984**, *18*, 78A–90A.

(10) Rappe, C.; Andersson, R.; Bergqvist, P.-A; Brohede, C.; Hansson, M.; Kjeller, L.-O.; Lindstrom, G.; Marklund, S.; Nygren, M.; Swanson, S. E.; Tysklind; M., Wiberg, K. *Chemosphere* **1987**, *16*, 1603–1618.

(11) Czuczwa, J. M.; McVetty, B. D.; Hites, R. A. *Chemosphere* **1985**, *14*, 623–626.

(12) Czuczwa, J. M.; Hites, R. A. *Environ. Sci. Technol.* **1986**, *20*, 195–200.

(13) Ryan, J. J.; Schecter, A.; Sun, W.-F.; Lizotte, R. In *Chlorinated Dioxins and Dibenzofurans in Perspective*; Rappe, C., Choudhary, G., Keith, L. H., Eds.; Lewis Publishers, Inc.: Chelsea, MI, 1986; pp 3–16.

(14) May, W. E.; Wasik, S. P.; Freeman, D. H. *Anal. Chem.* **1978**, *50*, 175–179.

(15) May, W. E.; Wasik, S. P.; Freeman, D. H. *Anal. Chem.* **1978**, *50*, 997–1000.

(16) Dickhut, R. M.; Andren, A. W.; Armstrong, D. E. *Environ. Sci. Technol.* **1986**, *20*, 807–810.

(17) Miller, M. M.; Ghodbane, S.; Wasik, S. P.; Tewari, Y. B.; Martire, D. E. *J. Chem. Eng. Data* **1984**, *29*, 184–190.

(18) Doucette, W. J.; Andren, A. W. *Chemosphere* **1988**, *17*, 243–252.

(19) Lodge, K. B. *Chemosphere* **1988**, *18*, 933–940.

(20) Hildebrand, J. H.; Prausnitz, J. M.; Scott, R. L. *Regular and Related Solutions*; Van Nostrand Reinhold: New York, 1970.

(21) Bruggeman, W. A.; Van der Steen, J.; Hutzinger, O. *J. Chromatogr.* **1982**, *238*, 335–346.

(22) Opperhuizen, A.; Gobas, F. A. P. C.; Van der Steen, J. M. D.; Hutzinger, O. *Environ. Sci. Technol.* **1988**, *22*, 638–646.

(23) Yalkowsky, S. H. *Ind. Eng. Chem. Fundam.* **1979**, *18*, 108–111.

(24) Rordorf, B. F. *Thermochim. Acta* **1987**, *112*, 117–122.

(25) Rordorf, B. F. *Chemosphere* **1989**, *18*, 783–788.

(26) Hermann, R. H. *J. Phys. Chem.* **1972**, *76*, 2754–2759.

(27) Mackay, D.; Mascarenhas, R.; Shiu, W. Y.; Valvani, S. C.; Yalkowsky, S. H. *Chemosphere* **1980**, *9*, 257–264.

(28) Gobas, F. A. P. C., personal communication.

(29) Opperhuizen, A. D.Sc. Thesis, University of Amsterdam, The Netherlands, 1986.

(30) Edward, J. T. *J. Chem. Educ.* **1970**, *47*, 261–270.

Distribution and Mobilization of Arsenic and Antimony Species in the Coeur D'Alene River, Idaho

Wai-Man Mok and Chien M. Wai*

Department of Chemistry, University of Idaho, Moscow, Idaho 83843

■ Sediments from the Main Stem and the South Fork of the Coeur d'Alene River are contaminated with As, Sb, and other heavy metals from the local mining operations. Water samples from the South Fork and the Main Stem showed high levels of As (0.11–1.64 $\mu g/L$) and Sb (0.23–8.25 $\mu g/L$) relative to those from the North Fork (0.26 $\mu g/L$ As and 0.17 $\mu g/L$ Sb). Arsenic(III) was found to be the predominant form in the waters of the South Fork and Main Stem of the Coeur d'Alene River, whereas the North Fork generally had higher As(V) concentrations. The major inorganic Sb species was Sb(V) in all three branches of the river. Leaching of As and Sb species from the contaminated Main Stem sediments depends on the pH values of the water as well as on the free iron oxides and manganese oxides present in the sediments. Factors controlling the distribution and mobilization of As and Sb species in this aquatic environment are discussed.

Introduction

Mining is the main industry along the South Fork of the Coeur d'Alene River in northern Idaho. The area is one of the major silver, lead, and zinc producing areas in the United States. Associated with the mining industry of the area has been the problem of heavy metal pollution (*1*). Mining and smelting wastes have been discharged into the South Fork of the river since mining began in this area some 80 years ago. The installation of settling ponds for mill wastes in 1968 has greatly reduced the present discharge of mining wastes into the river from the active mining operations. However, huge amounts of mine tailings have already been deposited in the river and spread to the valley due to flooding and the changing of river channels. These contaminated sediments are being leached to varying degrees by surface water and groundwater and are likely to be nonpoint sources of pollution in this area for years to come.

Antimony and arsenic are present in the mine wastes in significant amounts. The distribution and mobility of these two elements in the contaminated sediments of the Coeur d'Alene River system are not known. Sb and As are interesting for environmental studies because their toxicity and physiological behavior depend on their oxidation states. Biologically, As(III) is considered more toxic than As(V) (*2*). The relative toxicity of Sb(III) and Sb(V) is less known; however, soluble salts of Sb have been shown to be toxic (*3*). The United States Public Health Service (USPHS) recommends that the As concentration in drinking water should not exceed 10 $\mu g/L$. There is no criterion for Sb given by the USPHS. Knowledge of the chemical factors controlling the distribution and mobilization of the As and Sb species in natural water systems is important for environmental control and monitoring of these toxic metals as well as for an understanding of their geochemical and biological cyclings.

The Coeur d'Alene River system can be divided into three components: the North Fork, which supports a rather healthy aquatic community, the South Fork, which has received mining wastes for over 80 years, and the Main Stem, which has been affected by the conditions of the South Fork. The South Fork of the Coeur d'Alene River

Table I. Description of the Seven Selected Sediment-Sampling Sites

station	site description
SC-Main Stem	near Cataldo Mission flats, very close to station 5
SR-Main Stem	At station 7, near the bridge beyond Rose Lake
SB-Main Stem	near Blue Lake
SH-Main Stem	At station 8, near Harrison
SM-Main Stem	near the mouth of the Coeur d'Alene River
SN-North Fork	at station 3 before the North Fork enters the Main Stem
SS-South Fork	at station 2 of Smelterville Flats

is a shallow, swiftly flowing stream; the Main Stem of the river is much deeper and slower moving than the South Fork. The gradient of the South Fork is ~5.7 m/km, while the gradient of the main stem is only ~0.19 m/km (*4*). Because of the large gradient of the South Fork, most of the mine tailings discharged to the South Fork did not settle out until they reached the Main Stem.

The present work was undertaken to study the distribution and speciation of inorganic As and Sb species in the Coeur d'Alene River and to investigate the effects of the contaminated sediments on water quality. Factors affecting the mobility of As and Sb at the sediment–water interface are discussed. Besides As and Sb, current levels of Zn, Mn, Fe, and sulfate in the river are also reported.

Experimental Section

Sampling. Nine sampling stations were selected to study the distribution of As and Sb in the Coeur d'Alene River system (Figure 1). Samples were collected from December 1986 through June 1987 for this study. Water samples were collected in 1-L high-density linear polyethylene bottles. The containers were washed with nitric acid and rinsed with deionized water prior to sample collection. Water samples were filtered through 0.45-μm membranes and stored in a refrigerator at ~4 °C prior to chemical analysis, which usually took place within several days after collection. In laboratory experiments at room temperature with As(III) and As(V), Cherry et al. (*5*) found that no oxidation of As(III) was observed for at least 3 weeks. Andreae et al. (*6*) found no measurable change of Sb species and concentration over a 4-day span if the samples were stored in the dark at room temperature. For speciation measurements storage at 4 °C appears to be the safest method for natural water samples (*7*). No changes in the concentrations of As and Sb species in natural waters stored at 4 °C for 1 week were observed in our laboratory. Filtered samples were also preserved by acidification to pH 2 with HNO_3 for Zn, Mn, and Fe analysis.

Sediment samples were taken at seven selected locations (Table I). The sediments collected were at least 6 in. below the surface. They were taken with plastic shovels. The sediment samples were sealed in plastic bags and stored at 4 °C in a refrigerator until used. A sediment core (22 cm in length) was also taken from the delta area at the mouth of the Coeur d'Alene River with a core sampling apparatus. Six core increments were analyzed to study the
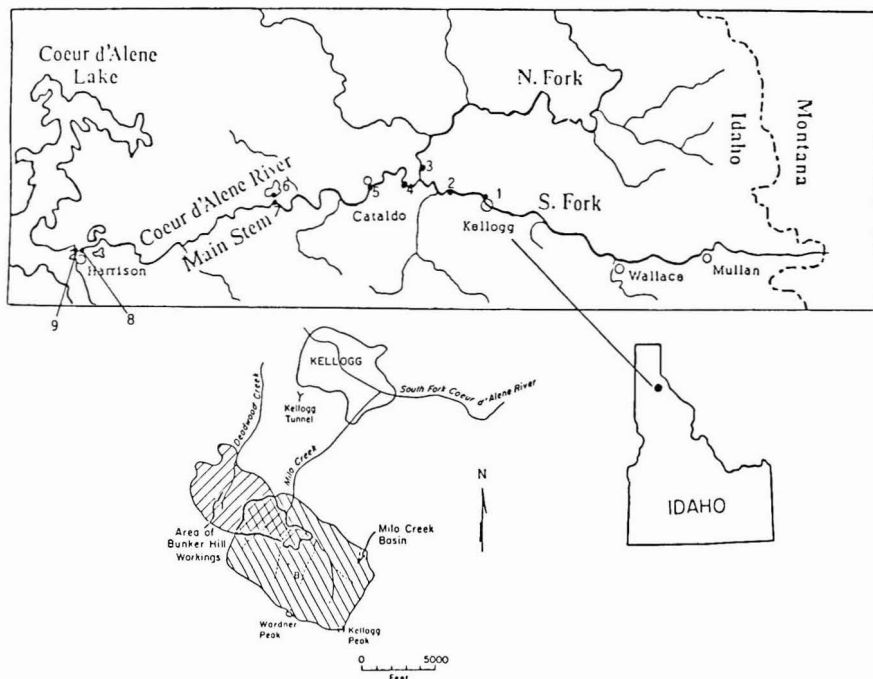
Figure 1. Location of the sampling stations in the Coeur d'Alene River.

vertical distribution of As and Sb in the sediment column.

Analysis of Water Samples. A pyrrolidinecarbodi-thioate (PCDT) extraction procedure was used for the simultaneous determination of trivalent and pentavalent inorganic species of arsenic and antimony in natural waters. The details of the extraction procedure are given in the literature (8). The extraction procedure not only concentrates As and Sb species but also eliminates common interfering ions, such as the alkali metals, alkaline earth metals, halogens, and phosphate. The applicability of this method to water samples with complex matrices and different chemical compositions has been reported (8).

Samples and standards were irradiated in a TRIGA nuclear reactor and counted with an Ortec Ge(Li) detector. The detector output was fed into an EG&G Ortec Adcam (Model 918) multichannel analyzer. Data from the analyzer were processed by EG&G Ortec software on an IBM-PC. The details of the sample preparation, irradiation, and counting for neutron activation analysis (NAA) are given elsewhere (8). A detection limit of 10^{-3} μg/L As and Sb can be achieved with this extraction method and neutron activation analysis. The coefficients of variation for analyses of replicate samples lie between 2 and 3%, and the recovery of As and Sb species spiked to water samples is always greater than 97%. Concentrations of Zn, Mn, and Fe were determined by using an IL-353 atomic absorption spectrophotometer or an ARL Model 35,000C inductively coupled plasma–atomic emission spectrometer. Sulfate was analyzed by a Dionex Model 2000-I ion chromatograph.

Leaching experiments were carried out to study the release of As, Sb, Zn, Mn, and Fe from the sediments. All experiments were conducted at room temperature under atmospheric pressure. In each system, a sample, usually 60 g of sediment, was placed in a 1-L high-density linear polyethylene bottle and 800 mL of distilled deionized water was added. The sediment–water mixture was kept in suspension by continuous stirring with a magnetic stirrer (9, 10). The leaching experiments involved the measurement of pH and the analysis of leachates for As, Sb, Zn, Mn, and Fe.

Arsenic and Sb in the sediments were determined by a nondestructive neutron activation technique. Samples for neutron activation analysis were first air-dried and ground to less than 200 mesh. Approximately 0.1 g of the dry sample was sealed in a $^2/_5$-dr polyethylene vial. Samples and standards were irradiated together for 2 h in the TRIGA reactor. After cooling for a few days, the samples were counted for 500–4000 s on the Ortec Ge(Li) detector. Mn, Zn, and Fe in the sediments were determined by a Rigaku 3370 automated X-Ray fluorescence spectrometer.

Results and Discussion

Water Quality Data. Table II summarizes the mean values and the ranges of As, Sb, and pH in the waters collected from the selected sites along the Coeur d'Alene River.

Stations 1 and 2, located in the South Fork of the river, have shown consistently high metal readings during the course of this study. Antimony concentrations as high as 8.3 and 6.8 μg/L have been noted at stations 1 and 2, respectively. Arsenic concentrations of 1.2 and 1.6 μg/L have also been observed at stations 1 and 2, respectively. Station 3 is at the lower end of the North Fork before it enters the Main Stem. During the period of this study, station 3 never showed As and Sb concentrations above 0.25 and 0.16 μg/L, respectively. Water quality within the Main Stem of the Coeur d'Alene River is affected by the mixing of the North Fork and South Fork waters. Station 4 is located just below the confluence of the North Fork and South Fork. The substantially lower As and Sb concentrations at station 4, compared with those observed at stations 1 and 2, reflect a dilution effect after mixing with the North Fork waters. Average As and Sb concentrations

Table II. Mean Values and Ranges of As, Sb, and pH in the Waters of the Coeur d'Alene River for the Sampling Period[a]

station	As(III)	As(III) + As(V)	Sb(III)	Sb(III) + Sb(V)	pH
1	0.484	0.670	0.064	4.443	7.53
	0.064–0.830	0.179–1.151	0.017–0.110	1.127–8.245	7.35–7.92
2	0.816	0.902	0.051	4.085	7.36
	0.096–1.370	0.166–1.636	0–0.125	1.112–6.758	7.24–7.49
3	0.039	0.125	0.016	0.093	7.51
	0.022–0.059	0.082–0.252	0–0.027	0.059–0.164	7.32–7.70
4	0.135	0.247	0.021	1.026	7.70
	0.082–0.190	0.112–0.351	0–0.039	0.328–1.893	7.27–9.07
5	0.127	0.220	0.025	0.773	7.42
	0.082–0.190	0.147–0.378	0–0.053	0.235–1.381	7.34–7.61
6	0.163	0.194	0.025	0.565	7.42
	0.126–0.190	0.134–0.293	0–0.046	0.502–0.751	7.09–7.62
7	0.237	0.290	0.029	0.722	7.44
	0.099–0.515	0.145–0.523	0.011–0.051	0.346–1.307	7.32–7.66
8	0.253	0.379	0.033	0.798	7.39
	0.139–0.470	0.286–0.476	0–0.047	0.294–1.270	7.33–7.50
9	0.354	0.630	0.019	0.829	7.53
	0.190–0.723	0.237–1.471	0–0.037	0.393–1.752	7.38–7.73

[a] Concentrations in micrograms per liter.
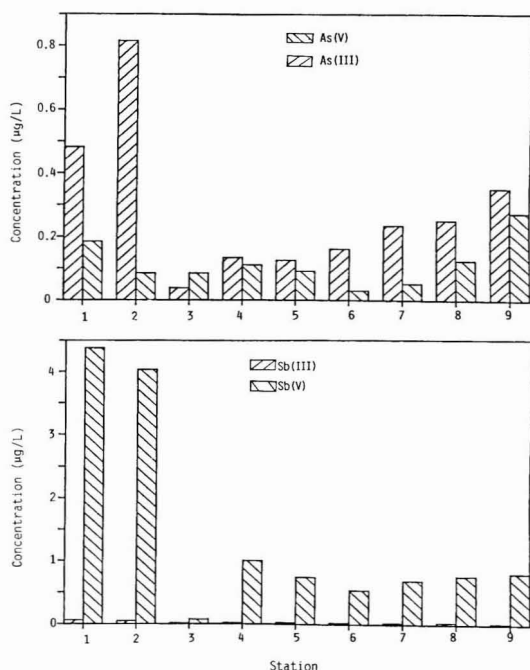
Figure 2. (a) Mean values of As(III) and As(V) and (b) mean values of Sb(III) and Sb(V) in the Coeur d'Alene River during the sampling period.

Table III. As and Sb Levels in North Fork of Coeur d'Alene River, in Lake Coeur d'Alene, and in St. Joe River

		concn, μg/L	
station	date	As(III) + As(V)	Sb(III) + Sb(V)
North Fork	6-26-87	0.115 ± 0.016	0.164 ± 0.029
Southern Lake Coeur d'Alene	8-15-87	0.357 ± 0.005	0.480 ± 0.011
Delta Area	8-15-87	0.440 ± 0.005	1.656 ± 0.020
St. Joe River	8-15-87	0.276 ± 0.004	0.044 ± 0.005
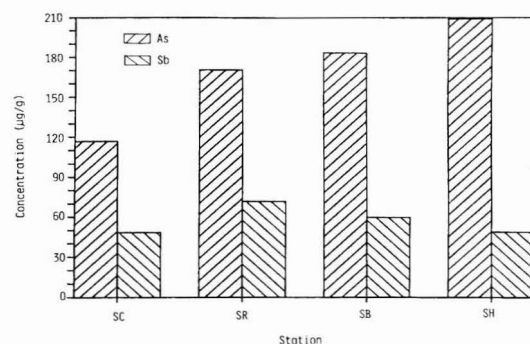
Figure 3. Concentrations of As and Sb in the surface sediments along the Main Stem of the Coeur d'Alene River.

in stations 5 and 7–9 along the Main Stem ranged from 0.11 to 1.47 μg/L and from 0.24 to 1.89 μg/L, respectively. The Main Stem waters generally have considerably lower concentrations of As and Sb compared to the South Fork waters.

Figure 2 shows the mean values of the trivalent and pentavalent As and Sb species in the river during the sampling period. As(III) is the predominant species in the Main Stem and South Fork, while a slightly higher concentration of As(V) is always observed in the North Fork. Contrary to As, the concentration of Sb(V) is always much higher than that of Sb(III) in all three branches of the river.

The St. Joe River, which lies south of the Coeur d'Alene River, is classified as a wild and scenic river by the Na-

tional Forest Service. Water of the St. Joe River should provide some information about the background values of As and Sb in the natural environment. In addition, water samples from the delta area in Coeur d'Alene Lake at the mouth of the Coeur d'Alene River and from the southern part of Coeur d'Alene Lake, which is considered to be much less polluted, were also analyzed. The results are listed in Table III. The As and Sb concentrations in the southern part of Lake Coeur d'Alene, about 0.36 and 0.48 μg/L, respectively, were lower than those in the delta area (0.44 and 1.66 μg/L for As and Sb, respectively). The total As concentration in the North Fork (0.12 μg/L) was comparable to the values from the St. Joe River. The total Sb level of the former, however, was higher than the level of the latter.

Figure 3 shows the concentrations of As and Sb in the surface sediments for the stations along the Main Stem of the river. Arsenic concentration in the sediments ap-

Table IV. Mean Values and Ranges of Zn, Mn, Fe, and Sulfate in the Waters of the Coeur d'Alene River for the Sampling Period[a]

station	Zn mean	Zn range	Mn mean	Mn range	Fe mean	Fe range	SO_4^{2-} mean	SO_4^{2-} range
1	1.48	0.67–2.05	0.16	0.07–0.26	0.02	0–0.06	23.11	6.41–40.23
2	2.73	0.79–4.23	0.98	0.17–1.84	0.23	0–0.73	54.27	7.57–120.38
3	0.02	0.01–0.03	<0.01	0–0.02	ND[b]	nil	2.69	2.13–3.34
4	0.75	0.40–1.17	0.34	0.10–0.47	0.07	0–0.19	17.00	5.31–35.18
5	0.47	0.19–0.75	0.23	0.05–0.38	0.07	0.01–0.31	12.64	4.37–24.73
6	0.04	0.01–0.08	0.14	0.08–0.24	0.15	0.11–0.21	7.95	6.66–9.00
7	0.52	0.25–1.03	0.30	0.07–0.79	0.11	0.04–0.23	13.03	4.20–26.60
8	0.53	0.24–1.07	0.29	0.09–0.71	0.12	0.04–0.21	13.30	4.43–26.75
9	0.25	0.18–0.43	0.17	0.09–0.26	0.11	0.08–0.19	7.86	4.08–12.75

[a] Concentrations in milligrams per liter. [b] ND, not detectable.
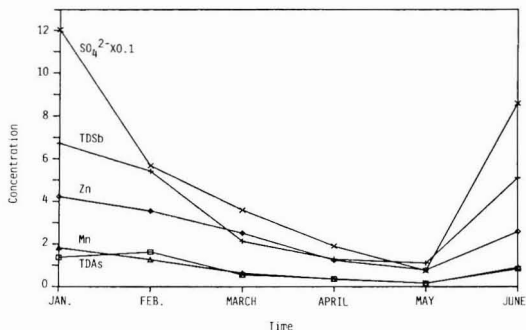
Figure 4. Variation in the concentrations of (TD)As, (TD)Sb, Zn, Mn, and SO_4^{2-} at station 2 as a function of time during the sampling period. (TD)As = As(III) + As(V), (TD)Sb = Sb(III) + Sb(V). Concentrations of As and Sb in micrograms per liter; concentrations of Zn, Mn, and SO_4^{2-} in milligrams per liter.

Table V. Concentrations of As, Sb, Zn, Mn, and Fe in the Sediments Collected from the Coeur d'Alene River[a]

sample	As	Sb	Zn	Mn	% Fe
			concn, $\mu g/g$		
SC	117.05	48.72	5703	6081	8.30
SR	170.43	72.11	9262	8163	10.49
SB	183.50	60.19	5679	11323	12.41
SH	209.09	49.20	4409	10021	11.82
SM	147.39	48.71	4148	8465	10.05
SN	10.68	1.91	142	186	2.57
SS	111.00	136.81	9430	17285	21.24

[a] As and Sb were determined by instrumental neutron activation analysis (INAA) based on quadruplicate analyses. Zn, Mn, and Fe were determined by XRF. Description of sampling sites is given in Table I.

pears to increase toward the mouth of the river (117 $\mu g/g$ at Cataldo, 209 $\mu g/g$ at Harrison). Although As concentration in the surface sediments was much higher than that of Sb (As/Sb ratios vary from 2 to 4), the As level in the water was relatively low (As/Sb ratios vary from 0.2 to 0.8).

Table IV summarizes the mean values and ranges of Zn, Fe, Mn, and sulfate in the Coeur d'Alene River waters during the sampling period. Zn, Mn, and sulfate were also used as water quality indicators because both $ZnSO_4$ and $MnSO_4$ are very soluble. High Zn, Mn, and Fe levels were observed at station 2 of the South Fork. Zn and Mn in the North Fork (station 3) were found only in trace amounts (<0.03 mg/L). Zn and Mn in the Main Stem have overall mean values of 0.50 and 0.27 mg/L, respectively, ranging from 0.18 to 1.07 mg/L for Zn and 0.05 to 0.79 mg/L for Mn. The mean values of sulfate concentrations in the river vary from 2.69 mg/L at station 3 of the North Fork to 54.27 mg/L at station 2 of the South Fork.

In general, the concentrations of As, Sb, SO_4^{2-}, and the other trace metals studied were found to be higher in the low flow of winter and lower in the high flow during the spring months at the time of snow melt. An increase of metal and sulfate concentrations was also observed in some stations in June when the water level falls down. Figure 4 shows the seasonal variations in the concentrations of the ions studied at station 2 during the sampling period. Similar trends were observed at other stations.

Station 6 was established in Rose Lake at a point close to the river. During high water in the spring, the river sometimes passes through a culvert and seeps into Rose Lake. This station was arbitrarily chosen to evaluate contamination from the community of the river. As(III) and Sb(V) were still the predominant species observed in the lake water samples. The low concentrations of Zn, Mn, and sulfate in the lake water suggested that there was no obvious correlation between Rose Lake and the Main Stem during the sampling period.

Leaching of As, Sb, and Other Metals from the Sediments. X-ray diffraction showed that the sediment samples were mainly composed of quartz, muscovite, and siderite with small quantities of kaolinite. Potassium feldspar existed in all samples. The clay fraction made up about 2.0–3.2% of the bulk sample and was composed of essentially the same minerals as found in the bulk samples. The diffraction patterns for the clay fraction were generally less intense than those of the bulk samples, implying a poorer crystallinity.

The As, Sb, Zn, Fe, and Mn contents of the sediments studied are presented in Table V. The North Fork sediments (SN) showed much lower metal contents than those from the Main Stem Coeur d'Alene River.

Six sediment samples, five from the Main Stem and one from the North Fork, were leached with deionized water under aerobic conditions with stirring. The description of sampling sites is given in Table I. Leachates from the sediments in all the leaching experiments showed very little variation in pH during the course of leaching. The mean pH in the leachates was 6.9. Cumulative releases of As and Sb from the Main Stem sediments (SR) are shown in Figure 5. Trends observed in other sediments from the Main Stem were similar to those of sediment SR. Sb(V) was the predominant Sb species released during leaching. Conversely, leaching under the same conditions resulted in the almost exclusive release of As(III). The releases of total arsenic [(TD)As = As(III) + As(V)] occurred mainly during the initial leaching period and appeared to approach asymptotic limits. Although the As content in the sediments was higher than that of Sb, the release of (TD)Sb always exceeded that of (TD)As after a short leaching period. The same trend was observed in the concentrations
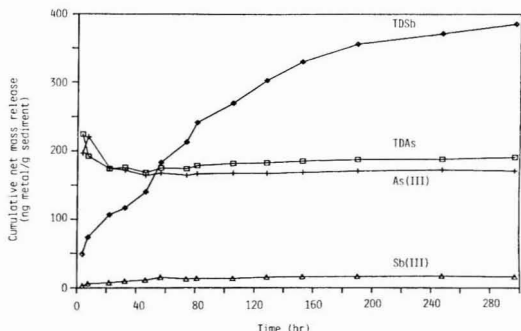
Figure 5. Cumulative releases of As and Sb from sediment SR. (TD)As = As(III) + As(V), (TD)Sb = Sb(III) + Sb(V).

of As and Sb in the South Fork and Main Stem waters. The leaching experiments yielded results correlating with the observed river water quality with respect to arsenic and antimony.

Leaching of metals from sediments in a river should also depend upon the flow of water. The effect was more pronounced at low flow because of longer sediment–water contact time and smaller water volume in the river. the As and Sb concentrations in the Coeur d'Alene River were always lower during the high flow rate in the spring runoff. Runoff from snow melt also served to dilute the effect of mineralized groundwaters added to the river system along parts of its upper reaches. Higher As and Sb concentrations were observed in the river water when the flow was low and groundwater discharge was the major source.

Sediments from the North Fork were relatively uncontaminated with mining wastes. Arsenic and antimony concentrations in the sediment samples from the North Fork of the river were $1/10$ to $1/35$ of those from the Main Stem. Leaching experiments also indicated that As(III) and Sb(V) were the major leachable species from the North Fork sediments. The amounts of As and Sb released during leaching were substantially lower than those from the Main Stem, in agreement with the water quality data observed in the river. However, the As(V) concentration was found to be slightly higher than that of As(III) in the North Fork water samples, in contrast to the results observed from the leaching experiments. Several competing processes could modify the concentrations of the arsenic species in natural waters, including oxidization of arsenite to arsenate or the reverse reaction, precipitation and adsorption reaction, etc. The kinetics of the arsenite–arsenate transformation in river waters are still not well understood.

The cumulative net mass release of Zn from sediment SR is much greater than those of Mn and Fe. For example, the cumulative release of Zn reached 105 $\mu g/g$ sediment after 300 h of leaching, whereas those of Mn and Fe were 12 and 5 $\mu g/g$ of sediment, respectively, during the same period of time. The other sediment samples from the Main Stem behaved similarly to SR in the leaching process. The releases of these metals from the Main Stem sediments were also substantially higher than those from the North Fork (sediment SN). The results are consistent with those observed in the river waters.

Depth Profiles of Arsenic and Antimony in Sediments. Table VI shows the vertical distribution of As, Sb, Fe, and Mn in a sediment core from the delta area of Lake Coeur d'Alene at the mouth of the Coeur d'Alene River. The surface sediments (0–7 cm) were brown, while those below were dark grey. The sediment core showed high As and Sb concentrations at the surface (197 $\mu g/g$ As and 58

Table VI. Vertical Distribution of As, Sb, Fe, and Mn in the Sediments from the Delta Area of Lake Coeur d'Alene (0–22 cm)[a]

depth, cm	concn, $\mu g/g$		concn, %	
	As	Sb	Fe	Mn
0.5	196.96	58.06	11.19	0.97
4.5	146.63	47.13	9.20	0.71
8.5	7.84	2.99	2.44	0.06
14.5	7.37	1.96	2.35	0.02
18.0	6.21	1.82	2.34	0.02
21.5	5.65	2.20	2.22	0.02

[a] As and Sb were determined by INAA based on quadruplicate analyses. Fe and Mn were determined by XRF.

Table VII. Arsenic and Antimony Distribution Coefficients (D) Following 10 Days of Leaching and the Amounts of Free Iron Oxides and Manganese Oxides[a]

sediment	D_{As}	D_{Sb}	% Fe as free iron oxides	% Mn as free manganese oxides
SC	2032	458	2.73	0.14
SR	902	194	2.41	0.10
SB	692	106	1.71	0.12
SH	990	256	2.27	0.11
SM	384	83	1.46	0.07

[a] Description of sampling sites is given in Table I.

$\mu g/g$ Sb), decreasing with depth to concentrations of a few micrograms per gram. The concentration profiles of As and Sb paralleled those of Fe and Mn, and the sediments showed a very strong correlation between the vertical distributions of As and Sb and those of Fe and Mn, with correlation coefficients of 0.99. The fixation of As in sediments has been attributed to adsorption onto hydrous iron oxide (11–13). Arsenic may also become incorporated into sediments by coprecipitation at the time of formation of the hydrous oxides (14–16). Associations between sediment As and Mn have also been reported (11, 17). Our results indicate that both As and Sb were associated with Fe and Mn. The abnormally high As and Sb concentrations in the surface sediments are likely due to upward migration of these elements through the sediments. It was reported that after burial of surface sediments, Fe, Mn, As, and Sb compounds could redissolve under reducing conditions at depth and migrate upward to the top layers where substantial amounts of As and Sb have become immobilized along with Fe and Mn in the oxidizing zone (11, 12, 17).

Effects of Free Iron Oxides and Manganese Oxides upon the Release of Arsenic and Antimony during Water–Sediment Interactions. Both iron oxides and manganese oxides possess high affinities for many trace metals. To examine the effects of sediment iron oxides and manganese oxides upon the partitioning of As and Sb between the river sediments and the water, the chromatographic distribution coefficient (D) was used and a citrate–dithionite extraction method (18–20) was employed to determine the amounts of free iron oxides and manganese oxides in the Main Stem sediments used in the leaching experiments. To obtain such D values, total As concentrations ($\mu g/g$) in sediments were divided by the cumulative net mass release of total As ($\mu g/g$) following 10 days of leaching. The same was true for Sb. The D values were obtained in our experiments following a procedure described in the literature (21). Values of D for the sediments and their corresponding free iron oxides and manganese oxides are summarized in Table VII. A high D value signifies that a trace element in the sediment was

Metal	pH				
	2.7	4.3	6.3	8.3	11.4
As(III)	3075.97	267.32	164.30	7.75	122.06
As(V)	5062.87	20.04	8.65	113.39	1744.74
Sb(III)	194.59	6.10	2.61	4.68	12.68
Sb(V)	8.89	10.60	96.06	1067.60	1605.53
Zn	1519.66	1028.06	39.85	1.51	3.21
Fe	7161.57	5.04	2.72	9.96	27.75
Mn	987.18	351.40	11.13	<0.10	1.24

[a] As and Sb concentrations in nanograms per gram of sediment. Other metals released are given in micrograms per gram of sediment.

retained more strongly than another one with a low D value.

The linear correlation coefficients between the distribution coefficients for As and free iron oxides and manganese oxides were 0.87 and 0.83, respectively. The corresponding correlation coefficients for Sb and free iron oxides and manganese oxides were 0.90 and 0.75, respectively. The results suggest that the existence of free iron oxides and manganese oxides in the sediments is a significant factor affecting the release of As and Sb during water–sediment interactions. The higher D values for As relative to Sb (Table VII) also suggest that the former is more strongly retained than the latter. Under weakly acidic to basic conditions, As(V) can be coprecipitated on hydrous iron oxides with the formation of the mineral scorodite ($FeAsO_4 \cdot 2H_2O$), which is very insoluble (14–16). It is speculated that both stronger adsorption of As on the existing oxide surfaces and the incorporation of As into the sediments by coprecipitation at the time of formation of hydrous oxides are factors responsible for the observation that, although As concentration was higher than Sb concentration in the sediments, the reverse was observed in the Main Stem and the South Fork river water. This also offers a plausible explanation for the dominance of As(III) in waters from the Main Stem and South Fork and in the sediment leachates. The trivalent As in the river waters probably exists as H_3AsO_3, which is the stable form of As(III) below pH 8 (5). Arsenic(III) in this form is mobile. Thus, the high As(III)/As(V) ratios observed presumably are caused by the immobilization of As(V) through coprecipitation and sorption onto the iron and manganese hydroxides (14).

Effect of pH on Mobilization of Arsenic and Antimony. On a regional scale, acid precipitation is probably an important factor affecting metal mobility in surface water. To study the release of arsenic and antimony with respect to acidity, sediment sample (SR) from the Main Stem was leached for 40 h at controlled pH. Table VIII presents the results. The releases of total As and Sb from the sediments in aqueous solution followed a predictable pattern of increasing release with decreasing pH. The release of As and Sb also rose sharply at high pH. This behavior is distinctive of As and Sb because they both possess an anion chemistry in aqueous solution.

The results indicate that pH variation not only influences the mobility of As and Sb, but also alters the distribution of the metal species. The observation of an enhanced As and Sb solubility both at low and at high pH in our leaching experiments is significant. Since lime treatment is a common method used to deal with acid mine drainage and waste waters related to mine tailings, the discharge of lime-treated waste water with high pH might result in a higher As and Sb release from the sediment in

contact. A near-neutral pH condition would favor the long-term stability of mine wastes with respect to As and Sb.

Conclusion

As(III) was the predominant form of inorganic As in the South Fork and Main Stem of the Coeur d'Alene River, whereas the North Fork generally had higher As(V) concentrations. The major inorganic Sb species was Sb(V) in all three branches of the river. The Main Stem sediments were highly contaminated with As and Sb. In general, the water quality observed in the field was correlated with the results observed from the laboratory leaching experiments. Interaction of water with the contaminated sediments was likely to be a major factor controlling the distribution of As and Sb species in that aquatic environment. Release of As and Sb was related to the free iron oxides and manganese oxides present in the sediments. Mobilization of As and Sb was more likely to occur in sediments low in iron oxides and manganese oxides. Arsenic was more strongly retained in the sediments than Sb, as reflected by the observation that, although the concentrations of As in the Main Stem sediments were higher than those of Sb, the reverse was true in the Main Stem river water and in the solutions of the leaching experiments. pH fluctuation in water also affected the release of As and Sb from sediments. Acid precipitation is an important factor affecting As and Sb mobility in surface water. On the other hand, the sharply increasing release of As and Sb at high pH might also influence the application of a lime treatment method to reduce metal content in acid mine drainage and waste waters related to mine tailings.

The extent to which As and Sb are leached into the river water is also dependent on the flow of the river. The effect is more pronounced at low flow. It is possible that even if there is zero discharge of mine wastes into the river in the future, the water quality of the river may remain affected by the leaching of the polluted sediments, and the concentrations of As and Sb in the Main Stem may still be higher than the geochemical background values. Water quality management planning for the Coeur d'Alene River should, therefore, also consider the nonpoint sources of contamination, including leaching of the river sediments.

The pollution problem existing in the sediments of the Coeur d'Alene River is primarily the result of the uncontrolled discharge of mine wastes into the river during past mining operations. The current data obtained from this area with respect to As and Sb will certainly be valuable to environmental planning and consideration for the Coeur d'Alene Mining District and other similar mining areas.

Literature Cited

(1) Davis, H. T. *Environ. Sci. Technol.* **1978**, *12*, 276.
(2) *Arsenic—Medical and Biological Effects of Environmental Pollutants*; National Academy of Sciences: Washington, DC, 1977.
(3) Luckey, T. D.; Venugopal, B. *Metal Toxicity in Mammals*; Plenum Press: New York, 1977; Vol. 1, p 139.
(4) Norbeck, P. M. M.S. Thesis, University of Idaho, Moscow, ID, 1974.
(5) Cherry, J. A.; Sahikh, A. U.; Tallman, D. E. *J. Hydrol.* **1979**, *43*, 373.
(6) Andreae, M. O.; Asmode, J. F.; Foster, P.; Dack, L. V. *Anal. Chem.* **1981**, *53*, 1766.
(7) Florence, T. M. *Talanta* **1982**, *29*, 345.
(8) Mok, W. M.; Wai, C. M. *Anal. Chem.* **1987**, *59*, 233.

(9) Wai, C. M.; Mok, W. M. A Chemical Speciation Approach to Evaluate Water Quality Problems in the Blackbird Mining Area, Idaho. Research Technical Report; Idaho Water Resources Research Institute; Moscow, ID, 1986; pp 61.

(10) Mok, W. M.; Wai, C. M. *Water Res.* **1989**, *23*, 7.

(11) Crecelius, E. A. *Limnol. Oceanogr.* **1975**, *20*, 441.

(12) Farmer, J. G.; Cross, J. D. *Radiochem. Radioanal. Lett.* **1979**, *39*, 429.

(13) Neal, C.; Elderfield, H.; Chester, R. *Mar. Chem.* **1979**, *7*, 207.

(14) Mok, W. M.; Riley, J. A.; Wai, C. M. *Water Res.* **1988**, *22*, 769.

(15) Aggett, J.; Lybley, S. *Environ. Sci. Technol.* **1986**, *20*, 183.

(16) Wilson, F. H.; Hawkins, D. B. *Environ. Geol.* **1978**, *2*, 195.

(17) Takamatsu, T.; Kawashima, M.; Koyama, M. *Water Res.* **1985**, *19*, 1029.

(18) Jackson, M. L. *Soil Chemical Analysis—Advanced Course,* 2nd ed.; University of Wisconsin: Madison, WI, 1969.

(19) Anderson, B. J.; Jenne, E. A. *Soil Sci.* **1970**, *109*, 163.

(20) Olson, R. V.; Roscoe, E. In *Methods of Soil Analysis,* 2nd ed.; Agronomy Monograph No. 9; Page, A. L., Ed.; University of Wisconsin: Madison, WI, 1982.

(21) Brannon, J. M.; Patrick, W. H., Jr. *Environ. Sci. Technol.* **1987**, *21*, 450.

Mercury Chemistry in Simulated Flue Gases Related to Waste Incineration Conditions

Björn Hall,* Oliver Lindqvist, and Evert Ljungström

Department of Inorganic Chemistry, Chalmers University of Technology and University of Göteborg, S 412 96 Göteborg, Sweden

■ A flue gas generator has been built in order to study mercury reactions. The generator consists of a propane-fueled furnace and a 12 m long temperature-controlled steel duct with a fabric filter. When vaporized (elemental) mercury was added to the propane flame in a concentration of 150 $\mu g/m^3$ and with 8% excess of oxygen, 20–30% of the mercury was oxidized after 0.8 s residence time in the furnace and the duct ($T > 500$ °C). In the presence of HCl(g) in the flue gas, most of the elemental mercury was oxidized after 0.8 s. The reaction product is assumed to be mercuric chloride. A "rereduction" of the oxidized mercury occurs when the temperature has decreased below 200 °C. This reduction is probably a heterogeneous reaction at the surface of the flue gas duct. Experiments with mercury and activated carbon powder [0.5–1.0 g/m^3, at NTP, specific surface 792 m^2/g (BET)] in the flue gas duct have also been performed. The results indicate that activated carbon may act as a catalyst in the oxidation of mercury.

Introduction

Combustion of fossil fuels and of municipal solid waste mobilizes a number of substances (*1*). Many of the components liberated in the combustion process are notorious pollutants; others are strongly suspected of being harmful. The rapidly growing insight into the environmental problems caused by combustion, combined with the constant need for energy production, has accelerated the development of techniques for emission control.

There are, however, flue gas components for which no simple cleanup process exists today. One such component is elemental mercury. It has been observed in several cases that mercury is partly associated with the solids from the flue gas that are captured in electrostatic precipitators and bag filters, hence less being emitted into the atmosphere. The mechanism behind this retention is not well-known (*2*) and needs to be studied further.

The actual environmental effects caused by mercury emissions depend on the deposition pattern and the levels already present. A small increase in deposition may cause levels to become unacceptable and give rise to severe environmental damage. In Sweden, for example, it has been known for some time that fish from a large number of lakes, especially in areas where acidification has proceeded, contain mercury at levels that make the fish unsuitable to eat, and thus the lakes have been "blacklisted". Most of these lakes do not have a local source of mercury and it is reasonable to assume that deposition from the air, directly on the lake or on its surrounding watershed, is the cause of the elevated mercury levels (*3*).

It is therefore of great importance to reduce mercury deposition and to study possible ways of reducing the emission of combustion-generated mercury into the atmosphere. One way of achieving this could be to find the optimal conditions for removal of mercury with the fly ash, in a stable and insoluble form. Laboratory studies of mercury's behavior in simulated flue gases related to waste incineration conditions have been performed (*4*), and the results of these experiments are reported in this paper.

Experimental Section

A small-scale, propane-fired flue gas generator was built to study chemical reactions of mercury in the flue gases. The apparatus is shown in Figure 1. The gas is produced in a furnace equipped with a low-pressure propane burner with a maximum output of 17 kW. The furnace is connected to a 12-m flue gas duct, which gives a residence time of ~3 s for the gas. Particulates and trace gases, e.g., HCl, SO_2, and Hg^0, may be introduced either through or after the flame. Following the duct is a fabric filter with a bypass where particulates may be separated from the gas. The actual dimensions of the apparatus were dictated by the need to pass particulates through the system and to be able to collect samples large enough to be analyzed for mercury. The flow of gas through the system is maintained by an induced draught ejector. The furnace and ducts are air cooled, and the cooling air may be recirculated or shut off at each duct section to produce a suitable temperature profile in the duct.

A simple computer-controlled data acquisition system collects and stores temperature and combustion parameter data during the experiments (Figure 2).
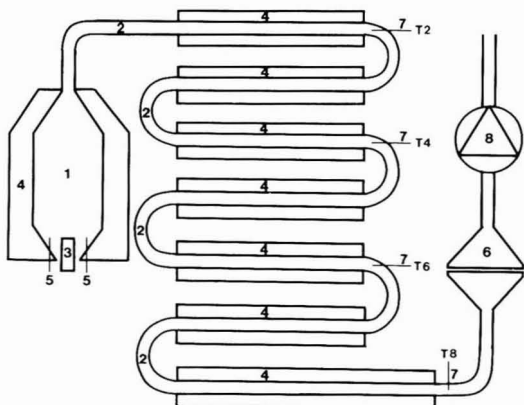
Figure 1. Schematic drawing of the flue gas generator. Key: (1) furnace, (2) flue gas duct, (3) propane burner, (4) cooling air jacket, (5) trace gas inlet, (6) fabric filter, (7) sampling probes, (8) induced draught ejector.
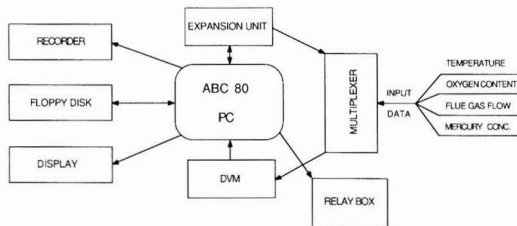
Figure 2. Data collection system.
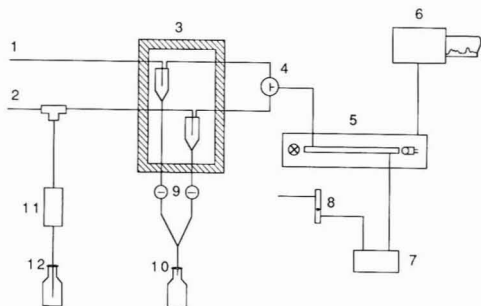
Figure 3. System for continuous measurement of mercury in flue gas. Key: (1) Hg⁰ line, (2) Hg(tot) line (3) ice box with gas/liquid separators, (4) three-way valve, (5) mercury analyzer, (6) recorder, (7) pump for gas (1 L/min), (8) gas flow meter, (9) drain valve, (10) drain, (11) pump for liquid (2 mL/min), (12) container with acidic Sn(II) solution.

Mercury is analyzed by the cold vapor atomic absorption (CVAA) technique by using an apparatus originally described by Iwasaki (5) but modified to measure both elemental and total mercury. A diagram of the analysis instrument is shown in Figure 3.

To analyze elemental mercury in the flue gas, a flow of 1 L/min is continuously drawn from one of the sampling points on the steel duct (cf. Figure 1), through a Teflon tube to a cooled liquid/gas separator where condensed water is separated. Since elemental mercury has a low solubility in water, the mercury vapor will pass into an 80 cm long absorption cell where the light absorption at 253.6 nm is measured. The detection limit in the present setup is 10 $\mu g/m^3$.

A measure of total mercury is obtained by sampling through a second line where an acidic tin(II) solution is
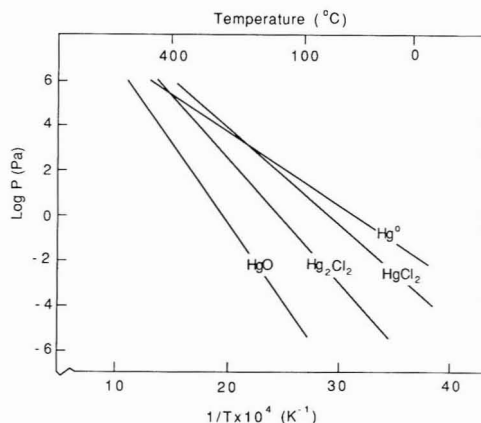
Figure 4. Vapor pressure over condensed phase vs temperature for some mercury compounds (9, 17–19).

in contact with the sampled gas and is transported with the gas to another liquid/gas separator. The mercury vapor then goes on to the absorption cell. Reactive forms of oxidized mercury, either gaseous or solid, are reduced to elemental mercury by the Sn(II) solution. The elemental mercury measured after reduction in this line is the sum of the original elemental mercury and the oxidized mercury at the sampling point. However, some forms of nonreactive oxidized mercury, such as mercury sulfide (3), are not reduced by this process and will escape detection if present in the flue gas.

Results and Discussion

The aim of the present project is to study the transformations of mercury in flue gases, with and without added trace gases and particulates. In coal, mercury is present mainly as the sulfide (6), while in domestic refuse, elemental mercury and mercuric oxide are dominant species. At combustion temperatures, in an oxidizing environment, elemental mercury will evaporate (Figure 4). Mercuric oxide is thermally unstable at temperatures above ca. 500 °C and decomposes into elemental mercury and oxygen (7). Under these conditions mercuric sulfide will also react with oxygen and produce elemental mercury and sulfur dioxide.

All chemical forms of mercury in the fuel are thus expected to leave the combustion zone as gaseous, elemental mercury with a partial pressure in the gas of $\sim 10^{-4}$ Pa in the coal case and an order of magnitude greater for refuse incineration (8). This is well below the saturation pressure, even at ambient temperature, as is shown in Figure 4. Thus, if no chemical or physical processes took place, the vapor would pass through the flue gas system and out into the atmosphere.

The temperature before the flue gas enters the duct is >600 °C and thus probably no HgO has been formed. As the flow gas gradually cools along the duct, it reaches the temperature range of 300–500 °C, where the oxidation of elemental mercury to HgO may occur (reaction 1). At temperatures lower than 300 °C, the reaction rate is probably too slow (7).

By use of total pressures over decomposing mercuric oxide as measured by Taylor and Hulett (9) and the calculated equilibrium values (10) for the reactions

$$Hg^0(g) + \frac{1}{2}O_2(g) \leftrightarrow HgO(g) \qquad (1)$$

and

$$HgO(g) \leftrightarrow HgO(s) \qquad (2)$$
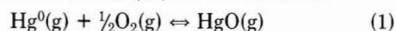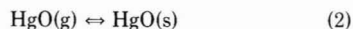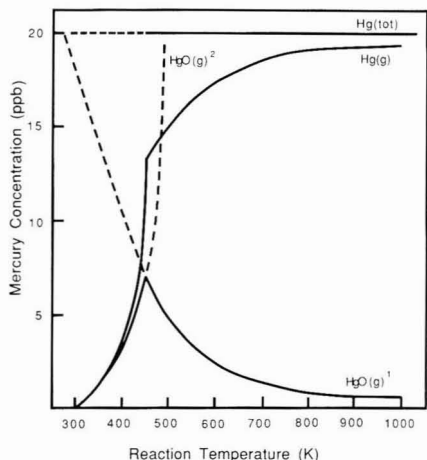
Figure 5. Theoretical calculations of the mercury and mercuric oxide concentrations in the gas phase with a total mercury concentration of 20 ppb and an oxygen concentration of 10 % [the data on HgO(g) are uncertain]. HgO(g)[1], concentration of mercuric oxide according to reaction 1. HgO(g)[2], concentration of mercuric oxide according to reaction 2.

it is possible to calculate the concentrations of Hg(g) and HgO(g) at different temperatures (Figure 5).

If trace amounts of hydrogen chloride are present, which is the case in waste incineration, several other reactions are possible in the cooling flue gas, e.g.:

$$HgO(g,s) + 2HCl(g) \Leftrightarrow HgCl_2(g) + H_2O(g) \quad (3)$$

$$2HCl(g) + \tfrac{1}{2}O_2(g) \Leftrightarrow Cl_2(g) + H_2O(g) \quad (4)$$

$$Hg^0(g) + Cl_2(g) \Leftrightarrow HgCl_2(g) \quad (5)$$

$$2Hg^0(g) + Cl_2(g) \Leftrightarrow Hg_2Cl_2(s) \quad (6)$$

$$Hg_2Cl_2(s) \Leftrightarrow Hg^0(g) + HgCl_2(g) \quad (7)$$
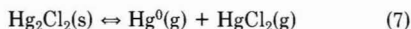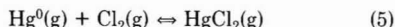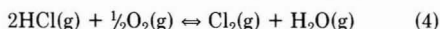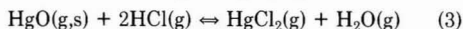
The sampling probes used in our investigation are made from stainless steel followed by Teflon tubing. Wang et al. (11) showed that gaseous mercuric chloride may react when it is passed through a stainless steel tube at 200 °C. They proposed the following reaction:

$$2HgCl_2(g) + H_2(g) \Leftrightarrow Hg_2Cl_2(s) + 2HCl(g) \quad (8)$$
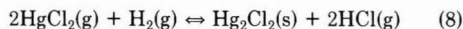
on the basis of HCl formation and that no elemental mercury was found in their study. The $H_2(g)$ was assumed to be hydrogen occluded in steel. Braun et al. (12) suggested that some rereduction of oxidized mercury may occur in the Teflon tubes ordinarily used for mercury sampling, especially when $SO_2(g)$ is present. Also, on the basis of thermodynamic considerations, Stevens et al. (13) proposed the possibility of a reaction between mercury oxide and sulfur dioxide in plumes from combustion as well as in ambient air.

Whether any of these effects may occur to any extent in the present measurement system is not known. There were no such indications, e.g., when elemental mercury from the calibrated mercury feed system was monitored, and it is thus assumed that they do not have any major effects on the results reported here. Nevertheless, this is a question of great interest for anyone dealing with mercury sampling in flue gases and ought to be further investigated.

Addition of Hg⁰(g). When only elemental mercury is added to the flue gas from the propane flame, oxygen,
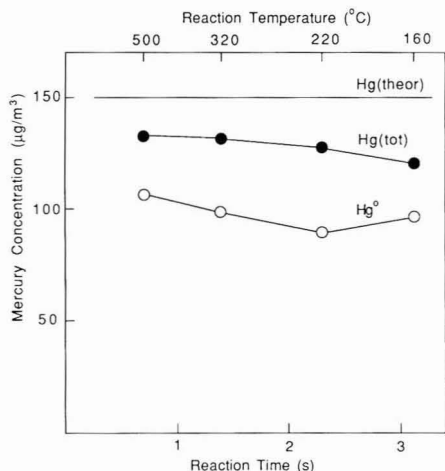
Figure 6. Mercury concentration vs reaction time/temperature. [O₂] = 8%.
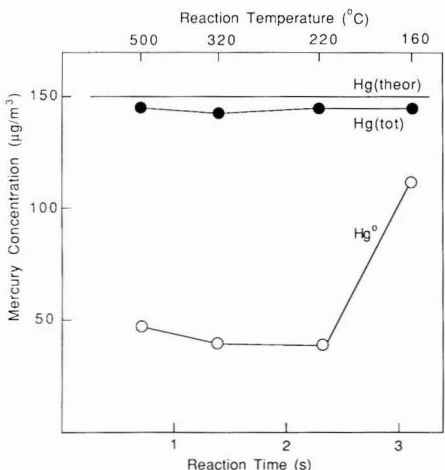
Figure 7. Mercury concentration vs reaction time/temperature. [HCl] = 250 ppm.

carbon dioxide, water vapor, and small amounts of carbon monoxide, nitrogen oxide, and organic compounds are present to react with the mercury. Figure 6 shows the amount of total and elemental mercury in the flue gas duct. It is reasonable to assume that reactions 1 and 2 are mainly responsible for the results obtained. The concentrations of both elemental and total mercury are decreasing slowly along the duct, except at the last sampling point, where a slight rise of elemental mercury occurs. A possible explanation is that solid HgO deposits in the duct. This is in agreement with the rather low estimated vapor pressure of HgO (Figure 4).

Addition of Hg⁰(g) + HCl(g). As can be seen from Figure 7, the fraction of elemental mercury drops when HCl(g) is added. In the experiments performed, HCl has been present in substantial excess, 50–250 ppm compared with 0.02 ppm Hg⁰. The main reaction appears to occur in the flame zone or in the flue gas at temperatures higher than 500 °C and is almost completed when the gas temperature has fallen below 500 °C. The mechanisms for oxidation and chloride formation are not known in detail, and both reactions 1 and 3 should be regarded as overall
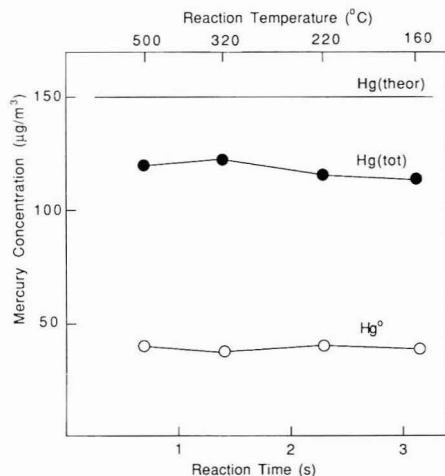
Figure 8. Mercury concentration vs reaction time/temperature. [Activated carbon] = 0.5 g/m³.

reactions only. Other reactions, such as 4–7, may also occur.

The almost constant and nearly theoretical value of the total Hg concentration shows that the product of the reaction between HCl and mercury is easily reduced and present in the vapor phase. Mercuric chloride is the most probable product, since it is reduced by tin(II) in the analytical procedure and has a high vapor pressure (Figure 4). This conclusion is in agreement with previous reports on solid waste incineration, where it has been proposed that nearly all mercury exists as mercury chlorides, predominantly mercury(II) chloride (14, 15).

At lower temperatures in the flue gas, around 150–200 °C at T8, a reduction of oxidized mercury (to elemental mercury) occurs in many of the experiments. We assume that steel corrosion induced by hydrochloric acid at these temperatures may give rise to an activated iron surface on which Hg(II) compounds may be reduced:

$$Fe + Hg(II) \Rightarrow Hg^0(g) + Fe(II) \qquad (9)$$
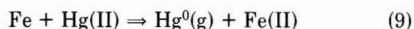
This rereduction process seems to be very sensitive to local variations in the steel surface of the duct and may be the explanation to the very different ratios Hg^0/Hg(tot) measured in combustion plants of similar construction. The understanding and control of this process may therefore be of critical importance for retaining mercury in its oxidized forms in filter fly ash.

Mercury and Activated Carbon. A noticeable oxidation of the metallic mercury is obtained even in the absence of HCl when activated carbon [0.5–1.0 g/m³, at NTP, specific surface 792 m²/g (BET)] is added to the flue gas. The total mercury concentration is, on the other hand, only slightly reduced, as shown in Figure 8.

P'yankov (16) showed in his work with mercury and ozone that activated carbon acts as a catalyst for the formation of mercuric oxide. It is quite possible that activated carbon can act as a catalyst even in the reaction between mercury and oxygen at elevated temperatures.

The carbon that was collected in the fabric filter at 150 °C contained 40–60 ppm mercury (μg of mercury/g of

carbon), which corresponds to between 13 and 20% of the mercury added. This value agrees well with the difference between the total amounts of mercury, with and without activated carbon.

Further Investigations. Investigations continue on the influence of sulfur dioxide, nitrogen dioxide, and fly ash particles on the chemical transformations of mercury in the flue gas simulator. The mechanisms and kinetics of important processes, such as reactions between elemental mercury and oxygen, between Hg and HCl, and between Hg(II) compounds and activated Fe surfaces, all in the temperature range of 100–800 °C, will also be studied in greater detail, in a continuous-flow reactor.

Registry No. HCl, 7647-01-0; Hg, 7439-97-6; HgO, 21908-53-2; carbon, 7440-44-0.

Literature Cited

(1) Cato, G. A. Field testing: Trace element and organic emissions from industrial boilers. Pb-261 263; U.S. Department of Commerce, Oct 1976.
(2) Lindqvist, O. *Waste Manage. Res.* **1986**, *4*, 35.
(3) Lindqvist, O.; Jernelöv, A.; Johansson, K.; Rodhe, H. Mercury in the Swedish environment: Global and local sources. Report SNV PM 1816; Distributed by the National Swedish Environmental Protection Board, Box 1302 S-171 25 Solna, Sweden, 1984.
(4) Hall, B.; Ljungström, E.; Lindqvist, O. Mercury retention in filter fly ash. Bränsleteknik, No. 263; Report to the Swedish Thermal Engineering Research Institute, Box 6405, S-113 82 Stockholm, Sweden (in Swedish with English abstract), 1987.
(5) Iwasaki, Y. Air Pollution Control Dept., Tokyo Metropolitan Research Institute for Environmental Protection, 175 Shinsuna Kotoku, Tokyo, Japan, personal communication, 1985.
(6) Royal Swedish Academy of Sciences Report 192; (in Swedish with English abstract), 1981.
(7) Sidgwick, N. V. *The Chemical Elements and their Compounds*; Oxford University Press: London, 1950.
(8) Airey, D. *Sci. Total Environ.* **1982**, *25*, 19.
(9) Taylor, G. B.; Hulett, G. H. *J. Phys. Chem.* **1913**, *17*, 565.
(10) Chase, M. W.; Davies, C. A.; Downey, J. R.; Frurip, D. J.; McDonald, R. A.; Syverud, A. N. *J. Phys. Chem. Ref. Data* **1985**, *14*(2).
(11) Wang, R. G.; Dillon, M. A.; Spence, D. *J. Chem. Phys.* **1983**, *79*(2), 1100.
(12) Braun, H.; Metzger, M.; Vogg, H. *Müll und Abfall* **1986**, *2*, 62.
(13) Stevens, R. D. S.; Reid, N. W.; Schroeder, W. H.; McLean, R. A. N. The chemical forms and lifetimes of mercury in the atmosphere. Second Symposium on Combustion and the Nonurban Troposphere, Williamsburg, VA, 25–28 May 1982.
(14) Vogg, H.; Braun, H.; Metzger, M.; Schneider, J. *Waste Manage. Res.* **1986**, *4*, 65.
(15) Bergström, J. G. T. *Waste Manage. Res.* **1986**, *4*, 57.
(16) P'yankov, V. A. *J. Gen. Chem. USSR (Engl. Transl.)* **1949**, *19*, 187.
(17) Smith, A.; Menzies, A. W. C. *J. Am. Chem. Soc.* **1910**, *32*, 1541.
(18) Pressions de vapeur du mercure et de ses chlorures, étude bibliographique. *Inf. Chim.* **1978**, *No. 182*, 227.
(19) Weast, R. C., Ed. *CRC Handbook of Chemistry and Physics*, 58th ed.; CRC Press: Boca Raton, FL, 1977–78.

Effect of pH, Temperature, and Concentration on the Adsorption of Cadmium on Goethite

Bruce B. Johnson

Department of Biological and Chemical Sciences, Bendigo College of Advanced Education, Bendigo, Victoria, 3550 Australia

■ Adsorption of cadmium onto goethite has been investigated as a function of both solution concentration and temperature. The pH range over which adsorption occurred was shifted to higher pH values as the initial cadmium concentration was increased and as the solution temperature was decreased. Over the temperature range studied (10–70 °C), the results of adsorption experiments carried out at pH 6.5 and 7.0 could be fitted by using a one-site Langmuir adsorption isotherm. However, at pH 7.5 a two-site Langmuir model was needed to fit the data. The integral heat of adsorption found from the Langmuir constants was ~13 kJ mol^{-1} at pH 6.5 and 7.0, while the two-site types at pH 7.5 yielded heats of adsorption of 20 and 6 kJ mol^{-1}, respectively. The isosteric heat of adsorption was also determined and found to decrease with increasing surface coverage.

Introduction

The adsorption of heavy metals by various substrates has been the subject of many studies over recent years. In particular, the effect of solution pH, the concentration of cation and substrate (1–4), the nature of the substrate (5–7), and the presence of competing ions (8–10) and of complexing ligands (11, 12) on adsorption have all been extensively investigated. However, very few studies have looked at the effect of temperature on adsorption (13–15). In most of these studies, the effect of temperature has generally been of secondary importance to the main thrust of the paper.

Temperature is an important variable in natural water systems, with seasonal variations of 30 °C not uncommon. In addition, substantial variation in water temperature occurs with depth in lakes and in the ocean. In particular, lakes used as reservoirs for water cooling of facilities like power stations often have temperature variations from 70 °C near the outlet pipe to 10 °C in more distant parts of the water storage. Obviously, if the extent of adsorption varies with temperature, this may have a significant impact on heavy-metal accumulation by sediments.

Trace-metal adsorption by soils is another important field. In countries like Australia with hot summers, it is not uncommon for surface soil temperatures to reach 50 °C, while in winter they fall below 5 °C. These substantial variations may have an effect on trace-element availability to plants if the fraction adsorbed varies with temperature. For example, a recent study by Schwartz et al. (16) has shown that the soil temperature in the root zone significantly affects the uptake of phosphorus and zinc by barley.

The present study investigates the effect of pH, solution concentration, and temperature on the adsorption of cadmium onto the hydrous metal oxide goethite (α-FeOOH). Cadmium was chosen because it is present in industrial wastes (e.g., from the plating and pigment industries) and is a contaminant in industrial gypsum, which is frequently applied to sodic soils. Cadmium is known to be toxic. Long-term exposure causes kidney damage and may also aid in the development of hypertension and prostate cancer (17, 18). In addition, studies by other groups have shown that the fraction of cadmium adsorbed increases markedly from pH 6 to 8 (19, 20), the range of

pH values shown by many natural water systems and soils. Goethite was chosen as the adsorbent because it has been shown that the hydrous oxides of iron and manganese adsorb trace metals more strongly than most other adsorbents (21, 22).

The results found indicate that the effect of temperature can be almost as important as pH in determining the adsorption behavior of cadmium.

Experimental Section

Goethite was prepared by dissolving analytical reagent grade Fe(NO$_3$)$_3$·9H$_2$O in doubly distilled water and aging for 24 h at pH 1.6 in a polyethylene beaker stirred with a Teflon-coated stirrer. KOH (2.5 M) was added dropwise until the pH reached 12.0, and the resulting suspension was aged for 5 days in an oven at 60 °C. The particles formed were then dialyzed in cellulose acetate tubing against doubly distilled water, which was changed twice daily for 5 days, before freeze drying. Care was taken throughout to avoid silicate contamination.

X-ray powder diffraction traces confirmed that goethite was present, with no peaks from other hydrous iron oxides evident. The surface area was determined to be 76 m^2 g^{-1} by the BET method, after outgassing at 60 °C overnight. The pH$_{IEP}$ was determined at 25 °C at 9.1 by measurement of the microelectrophoretic mobility of a suspension, using a Rank Bros Model II instrument.

The first set of adsorption runs involved a survey of the adsorption characteristics of cadmium on goethite. Experiments were performed in a water-jacketed reaction vessel, which maintained the constant temperature needed. The required mass of goethite (55 m^2/L) was added to doubly distilled water in the vessel and sonicated to break up the goethite aggregates. The ionic strength was adjusted to 1.0×10^{-2} M with KNO$_3$, the pH adjusted to the starting pH of the experiment (usually pH 4.0), and the system left stirring overnight with nitrogen bubbling through the solution.

The following day, the required cadmium concentration was added to the reaction solution and the pH electrode recalibrated with buffer solutions kept at the temperature of the experiment. After an equilibration time of 20–30 min, a sample was removed for centrifuging and the pH of the reaction solution adjusted upward with KOH. The equilibration time was chosen after preliminary experiments showed that the initial adsorption reaction was completed within 30 min. In all, 20–24 samples were taken covering the pH range from 4 to 10. Each was maintained at the experimental temperature before and during centrifugation. The samples were then analyzed by flame atomic absorption spectrophotometry.

In the second set of experiments a similar vessel was used, but the reaction solution was maintained at a constant pH by using a Metrohm automatic titrator. After overnight equilibration of a goethite suspension at the required pH and temperature, the concentration of cadmium in the solution was gradually increased with measured aliquots of a cadmium solution whose pH had previously been matched with that of the experiment. Samples were removed after each cadmium addition and im-
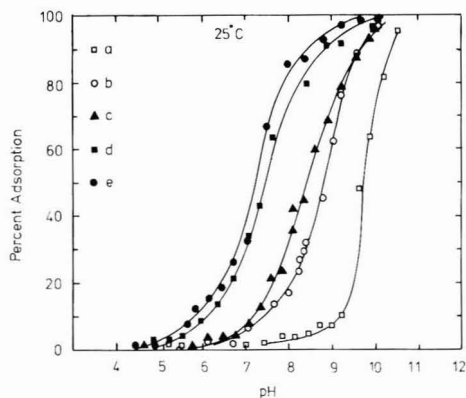
Figure 1. (a) Precipitation curve for 1×10^{-4} M Cd at 25 °C, $I = 0.01$ M KNO_3. (b)–(e) Adsorption of cadmium at various concentrations on goethite: 55 m^2/L, $I = 0.01$ M KNO_3 at 25 °C; (b) 2×10^{-4} M; (c) 1×10^{-4} M; (d) 1×10^{-5} M; (e) 1×10^{-6} M.
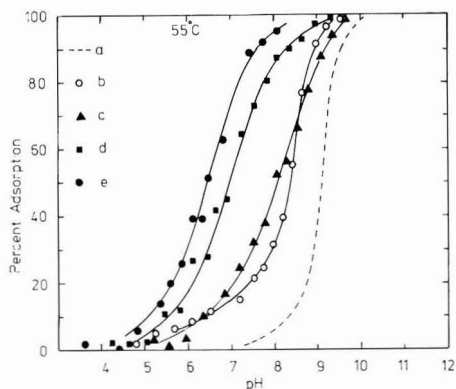
Figure 2. (a) Precipitation curve for 1×10^{-4} M Cd at 55 °C, $I = 0.01$ M KNO_3. (b)–(e) Adsorption of cadmium at various concentrations on goethite: 55 m^2/L, $I = 0.01$ M KNO_3, at 55 °C; (b) 3×10^{-4} M; (c) 1×10^{-4} M; (d) 1×10^{-5} M; (e) 1×10^{-6} M.

mediately filtered with Nuclepore 0.22-μm membrane filters. These filters had previously been shown not to significantly adsorb cadmium, but as an additional precaution, the standard solutions used in the atomic absorption analysis were also subjected to filtration through identical Nuclepore filters at the temperature of the experiment.

Results and Discussion

Effect of pH and Concentration. Figures 1 and 2 illustrate the effect of pH and initial cadmium concentration on the adsorption of cadmium onto goethite at two temperatures. All experiments show the bulk of the adsorption occurring over a relatively narrow pH range of ~2 units. This pH range (or adsorption edge) moves to higher pH as the initial adsorbate concentration is increased. These features have been noted as characteristics of metal ion adsorption in several previous adsorption studies (1, 3, 15).

The curve shapes of all of the concentrations are similar until the initial cadmium concentration is greater than 1×10^{-4} M. Both the 2×10^{-4} M curve at 25 °C and the 3×10^{-4} M curve at 55 °C have significantly steeper shapes than the other adsorption edges. Comparison with the shapes of the precipitation curves for cadmium in the absence of goethite, which show a similar rapid decrease

in concentration of metal ion in solution, suggests that cadmium is precipitating from solution at these higher concentrations, well before adsorption is complete. This appears to occur because the adsorption edge has been displaced into the pH region where cadmium precipitation from solution occurs.

Whether or not the $Cd(OH)_2$ formed absorbs on the goethite surface is impossible to tell from these experiments. This precipitation occurs at pH values below the precipitation curves shown in Figures 1 and 2 for two reasons. First, the precipitation curves shown are for 1×10^{-4} M cadmium solutions. Even allowing for this, however, the pH values are lower than expected, suggesting that the surface plays a significant role in the precipitation process. Second, since the IEP of the goethite is 9.1, and that of $Cd(OH)_2$ is >10.5 (23), the charge at the shear plane is positive over the pH range of adsorption. Hence, the hydroxide ion concentration in the vicinity of the surface should be greater than that in bulk solution. The paper by Farley et al. (24), which proposes a model for adsorption of cations that allows for both surface adsorption and precipitation, suggests that precipitation may be a valid description of the sorption of cations onto metal oxides.

If all adsorption sites on the goethite surface were equally favorable for adsorption, we would expect the position of the percent adsorption versus pH curves to be independent of initial cadmium concentration. Although Figures 1 and 2 indicate that this is not the case, since the adsorption edge is seen to shift to higher pH values at higher initial cadmium concentrations, the results do show that at concentrations below 5×10^{-6} M the curves tend toward a single line. A similar trend is evident in the results of Benjamin and Leckie (3), who investigated the adsorption of cadmium onto amorphous iron oxyhydroxide. They found that where the ratio of initial mole of cadmium to available surface area was very low, fractional adsorption was independent of the initial cadmium concentration. Deviation from this Langmuir behavior at higher concentrations was explained by suggesting the presence of a distribution of site types with different adsorption characteristics. This suggestion appears the most probable explanation of the effect of initial cadmium concentration on fraction adsorbed found in this study for goethite.

From infrared studies of the goethite surface, it has been shown that the surface hydroxyl groups can be coordinated to one, two, or three iron atoms, giving sites with very different reactivities (25). Because of surface roughness on an atomic scale, there will also be differences in reactivity between sites with the same coordination. Together, these effects should generate a surface with a wide range of adsorption energies. Adsorption sites with greatest reactivity will be occupied first, leaving sites of lower reactivity as the surface is progressively covered. Hence higher solution pH is required, increasing the extent of hydrolysis of the adsorbing ions (and decreasing the positive charge on the ions) before adsorption can occur against the unfavorable charge present at the surface, onto these sites of lower reactivity.

Effect of Temperature. Experiments were conducted at five temperatures between 10 and 70 °C, and at a range of initial cadmium concentrations between 5×10^{-7} and 3×10^{-4} M. Figures 3 and 4 show the results obtained at two such initial concentrations and are typical of the other results found. It can be seen that the adsorption edge is shifted to lower pH values as the temperature is increased. Hence, for initial cadmium concentrations of 1×10^{-4} M, at any pH in the range from pH 6 to 9, more cadmium is

Table I. Variation in $pH_{50\%ads}$ with Initial Cadmium Concentration and Temperature

	initial Cd(II) concn/M						
$T/°C$	3×10^{-4}	1×10^{-4}	3×10^{-5}	1×10^{-5}	3×10^{-6}	1×10^{-6}	5×10^{-7}
10	9.1	9.0	8.2	7.5	7.4	7.0	7.0
25	8.8[a]	8.5	7.8[b]	7.4	7.3	7.1	7.0
40	8.8	8.4	7.6	7.1	7.0	6.6	6.6
55	8.4	8.1	7.2	7.0	6.6	6.4	6.2
70	8.1	7.8	7.2	6.9	6.5	6.4	6.5

[a] 2×10^{-4} M Cd(II). [b] 2×10^{-5} M Cd(II).
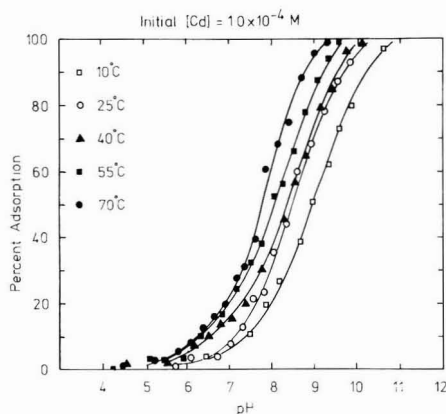
Figure 3. Adsorption of 1×10^{-4} M Cd on goethite: 55 m²/L, I = 0.01 M KNO₃, at temperatures in the range 10–70 °C.
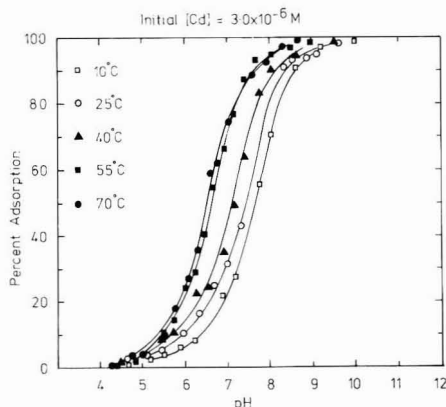
Figure 4. Adsorption of 3×10^{-6} M Cd on goethite: 55 m²/L, I = 0.01 M KNO₃, at temperatures in the range 10–70 °C.

Figure 5. Langmuir adsorption isotherms of cadmium adsorbed on goethite: 55 m²/L, I = 0.01 M KNO₃, at pH 6.5.

adsorbed from solution at higher temperatures. For example, Figure 3 shows that, at pH 8.0, the percent cadmium adsorbed varies from 20% at 10 °C to 60% at 70 °C. This effect is even more dramatic for the 3×10^{-6} M solutions shown in Figure 4, where the adsorption curves are slightly steeper. Here at pH 7.0, the percent cadmium adsorbed increases from 22% at 10 °C to 75% at 70 °C.

A summary of the results obtained is shown in Table I. The pH given at each concentration and temperature is that required for 50% adsorption of the initial cadmium concentration. Both temperature and initial cadmium concentration are seen to have a marked effect on adsorption, with higher temperatures and lower concentrations causing a decrease in $pH_{50\%ads}$. The results shown in the table indicate that the pH required to adsorb 50% of the cadmium decreases by ~1.0 pH unit at concentra-

tions above 1×10^{-5} M and by ~0.6 at lower concentrations, over the temperature range from 10 to 70 °C.

This decrease in the pH required to adsorb cations onto metal oxides with increasing temperature has also been noted by Tewari and Lee (14) for the adsorption of cobalt on TiO₂, ZrO₂, NiFe₂O₄, and Al₂O₃, and by Tamura et al. (15) for cobalt adsorption onto spherical magnetite particles.

Application of Langmuir Isotherm Equation. From the percent adsorption versus pH plots, pH values of 6.5, 7.0, and 7.5 were chosen as suitable for a set of experiments in which pH and temperature were fixed while the cadmium concentration was varied. Only between pH 6.5 and 7.5 did significant adsorption occur at all of the temperatures and concentrations investigated. The results obtained from this investigation were first analyzed by using the Langmuir adsorption isotherm, which can be expressed in a linear form as

$$C/N = C/N_m + 1/kN_m$$

In this equation, C is the equilibrium solution concentration, N is the amount of adsorbate adsorbed per unit area of adsorbent, N_m is the amount of adsorbate required to form a monolayer on available surface sites, and k is the equilibrium constant for the adsorption–desorption process.

Examples of the results obtained at each pH for a number of temperatures are shown in Figures 5–7. While it can be seen that the results at pH 6.5 and 7.0 can be
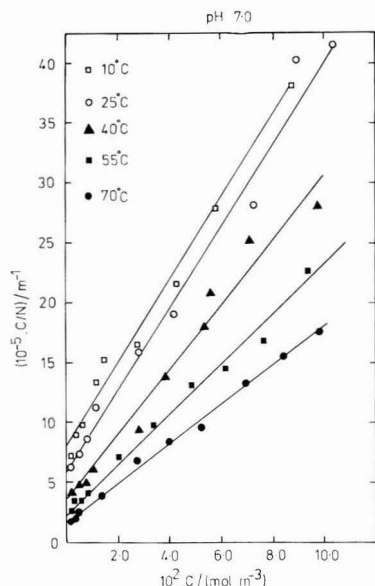
Figure 6. Langmuir adsorption isotherms of cadmium adsorbed on goethite: 55 m²/L, I = 0.01 M KNO$_3$, at pH 7.0.
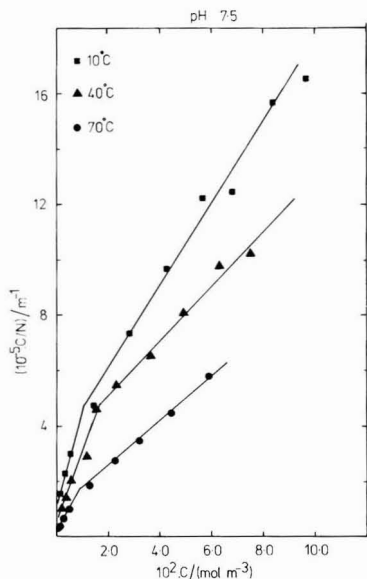
Figure 7. Langmuir adsorption isotherms of cadmium adsorbed on goethite: 55 m²/L, I = 0.01 M KNO$_3$, at pH 7.5.

fitted by a simple straight line, the results at pH 7.5 quite obviously cannot.

It is somewhat surprising that the Langmuir one-site model fits the data so well at pH 6.5 and 7.0 (Figures 5 and 6), since the equation is derived on the basis that all adsorption sites have equal energy, while the percent adsorption versus pH curves shown earlier clearly suggested a range of site energies. However, Hiemenz (26) noted that the Langmuir equation gives adequate results in many cases where surface heterogeneity is known to be present.

The results at pH 7.5 (Figure 7) show marked deviation from linearity at low concentrations, but can be fitted by assuming two different site types with differing adsorption

Table II. Langmuir Isotherm Constants for Cadmium Adsorption at pH 6.5, 7.0, and 7.5 and Various Temperatures

	T/K				
	283	298	313	328	343
		pH 6.5			
$10^2 N_m/\text{mol m}^{-2}$	1.8	2.7	2.7	3.2	3.3
$k/\text{m}^3 \text{ mol}^{-1}$	21	21	31	39	45
		pH 7.0			
$10^7 N_m/\text{mol m}^{-2}$	3.0	3.2	3.6	5.9	6.0
$k/\text{m}^3 \text{ mol}^{-1}$	41	64	80	110	109
		pH 7.5			
$10^7 N_{m1}/\text{mol m}^{-2}$	1.6	1.5	2.1	2.7	3.3
$k_1/\text{m}^3 \text{mol}^{-1}$	519	703	931	1623	2247
$10^7 N_{m2}/\text{mol m}^{-2}$	5.5	5.1	6.5	7.8	9.5
$k_2/\text{m}^3 \text{ mol}^{-1}$	28	36	36	38	49

energies. The Langmuir two-site model, which can be expressed as

$$\theta = \frac{N_1}{N_{m1}} + \frac{N_2}{N_{m2}} = \frac{k_1 C}{1 + k_1 C} + \frac{k_2 C}{1 + k_2 C}$$

where θ is the overall fractional surface coverage, has been used before to fit adsorption data (27) when plots of C/N versus C have yielded two linear regions. The values of N_m and k for the two-site types in Figure 7 were determined by an iterative, least-squares fitting program, with starting values estimated from the slopes and intecepts of the two straight lines. These results, together with those obtained at pH 6.5 and 7.0 (Figures 5 and 6), provide the values for N_m and k as a function of temperature and pH shown in Table II.

At each pH, two trends are immediately evident. The first is the increase in k with temperature. This result conforms with the trend to increased adsorption with temperature noted earlier and suggests that the overall adsorption process is endothermic. The second trend is the increase in the value of N_m with temperature. It is interesting to note that, at each pH, the value of N_m approximately doubles as the temperature increases from 10 to 70 °C. While this increase may be due to an increase with temperature in the number of surface sites available for adsorption, it is more likely to be due to a decrease in the size of the adsorbing species, especially as it is independent of the solution pH. This could well occur due to progressive desolvation of the adsorbing ion as the solution temperature rises.

The PZC of the goethite used in this study (determined by surface charge titration) varied from pH 8.5 at 10 °C to pH 7.8 at 70 °C. At pH values well below the PZC, the majority of the surface sites will be positively charged, (SOH$_2^+$). As the PZC is approached, increasing numbers will be neutralized, forming SOH, and a small number will acquire a negative charge, forming SO$^-$ before the PZC is reached. Given that the adsorbing species is most probably positively charged (Cd^{2+} or CdOH$^+$), adsorption will occur most readily on neutral and negatively charged sites. The increase in N_m with increasing pH at fixed temperature is therefore likely to be due to an increase in the fraction of neutral sites available for adsorption, as the PZC is approached.

The emergence of a second type at pH 7.5 may well result from the presence of significant numbers of negatively charged surface sites at this higher pH, which provide for a strong electrostatic attraction between the surface and the adsorbing cadmium species. The values of the parameter k, which is a measure of the equilibrium

constant for the adsorption reaction, are more than an order of magnitude higher on these new surface sites than on the neutral sites, as would be expected with the addition of a favorable electrostatic interaction.

If the species adsorbing at 25 °C is a hydrated cadmium ion ($r = r_{Cd^{2+}} + 2r_{H_2O}$), as has frequently been suggested, the maximum adsorption density should be $\sim 3.5 \times 10^{-6}$ mol m^{-2}. The observed value at pH 7.5 is only 15% of this theoretical figure, indicating that even at pH 7.5 much of the surface is not available for adsorption. Expressed as an area, at 25 °C and pH 7.5, each adsorbing ion occupies ~ 3 nm^2, compared with 0.44 nm^2 required for adsorption of a hydrated cadmium ion. The area per adsorption site on goethite (where an adsorption site is taken to be a surface hydroxyl group) found in other work varies from 0.05 nm^2 [tritium exchange (28)] to 0.4 nm^2 [titration in 1 M NaCl (29)]. Hence, even taking the largest value, sufficient sites are available on the surface to accommodate the monolayer of hydrated cadmium ions. The low experimental adsorption density can be accounted for by assuming that only a relatively small fraction of the goethite surface is available for adsorption of cadmium even at pH 7.5. It has been shown that the goethite surface has similar numbers of three different types of surface sites (25). If only one of these sites adsorbed cadmium species, then the value of N_m found would be reasonably accounted for given the possibility of lateral repulsion between adsorbed species and the fact that a significant fraction of the surface sites are positively charged at the pH of the experiments.

Reactions Contributing to k. The adsorption of cadmium onto goethite in these experiments involves a number of equilibrium steps. The surface charge arises through interaction with potential determining ions.

$$SOH_2^+ \rightleftharpoons SOH + H_S^+$$

$$SOH \rightleftharpoons SO^- + H_S^+$$
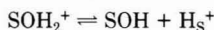
The charged surface may then interact with electrolyte ions present in solution

$$SO^- + K^+ \rightleftharpoons SO^-K^+$$

$$SOH_2^+ + NO_3^- \rightleftharpoons SOH_2^+NO_3^-$$
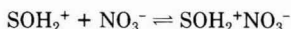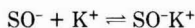
or with cadmium species in solution. When considering cadmium adsorption, account must be taken not only of the bare cation, but also of the hydrolyzed species present at any pH. Hence, possible adsorption reactions include the following:

$$SO^- + Cd^{2+} \rightleftharpoons SOCd^+$$

$$SO^- + CdOH^+ \rightleftharpoons SOCdOH$$

$$SO^- + Cd(OH)_2 \rightleftharpoons SOCd(OH)_2^-$$

$$SOH + Cd^{2+} \rightleftharpoons SOCd^+ + H^+$$

$$SOH + CdOH^+ \rightleftharpoons SOCdOH + H^+$$
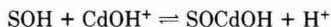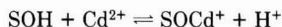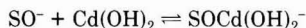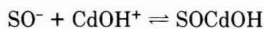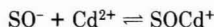
Each of these reactions has an associated equilibrium constant, and all will vary with temperature. The value of k obtained from a Langmuir analysis is the net result of all of these surface reactions and, therefore, represents the equilibrium constant for the overall adsorption process.

Estimation of the Heat of Adsorption from Langmuir Constants. From the variation in k with temperature, the enthalpy change accompanying adsorption can be obtained via the van't Hoff isochore.

$$\frac{\delta \ln k}{\delta T} = \frac{\Delta H_m}{RT^2}$$
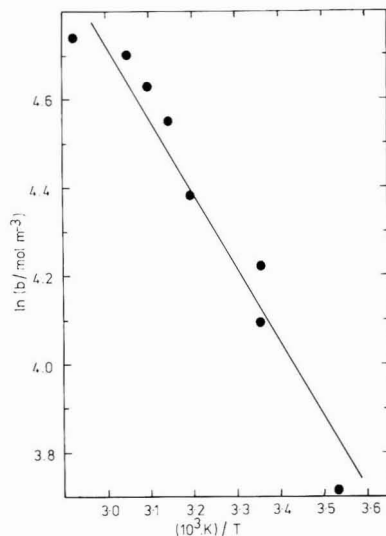
Figure 8. Plot of ln k vs 1/T for cadmium adsorption on goethite at pH 7.

A plot of ln k versus $1/T$ should yield a straight line from whose slope the integral heat of adsorption can be calculated. This heat of adsorption is also that for the overall adsorption process. No conclusions about the heat of adsorption for any of the various processes involved in adsorption can be drawn from these data.

Figure 8 shows such a plot, which includes the results shown in Table II for cadmium adsorption at pH 7.0. Similar plots were obtained at pH 6.5 and for the two-site types at pH 7.5. The resulting heats of adsorption are listed.

pH 6.5 $\Delta H_{m,ads} = (12.6 \pm 1.6)$ kJ mol^{-1}

pH 7.0 $\Delta H_{m,ads} = (13.7 \pm 2.0)$ kJ mol^{-1}

pH 7.5

  site type 1 $\Delta H_{m,ads} = (20.1 \pm 1.8)$ kJ mol^{-1}

  site type 2 $\Delta H_{m,ads} = (6.3 \pm 1.4)$ kJ mol^{-1}

The results indicate little variation in the heat of adsorption with pH while one site type adequately describes the system. However, where two site types are present at pH 7.5, there is a rather greater dependence of adsorption on temperature for site type 1 and a lesser dependence for site type 2.

Variation in Heat of Adsorption with Coverage. An estimate of the variation in heat of adsorption with coverage can be found from the Clausius–Clapeyron equation:

$$\frac{d \ln C_\theta}{dT} = \frac{\Delta H_\theta}{RT^2}$$

where C_θ is the equilibrium solution concentration required to achieve the surface coverage θ. Since analysis with the Langmuir equation had indicated that N_m increased with temperature, the value of N required to obtain a fixed value of θ also varied with temperature. The values used for N_m are those from Table II, with N_m for the second site type being used at pH 7.5. Typical graphs of ln C_θ versus $1/T$ are shown in Figure 9, while the values obtained for
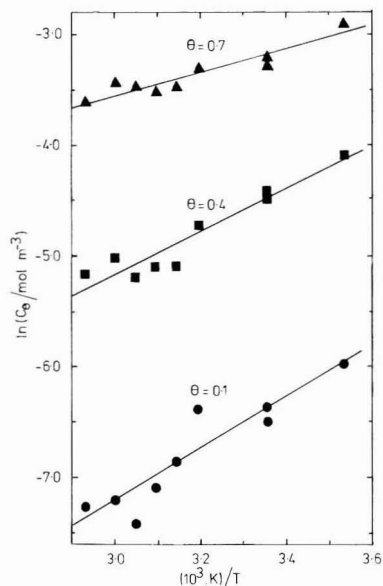
Figure 9. Plots of ln C_θ vs $1/T$ for cadmium adsorption on goethite at pH 7.
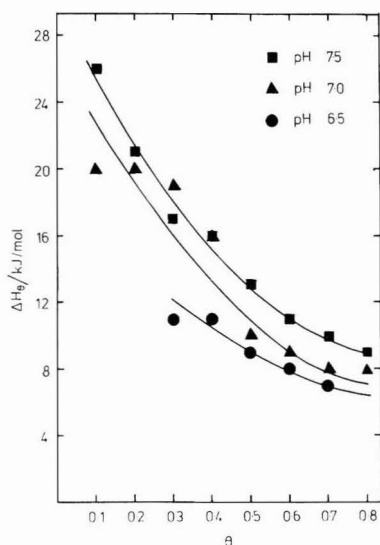
Figure 10. Plots of ΔH_θ vs θ for cadmium adsorption on goethite at pH 6.5, 7.0, and 7.5.

ΔH_θ at each pH are indicated graphically as a function of θ in Figure 10. Heats of adsorption at low θ values were not obtained at pH 6.5 due to the difficulty in obtaining accurate experimental data for N, especially at low temperatures.

As expected, there is a marked decrease in the heat of adsorption with increasing surface coverage at the three pH values studied. The values do not tend toward the results found from the Langmuir constants, as has previously been reported (13, 14). At each pH, the results in Figure 10 suggest that the value of ΔH_θ appears to be tending toward ~6 kJ mol⁻¹ as θ tends to 1.0. This agrees well with the value of the heat of adsorption found for the second site type at pH 7.5 by using the Langmuir analysis and suggests the second site enthalpy corresponds to the

heat of adsorption near monolayer coverage. It is also interesting to note that the heat of adsorption for the first site at pH 7.5 is similar to the ΔH_θ values found at low θ for pH 7.0 and 7.5 in Figure 10, suggesting that it may represent the low coverage limit.

Generally speaking, the values found for the heat of adsorption are somewhat smaller than those found by Tewari et al. (14) for cobalt adsorption onto various substrates. It is difficult to compare the results directly, however, as neither the adsorbate nor the adsorbents correspond, and also, they chose to determine ΔH_θ using a fixed N, independent of the variation of N_m with temperature.

In summary, the fraction of the initial cadmium concentration adsorbed by goethite depends on the solution pH, the initial cadmium concentration, and the temperature. The effect of temperature is quite significant. An increase in temperature from 10 to 70 °C results in up to 3 times as much cadmium adsorbing at pH values in the adsorption edge. Since the critical pH range for cadmium adsorption is between pH 6 and 9, this suggests that seasonal temperature variations may markedly affect the extent to which cadmium is retained by soils and sediments.

Registry No. Cd, 7440-43-9; goethite, 1310-14-1.

Literature Cited

(1) James, R. O.; Healy, T. W. *J. Colloid Interface Sci.* **1972**, *40*, 42–52.
(2) Murray, J. W. *Geochim. Cosmochim. Acta* **1975**, *39*, 635–647.
(3) Benjamin, M. M.; Leckie, J. O. *J. Colloid Interface Sci.* **1981**, *79*, 209–221.
(4) Dzombak, D, A.; Morel, F. M. M. *J. Colloid Interface Sci.* **1986**, *112*, 588–598.
(5) James, R. O.; MacNaughton, M. G. *Geochim. Cosmochim. Acta* **1977**, *41*, 1549–1555.
(6) Davies-Colley, R. J.; Nelson, P. O.; Williamson, K. J. *Environ. Sci. Technol.* **1984**, *18*, 491–499.
(7) Tiller, K. G.; Gerth, J.; Brümmer, G. *Geoderma* **1984**, *34*, 17–35.
(8) Gadde, R. R.; Laitinen, H. A. *Anal. Chem.* **1974**, *46*, 2022–2026.
(9) Benjamin, M. M.; Leckie, J. O. *Environ. Sci. Technol.* **1982**, *16*, 162–170.
(10) McLelland, J. A. M.App.Sc. Thesis, Bendigo C.A.E., Bendigo, Victoria, Australia, 1986.
(11) Davis, J. A.; Leckie, J. O. *Environ. Sci. Technol.* **1978**, *12*, 1309–1315.
(12) MacNaughton, M. G.; James, R. O. *J. Colloid Interface Sci.* **1974**, *47*, 431–440.
(13) Tewari, P. H.; Campbell, A. B.; Lee, W. *Can. J. Chem.* **1972**, *50*, 1642–1648.
(14) Tewari, P. H.; Lee, W. *J. Colloid Interface Sci.* **1975**, *52*, 77–88.
(15) Tamura, H.; Matijević, E.; Meites, L. *J. Colloid Interface Sci.* **1983**, *92*, 303–314.
(16) Schwartz, S. M.; Welch, R. W.; Grunes, D. L.; Cary, E. E.; Norvell, W. A.; Gilbert, M. D.; Meredith, M. P.; Sanchirico, C. A. *Soil Sci. Soc. Am. J.* **1987**, *51*, 371–375.
(17) Elinder, C. G. *Int. J. Environ. Stud.* **1982**, *19*, 187–193.
(18) Bretherick, L., Ed. *Hazards in the Chemical Laboratory*, 3rd ed.; Royal Society of Chemistry: London, 1981.
(19) Harding, I. H.; Healy, T. W. *Prog. Water Technol.* **1979**, *11*, 265–273.
(20) Millward, G. E. *Environ. Technol. Lett.* **1980**, *1*, 394–399.
(21) Jenne, E. A. In *Trace Inorganics in Water*; Gould, R. F., Ed.; ACS Symposium Series 73; American Chemical Society: Washington, DC, 1968; pp 337–387.
(22) Borggaard, O. K. *J. Soil Sci.* **1987**, *38*, 229–238.
(23) Parks, G. A. *Chem. Rev.* **1965**, *65*, 177–198.
(24) Farley, K. J.; Dzombak, D. A.; Morel, F. M. M. *J. Colloid Interface Sci.* **1985**, *106*, 226–242.

(25) Russell, J. D.; Parfitt, R. L.; Fraser, A. R.; Farmer, V. C. *Nature* 1974, *248*, 220–221.

(26) Hiemenz, P. C. *Principles of Colloid and Surface Chemistry*, 2nd ed.; Marcel Dekker: New York, 1986; p 405.

(27) Kinniburgh, D. G.; Barker, J. A.; Whitfield, M. *J. Colloid Interface Sci.* 1983, *95*, 370–384.

(28) Yates, D. E.; Grieser, F.; Cooper, R.; Healy, T. W. *Aust. J. Chem.* 1977, *30*, 1655–1660.

(29) Balistrieri, L. S.; Murray, J. W. *Geochim. Cosmochim. Acta* 1982, *46*, 1253–1265.

Sorption of Aminonaphthalene and Quinoline on Amorphous Silica

John M. Zachara,* Calvin C. Ainsworth, Christina E. Cowan, and Ronald L. Schmidt

Pacific Northwest Laboratory, P.O. Box 999, Richland, Washington 99352

■ The adsorption of quinoline and aminonaphthalene was investigated from aqueous solution on amorphous silica (SiO₂). Amorphous SiO₂ was not a strong adsorbent of these compounds and quinoline was adsorbed more strongly than aminonaphthalene. The adsorption of both compounds varied with pH. A maximum in adsorption occurred near their respective pK_a's. Temperature effects were significant, suggesting enthalpy contributions in the range of H bonding. Both compounds appeared to adsorb via identical mechanisms that included H bonding and ion exchange. The greater basicity of quinoline combined with (1) the enhanced electron-donating properties of the heteroatom N and (2) the delocalized π-bonded ring system were proposed to account for its stronger adsorption. Aminonaphthalene showed greater exclusion from the internal region of porous SiO₂, indicating that the compounds orient differently at the surface. The triple-layer adsorption model and three outer-sphere surface complexes were used to model the adsorption data. Good predictions of adsorption isotherms and the effects of ionic strength and electrolyte cation were obtained.

Introduction

Shallow, near-surface aquifers are often the recipients of contaminants because of their high permeability and linkage to the vadoze zone and soils (*1*, *2*). Quartz and feldspars commonly dominate their mineralogy (*3–7*). Hydrophobic organic compounds are, in general, poorly retarded in these subsurface systems because the organic carbon content is low and sorption is minimal on silica, layer lattice silicate, or iron/aluminum oxide surfaces (*3*, *8*). In contrast, hydrophobic ionizable organic compounds, including organic acids and bases, interact with specific surface sites on mineral surfaces, thereby retarding their migration (*9*, *10*).

Organic bases containing nitrogen are common to coal and petroleum products, and their wastes and tars, as well as other industrial processes (*11*). These compounds ionize to organic cations and are strongly adsorbed by layer silicates that possess negative charge (*12*). Silica also represents a potential subsurface sorbent of organic bases because its surface contains weakly acidic silanol groups that ionize to negatively charged sites above pH 5 (*13*, *14*). Silica behaves as an ion exchanger, forming both inner- and outer-sphere surface complexes with inorganic cations (*13*, *15–17*).

Infrared spectroscopy has shown that hydrogen bonding, charge-transfer reactions, and electrostatic interactions control the sorption of organic bases (alkyl aliphatic amines and selected aromatic amines and pyridines) on silica from the vapor phase (*18–22*) and aprotic organic solvents (*22–26*). Little comparable information exists on the sorption of aromatic amines and heterocyclic aromatic compounds on silica from aqueous solution, which could be used to assess the behavior of these compounds in groundwater in contact with silica-rich sediments.

The sorption of quinoline and aminonaphthalene on porous and nonporous amorphous silica was investigated in this paper. These compounds differ in their size, pK_a, and aqueous solubility. Sorption was measured over a range in sorbate concentration, pH, electrolyte concentration, electrolyte cation, and temperature to examine the surface reaction and establish the presence of specific types of surface complexes. A site-binding model was used to evaluate the consistency of specific surface reactions with the sorption data.

Experimental Procedures

Sorbates. 1-Aminonaphthalene and quinoline (99% purity, Aldrich Chemical Co.) were used without further purification for sorbate stock solutions. These stock solutions were spiked with ¹⁴C-labeled aminonaphthalene or quinoline (Sigma Chemical Co.) that had been purified by high-pressure liquid chromatography (HPLC). The radiochemical purity of the ¹⁴C-labeled compounds was >99% and their specific activity was approximately 10 mCi mmol⁻¹. Selected physicochemical properties of the sorbate molecules are summarized in Table I.

Porous and Amorphous SiO₂. Microporous, amorphous, Merck silica gel [SiO₂(ap), Aldrich] was prepared by first washing in acid (0.1 M HCl) and then repeatedly (~10 times) in distilled/deionized water until chloride free. The SiO₂(ap) was then dried at 100 °C. The microporous silica gel was reported by the supplier to have a surface area of 675 m² g⁻¹, a particle size of 212–500 μm, a pore size of 4.0 nm, and a pore volume of 0.68 cm³ g⁻¹.

Nonmicroporous, amorphous SiO₂ [SiO₂(ac)] was prepared by adding dry Aerosil 200 (Degussa, Inc.) to 0.01 M NaCl to yield a suspension with a 1:10 solids to solution ratio. The SiO₂(ac) had a surface area of 183 m² g⁻¹, a particle size of 0.012 μm, and no internal pore space.

General Experimental Procedures. Sorption experiments were conducted in an incubator–shaker controlled to within 0.5 °C of the desired temperature, which was usually 25 °C. Preweighed 25-mL Corex centrifuge tubes, sealed with Teflon-lined silicon rubber septa, were used for all equilibrations. Sorption experiments were performed with a single sorbate concentration over a range in pH (sorption edges) and with variable sorbate concentration at a single pH (isotherms). Unless otherwise indicated, the electrolyte was 0.01 M NaCl and the titrants for controlling pH were 0.1 M NaOH and 0.1 M HCl. The sorbent concentration was 50 g of SiO₂ L⁻¹ (1:20 solids to solution ratio). The masses of dry SiO₂(ap) or SiO₂(ac) suspension, aminonaphthalene or quinoline stock, and

Table I. Physical Properties of Quinoline and Aminonaphthalene

compound	structure	K_a	dimens,[a] Å X	dimens,[a] Å Y	solub, mg/L	K_{ow}	TSASA,[b] Å²	TSA,[b] Å²	TV,[b] Å³	D,[c] D		σ^{+d}
quinoline		$10^{-4.93}$	8.5	7.2	6000	~110	301.75	141.70	121.16	2.20	NH	+0.071
aminonaphthalene		$10^{-3.93}$	8.7	8.0	1700	166	325.70	159.43	136.88	1.88	NH₂	+0.571

[a] Dimensions estimated from internuclear angles and distances calculated according to the INDO/S approximation (54). X is horizontal distance; Y is vertical distance. [b] Total solvent accessible surface area, total van der Waals surface area, and total volume, respectively, as defined by and calculated according to Pearlman (55, 56). [c] Dipole moment (debyes) for B calculated according to the INDO/S approximation (54). [d] Formal charge on BH⁺ cation centers (Mulliken) calculated according to the INDO/S approximation (54).

titrant plus electrolyte were measured to enable strict mass accounting. Replicate tubes were used at each pH value or sorbate concentration. Following overnight equilibration of the SiO_2 suspension with the organic sorbate (approximately 10 000 cpm initial activity), the tubes were centrifuged: 10 min at 5000 rcf for SiO_2(ap) and 1 h at 5000 rcf for SiO_2(ac). Two aliquots for liquid scintillation counting were removed from each tube to tared vials. The mass of the analytical aliquots were recorded, and final pH was measured in the remaining equilibrium solution.

Sorption Kinetics and Compound Stability. One gram of SiO_2(ap) was equilibrated with 18 mL of 0.01 M NaCl overnight in each of a group of Corex tubes. After the pH of the suspensions was adjusted to pH 4 or 6, 1 mL of aminonaphthalene stock and sufficient electrolyte to bring the total volume to 20 mL were added to each tube. The suspensions were then equilibrated for periods of time ranging from 0.5 h to 1 week. The percent removal of both compounds reached steady state rapidly, within 0.5 h (data not shown). These steady–state concentrations remained stable for over 48 h, and direct analysis by HPLC indicated that no conversion of the compounds had occurred.

Sorption Edge Experiments. The sorption of quinoline and aminonaphthalene over a range in pH was investigated by using a jacketed-water cooled/heated reaction flask attached to a titrator fitted with a Ross combination electrode. The experiment was begun by maintaining a SiO_2(ap or ac)/NaCl(aq) suspension at pH 8 overnight at the appropriate temperature (10, 25, or 40 °C). The sorbate stock solution was then added. The suspension was held at pH 8 for 30 min and two 10-mL aliquots of the suspension were transferred to Corex tubes. The pH of the suspension was adjusted to pH 7.5 and maintained for 30 min before another pair of 10-mL aliquots were removed. This procedure was continued by reducing the pH in 0.5-unit increments to pH 2.5. The sealed tubes were then removed to a gas-tight chamber in the incubator–shaker. The chamber was flushed with N_2 and the suspensions were equilibrated overnight. Centrifugation, ¹⁴C analyses, and final pH measurements were conducted as described above.

Sorption Isotherms. Isotherm experiments with SiO_2(ap or ac) were conducted using the titrator with pH = pK_a of the sorbates (BH⁺ = B) and at pH = pK_a + 3 (B ≫ BH⁺). Once the desired pH of a SiO_2 suspension had been stabilized, aliquots (10 mL) of the suspension were transferred to preweighed centrifuge tubes. After weighing to determine the mass of suspension in each tube, 0.5-mL aliquots of the appropriate organic solute stock solution were added to replicates tubes to yield a sorbate concentration range of 1.0×10^{-8}–1.0×10^{-4} M. The tubes were then equilibrated overnight, centrifuged, and sampled as described above for the sorption edge experiments. Iso-

Table II. Reactions and Associated Equilibrium Constants Used in Modeling Sorption of the Organic Compounds to Silica

reactions	constants
$H^+ + OH^- = H_2O$	14.00
$B + H^+ = BH^+$	pK_a of compd
$SiOH + H^+ = SiOH_2^+$	-0.95^a
$SiOH = SiO^- + H^+$	-6.8^a
$SiOH + Na^+ = SiO^--Na^+ + H^+$	-7.0^a
$SiOH + Ca^{2+} = SiO^--Ca^{2+} + H^+$	-7.32^b

[a] From Riese (32) for α-SiO_2. [b] This study.

therms were measured on SiO_2(ap) at 25 °C in 0.01 M NaCl, 1.0 M NaCl, and 0.005 M $CaCl_2$, and on SiO_2(ac) at 10, 25, and 40 °C in 0.01 M NaCl.

Sorption Modeling. a. SiO_2(ac). Data from the sorption edge experiments were used with the program FITEQL (27, 28) to fit sorption constants for hypothesized sorption reactions. The triple-layer model (TLM) (28, 29) was used. We note that alternative approaches requiring less parameterization exist to the TLM to describe the ionization behavior of SiO_2 (30). The TLM was used because (1) the organic sorbate surface complexes were thought to be outer sphere and (2) the model contains different adsorption planes that could be used to simulate H-bonded and electrostatic surface complexes. The solution speciation and acidity/electrolyte constants that were used in the TLM modeling are given in Table II. The site density, outer layer capacitance, and inner layer capacitance used for both SiO_2(ac) and SiO_2(ap) were 5.0 sites nm⁻² (31), 0.20 F m⁻², and 1.25 F m⁻², respectively. The TLM surface acidity and electrolyte constants for SiO_2 were taken from Riese (32) for α-SiO_2 in NaNO₃ electrolyte. These values were similar to TLM constants reported by Davis (33) for SiO_2 derived from the data of Abendroth (13). Previous studies (34) showed that the results of the FITEQL modeling are not affected significantly by variations in the inner and outer layer capacitances; therefore, these values were fixed for all the analyses presented in this paper. Several different combinations of surface complexes were evaluated to determine the best set of reactions that fit the data from the sorption edge experiments. These reactions and their equilibrium constants were used to model the sorption isotherms for SiO_2(ac).

b. SiO_2(ap). The sorption reactions and constants fitted for quinoline and aminonaphthalene on SiO_2(ac) were used to model the sorption edge and isotherm data on SiO_2(ap). Because the surface area of the SiO_2(ap) accessible to the two compounds was not known, the total number of sites was used in FITEQL as a fitting parameter. The active surface area was calculated from the total number of sites fitted by the model using the site density
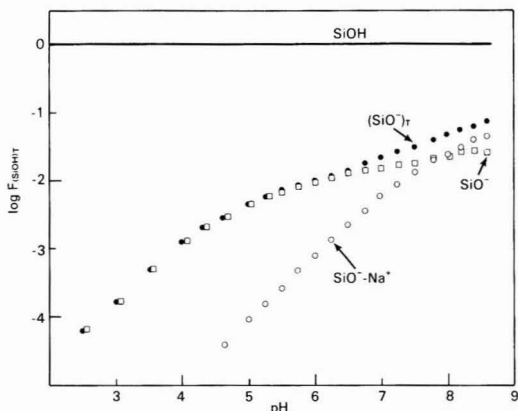
Figure 1. Calculated fractional distribution of surface sites on SiO_2 using the TLM and constants in Tables I and II. Electrolyte composition was 0.01 M NaCl.

Figure 2. Fractional sorption of quinoline on $SiO_2(ac)$ and $SiO_2(ap)$ as a function of pH. Electrolyte composition was 0.01 M NaCl.

Figure 3. Fractional sorption of aminonaphthalene on $SiO_2(ac)$ and $SiO_2(ap)$ as a function of pH. Electrolyte composition was 0.01 M NaCl.

and solid to solution concentration. The sorption isotherm data were modeled as described for the $SiO_2(ac)$, using the average estimated surface area for the $SiO_2(ap)$ and the sorption reactions and constants for quinoline and aminonaphthalene on $SiO_2(ac)$.

c. Calcium Sorption on $SiO_2(ac)$. Sorption constants for calcium on $SiO_2(ac)$ were determined to model quinoline and aminonaphthalene sorption on $SiO_2(ap)$ in 0.005 M $CaCl_2$ electrolyte. The sorption constants were fitted from Ca^{2+} fractional sorption data over the pH range 4.5–8.5. The initial Ca^{2+} concentration was 1.0×10^{-4} M, the electrolyte was 0.01 M NaCl, and the $SiO_2(ac)$ was at 50 g L^{-1}. The pH of 50% sorption was 7.2 (not shown). The fitted sorption reaction was

$$SiOH + Ca^{2+} = SiO^--Ca^{2+} + H^+ \quad (1)$$
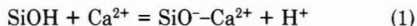
The Ca^{2+} constant was used along with the estimated surface area of $SiO_2(ap)$ and the other surface complexation constants on $SiO_2(ac)$ to model the quinoline and aminonaphthalene isotherms on $SiO_2(ap)$ in 0.005 M $CaCl_2$.

Calculation of Surface Charge on $SiO_2(ac)$. The calculated fraction of surface sites on $SiO_2(ac)$ that are negatively charged over the conditions used in the sorption experiments is shown in Figure 1. The extent of surface ionization and complex formation with Na was calculated with TLM by use of the silica properties mentioned previously and the constants in Table II. Neutral sites dominate the surface over the pH range and the fraction of ionized sites reaches a maximum of approximately 3% (log $F \simeq -1.5$) at pH 8.5.

Results and Discussion

Sorption at 25 °C. a. Sorption Edges. Both quinoline and aminonaphthalene were sorbed on silica (Figures 2 and 3). Sorption varied with pH in an identical way for both compounds, with a maximum in sorption noted at a pH near the compound pK_a. Increased ionization of SiOH to SiO^- groups above the pK_{SiO^-} had no apparent effect on the sorption of either compound. Quinoline was sorbed more strongly than aminonaphthalene over the entire pH range by a factor of approximately 2.

The sorption of quinoline and aminonaphthalene on SiO_2 differed from that of inorganic cations. Inorganic cations display an abrupt pH edge where sorption increases rapidly from near 0 to 100% (see, for example, ref 13). This rapid increase in cation sorption is due to the development of negative charge on SiO_2 (Figure 1) and the
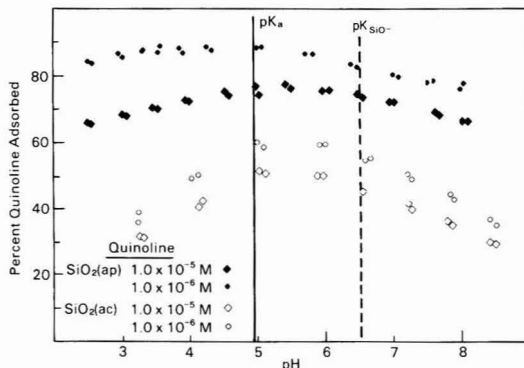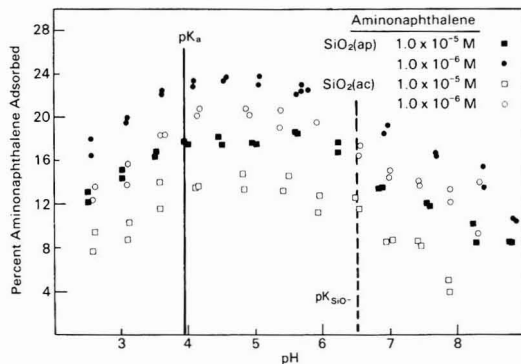
hydrolysis of the sorbing ion. The pH of maximum sorption for quinoline and aminonaphthalene occurred when the silica surface carried little negative charge, which suggested binding of the organic molecule or organic cation to neutral sites.

The two organic compounds displayed concentration-dependent sorption on both types of silica. Fractional sorption at a given pH decreased with an increase in the initial concentration of the compound from 10^{-6} to 10^{-5} M (Figures 2 and 3). Both compounds exhibited greater affinity on a mass basis for $SiO_2(ap)$ (Figures 2 and 3), which has a 3-fold greater surface area. The increase in sorption of $SiO_2(ap)$ over $SiO_2(ac)$, however, was less than proportional to its increase in surface area, implying that the internal pore space was only partly available. The increase in quinoline sorption on $SiO_2(ap)$ over $SiO_2(ac)$ ($\simeq 20–30\%$) was far greater than that observed for aminonaphthalene ($\simeq 5\%$).

b. Sorption Isotherms. Both compounds produced curvilinear isotherms when plotted on an arithmetic scale that were mostly linearized on a log–log basis (Figure 4). The log–log isotherms showed slight curvature above log $C_e \simeq -5.5$, possibly signifying the onset of surface saturation. As in the pH edge experiments, more quinoline was sorbed than aminonaphthalene. The log–log isotherms for both compounds exhibited similar slope, and the quinoline isotherms were displaced 0.75 log unit to a higher sorption density (Figure 4).

In agreement with Figures 2 and 3, variation in pH had a small effect on the isotherms (Figure 4). Sorption was lower at the higher pH, by a factor of 0.4 log unit for quinoline and 0.2 log unit for aminonaphthalene. For each

Table III. Isotherm Parameters for Quinoline Sorption on SiO_2(ap) and SiO_2(ac)

solid	pH	electrolyte	temp, °C	$\log K$, L mol^{-1}	M, mol g^{-1}	N	R^2	RMS
SiO_2(ap)	5.0	0.01 M NaCl	25	4.58	3.27×10^{-6}	0.934	0.999	0.040
SiO_2(ap)	5.0	1.00 M NaCl	25	4.42	3.60×10^{-6}	0.946	0.999	0.029
SiO_2(ap)	5.0	0.01 M CaCl$_2$	25	4.73	3.03×10^{-6}	0.932	0.998	0.050
SiO_2(ap)	8.0	0.01 M NaCl	25	4.45	2.56×10^{-6}	0.944	0.999	0.041
SiO_2(ap)	8.0	0.01 M CaCl$_2$	25	4.52	2.17×10^{-6}	0.942	0.998	0.048
SiO_2(ac)	5.0	0.01 M NaCl	25	4.76	1.70×10^{-6}	0.922	0.999	0.045
SiO_2(ac)	5.0	0.01 M NaCl	25	4.67	1.61×10^{-6}	0.973	0.999	0.029
SiO_2(ac)	5.0	0.01 M NaCl	25	4.58	2.48×10^{-6}	0.916	0.999	0.039
SiO_2(ac)	5.0	0.01 M NaCl	10	4.76	1.77×10^{-6}	1.000	0.999	0.036
SiO_2(ac)	5.0	0.01 M NaCl	40	4.41	1.48×10^{-6}	0.942	0.999	0.043

[a] The Langmuir–Freundlich equation is $S = (KC^N)M/[1 + KC^N]$ where S is the sorbed concentration, C is the aqueous equilibrium sorbate concentration, K is the binding constant, M is the adsorption maximum, and N is an empirical parameter reflecting surface heterogeneity.

Table IV. Isotherm Parameters for Aminonaphthalene Sorption on SiO_2(ap) and SiO_2(ac)

solid	pH	electrolyte	temp, °C	$\log K$, L mol^{-1}	M mol g^{-1}	N	R^2	RMS
SiO_2(ap)	4.0	0.01 M NaCl	25	3.70	1.06×10^{-6}	0.962	0.999	0.026
SiO_2(ap)	4.0	1.00 M NaCl	25	4.01	7.64×10^{-7}	0.968	0.999	0.030
SiO_2(ap)	4.0	0.01 M CaCl$_2$	25	3.93	8.94×10^{-7}	0.986	0.999	0.031
SiO_2(ap)	7.0	0.01 M NaCl	25	3.67	8.46×10^{-7}	0.986	0.999	0.024
SiO_2(ap)	7.0	0.01 M CaCl$_2$	25	3.99	4.28×10^{-7}	1.02	0.999	0.037
SiO_2(ac)	4.0	0.01 M NaCl	25	4.51	4.47×10^{-7}	0.852	0.982	0.156
SiO_2(ac)	4.0	0.01 M NaCl	25	3.92	1.15×10^{-6}	0.887	0.999	0.031
SiO_2(ac)	4.0	0.01 M NaCl	10	3.98	1.11×10^{-6}	0.929	0.999	0.012
SiO_2(ac)	4.0	0.01 M NaCl	40	4.21	4.26×10^{-7}	0.882	0.999	0.029

[a] Parameters as defined in Table III.

compound the log–log isotherms at the two pH values were parallel, which suggested that the degree of pH dependency observed for the sorption of 10^{-6} and 10^{-5} M concentrations in Figures 2 and 3 occurred over the entire sorbate concentration range spanned by the isotherms (10^{-8}–10^{-4} M).

The electrolyte composition and ionic strength had minor effects on compound sorption. At comparable ionic strength ($I \simeq 0.01$), sorption was slightly higher in Ca^{2+} electrolyte (0.005 M CaCl$_2$) than in Na$^+$ electrolyte (0.01 M NaCl) (Figure 4). At equal ionization fractions, (pH 5 and 4 for quinoline and aminonaphthalene, respectively), an increase in ionic strength from $I = 0.01$ to $I = 1.0$ caused a slight increase in quinoline sorption and a small decrease in aminonaphthalene sorption. The lack of ionic strength and cation effects suggested that the surface complexes either were strong and inner sphere (35) or were dominated by interaction with neutral sites where competition with the electrolyte cations was minimal.

The log–log isotherms could be described with Freundlich, multisite Langmuir, and Langmuir–Freundlich (L–F) isotherm equations (36). The Langmuir–Freundlich equation exhibited the lowest root mean square (RMS) deviation (RMS, shown only for the L–F equation in Tables III and IV). Unlike the Freundlich equation, which yields a linear log–log transform, the L–F equation with its additional adjustable parameter (an adsorption maximum M) was able to simulate the curvature in the log–log isotherms of Figure 4 at high surface coverage. Analyses of the individual replicate isotherms for both compounds on SiO_2(ac) at 25 °C (Tables III and IV) show the extent of variability in the isotherm parameters.

The sorption maxima (M; Table III and IV) for quinoline on both SiO_2 sorbents [(2.4–5.7) $\times 10^{-6}$ mol g^{-1}, extrapolated from the Langmuir–Freundlich equation] exceeded that of aminonaphthalene [(0.7–1.6) $\times 10^{-6}$ mol g^{-1}]
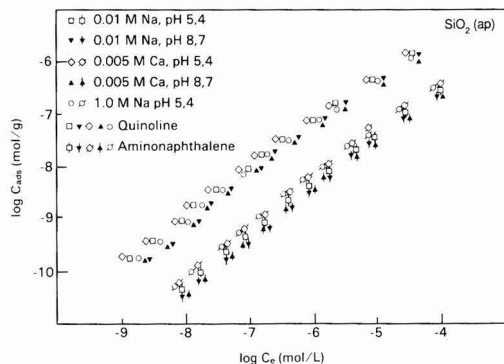
Figure 4. Sorption isotherms of quinoline and aminonaphthalene on SiO_2(ap) at different pH levels, ionic strength, and electrolyte composition.

by factors of 2–4 (Tables III and IV). The sorption maxima for both compounds on SiO_2(ap) were not proportionally larger than their maxima on SiO_2(ac). The sorption maxima for quinoline on SiO_2(ap) in 0.01 M NaCl (3.96×10^{-6} mol g^{-1} at pH 5 and 2.75×10^{-6} mol g^{-1} at pH 8) were well below (1) the total concentration of SiOH sites and (2) the computed concentrations of SiO$^-$ sites at pH 5 (2.45×10^{-5} mol g^{-1}), and the $[SiO^-]_T$ and SiO$^-$ site concentrations (2.56×10^{-4} and 1.17×10^{-4} mol g^{-1}, respectively) at pH 8. On SiO_2(ac), where the total surface area was readily accessible to the compounds, the extrapolated maximum for quinoline at pH 5 in 0.01 M NaCl (2.48×10^{-6} mol g^{-1}) was below the total concentration of SiOH sites but was close to the computed concentration of SiO$^-$ sites (6.63×10^{-6} mol g^{-1}).

Temperature Effects. Temperature affected the sorption of both quinoline and aminonaphthalene on

Figure 5. Effect of temperature on the fractional sorption of quinoline on $SiO_2(ac)$ over a range in pH. Electrolyte composition was 0.01 M.

Figure 6. Effect of temperature on quinoline and aminonaphthalene sorption on $SiO_2(ac)$. pH was near their pK_a values. Solid lines show Langmuir–Freundlich isotherm fits to the data.

Table V. Isosteric Heat of Sorption of Quinoline and Aminonaphthalene on $SiO_2(ac)$

sorptn dens, log mol g^{-1}	ΔH, kJ mol^{-1}	
	10–25 °C	25–40 °C
	Quinoline	
−6.00	−35.3	−60.2
−7.00	−25.0	−46.0
−8.00	−21.6	−41.8
−9.00	−18.5	−37.8
−10.0	−15.5	−33.8
−11.0	−12.5	−29.9
	Aminonaphthalene	
−6.40	−20.3	−39.5
−7.00	−17.1	−39.5
−8.00	−11.7	−29.2
−9.00	−6.44	−27.7
−10.0	−1.15	−26.9
−11.0	0.99	−26.2

the same Γ. The isosteric heat of sorption is a macroscopic measurement incorporating the effects of solute–surface, solute–solvent, and solvent–surface interactions and changes that accompany sorption (*39*).

The isosteric heat of sorption was exothermic and varied with both surface coverage and temperature interval (Table V). The isosteric heat of sorption for nonionic organic compounds on dehydrated mineral surfaces (*38*) and phenoxyacetic acid anions on hydrated mineral surfaces (*40*) decreased with surface coverage. Surface site heterogeneity was proposed to cause these trends. In direct contrast, $\overline{\Delta H_\Gamma}$ for both quinoline and aminonaphthalene increased with sorption density on $SiO_2(ac)$. Lateral interaction between sorbate molecules on the silica surface may cause this trend in enthalpy (*39*). McCloskey and Bayer (*41*) also observed an increase in $\overline{\Delta H_\Gamma}$ with surface loading for fluridone sorption on smectitic soil. Quinoline exhibited a higher $\overline{\Delta H_\Gamma}$ (−12.5 to −60.2 kJ mol^{-1}) than did aminonaphthalene (0.99 to −39.5 kJ mol^{-1}). These enthalpies span the ranges reported for van der Waals and hydrogen bonding of −20 to −60 kJ mol^{-1} (*39, 42*). Our values were lower than those observed for butylamine sorption on silica from *n*-hexane (−190 kJ mol^{-1}) where specific complexation with ionized sites was the proposed mechanism (*24*).

Sorption Modeling. a. Sorption Edges. The sorption data in Figures 2 and 3 could only be reproduced with FITEQL/TLM (Figure 7) using the three following surface reactions:

$$SiOH + B = SiO^- - BH^+ \qquad (3)$$

$$SiOH + B = SiOH - B \qquad (4)$$

$$SiOH + B + H^+ = SiOH - BH^+ \qquad (5)$$
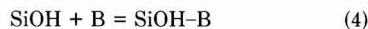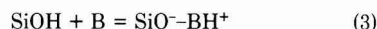
These surface species were required for both quinoline and aminonaphthalene; they are hypothesized species that lead to agreement between model calculations and the experimental data. All combinations of only two surface species lead to poor agreement with the experimental data. Sorption constants for the quinoline surface species varied between replicate experiments by as much as 30% (Table VI). The constants also showed some variation at different sorbate concentrations (Table VI), with the greatest difference observed for the $SiO^- - BH^+$ complex.

The $SiOH - B$ and $SiO^- - BH^+$ surface species represent outer-sphere hydrogen-bonded and ion-exchange complexes, respectively. While these two complexes exhibit the same reaction stoichiometry (eq. 3 and 4), they are viewed as distinct species within the TLM with H$^+$ residing

$SiO_2(ac)$, indicating enthalpy contributions to the free energy of sorption. A reduction in temperature to 10 °C increased sorption, while an increase in temperature to 40 °C decreased sorption (shown in Figure 5 for quinoline only). The effects of temperature were uniform over the pH range, indicating that enthalpy contributions were independent of the aqueous speciation of the compounds. Enthalpy was important even above the pK_a when the neutral compound was the predominant solution species. A slight enhancement in the sorption maxima was observed at 10 °C. In contrast to these findings, entropy dominated the free energy of exchange of alkyl ammonium ions on sodium montmorillonite (*37*) and the free energy of sorption of hydrophobic organic compounds on mineral surfaces (*38*).

Isotherms for both compounds on $SiO_2(ac)$ varied with temperature (Figure 6). As observed in Figure 5, sorption was highest at 10 °C. Temperature effects were greater for quinoline, and the isotherms for each compound were parallel at the different temperatures (Figure 6, Tables III and IV). The extrapolated L–F isotherm parameters show a reduction in K (L–F binding constant) with increasing temperature, and a relatively constant sorption maximum.

The isosteric heat of sorption ($\overline{\Delta H_\Gamma}$) was calculated as a function of sorption density (Γ) by use of the Clausius–Clapeyron equation (*38*):

$$\overline{\Delta H_\Gamma} = R \ln (C_2/C_1)/(1/T_2 - 1/T_1) \qquad (2)$$

where R is the gas constant, C_2 is the equilibrium concentration of the solute at temperature T_2 at the specified Γ, and C_1 is the equilibrium solute concentration at T_1 at

SiO₂(ac), Aminonaphthalene = 10⁻⁶M

Percent Adsorbed

SiOH-BH·
SiOH-B
SiO·-BH·

pH

SiO₂(ac), Quinoline = 10⁻⁶M

Percent Adsorbed

SiOH-BH·
SiOH-B
SiO·-BH·

pH

Figure 7. TLM modeling of aminonaphthalene and quinoline sorption on SiO₂(ac) in 0.01 M NaCl. The solid line is the summation of all the species.

Table VI. Sorption Constants for Quinoline and Aminonaphthalene on SiO₂(ac)

concn, M	log K sorption constants for surface species		
	SiO–BH⁺	SiOH–B	SiOH–BH⁺
quinoline			
10⁻⁶	0.890 ± 0.12	0.650 ± 0.08	5.68 ± 0.14
10⁻⁵	0.576 ± 0.19	0.669 ± 0.14	5.58 ± 0.17
aminonaphthalene			
10⁻⁶	0.306	0.034	4.25
10⁻⁵	0.229	−0.476	4.06

in the 0 plane for the SiOH–B complex and within the β plane for SiO⁻–BH⁺. The existence of these separate species is supported by infrared (43) and sorption studies (44, 45). The SiOH–BH⁺ complex may be viewed as an analogue of SiOH₂⁺ that is stabilized by electron sharing with Si-bound oxygen, which exhibits a negative dipole moment. A similar complex was postulated to form for quaternary ammonium cations (46) and water (47) on SiO₂.

After the effects of surface and solution ionization reactions were removed, SiO⁻–BH⁺ was the most stable calculated surface complex, followed by SiOH–BH⁺ (Table VII). The strength of the SiO⁻–BH⁺ complex exceeded that of both SiO⁻–Na⁺ and SiO⁻–Ca²⁺, indicating stabilization of the organic surface complex by hydrophobic forces or surface H bonding with the π electron cloud. The model calculations in Figure 7, however, suggested that sorption of the ionized and molecular species to neutral SiOH groups contributed more to the total adsorption than the ion-exchange complex (SiO⁻–BH⁺). The SiOH–BH⁺ and SiOH–B complexes dominated total sorption because of the large excess of SiOH sites compared to SiO⁻ sites (Figure 1) and because [BH⁺]aq was small when [SiO⁻]T was large.

The constants in Table VI for SiO₂(ac) were used along with the sorption edge data for SiO₂(ap) in Figures 2 and 3 in FITEQL to estimate a surface area for SiO₂(ap) that was accessible to the two compounds. Less than 50% of the

Table VII. Intrinsic Strength of Quinoline and Aminonaphthalene Surface Complexes

reaction	log K
Quinoline (10⁻⁶ M)	
SiO⁻ + QH⁺ = SiO⁻–QH⁺	2.76
SiOH + QH⁺ = SiOH–QH⁺	0.75
SiOH + Q = SiOH–Q	0.65
Aminonaphthalene (10⁻⁶ M)	
SiO⁻ + AH⁺ = SiO⁻–AH⁺	2.18
SiOH + AH⁺ = SiOH–AH⁺	0.32
SiOH + A = SiOH–A	0.034
Na⁺	
SiO⁻ + Na⁺ = SiO⁻–Na⁺	−0.2
Ca²⁺ (10⁻⁴ M)	
SiO⁻ – Ca²⁺ = SiO⁻–Ca²⁺	−0.5

total surface area on SiO₂(ap) (258.2 m² g⁻¹) was calculated to be available to aminonaphthalene. In contrast, the entire surface area of SiO₂(ap) was calculated to be accessible to quinoline. Size considerations alone cannot fully account for the apparent inaccessibility of the internal pore space of SiO₂(ap) to aminonaphthalene, because the average 4.0-nm pore size is at least 4 times larger than the long dimension of the compounds (Table I). A range in pore diameter about the 4.0-nm average is expected (48), and aminonaphthalene sorption in the smaller diameter pore regions may be sterically inhibited because of its larger molecular volume (Table I) and the bulky amine group. Specifically, the amine group may be physically unable to interact with hydrated SiOH sites in the narrow pore areas. For alkylamines, Van Cauwelaert et al. (20) suggested that steric factors influence sorption on SiO₂, while Rochester and Yong (43) saw no evidence of such effects. Steric interactions appeared to have little influence on the sorption of substituted pyridines on SiO₂ from CCl₄ (23).

b. Sorption Isotherms. The constants in Tables I and VI (for 10⁻⁶ M sorbate concentrations) and the active surface area estimated for SiO₂(ap) were used to simulate the sorption isotherms in Figure 4 and the 25 °C isotherms in Figure 6. The calculated isotherms exhibited similar slopes and good agreement with the experimental data (shown for selected isotherms in Figure 8). Because the isotherms were nonlinear, the use of a single set of sorption constants yields a slight underprediction of sorption at low C_e and an overprediction at high C_e (Figure 8). The inflection or pivot point to this over- or underprediction was the approximate sorbate concentration at which the constants were fit. The difference between the measured and predicted fractional sorption at initial sorbate concentrations of 5.0×10^{-7} and 1×10^{-5} M ranged from +30.0% to −3.4% (Table VIII). The agreement was usually within 10% for SiO₂(ap), and higher for SiO₂(ac). The close agreement for SiO₂(ap) suggested that the effective surface area of the sorbent for each compound was independent of surface coverage. Thus, the increased diffusional gradient created at higher aminonaphthalene concentrations did not increase access to the internal pore space of SiO₂(ap).

The model calculations correctly predicted the direction and magnitude of the shift in the isotherms, relative to those in 0.01 M NaCl at pH 5 for quinoline and pH 4 for aminonaphthalene, that occurred in the presence of increased ionic strength (1.0 M NaCl, predictions not shown) and Ca²⁺ (0.005 M CaCl₂; Figure 8b). The small effect of ionic strength and Ca²⁺ on compound sorption (Figure 4, Figure 8b) was consistent with the calculated dominance

a) SiO$_2$ (ap), 0.01 M NaCl

b) SiO$_2$ (ap), 0.005 M CaCl$_2$
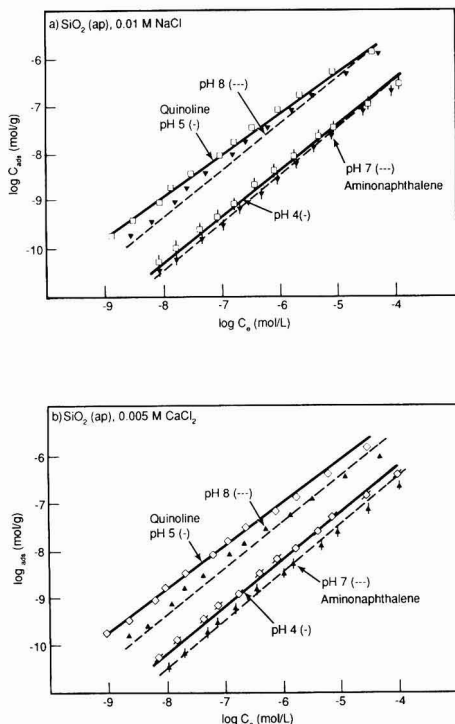
Figure 8. TLM predictions of selected isotherms for SiO$_2$(ap) in Figure 4. Solid and dashed lines represent model calculations.

Table VIII. Percent Difference between Experimental and Predicted Sorption Isotherms[a]

conditions	% diff[b]	% diff[c]
Quinoline on SiO$_2$(ac)		
0.01 M NaCl, pH 5	30.0	15.3
Quinoline on SiO$_2$(ap)		
0.01 M NaCl, pH 5	0.97	−3.4
0.01 M NaCl, pH 8	9.0	3.4
1.0 M NaCl, pH 5	−0.09	−8.4
0.005 M CaCl$_2$, pH 5	4.7	1.0
0.005 M CaCl$_2$, pH 8	11.8	6.2
Aminonaphthalene on SiO$_2$(ac)		
0.01 M NaCl, pH 4	12.1	7.2
0.01 M NaCl, pH 7	19.4	2.66
Aminonaphthalene on SiO$_2$(ap)		
0.01 M NaCl, pH 4	0.1	−3.71
0.01 M NaCl, pH 7	4.0	−2.60
1.0 M NaCl, pH 4	9.3	2.1
0.005 M CaCl$_2$, pH 4	3.8	2.9
0.005 M CaCl$_2$, pH 7	3.8	4.6

[a] Constants for 10^{-6} M initial sorbate concentrations in Table VI were used. [b] (Measured % adsorbed) − (predicted % adsorbed) at an initial concentration of 5.0×10^{-7} M. [c] (Measured % adsorbed) − (predicted % adsorbed) at an initial concentration of 1.0×10^{-5} M.

of surface complexes on neutral SiOH sites. Increased Na$^+$ concentrations and Ca^{2+} will decrease free SiO$^-$, which would reduce aminonaphthalene and quinoline sorption if they were binding primarily to SiO$^-$ sites. The predicted three species surface speciation model (Figure 7) was, therefore, consistent with the pH, concentration, and ionic strength influences on quinoline and aminonaphthalene sorption (Figure 8).

Reasons for Selectivity Differences. The shift ($\Delta\nu_{OH}$) in the infrared O–H stretching band of the free SiOH hydroxyls (3750 cm^{-1}) that accompanies adsorption from the gas phase or organic solvents (e.g., CCl$_4$) has been repeatedly used as a measure of sorbate binding strength on SiO$_2$. The shift has been correlated with the enthalpy of sorption, ΔH_{ads} (49, 50) and the extent of H bonding and charge transfer. Combined with spectral data on the sorbate, $\Delta\nu_{OH}$ has been used to determine the extent of covalency, charge transfer, and ionicity of the surface complexes (18, 21–23, 25, 43, 51). For organic N bases, $\Delta\nu_{OH}$ and, therefore, ΔH_{ads} have been shown to increase with increasing basicity of the sorbate (20, 23, 43). Griffiths et al. (23) demonstrated that $\Delta\nu_{OH}$ increases with electron donor substituent groups that promote stronger interaction with the hydroxyl groups (20, 43).

Consistent with the above observations, aniline (pK_a = 4.93) is observed to have a lower $\Delta\nu_{OH}$ (ΔH_{ads}) in CCl$_4$ (51) than pyridine (pK_a = 5.52) (23). Resonance structures withdraw electron density from N to the ring, making aniline a weaker base than pyridine (52). While $\Delta\nu_{OH}$ data are not available for quinoline and aminonaphthalene, their isosteric heats of sorption and sorption behavior in water agree with these observations. Aminonaphthalene is a weaker base, has a lower pK_a (Table I), and, therefore, forms weaker bonds with acidic SiOH groups than quinoline.

Physical properties of the two compounds related to the electronic configuration of the ring are also consistent with their sorption. Water interacts strongly with the SiO$_2$ surface (47, 48), and H$_2$O as a lone-pair adsorbate competes with the aromatic amine and heteroatom N compounds for H-bonding SiOH sites on SiO$_2$. Quinoline is a better competitor with H$_2$O than aminonaphthalene because it forms stronger H bonds. The stronger H-bonding character of quinoline is manifested in its higher dipole moment and aqueous solubility (Table I). As a cation, QH$^+$ may be more strongly bound than AH$^+$ to SiO$^-$ sites because positive charge is delocalized throughout the aromatic ring structure of QH$^+$. Delocalization of charge to H atoms around the periphery of the ring system leads to a lower formal charge on the NH atom centers of the quinolinium ion as compared to the NH$_3$ atom centers of the aminonaphthalene cation (Table I). Delocalization allows for a larger interaction electrostatic area of overlap integral with the surface (53).

Significance to Field Attenuation. Retardation factors were calculated to determine whether SiO$_2$ surfaces can attenuate quinoline and aminonaphthalene migration in the subsurface. With the data in Figures 2 and 3 for 10^{-6} M initial concentrations at maximum sorption on SiO$_2$(ac), distribution coefficients (K_d's in L m^{-2}) of 1.34 $\times 10^{-4}$ and 2.73×10^{-5} were calculated for quinoline and aminonaphthalene, respectively. If, for example, a subsurface material is assumed to have a SiO$_2$ surface area of 10 m^2 g^{-1}, then K_d's (mL g^{-1}) of approximately 1.34 and 0.273 for quinoline and aminonaphthalene could be anticipated. The further assumption of a bulk density of 1.5 g cm^{-3} and porosity of 0.5 yields retardation factors (R_f, ref 51) of 4.02 and 1.82 for quinoline and aminonaphthalene, respectively. The subsurface migration rates of these two solutes would, therefore, be approximately 25% (quinoline) and 55% (aminonaphthalene) of the linear velocity of the groundwater.

Conclusions

Quinoline was more strongly sorbed than aminonaphthalene under all experimental conditions. The heterocycle nitrogen promoted a stronger interaction with

the silica surface than did nitrogen within the aromatic amine group. The two compounds adsorbed to silica via a similar mechanism, as shown by their parallel isotherms and the similar effects that both temperature and pH had on sorption. Surface complexes involving the neutral compound (B) and/or neutral sites (SiOH) were found to be important as evidenced by the insensitivity of sorption to ionic strength and electrolyte cation. Only aminonaphthalene was excluded from the internal space of porous silica, which indicated that the two compounds oriented differently at the surface and that steric factors were potentially important.

A three-complex surface model provided good descriptions of compound sorption on porous and nonporous silica at different pHs and sorbate concentrations. The model correctly predicted the small effects of ionic strength and electrolyte cation on N aromatic compound sorption. The surface complexes represented electrostatically bound and H-bonded sorbate molecules on the surface and were consistent with the calculated isosteric sorption enthalpies. The greater stability of the quinoline surface complexes, as compared with aminonaphthalene, was consistent with the greater basicity of quinoline and its ability to delocalize charge through its ring structure.

Sorption to silica, such as quartz sand grains in groundwater, can retard quinoline and, to a lesser extent, aminonaphthalene migration. Silica surface areas in excess of 2 $m^2 g^{-1}$ in the saturated zone are required before sorption effects are observed or become significant.

Acknowledgments

Registry No. SiO$_2$, 7631-86-9; quinoline, 91-22-5; aminonaphthalene, 25168-10-9.

Literature Cited

(1) Cherry, J. A.; Gillham, R. W.; Barker, J. F. *Groundwater Contamination* (*Studies in Geophysics*); National Academy Press: Washington, DC, 1984; Chapter 3, pp 46–64.
(2) Mackay, D. M.; Roberts, P. V.; Cherry, J. A. *Environ. Sci. Technol.* **1985**, *19*, 384–392.
(3) Goerlitz, D. F.; Troutman, D. E.; Godsy, E. M.; Franks, B. J. *Environ. Sci. Technol.* **1985**, *19*, 955–961.
(4) Jackson, R. E.; Inch, K. J. *Environ. Sci. Technol.* **1983**, *17*, 231–237.
(5) Kipp, K. L.; Stollenwerk, K. G.; Grove, D. B. *Water Resour. Res.* **1986**, *22*, 519–530.
(6) Patterson, R. J.; Spoel, T. *Water Resour. Res.* **1981**, *17*, 513–520.
(7) Stollenwerk, K. G.; Grove, D. B. *J. Environ. Qual.* **1985**, *14*, 150–155.
(8) Estes, T. J.; Shah, R. V.; Vilker, V. L. *Environ. Sci. Technol.* **1988**, *22*, 377–381.
(9) Kummert, R.; Stumm, W. *J. Colloid Interface Sci.* **1980**, *75*, 373–382.
(10) Zachara, J. M.; Ainsworth, C. C.; Felice, L. J.; Resch, C. T. *Environ. Sci. Technol.* **1986**, *20*, 620–627.
(11) Zachara, J. M.; Felice, L. J.; Riley, R. G.; Harrison, F. L.; Mallon, B. *The Selection of Organic Chemicals for Subsurface Transport Research*; U.S. Department of Energy; Office of Health and Environmental Research; Ecological Research Division: Washington, DC, 1985; DOE/ER-0217.
(12) Zachara, J. M.; Ainsworth, C. C.; Schmidt, R. L.; Resch, C. T. *J. Contam. Hydrol.* **1988**, *2*, 343–364.
(13) Abendroth, R. P. *J. Colloid Interface Sci.* **1970**, *34*, 591–596.
(14) Schindler, P. W.; Kamber, H. R. *Helv. Chim. Acta* **1968**, *51*, 1781–1786.
(15) Schindler, P. W.; Furst, B.; Dick, R.; Wolf, P. U. *J. Colloid Interface Sci.* **1976**, *55*, 469–475.
(16) Ahrland, S.; Grenthe, I.; Noren, B. *Acta. Chem. Scand.* **1960**, *5*, 1059–1076.
(17) Tadros, T. F.; Lyklema, J. *J. Electroanal. Chem.* **1968**, *17*, 267–275.
(18) Basila, M. R. *J. Chem. Phys.* **1961**, *35*, 1151–1158.
(19) Kagel, R. O. *J. Phys. Chem.* **1970**, *74*, 4518–4519.
(20) Van Cauwelaert, F. H.; Vermoortele, F.; Uytterhoeven, J. B. *Discuss. Faraday Soc.* **1971**, *52*, 66–76.
(21) Rochester, C. H.; Trebilco, D. A. *Chem. Ind.* (*London*) **1978**, *20*, 348–349.
(22) Child, M. J.; Heywood, M. J.; Pulton, S. K.; Vicary, G. A.; Yond, G. H.; Rochester, C. H. *J. Colloid Interface Sci.* **1982**, *89*, 202–208.
(23) Griffiths, D. M.; Marshall, K.; Rochester, C. H. *J. Chem. Soc., Faraday Trans. 1* **1974**, *70*, 400–410.
(24) Jednačak-Bišćan, J.; Pravdic, V. *J. Colloid Interface Sci.* **1982**, *90*, 44–50.
(25) Child, M. J.; Heywood, M. J.; Pulton, S. K.; Vicary, G. A.; Yond, G. H.; Rochester, C. H. *J. Chem. Soc., Faraday Trans. 1* **1982**, *78*, 2005–2010.
(26) Sayed, M. B.; Cooney, R. P. *J. Colloid Interface Sci.* **1983**, *91*, 552–559.
(27) Westall, J. C. FITEQL, A Program for Determination of Chemical Equilibrium Constants from Experimental Data. User's Guide Version 1.2; Report no. 82-01; Oregon State University: Corvallis, OR, 1982.
(28) Westall, J. C. FITEQL, A Program for Determination of Chemical Equilibrium Constants from Experimental Data. Version 2.0; Report no. 82-02; Oregon State University: Corvallis, OR, 1982.
(29) Davis, J. A.; Leckie, J. O. *J. Colloid Interface Sci.* **1978**, *67*, 90–107.
(30) Marinsky, J. A. In *Aquatic Surface Chemistry*; Stumm, W., Ed.; John Wiley and Sons: New York, 1987; pp 49–81.
(31) Zhuravlev, L. T. *Langmuir* **1986**, *3*, 318–319.
(32) Riese, A. C. Ph.D. Thesis, Colorado School of Mines, Boulder, CO, 1982.
(33) Davis, J. A. Ph.D. Thesis, Stanford University, 1978.
(34) Zachara, J. M.; Cowan, C. E.; Schmidt, R. L.; Ainsworth, C. C. *Clays Clay Miner.* **1987**, *4*, 317–326.
(35) Hayes, K. F.; Leckie, J. O. *J. Colloid Interface Sci.* **1987**, *115*, 564–572.
(36) Kinniburgh, D. G. *Environ. Sci. Technol.* **1986**, *20*, 895–904.
(37) Vansant, E. F.; Uytterhoeven, J. B. *Clays Clay Miner.* **1972**, *20*, 47–54.
(38) Chiou, C. T.; Stroup, T. D. *Environ. Sci. Technol.* **1985**, *19*, 1196–1200.
(39) Burchill, S.; Hayes, M. H. B.; Greenland, D. J. In *The Chemistry of Soil Processes*; Greenland, D. J., Hayes, M. B. B., Eds.; John Wiley and Sons: New York, 1981.
(40) Hague, R.; Sexton, R. *J. Colloid Interface Sci.* **1968**, *27*, 818–827.
(41) McCloskey, W. B.; Bayer, D. E. *Soil Sci. Soc. Am. J.* **1987**, *51*, 605–612.
(42) Kiselev, A. V. *J. Chromatogr.* **1970**, *49*, 84–129.
(43) Rochester, C. H.; Yong, G. H. *J. Chem. Soc., Faraday Trans. 1* **1980**, *76*, 1158–1165.
(44) Allingham, M. M.; Cullen, J. M.; Giles, C. H.; Jain, S. K.; Woods, J. S. *J. Appl. Chem.* **1958**, *8*, 108–116.
(45) Haldeman, R. G.; Emmett, P H. *J. Phys. Chem.* **1955**, *59*, 1039.
(46) Blackman, L. C. F.; Harrop, R. *Nature* **1965**, *208*, 777–778.
(47) Grivtsov, A. G.; Zhuravlev, L. T.; Gerasimova, G. A.; Khazin, L. G. *J. Colloid Interface Sci.* **1988**, *126*, 397–407.
(48) Iler, R. K. *The Chemistry of Silica*; John Wiley and Sons: New York, 1979.
(49) Kitao, T.; Jarboe, C. H. *J. Org. Chem.* **1967**, *32*, 407–410.
(50) Vinogradov, S. N.; Linnell, R. H. *Hydrogen Bonding*; Van Nostrand Reinhold Co.: New York, 1971.

(51) Low, M. J. D.; Hasegawa, M. *J. Colloid Interface Sci.* **1968**, 26, 95–101.

(52) Morrison, R. T.; Boyd, R. N. *Organic Chemistry*; Allyn and Bacon: Boston, MA, 1974.

(53) Maes, A.; Leemput, L. V.; Cremers, A.; Uytterhoeven, J. *J. Colloid Interface Sci.* **1980**, 77, 14–20.

(54) Zerner, M. C. *Ann. N.Y. Acad. Sci.* **1981**, 35, 367.

(55) Pearlman, R. S. In *Physical Chemical Properties of Drugs*; Marcel Dekker: New York, 1972; pp 321–347.

(56) Pearlman, R. S. *Quantum Chem. Prog. Exch. Bull.* **1981**, 1, 15.

Dissolution Kinetics of Minerals in the Presence of Sorbing and Complexing Ligands

Cheng-Fang Lin and Mark M. Benjamin*

Department of Civil Engineering, FX-10, University of Washington, Seattle, Washington 98195

■ This study investigated and modeled the important reactions controlling oxide dissolution in a system containing strongly complexing and strongly sorbing ligands. Polyphosphate and ferrihydrite were the model ligand and oxide studied, respectively. The dissolution of ferrihydrite in these systems is via a process called ligand-promoted dissolution, which is controlled by a surface reaction and is initiated by sorption of tripolyphosphates. Fe and tripolyphosphate leave the surface as one entity. If empty surface sites are available, Fe-tripolyphosphate complexes that are released to solution can quickly readsorb to the surface, forming a species different from the precursor to the dissolution reaction. The strong adsorption of complexes counteracts the iron dissolution reaction and leads to nonlinear net dissolution kinetics. An adsorption/dissolution kinetic model is developed that successfully simulates the experimental observations here as well as previous work reported in the literature for systems where adsorption of free ligands and complexes is much weaker.

Introduction

The surfaces of iron and aluminum oxides (and hydroxides) are capable of coordinating with (i.e., adsorbing) dissolved anions via ligand-exchange reactions (*1–3*). Several studies have shown that the solubility and the rate of dissolution of sparingly soluble oxides can be significantly increased by certain sorbing anions and organic substances (*4–7*). The increased rate of dissolution has been attributed to surface processes initiated by the sorbed species (*8–10*). Although the dissolution rate of these oxides may at times be limited by solid- or liquid-phase transport processes (*11–16*), Stumm and co-workers (*16, 17*) concluded that in most cases the rate of dissolution of slightly soluble oxides is controlled by the rate of surface chemical reactions.

Some dissolution processes include reduction of the structural metal ion; in such cases dissolution involves the adsorption of reductants, precursor complex formation, electron transfer, release of oxidized adsorbate (anionic ligand or organic substance), and the release of reduced structural metal ion (*10, 18*). The reaction steps for nonreductive dissolution can be represented as follows (*6*):

(1) adsorption of ligand

$$Fe-O-Fe-|-OH + L = Fe-O-Fe-|-L + OH^-$$

(2) formation of precursor complex

$$Fe-O-Fe-|-L = Fe-O-|-FeL$$
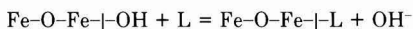
(3) detachment of metal ion and generation of new site

$$Fe-O-|-FeL + H_2O \rightarrow Fe-|-OH + FeL + OH$$
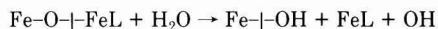
Once ligands adsorb to the surface, they may begin to polarize, weaken, and finally break the metal–oxygen bonds, causing the release of metal into solution. The overall process is referred to as "ligand-promoted dissolution" (*6*). In the absence of anionic ligands and under acidic conditions, surface hydroxyl groups are protonated. These protonated surface OH groups can also initiate the dissolution process in a way analogous to that caused by sorbed ligands. This is called "proton-promoted dissolution" (*6*).

Stumm and co-workers (*6, 7*) combined the surface complexation model of adsorption with the concepts of ligand-promoted dissolution to develop an overall model of the dissolution process. Specifically, the ligand-promoted dissolution rate of an oxide is presumed to be directly related to the concentration of "precursor complexes" on the surface: $R_L = k[Me-O-|-MeL]$, where R_L, k, and $[Me-O-|-MeL]$ denote the ligand-promoted dissolution rate, a first-order rate constant, and the concentration of precursor complex, respectively. They suggested that in general the concentration of precursor complexes (which are not amenable to direct experimental analysis) will be proportional to the concentration of adsorbed ligands (which is easily measured). In such cases, $R_L = K_L C^s_L$, where K_L and C^s_L denote the ligand-promoted dissolution rate constant and the sorbed ligand concentration. If sorption of the ligand is fairly weak, C^s_L will be small and a large number of surface sites will be vacant, even when the soluble ligand concentration is large. Under these conditions, C^s_L attains a pseudo steady state, and a constant dissolution rate can be established and maintained in a system for a fairly long period of time.

Despite the undeniable importance of linear ligand-promoted dissolution kinetics ($R_L = K_L C^s_L$) in many systems, a number of studies have shown that under certain conditions the rate of dissolution decreases as dissolution proceeds and that the relationship between the dissolution rate and the adsorbed ligand concentration can be nonlinear (*4, 5, 9, 19*). These observations have been attributed to a decrease in oxide surface area, heterogeneity of the surface, and the adsorption of released metal ions (*18*).

The majority of the studies described above were conducted with weakly sorbing ligands. The controlling reactions might be quite different in systems with strongly sorbing ligands. The current study investigated the applicability of available models in systems of strongly
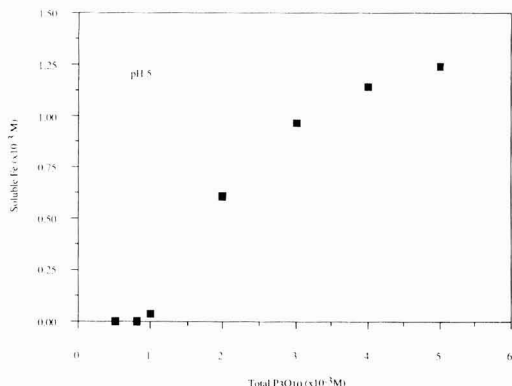
Figure 1. Dissolved Fe after 2-h contact of ferrihydrite (10^{-2} M as Fe) with tripolyphosphate. Dissolution does not occur until the tripolyphosphate concentration is $> 10^{-3}$ M.

sorbing ligands. As will be shown, the sorption of released metal–ligand complexes can be extremely important in such systems and, in fact, can control the overall kinetics of dissolution. In this paper, the experimental evidence supporting the importance of this reaction is presented, and the adsorption/dissolution kinetic model is expanded to include the reaction and explore the conditions under which it must be considered.

Experimental Section

All chemicals used in this study were analytical grade. Tripolyphosphate was the strongly sorbing ligand investigated. Stock solutions of 0.1 and 0.01 M sodium tripolyphosphate ($Na_5P_3O_{10}$) were prepared and stored at 4 °C in the dark.

Preparation of Ferrihydrite. The slightly soluble oxide chosen for study was ferrihydrite, which was prepared in batch for each experiment by adding ferric nitrate stock solution to a 0.1 M $NaNO_3$ solution at room temperature (22 ± 2 °C) under a nitrogen atmosphere. The solution was rapidly titrated to pH 8.0 with NaOH, and the slurry was aged at pH 8.0 ± 0.2 for 2 h before beginning the dissolution experiments.

Dissolution Kinetics. Dissolution experiments were carried out at room temperature and at 1.5 °C. Ferrihydrite concentration was 10^{-2} M Fe, and total tripolyphosphate concentrations were from 5×10^{-4} to 2×10^{-2} M. Both the suspension and stock tripolyphosphates were preadjusted to pH 5. After the ferrihydrite and tripolyphosphate were mixed, system pH was kept at 5.0 by using a Metrohm autotitrator. Normally, the dissolution reaction was allowed to proceed for 4 h. Sample aliquots were withdrawn at predetermined intervals and filtered immediately through 0.1-μm membrane filters; soluble Fe was operationally defined as the total Fe in the filtrate.

Longer term (7 days) experiments were also conducted to investigate the stoichiometric relationship between soluble Fe species and tripolyphosphate species at equilibrium conditions. For these experiments, the system temperature was 1.5 °C and pH was 5.0.

Fe and Phosphorus Analyses. Analyses of metals and phosphorus all followed recommended procedures (20). Fe concentrations in solution were determined by inductively coupled plasma (ICP) spectrometry. Both the standards and sample dilutions were made in 0.1 M $NaNO_3$ or 0.01 M $NaNO_3$. All solutions were adjusted to pH less than 3 prior to analysis. Polyphosphates were hydrolyzed to orthophosphate by boiling with acid and potassium per-
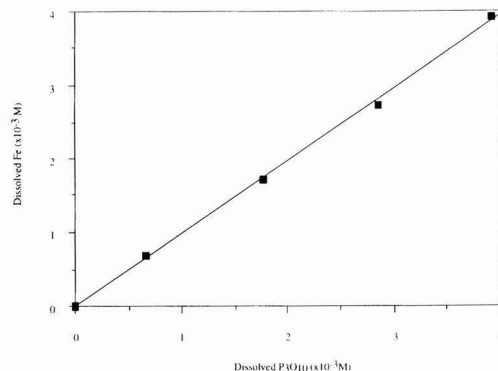
Figure 2. Concentrations of soluble Fe and tripolyphosphate after 7-days contact with ferrihydrite at pH 5.
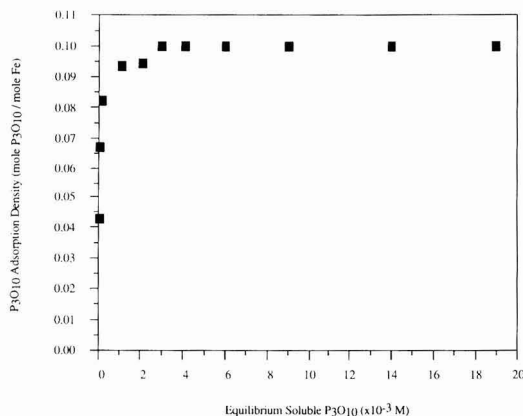
Figure 3. Adsorption isotherm of tripolyphosphate on ferrihydrite at pH 5. The maximum surface P_3O_{10} concentration is $\sim$0.1 mol of P_3O_{10}/mol of Fe and is attained at very low soluble P_3O_{10} concentrations.

sulfate for 30 min in an autoclave, after which phosphorus was determined colorimetrically following the ascorbic acid method (Standard Methods 424F). A Perkin-Elmer Lambda 3 UV/vis spectrophotometer was used for these measurements.

Results

Our previous study on the effect of polyphosphates on metal sorption behavior (21) revealed that the dissolved Fe concentration after 2 h is approximately proportional to the total tripolyphosphate added, as shown in Figure 1. However, dissolution did not occur in that system until the tripolyphosphate concentration was greater than $\sim 10^{-3}$ M, corresponding to a ratio of $\sim$0.1 mol of total tripolyphosphate/mol of Fe. The importance of the ligand in this process is apparent from Figure 2, which shows the soluble Fe concentration as a function of soluble tripolyphosphate concentration at pH 5 after 7 days of contact. The plot is linear, passing through (0, 0) with a slope of 0.98. Since no iron dissolves under similar conditions in the absence of tripolyphosphate, it is reasonable to conclude that essentially every iron ion in solution is complexed by tripolyphosphate, and vice versa. The adsorption isotherm for a tripolyphosphate/ferrihydrite system is shown in Figure 3. Adsorption of P_3O_{10} is very strong, and almost all the P_3O_{10} in the system is adsorbed until the surface is saturated ($\Gamma_{pmax} = 0.1$ mol of P_3O_{10}/mol of Fe), after which P_3O_{10} can be detected in solution.
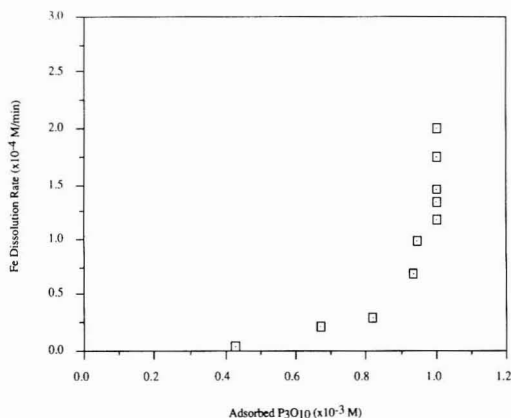
Figure 4. Dependence of dissolution rate on the concentration of adsorbed tripolyphosphate in the system. Reaction time is 1.0 min. Note that the maximum surface P_3O_{10} concentration is $\sim 10^{-3}$ mol/L, corresponding to the maximum adsorption density (0.1 mol of P_3O_{10}/mol of Fe) times the Fe concentration in the system, 1×10^{-2} M. The rate is clearly not linearly proportional to C^s_L.

According to the ligand-promoted reaction model, dissolution of oxides is initiated by adsorption of anions through surface complexation reactions, and the rate of dissolution is approximately proportional to the adsorbed ligand concentration (C^s_L). By contrast, Figure 1 and 3 indicate that in our system dissolution is negligible as the adsorbed ligand concentration increases from 0 to its saturation value. Thereafter, dissolution increases steadily as more polyphosphate is added to the system, even though C^s_L remains approximately constant. The average dissolution rates for the first minute of reaction are plotted as a function of the concentration of adsorbed P_3O_{10} in Figure 4; the nonlinearity of the relationship is obvious.

Figure 5 shows the kinetics of ferrihydrite dissolution in the presence of 5×10^{-4} to 4×10^{-3} M tripolyphosphate at pH 5. In systems containing 5×10^{-4}, 8×10^{-4}, and 10^{-3} M tripolyphosphate (Figure 5A), total soluble Fe concentration increases in the first 1, 4, and 15 min, respectively, and decreases thereafter. [A similar pattern was observed at pH 7, 8, and 10 for systems containing 8×10^{-4} M P_3O_{10} (*21*).] At higher total tripolyphosphate concentrations (Figure 5B), dissolution kinetics appear to follow a nonlinear rate law, and no longer term decrease in soluble Fe concentration is observed. It is obvious from these two figures that the rates of ferrihydrite dissolution in the systems studied are not constant; rates of dissolution decrease as reaction proceeds, and in some cases the net dissolution rate becomes negative.

Continually decreasing dissolution rates over time have been reported before (*18, 19*) and have been attributed to reductions in surface area and to surface heterogeneity. Although these explanations might be appropriate for other systems, they cannot explain the results in the current study. Neither a decrease in surface area nor surface heterogeneity could cause Fe to return to the surface after it had dissolved, as shown in Figure 5A. The results imply that there is a reaction opposing the detachment step that can lead to a net reversal of the dissolution reaction. To our knowledge, no experimental evidence of such a reaction has been presented previously. For the time scale of these experiments, this reaction is significant and the decrease in dissolved Fe concentration is obvious only at the lower tripolyphosphate concentrations studied. At high tripolyphosphate concentrations, this "reverse dissolution" reaction may be overwhelmed
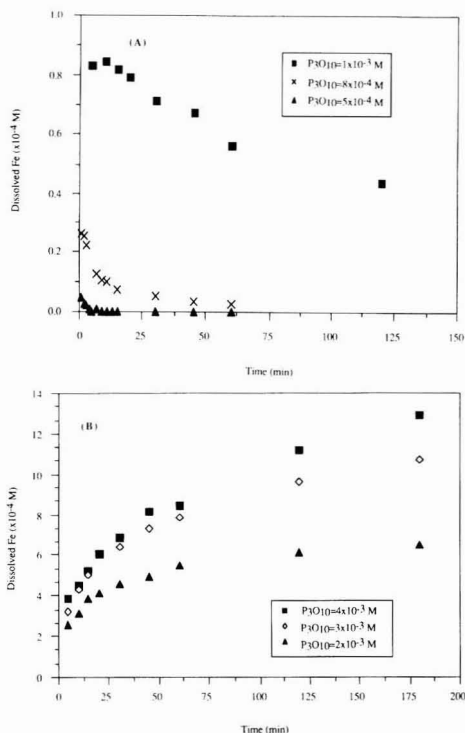
Figure 5. Dissolution kinetics at pH 5 in systems with 5×10^{-4} to 4×10^{-3} M tripolyphosphate. An increase followed by a decrease in dissolved Fe concentration is evident at total P_3O_{10} less than or equal to 10^{-3} M.

by the detachment step, so that the net change in Fe concentration in those systems is positive at all times.

There are two ways to account conceptually for the loss of dissolved Fe from solution: precipitation and adsorption. Since the dissolution of ferrihydrite is promoted by surface coordination reactions between tripolyphosphates and structural iron ions, iron is presumed to leave the surface together with tripolyphosphate as a complex. The fate and ultimate concentration of iron in solution depend on the stability constants and the sorption behavior of these complexes. The released Fe–tripolyphosphate complexes might dissociate, allowing free iron to reprecipitate or adsorb, or the complexes might adsorb and remove Fe from solution, if surface sites are available and if the adsorptive reaction is favorable. While either scenario (dissociation of the complexes followed by sorption or reprecipitation of the Fe; or adsorption of the complexes) is plausible conceptually, the former is not consistent with the experimental results, as shown below.

Consider a set of reactions in series:

$$A + B \leftrightarrow I_1 \leftrightarrow I_2 \leftrightarrow ... \leftrightarrow I_n \leftrightarrow P$$
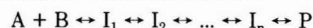
in which A and B are reactants, I_i are intermediates, and P is a product. For a system initially containing only A and B, the time profiles for the concentrations of all species are shown in Figure 6. While the concentrations of the species I_i may increase, peak, and then decrease, that of P can only increase toward its equilibrium value; it can never exceed that value, even transiently. This is true even if the reaction forming P is reversible, or if P can react to form A, B, or any intermediate directly.

With respect to the system under consideration, the reactants A and B are surface structural iron atoms and

Table I. Kinetic Expressions for the Proposed Dissolution Reactions of Ferrihydrite in the Presence of Tripolyphosphate (Figure 6)[a]

surface species

$d[\text{Fe--}|\text{--L}]/dt = k_1[\text{S1}][\text{L}] - k_2[\text{Fe--}|\text{--L}] - k_3[\text{Fe--}|\text{--L}] + k_4[\text{Fe--O--}|\text{--FeL}]$

$d[\text{Fe--O--}|\text{--FeL}]/dt = k_3[\text{Fe--}|\text{--L}] - k_4[\text{Fe--O--}|\text{--FeL}] - k_5[\text{Fe--O--}|\text{--FeL}] + k_6[\text{S1}][\text{FeL}]$

$d[\text{Fe--}|\text{--LFe}]/dt = k_{11}[\text{S1}][\text{FeL}] - k_{12}[\text{Fe--}|\text{--LFe}]$

solution species

$d[\text{FeL}]/dt = k_5[\text{Fe--O--}|\text{--FeL}] - k_6[\text{FeL}] - k_7[\text{FeL}] + k_8[\text{Fe}][\text{L}] - k_{11}[\text{S1}][\text{FeL}] + k_{12}[\text{Fe--}|\text{--LFe}]$

$d[\text{L}]/dt = -k_1[\text{S1}][\text{L}] + k_2[\text{Fe--}|\text{--L}] + k_7[\text{FeL}] - k_8[\text{Fe}][\text{L}]$

$d[\text{Fe}]/dt = k_7[\text{FeL}] - k_8[\text{Fe}][\text{L}] + k_9([\text{S1}] + [\text{S2}]) - k_{10}([\text{S1}] + [\text{S2}])[\text{Fe}]$

ligand-active sites

$d[\text{S1}]/dt = -k_1[\text{S1}][\text{L}] + k_2[\text{Fe--}|\text{--L}] + k_5[\text{Fe--O--}|\text{--FeL}] - k_6[\text{FeL}] - k_{11}[\text{FeL}] + k_{12}[\text{Fe--}|\text{--LFe}]$

H$^+$-active sites

$d[\text{S2}]/dt = k_9[\text{S1}] - k_{10}[\text{Fe}][\text{S1}]$

[a] [S1] represents the concentration of ligand-active sites; [S2] represents sites that can undergo proton-promoted dissolution only.
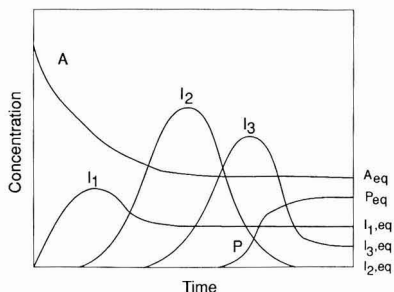
Figure 6. Time profiles for the concentrations of all species for a system initially containing only A. $I_{i,\text{eq}}$, A_{eq}, and P_{eq} represent the equilibrium concentrations for the various species.

dissolved polyphosphate, and the intermediate species might be adsorbed polyphosphate, precursor complexes, etc. For the concentration of dissolved Fe complexes to increase and later decrease, the dissolved complex must be an intermediate that reacts to form a product different from any of the species that preceded it in the reaction sequence. A scenario in which the complexes dissociate and Fe returns to the surface via a sorption or precipitation reaction does not meet this requirement. In such a case the concentration of dissolved complex could increase, but could never decrease as it was observed to do. We conclude that the reaction sequence includes dissolved Fe–polyphosphate complexes as intermediate species that subsequently adsorb to form a new surface species, different from any of the precursor species. Since all the Fe in solution is apparently in complexed form and since other metal–tripolyphosphate complexes have been shown to adsorb strongly to ferrihydrite (21), this scenario seems entirely plausible. In the subsequent discussion, we suggest a possible structure for such a surface species.

The kinetic results observed here can be interpreted by modifying the ligand-promoted dissolution model of Stumm et al. (22) to include the adsorption of Fe–tripolyphosphate complexes. The proposed sequence of events is that the detachment of metal from the surface is initiated as ligands adsorb. The soluble iron concentration at any time represents the net effect of a forward reaction (release of Fe complexes into solution) and a backward reaction (return of the complexes to the surface). Which reaction prevails depends on the relative concentration of surface sites and tripolyphosphate. The results presented in Figure 5 clearly indicate that adsorption of tripolyphosphate is fast and leads to rapid release of iron from the surface (the shortest sampling time is 1 min). If the total tripolyphosphate in the system is less than the amount required to saturate the surface, Fe–P$_3$O$_{10}$ complexes can readsorb, and after a few minutes, the backward

reaction overwhelms the forward reaction. As a result, the Fe concentration in solution decreases. On the other hand, if the total tripolyphosphate concentration in the system exceeds the amount necessary to saturate the surface, the surface lacks capacity for all the dissolved Fe–tripolyphosphate complexes to adsorb. Both the forward and reverse reactions proceed; however, the forward reaction prevails, resulting in apparent nonlinear kinetics (Figure 5B).

The essential aspect of the above scenario is that Fe–P$_3$O$_{10}$ complexes must adsorb to form a surface species different from those that led to Fe dissolution. We have also argued that Fe is initially released to solution as a complex by a ligand-promoted reaction. The possibility that Fe originally enters solution as uncomplexed, free Fe^{3+} ions released from bare surfaces sites, followed by very rapid coordination with dissolved tripolyphosphate and adsorption of complexes, cannot be absolutely ruled out. If this were the case, however, the overall dissolution process would be controlled by the proton-promoted dissolution reaction. On the basis of the proton-promoted dissolution rates of other iron oxides (7, 23), it is highly unlikely that such a reaction could dissolve 6% of 10^{-2} M ferrihydrite in 2 h, as occurred in the system with 2 × 10^{-3} M tripolyphosphate. Thus, we conclude that release of Fe–P$_3$O$_{10}$ complexes from the surface, followed by their readsorption to form a new surface species, is the most likely sequence of events occurring in the systems studied. In the next section, the adsorption/dissolution kinetic model of Stumm and co-workers (6, 7) is extended to incorporate this readsorption reaction.

Model Development and Verification

The proposed dominant reaction sequence for the dissolution of ferrihydrite in the presence of polyphosphate is (1) adsorption of tripolyphosphate, (2) formation of precursor complexes from sorbed tripolyphosphates, (3) release of precursor complexes, and (4) adsorption of complexes. After Fe–tripolyphosphate is released to solution, it will undergo dissociation and association reactions. In addition to the detachment of iron by release of precursor complexes, Fe may be released from vacant surface sites via proton-promoted dissolution and may reprecipitate. A schematic representation of the relevant reactions is presented in Figure 7, in which the forward and reverse reaction rate constants are noted. The kinetic expressions for the reactions in Figure 7 are grouped in Table I, where P$_3$O$_{10}$ is represented as L.

As noted earlier, when FeL adsorbs it must form a surface species different from the dissolution precursor. Such a species might have the ligand bound directly to the surface, although other configurations are also possible. In this conceptual model, rapid adsorption of L leads to
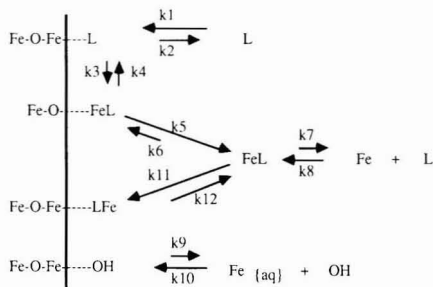
Figure 7. Schematic representation of the reactions for the dissolution of ferrihydrite in the presence of tripolyphosphate. L represents tripolyphosphate. k_i is the rate constant. The precursor complex (Fe–O–|–FeL) is derived from the adsorbed ligand (Fe–O–Fe–|–L). Dissolved FeL can adsorb to form a surface complex (Fe–O–Fe–|–LFe) different from the one in the dissolution sequence.

Table II. Assumptions for Adsorption/Dissolution Kinetic Model

1. $[S1] = 0.10[Fe]_T$
2. $[S2] = 0.77[Fe]_T$
3. a surface reaction is the rate-determining step
4. the precursor complex, Fe–O–|–FeL, is derived from surface ligands

the formation of a weakly adsorbed surface FeL complex, which is then released to solution. Once in solution, FeL can return to the surface as a strongly sorbed complex. In particular, if the complex does adsorb with the polyphosphate attaching to the surface, it is reasonable to assume that adsorption of the complex and adsorption of free ligand are competing reactions. If the concentration of free L in solution is low and the adsorption density of L is less than Γ_{pmax}, FeL can adsorb, decreasing the total soluble iron concentration; however, if free dissolved L is large, return of the complex to the surface could be impeded.

Several assumptions were made before the kinetic rate constants of this model were optimized. The assumptions are listed in Table II. The total concentration of adsorbing sites ([S1]) used in the model was $0.1[Fe]_T$. This number is obtained from the adsorption isotherm of tripolyphosphate. [S1] + [S2] is the proton-exchange capacity of ferrihydrite, which is ~0.87 mol/mol of Fe, based on the results of Davis and Leckie (24). The third assumption is the central assumption of surface reaction controlled dissolution. Zutic and Stumm (16) reported that for amorphous oxides and anions with small molecular size like F^-, both diffusion and the surface reactions have to be considered in the rate-determining step. However, if a ligand has a molecular size larger than F^-, as in the current case, the detachment step is more likely to be critical (16). Thus, it is justified to assume that a surface reaction is the rate-determining step. The final assumption is that the precursor complexes, which relate directly to the rate of dissolution, are derived from adsorbed uncomplexed ligands only. An adsorbed iron–tripolyphosphate complex, Fe–|–LFe, may lead to the formation of a binuclear precursor complex (Fe–O–Fe–|–LFe → Fe–O–|–FeLFe), but such a complex would probably be less capable of facilitating the detachment step. Computer codes based on the kinetic expressions in Table I were attached to NPSOL, a nonlinear optimization programming computer package (25). Kinetic results from the system with 2×10^{-3} M tripolyphosphate and 10^{-2} M ($[Fe]_T$) ferrihydrite at pH 5 were then used to optimize the rate constants in the model.
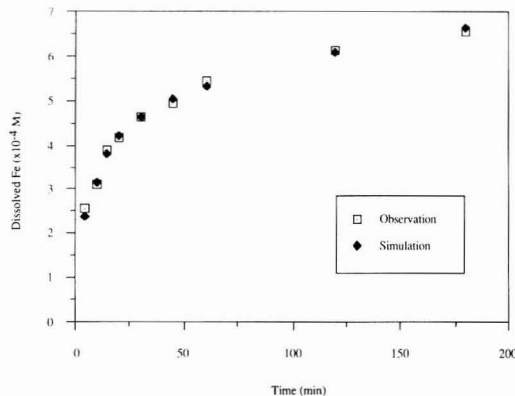
Figure 8. Optimization results for system with 10^{-2} M ($[Fe]_T$) ferrihydrite and 2×10^{-3} M tripolyphosphate.

Table III. Optimized Kinetic Constants Used To Model Experimental Data

k_1	1.10×10^3 M^{-1} min^{-1}	k_7	3.22×10^{-4} min^{-1}
k_2	1.25×10^{-6} min^{-1}	k_8	2.22×10^4 M^{-1} min^{-1}
k_3	4.93×10^{-1} min^{-1}	k_9	7.32×10^{-5} min^{-1}
k_4	2.84×10^2 min^{-1}	k_{10}	2.81×10^4 M^{-1} min^{-1}
k_5	8.95×10^1 min^{-1}	k_{11}	5.77×10^3 M^{-1} min^{-1}
k_6	6.45×10^1 M^{-1} min^{-1}	k_{12}	1.26×10^{-2} min^{-1}

Optimization results are presented in Figure 8 and Table III. Model simulations fit the experimental data very well. The optimized rate constants were then used to model the systems with 1×10^{-3} and 3×10^{-3} M tripolyphosphate. Model simulations are compared with experimental observations in Figure 9. The model not only fits the system with 3×10^{-3} M tripolyphosphate quite well (Figure 9B) but also successfully predicts an increase followed by a slow decrease in soluble iron concentration in the system with 1×10^{-3} M tripolyphosphate. For even lower and higher tripolyphosphate concentrations, 8×10^{-4} and 4×10^{-3} M, this model still gave reasonably good predictions (Figure 9C,D). It is not surprising that the quantitative predictions were not always excellent, since factors such as changes in the reactive site density (which might decrease during the reaction period), electrostatic interactions, and lateral interactions between surface molecules were not considered. Indeed, it has been established that the adsorption of polyphosphates can be greatly affected by surface negative charge (21).

The model would be able to simulate the kinetic results for systems containing total tripolyphosphate greater than 1×10^{-3} M reasonably well even without considering the adsorption of complexes (k_{11} and k_{12} in Figure 7). Similar kinetic curves have been reported in the literature fairly often. However, if k_{11} and k_{12} are removed from the model, it is impossible to reproduce the data or even the pattern in systems with total tripolyphosphate less than or equal to 1×10^{-3} M, i.e., under conditions where there is a period with a net negative dissolution rate. For instance, when the data from the system containing 1×10^{-3} M tripolyphosphate are used to determine the best-fit rate constants (Figure 10), the model simulates the experimental results very well when k_{11} and k_{12} are included. However, it cannot simulate the observed trend of an increase followed by a slow decrease in soluble iron concentration when k_{11} and k_{12} are excluded. As noted earlier, the reason for this can be understood by inspecting reactions 5 (k_5) and 6 (k_6) in Figure 7. The model construct is such that as the
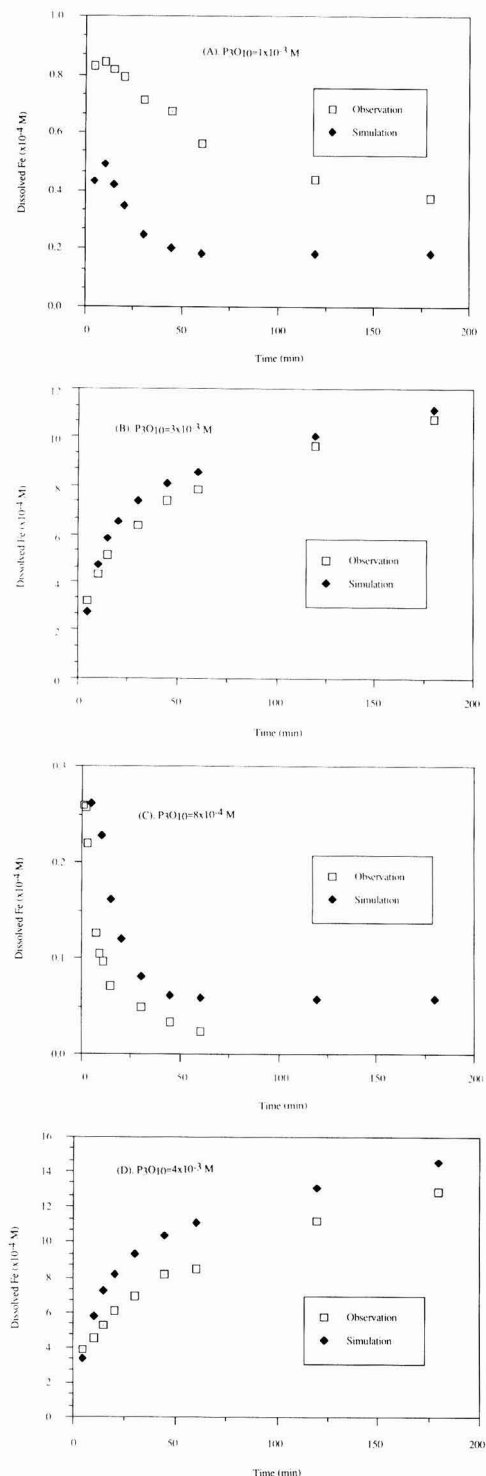
Figure 9. Simulation results for systems with 10^{-3}, 3×10^{-3}, 8×10^{-4}, and 4×10^{-3} M tripolyphosphate. The rate constants for the simulation were optimized based on the system with 2×10^{-3} M P_3O_{10} (Figure 8.)
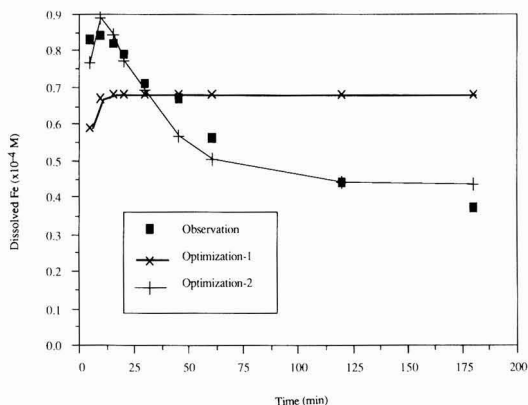
Figure 10. Best fit model results for the system with 10^{-3} M total tripolyphosphate, including ($+$, optimization-1) and excluding ($\times$, optimization-2) the sorption of Fe–P_3O_{10} complexes. When sorption of the complexes is excluded, the model cannot predict an increase and subsequent decrease in Fe concentration.

forward detachment reaction (k_5) and reverse sorption reaction (k_6) approach equilibrium, it is impossible to overshoot the equilibrium condition. Only if Fe returns to the surface by some reaction that produces a new surface species can this pattern be generated.

In most oxide dissolution studies, the observed dissolved metal ion concentration has increased monotonically with time. For such systems, the experimental results are easily modeled without considering sorption of complexes. However, those models can only reproduce results where the net rate of dissolution is always positive. Even though Waite et al. (18) noted that released structural metal ions could adsorb to the surface, no direct evidence for the reaction was presented in their work. In this study, the experimental work and the adsorption/dissolution kinetic model show clearly that adsorption of released complexes plays a significant role in the overall dissolution reaction and leads to an apparent negative dissolution rate. This reaction could easily be overlooked if the total ligand concentrations and the time steps in the kinetic studies were not adequately selected.

With the aid of this kinetic model, some of the reactions at the interface can be evaluated in detail, and the relative importance of the various proposed reactions and surface species can be examined. Figure 11 shows the surface and solution species concentrations predicted by the model as a function of time for a system with 1×10^{-3} M tripolyphosphate. [The model development is such that all the proposed adsorbed tripolyphosphate species, i.e., Fe–|–L, Fe–|–FeL, and Fe–|–LFe, are considered to be monodentate complexes, even though other types of complexes, e.g., bidentate $(FeO)_2FeL$ are possible.] Interestingly, the concentration of precursor complexes is always extremely low. This concentration is kept very low because the complex rapidly enters solution as FeL, which then can readsorb as the proposed alternative adsorbed complex. The speed of the dissolution reaction allows even this low concentration of precursors to release significant amounts of iron to solution rapidly. Adsorbed free ligand concentration (Fe–|–L) increases rapidly in the first 2–3 min (Figure 11B), leading to the formation of precursor. Starting at around $t = 3$ min, the formation of Fe–|–L by sorption of free L is slower than the conversion of Fe–|–L to precursor complexes (Fe–|–FeL), so the concentration of adsorbed free ligands (Fe–|–L) decreases. Fe–|–LFe becomes the predominant surface species over Fe–|–L in
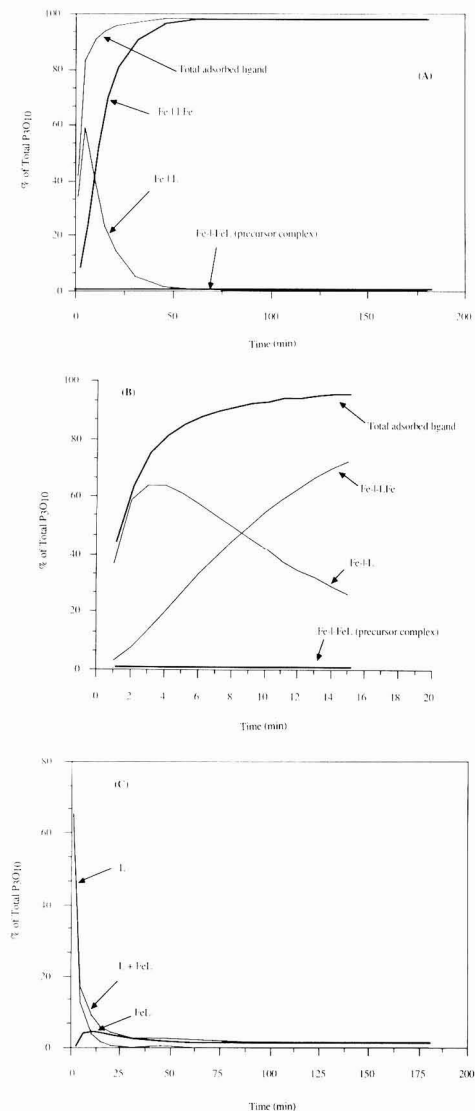
Figure 11. Model-predicted sorbed (A and B) and dissolved (C) tripolyphosphate speciation for a system containing 10^{-3} M P_3O_{10}. (B) is the same as (A), with an expanded scale from 0 to 20 min.

$\sim$10 min, and the concentration of Fe–L reaches negligible values by $t = \sim$40 min.

As each precursor complex leaves the surface, dissolved L and dissolved FeL compete to sorb to the newly available site. The sorption of LFe (in the form Fe–|–LFe) temporarily stops the dissolution at that site, while sorption of L initiates a new dissolution sequence. Soon, most surface sites are occupied by FeL (as Fe–|–LFe). The dissolution reaction slows because free ligands in solution are unable to compete effectively with FeL for these sites. The whole process can be treated as the conversion of Fe–|–L plus L in the early stages of reaction ($t < 10$ min) to Fe–|–LFe plus FeL in the later stages ($t > 25$ min); in the end, all the adsorbed tripolyphosphate is in the form Fe–|–LFe, and all the soluble tripolyphosphate is present as FeL.

The previous discussion described systems where total tripolyphosphate was less than that necessary to saturate the surface. Figure 12 presents typical model output for
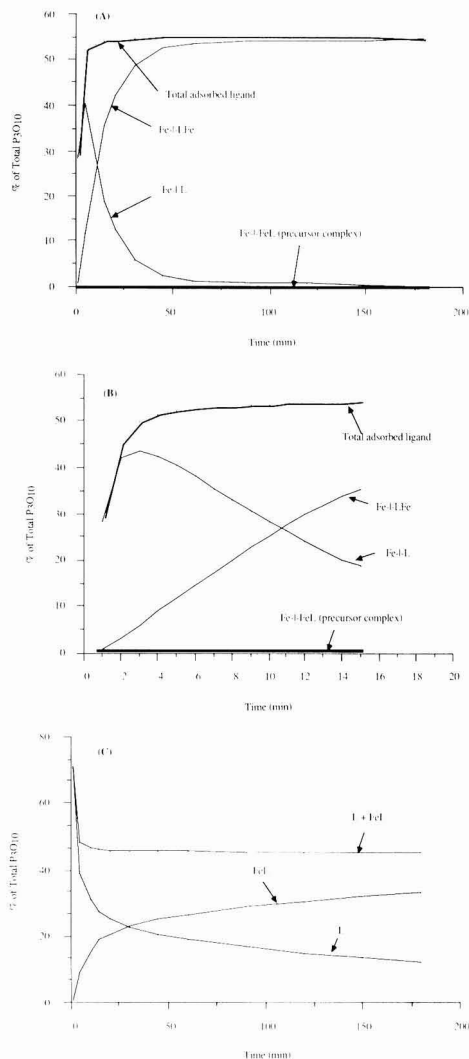
Figure 12. Model-predicted sorbed (A and B) and dissolved (C) tripolyphosphate speciation for a system containing 2×10^{-3} M P_3O_{10}. (B) is the same as (A), with an expanded scale from 0 to 20 min.

the alternative case, where total tripolyphosphate is greater than that necessary to saturate the surface. The early stages of the reaction are not very different in the two cases. Fe–|–L is the predominant surface species up to $\sim$10 min (Figure 12B). However, the concentration of Fe–|–L peaks and then starts to decrease after 2 min, while Fe–|–LFe increases (Figure 12B). As the surface is gradually enriched in Fe–|–LFe at the expense of Fe–|–L, the release of iron is retarded. After $\sim$1 h, almost all surface sites available for binding ligands are occupied by complexes in the form Fe–|–LFe (Figure 12A). From this point on, dissolution is very slow, proceeding only to the extent that free L in solution can occupy a free site during the short interval between desorption of LFe from a surface site and resorption of the same or a different LFe complex from solution. This process proceeds continuously until, at equilibrium, all the ligands in the system, both in solution (Figure 2) and at the surface, are complexed.

The dissolution of ferrihydrite in the presence of tripolyphosphate is a typical example of the situation where
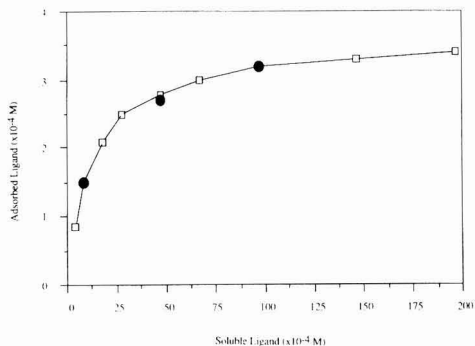
Figure 13. Simulation of the dissolution of δ-Al$_2$O$_3$ in the presence of salicylate at pH 5. The plot shows adsorbed ligand concentration as a function of bulk ligand concentration in the system. Solid circles represent the data of Furrer and Stumm (*6*). Open squares represent data generated by this model.
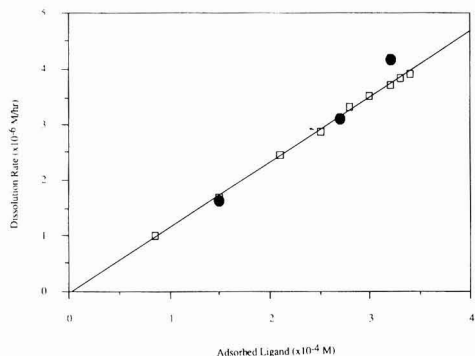
Figure 14. Simulation of the dissolution of δ-Al$_2$O$_3$ in the presence of salicylate at pH 5. The plot shows the dissolution rate as a function of the adsorbed ligand concentration. The adsorption of complexes was ignored. Solid circles represent the data of Furrer and Stumm (*6*). Open squares represent data generated by this model. The value of K_L in $R_L = K_L C^s_L$ for the simulation is 1.17 h^{-1}.

the dissolution reaction is rapid, and complexes are strongly sorbing. The model can also be applied to another limiting case where adsorption of ligands and/or complexes is much weaker, the dissolution reaction is far from equilibrium, and complexes do not sorb. One example of such a system is represented by the work of Furrer and Stumm (*6*) on the dissolution of δ-Al$_2$O$_3$ in the presence of salicylate. In that work, 0.06% of 2×10^{-2} M Al dissolved at pH 5 in the presence of 5×10^{-3} M salicylate in 4 h, i.e., dissolution is ~2 orders of magnitude slower than in our study. Figures 13 and 14 show the fit of our model to their adsorption and dissolution data. In this case, k_{11} and k_{12} could be ignored since the sorption of Al–salicylate complexes is negligible. In this and similar systems dissolution kinetics follow a linear rate law; i.e., a plot of soluble metal concentration vs time is linear. As expected, the rate of dissolution is linearly proportional to the adsorbed ligand concentration, i.e., $R_L = K_L C^s_L$ (Figure 14).

To evaluate the effects of the adsorption of metal–ligand complexes on the linear relationship between R_L and C^s_L, reaction steps 11 and 12 in Figure 7 can be added to the model. In other words, we will simulate what might have occurred if Al–salicylate complexes sorbed in that system. For the purpose of illustration, k_{11} (the kinetic constant for the adsorption of complex) was set to equal k_1 (the kinetic constant for the adsorption of ligand), and k_{12} (desorption of complex) was set to one-tenth of k_2 (de-
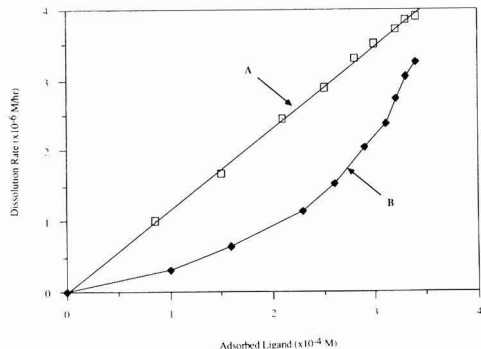
Figure 15. Simulation of the dissolution of δ-Al$_2$O$_3$ in the presence of salicylate at pH 5: dissolution rate as a function of adsorbed ligand concentration. Curve A represents a system where the adsorption of complexes was ignored; the rate of dissolution is linearly proportional to surface ligand concentration. Curve B represents a system where the adsorption of complexes is included; the rate of dissolution is not proportional to surface ligand concentration. The total adsorbed ligand concentrations are close in both conditions.

sorption of ligand), simulating a condition where the complex adsorbs more strongly than a free ligand. The remaining constants were kept the same as in the previous simulation, so that the adsorbed ligand concentrations were close in both conditions. Model results are presented in Figure 15, curve B, showing that, under these conditions, the dissolution rate is no longer linear with C^s_L. Curve A in Figure 15 represents the same condition except that k_{11} and k_{12} are 0. It is obvious that without considering the adsorption of complexes, linear relationships between the dissolution rate and adsorbed ligand concentration are always obtained; however, when the adsorption of complexes is considered, the rate of dissolution is inhibited and nonlinear relationships are obtained.

When the complete set of possible surface reactions is considered, it becomes clear that most previous studies represent a limiting case where sorption is very weak, and the current study represents the other extreme where sorption is very strong. There are many environmentally important ligands, particularly humic acids, which are likely to behave more like polyphosphate than salicylate in this regard. While the linear rate model of Stumm and co-workers (*6, 7*) can accurately represent the first limiting case, the proposed model can represent both extremes and the continuum of intermediate situations and, therefore, is likely to be useful over a wider range of environmental conditions.

Summary

The dissolution of ferrihydrite can be greatly enhanced in the presence of polyphosphates via a process called ligand-promoted dissolution. Depending on the total tripolyphosphate concentration, total soluble iron concentration may increase in the first few minutes and decrease thereafter or increase continuously at a decreasing rate. Generally, the former pattern is observed at a total tripolyphosphate concentration less than that which the surface can potentially adsorb. Under these conditions, adsorption of the released, tripolyphosphate-complexed Fe dominates over the dissolution of Fe, resulting in a decrease in the soluble Fe concentration. At total tripolyphosphate concentrations greater than that necessary to saturate the surface, dissolution of Fe overwhelms the adsorption of Fe–tripolyphosphate complexes, resulting in a continuous increase in soluble Fe concentration.

Ultimately, the equilibrium dissolved iron concentration is approximately equal to the soluble tripolyphosphate concentration.

An adsorption/dissolution kinetic model was developed based on the surface complexation model of adsorption. It considers the adsorption of free tripolyphosphates, formation of precursor complexes, release of precursor complexes, and the adsorption of Fe–tripolyphosphate complexes in a form different from that of precursor complexes. The model successfully simulates the experimental observations for ferrihydrite dissolution (10^{-2} M as Fe) for the tripolyphosphate concentrations studied (8×10^{-4}–4×10^{-3} M). The model confirms that the adsorption of released complexes plays a very significant role in the overall dissolution reaction. It is also consistent with the suggestions of previous workers that the rate-limiting step in the dissolution process is release of the precursor complex, and that the concentration of this complex is extremely small compared to those of other surface species. This reaction accounts for the nonlinear relationship between adsorbed ligand concentration and dissolution rate.

The conditions investigated in this study are representative of environments where the adsorption of ligands is strong and fast, the dissolution reaction is rapid, and complexes are strongly sorbing. The rapid release and strong sorption of metal–ligand complexes can explain the nonlinear dissolution kinetics and the apparent negative dissolution rates observed in some such systems. Previous studies have focused on systems where sorption of ligands and complexes is weak, and the dissolution reaction is relatively slow. By adjusting the values of rate constants, the model was shown to be equally applicable to both types of systems.

Literature Cited

(1) Kummert, R.; Stumm, W. J. Colloid Interface Sci. 1980, 75, 373.
(2) Sigg, L.; Stumm, W. Colloids Surf. 1980, 2, 101.
(3) Stumm, W.; Kummert, R.; Sigg, L. Croat. Chem. Acta 1980, 53, 291.
(4) Shying, M. E.; Florence, T. M. J. Inorg. Nucl. Chem. 1970, 32, 3493.
(5) Shying, M. E.; Florence, T. M. J. Inorg. Nucl. Chem. 1972, 34, 213.
(6) Furrer, G.; Stumm, W. Geochim. Cosmochim. Acta 1986, 50, 1847.
(7) Zinder, B.; Furrer, G.; Stumm, W. Geochim. Cosmochim. Acta 1986, 50, 1861.
(8) Stumm, W.; Furrer, G.; Kunz, B. Croat. Chem. Acta 1983, 56, 593.
(9) Waite, T. D.; Morel, F. M. M. Environ. Sci. Technol. 1984, 18, 860.
(10) Stone, A. T.; Morgan, J. J. In Aquatic Surface Chemistry; Stumm, W., Ed.; John Wiley & Sons: New York, 1987; Chapter 9, pp 221–254.
(11) Wollast, R. Geochim. Cosmochim. Acta 1967, 31, 635.
(12) Luce, R. W.; Bartlett, R. W.; Parks, G. A. Geochim. Cosmochim. Acta 1972, 36, 35.
(13) Busenberg, E.; Clemency, C. Geochim. Cosmochim. Acta 1976, 40, 41.
(14) Chou, L.; Wollast, R. Geochim. Cosmochim. Acta 1984, 48, 2205.
(15) Chou, L.; Wollast, R. Am. J. Sci. 1985, 285, 963.
(16) Zutic, V.; Stumm, W. Geochim. Cosmochim. Acta 1984, 48, 1493.
(17) Furrer, G.; Stumm, W. Chimia 1983, 37, 338.
(18) Waite, T. D.; Wrigley, I. C.; Szymczak, R. Environ. Sci. Technol. 1988, 22, 778.
(19) Waite, D. T.; Torikov, A. J. Colloid Interface Sci. 1987, 119, 228.
(20) Standard Methods for the Examination of Water and Wastewater, 16th ed.; Franson, M. A. H., Ed.; American Public Health Association: Washington, DC, 1985.
(21) Lin, C. F. Ph.D. Thesis, University of Washington, 1989.
(22) Stumm, W.; Wehrli, B.; Wieland, E. Croat. Chem. Acta 1987, 60, 429.
(23) Rubin, J.; Matijevic, E. J. Colloid Interface Sci. 1979, 68, 408.
(24) Davis, J. A.; Leckie, J. O. J. Colloid Interface Sci. 1978, 67, 90.
(25) Gill, P. E. In User's Guide for NPSOL, Version 4.0; Department of Operation Research: Standford University, CA, 1986.

Sampling Bias Caused by Materials Used To Monitor Halocarbons in Groundwater

Glenn W. Reynolds,[†] **John T. Hoff,**[*] **and Robert W. Gillham**

Waterloo Centre for Groundwater Research and Department of Earth Sciences, University of Waterloo, Waterloo, Ontario, Canada, N2L 3G1

■ Laboratory experiments were conducted to evaluate materials used in the construction of groundwater monitors for their potential to cause sampling bias. Ten materials were exposed to low concentrations of five halogenated hydrocarbons in water for periods up to 5 weeks. Borosilicate glass was the only material that did not diminish the halocarbon concentrations. Three metals, including stainless steel, apparently transformed the compounds. Six synthetic polymers, including poly(tetrafluoroethylene) and rigid poly(vinyl chloride), absorbed the compounds. The sorption rates were dependent on flexibility of the polymer, water solubility of the compound, solution volume to polymer surface area ratio, and temperature. A diffusion model explained the concentration histories of solutions exposed to polymers, and the diffusion mechanism was confirmed by direct measurement of halocarbon distributions in several of the polymers. The experimentally determined diffusivities and polymer–water partition coefficients for polyethylene were consistent with literature data.

Introduction

The importance of obtaining representative samples of groundwater for the determination of organic contaminants has motivated many studies of sampling techniques. Systematic errors arising from volatilization (1–4), sorption–desorption (3–10), and leaching (11, 12) have been documented. Work in our laboratory has focused on evaluating the potential of synthetic polymers and other materials used in groundwater monitors to absorb and release common organic contaminants (13–16).

Synthetic polymers are widely used in the construction of groundwater monitoring equipment. The fact that synthetic polymers are also employed to extract and preconcentrate water samples for the determination of soluble organics suggests that sorption might be a common source of error in sampling groundwater for organic contaminants. A question of current importance is whether to use poly(tetrafluoroethylene) or less expensive rigid poly(vinyl chloride) pipe to encase monitoring wells. Another question concerns the use of polymer tubing to convey water samples to the surface. A quantitative understanding of the processes by which organic compounds are absorbed by synthetic polymers is requisite to the design and effective use of sampling equipment constructed from synthetic polymers.

This paper reports the results of laboratory experiments to measure the sorption of halogenated organic compounds by synthetic polymers and other materials used in groundwater monitors. Two techniques were employed: (1) Conventional sorption measurements were carried out to determine the rates under conditions resembling those in a well; diffusivities and polymer–water partition coefficients were estimated from these data. (2) A scanning

electron microscope with an energy-dispersive X-ray analyzer was used to confirm the mechanism of sorption and to measure the diffusivities independently. This paper interprets the results of the experiments in light of other studies of the sorption of organic compounds by synthetic polymers and suggests a strategy for controlling sampling bias.

Experimental Methods

The sorption experiments were designed to examine the sorption rates associated with materials used in groundwater monitoring wells. Ten materials were evaluated: borosilicate glass tubing, 316 stainless steel tubing, aluminum tubing, galvanized steel sheet, rigid poly(vinyl chloride) rod (RPVC), poly(tetrafluoroethylene) tubing (Teflon, PTFE), Nylon 6,6 plate (NYL), polypropylene tubing (PP), low-density polyethylene tubing (LDPE), and latex rubber tubing (LAT). Most of these are or have been commonly used as well casing, screening, or transfer-line tubing materials; glass and latex rubber were included to represent the extremes of minimal and maximal sorption. The five organic compounds used in the experiments were 1,1,1-trichloroethane (TRI), 1,1,2,2-tetrachloroethane (TET), hexachloroethane (HEX), bromoform (BRO), and tetrachloroethylene (TEY). Among these compounds are some of the most common organic contaminants in groundwater.

Each material was washed, cut into pieces, and distributed equally among 30 160-mL glass hypovials. An additional 15 hypovials, which did not contain materials to be tested, served as controls. The hypovials were filled without headspace from a glass carboy containing an aqueous solution of the compounds at concentrations ranging from 20 to 45 μg L^{-1}. These concentrations are similar to the drinking water standards for low molecular weight halocarbons. The hypovials were immediately sealed with Teflon-faced silicone rubber septa and stored in the dark at 22 °C until sampled. The hypovials were not shaken continuously but were occasionally tilted back and forth to simulate near-stagnant conditions in a monitoring well. The shapes of the materials varied, but the ratio of the volume of solution to the surface area of material was nearly constant, being ~0.35 cm. This ratio would be experienced in a monitoring well cased with material having an internal diameter of ~1.4 cm.

Two hypovials containing the material to be tested and one control hypovial were sacrificed at the following times: 5, 15, and 30 min; 1, 3, 6, and 12 h; 1, 2, and 4 days; and 1, 2, 3, 4, and 5 weeks. The concentrations of the five compounds in the solutions were determined in duplicate by GLC. A modified pentane extraction was used to preconcentrate the samples (17). The extracts were injected into a Hewlett-Packard 5710A gas chromatograph equipped with a ^{63}Ni electron-capture detector. The column was packed with 10% UCON polar 50 HB5100 on 80–100-mesh Chromosorb. The detection limits (μg L^{-1}) were approximately 3.0 for TRI, 1.0 for BRO, 0.5 for TET and TEY, and 0.05 for HEX.

[†]Present address: Gartner Lee Limited, 140 Renfrew Drive, Markham, Ontario, Canada, L3R 8B6.

Additional experiments were conducted to determine the effects of temperature, concentration, and solution volume to polymer surface area ratio on sorption of the compounds by LDPE. To evaluate the effect of temperature, a set of hypovials containing LDPE was carried through the above procedure except that the hypovials were stored at 10 °C. To evaluate the effect of the volume to area ratio, a set of hypovials containing LDPE was carried through the procedure at a ratio of 0.60 cm. To determine whether the initial concentration would affect the rate of sorption, LDPE pieces were inserted into 16 hypovials as previously described. The vials were filled with buffered organic-free water and capped. Duplicate vials were spiked to known concentrations by injecting small aliquots of concentrated methanol stock solution containing the five compounds. The initial concentrations varied from approximately 5 to 100 μg L^{-1} for all of the compounds except HEX, which varied from approximately 2.5 to 50 μg L^{-1}. The hypovials were stored at 22 °C and sampled after 157 min.

Concentration distributions within the polymers were measured directly with a scanning electron microscope (SEM; JEOL Model JSM-840, operated at 25 keV) equipped with an energy-dispersive X-ray analyzer (EDAX; Kevex Analyst 8000). The compounds were those used in the sorption experiments, and the polymers were RPVC, PTFE, PP, and LDPE. A 6-cm segment of the polymer tubing was suspended in a stoppered Erlenmeyer flask containing a saturated solution of the compound. The solution was stirred continuously by a magnetic stirrer. After 30–360 min of exposure, the piece was removed from the solution and a 2-mm transverse section was cut from the middle. The section was immediately mounted on an aluminum stub with graphite cement and placed into the vacuum chamber of a gold-coating device. After a 30-nm layer of gold was deposited, the stub was quickly transferred to the sample chamber of the SEM. Typically, 7 min elapsed between removing the piece from the solution and measuring the concentration distribution. The electron beam caused the halogen atoms to fluoresce, and it was assumed that the rate of X-ray production was proportional to the concentration of the compound. No attempt was made to determine the absolute concentration. For a qualitative determination of a concentration profile, the electron beam was slowly scanned across the cut surface of the section and the intensity of the halogen X-rays produced was photographed; X-ray dot maps were also used to visualize concentration distributions. For a more quantitative determination, a series of discrete line analyses (30-s counting times) was made at 100-μm intervals across the cut surface of the specimen. Similar techniques have been used to study the interdiffusion of poly(vinyl chloride in poly(caprolactone) (18).

Results and Discussion

Sorption Experiments. The data for each experiment (material–compound combination) were plotted as a concentration history showing relative concentration versus time. The relative concentration was computed by dividing the concentration remaining in solution, C, by the initial concentration, C_0. To facilitate comparisons, the experimental data were grouped according to compound or material and plotted on common axes. Illustrative plots are shown in Figure 1. The polymer data were presented in Reynolds and Gillham (14) and the complete data set is contained in Reynolds (13). Each plotted point is the mean of four measurements (duplicate measurements from duplicate hypovials). The standard deviation of the relative concentration was usually less than 0.03; error bars
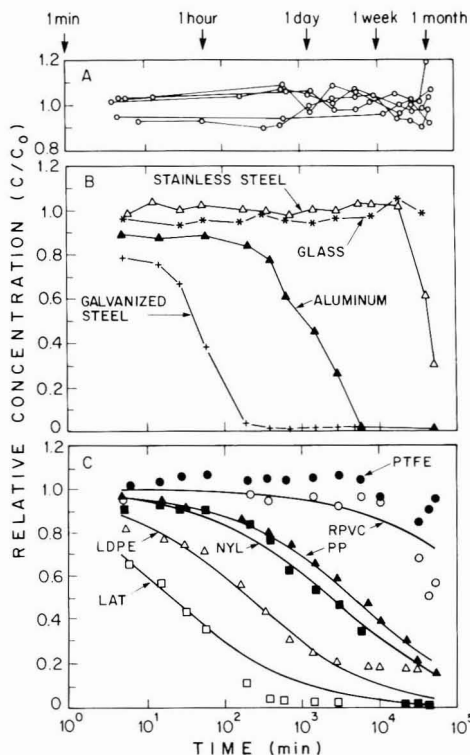
Figure 1. Relative concentration of bromoform, C/C_0, versus time in (A) control hypovials, (B) hypovials containing glass and metals, and (C) hypovials containing polymers. The smooth curves in (C) represent least-squares fits to the data for the diffusive transport model (eq 5).

were not indicated for the sake of clarity. The control concentrations remained essentially constant, indicating that interactions with the hypovials were too small to be measured.

Glass was the only material of the 10 tested that did not cause a reduction in solution concentration for at least one compound over the 34-day period of observation. Of the metals, stainless steel was the least reactive, causing reductions of only two compounds, BRO and HEX; the reductions were substantial however, amounting to 70% after 5 weeks. Aluminum caused reductions greater than or equal to 90% for four of the five compounds, the exception being TEY. Galvanized steel caused reductions greater than or equal to 99% for all compounds. The time for a 50% reduction in solution concentration can be used as a measure of the rate of compound disappearance. Table I shows that the compound disappearance rates decreased in the order galvanized steel > aluminum > stainless steel. The order in which the compounds disappeared from solution was BRO > HEX > TRI > TET > TEY.

It is unlikely that sorption would substantially deplete halocarbon concentrations in hypovials containing impenetrable materials at the volume to surface area ratios and solution concentrations used in these experiments. Gillham and O'Hannesin (16) measured sorption of monoaromatic hydrocarbons by polymers and stainless steel using very similar methods, and no losses were observed for stainless steel. Sorption of organic contaminants by glass has been observed (7, 19), but for compounds having much lower water solubilities.

The reduction of halocarbon concentrations in vials containing the metals is believed to have been caused by

Table I. Times for 50% Reduction of Solution Concentration in the Hypovials Containing the Metals

metal	50% reduction time[a]/min				
	BRO	HEX	TRI	TET	TEY
stainless steel	45000	45000	>50000	>50000	>50000
aluminum	1200	3000	8000	23000	>50000
galvanized steel	45	45	90	170	1000

[a] Compounds are identified in the first paragraph of Experimental Methods.

reactions involving the metal surfaces or metal ions released from the surfaces. Vogel et al. (20) summarized the current understanding of abiotic transformations of halogenated aliphatic compounds in natural water. Polyhalogenated aliphatic compounds can undergo reductive hydrogenolysis in the presence of transition metals and transition-metal complexes. In this reaction, a hydrogen atom replaces a halogen substituent and the transition metal is oxidized. Such reactions are relatively slow in nature, but the rates would be higher with an abundant supply of reduced metal present.

Halocarbon concentrations declined rapidly after an initial delay period in vials containing the metals, whereas concentrations declined more gradually in vials containing the polymers. (See Figure 1.) The delay may be related to the time required to deplete dissolved oxygen or for significant concentrations of transition-metal ions to accumulate. It was also observed that the order in which the compounds disappeared was different when metals were present than when polymers were present. (See below.) The more halogenated compounds were generally removed before the less halogenated compounds in solutions exposed to the metals, and this is consistent with the postulated mechanism. Interpretation of the order of compound disappearance is complicated by the fact that all of the compounds were initially present. The less halogenated compounds could thus be augmented by reductive hydrogenolysis of the more halogenated compounds. Unidentified peaks were seen in the chromatograms from hypovials containing the metals; the peaks were probably reaction products. The fact that stainless steel showed the lowest activity of the three metals in the sorption experiments is probably related to the fact that it is the most inert with respect to corrosion.

All of the polymers reduced the solution concentrations of at least three of the five compounds tested. The total extent of reduction ranged from not detectable to 99%, and the time for a 50% reduction ranged from 10 to over 50 000 min. A nonparametric analysis of variance, the Quade test (21), was used to determine the statistically significant trends in compound disappearance rates. Rankings were developed by comparing concentration history plots for the experiments having a solution volume to polymer surface area ratio of approximately 0.35 cm and a temperature of 22 °C. The results indicate that both factors, polymer and compound, are significant at a level of 1%. The rates vary more among polymers than among compounds. The compound disappearance rates decrease in the order LAT > LDPE > PP > NYL > PTFE > RPVC, and the corresponding trend for the compounds is TEY > HEX > TRI > BRO > TET. Multiple comparison tests indicate that not all of the inequalities are significant at a level of 5%. For example, the rates for RPVC and PTFE cannot be distinguished, nor can those of NYL and PP.

A nonparametric ANOVA of Gillham and O'Hannesin's (16) sorption experiment data for polymers also reveals significant trends in compound disappearance rate. The order for the polymers is flexible PVC > LDPE > PTFE > poly(vinylidene fluoride) > rigid PVC, and the order for the compounds is p-xylene > m-xylene > ethylbenzene > o-xylene > toluene > benzene. As before, not all of the inequalities are significant. Considering both data sets, it is evident that a qualitative relationship exists between the type of polymer and the rate at which the compounds were removed from solution. The sorption rates were highest for the most flexible polymers (LAT, flexible PVC, LDPE) and lowest for the most rigid polymers (RPVC, epoxy-fiberglass, PTFE). This is consistent with the results of Barcelona et al. (9), who conducted similar experiments with five polymer tubing materials. It is also apparent that the less soluble compounds were removed from solution more rapidly than the more soluble compounds. (See section on diffusive transport model.)

SEM Experiments. The concentration distributions of halogenated hydrocarbons in LDPE and PP clearly showed penetration and diffusion of the compounds in the polymers. Figure 2A shows a line-scan photo of the concentration of TEY in LDPE tubing. The concentration profiles of halocarbons in LDPE and PP resembled those expected for diffusion from a solution of constant concentration into a plane sheet. When a semiinfinite solid is exposed to a solution of constant concentration, and the diffusivity of the solute is constant, the concentration of the solute in the solid has the form (22)

$$c(x,t)/(CK) = \text{erfc } [x/(4Dt)^{1/2}] \quad (1)$$

where $c(x,t)$ is the concentration in the solid (g cm^{-3}), C is the concentration in the solution (g cm^{-3}), K is the equilibrium partition coefficient (dimensionless), D is the diffusivity of the solute in the solid (cm^2 s^{-1}), x is the penetration distance in the solid (cm), and t is the exposure time (s). Profiles approximating this form were observed for short exposure times in LDPE and PP. The rounding of the outer edges of the profiles in Figure 2A is probably due to relaxation that occurred after the polymer was removed from the solution.

The concentration profiles of TRI, BRO, and TEY were measured as accurately as possible in LDPE with the technique described earlier. An illustrative plot of X-ray intensity versus penetration distance is shown in Figure 2B. The diffusivities, calculated by fitting the profiles to eq 1 at $c/CK = 0.5$, ranged from 3×10^{-8} to 8×10^{-8} cm^2 s^{-1}. The SEM-measured diffusivities, which were determined at saturation concentrations, are $\sim$1 order of magnitude higher than those obtained from the sorption experiments at trace concentrations. (See below.) Diffusivity often depends on sorbed penetrant concentration for condensable organic vapors in polymers (23). In a study by Rogers et al. (24), the diffusivities of several organic vapors in LDPE increased by factors of 7–18 as activity increased from zero to 1.

It was not possible to measure the diffusivities in PTFE, because the halocarbon concentrations were below detection. Only the concentration profile of BRO could be measured in RPVC, due to interference from the large amount of chlorine present in the polymer. This profile was unlike those seen in LDPE and PP in that it was sharp

Table II. Values for log (K^2D)/cm^2 s^{-1} Obtained by Fitting the Sorption Experiment Data to the Diffusive Transport Model (eq 5)

		log $(K^2D)^a$/cm^2 s^{-1}				
polymer[a]	A^c/cm	TEY	HEX	TRI	BRO	TET
RPVC	0.337	-7.8	-8.0	d	-8.5	d
PTFE	0.358	-5.7	-7.9	-8.0	d	-9.2
NYL	0.321	-6.4	-5.7	-7.5	-6.4	-6.6
PP	0.365	-4.4	-4.4	-6.5	-6.6	-7.3
LDPE	0.372	-4.0	-4.0	-5.0	-5.2	-5.9
LDPE	0.602	e	e	-4.8	-5.2	-6.2
LDPE[b]	0.372	-4.3	-4.4	e	-6.1	-6.7
LAT	0.355	-3.9	-3.8	-4.1	-4.1	-4.4

[a] The polymers and compounds are identified in the first paragraph of Experimental Methods. [b] The experiment was done at 10 °C; all other experiments were done at 22 °C. [c] A = (solution volume)/(polymer surface area). [d] Amount of sorption was too small to estimate K^2D. [e] Experiment was not done.
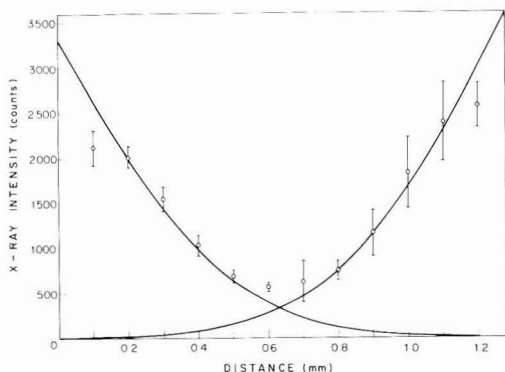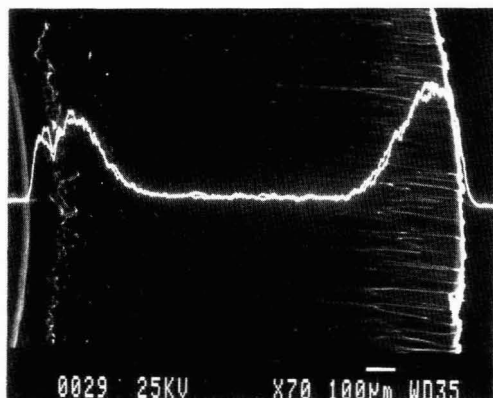
Figure 2. (A) (Top) X-ray line-scan photo of a transverse section cut from the middle of a 6-cm length of LDPE tubing that was exposed to a saturated solution of TRI for 80 min. Superimposed on the secondary electron image of the section are two traces of Cl Kα X-rays generated by scanning the electron beam horizontally across the section; upward deflection indicates increasing intensity. The curved inside and outside edges of the section are seen at the extreme left and right margins of the photo. (B) (Bottom) chlorine Kα X-ray intensity (counts, 30-s counting time) versus distance in LDPE plate (~1.2-mm thickness) after exposure to a saturated solution of TET for 165 min. Each plotted point is the mean of four measurements; the 95% confidence intervals are indicated. The curves drawn in the figure represent eq 1 with D equal to 7×10^{-8} cm^2 s^{-1}.

and steplike. It was also observed that RPVC was swelled and plasticized by the BRO solution. Non-Fickian behavior is often observed in glassy polymers at high concentrations of organic penetrant. In such systems sorption is controlled by the slow, relative to diffusion, relaxation (swelling) of polymer structure induced by strong inter-

actions between the penetrant molecules and the polymer (23, 25).

Diffusive Transport Model. In the following sections, the sorption experiment data are analyzed by a diffusive transport model and the values of the sorption parameters obtained are compared with relevant data from studies of the sorption of organic vapors by synthetic polymers. The experimental system is represented by an infinite sheet of polymer material suspended in a well-stirred solution of limited volume. One-dimensional geometry was used for convenience and generality; this simplification should not introduce large errors into the calculation of the sorption parameters. The thickness of the sheet is $2L$ (cm) and the thickness of the solution in contact with both sides of the sheet is $2A$ (cm). The equations that relate the concentration in the sheet, $c(x,t)$, to that in the solution, $C(t)$, are (ref 22, pp 56–60)

$$\partial c / \partial t = D(\partial^2 c / \partial x^2) \tag{2}$$

$$(A/K)(\partial C / \partial t) = \mp D(\partial c / \partial x) \text{ at } x = \pm L \text{ and } t > 0 \tag{3}$$

$$C = C_0; c = 0 \text{ for } -L < x < L \text{ at } t = 0 \tag{4}$$

where K is the polymer–water partition coefficient (dimensionless) and D is the diffusivity (cm^2 s^{-1}). Both K and D are assumed to be constant. The exact solution is an infinite series; an approximate solution, appropriate for small t, is (26)

$$C/C_0 = \exp(T/\alpha^2) \text{ erfc } [(T/\alpha^2)^{1/2}] \tag{5}$$

where C and C_0 are the solution concentrations at t and $t = 0$, respectively, $T = Dt/L^2$, and $\alpha = A/KL$. This function was fitted to the concentration histories by an iterative least-squares procedure. Since the value of A was known (it is the ratio of solution volume to polymer surface area), the value of K^2D (cm^2 s^{-1}) was calculated for each polymer.

The concentration histories generally conformed to eq 5, except when t was large and α was not small, indicating that the model provides an adequate representation of the experimental data. The agreement between the model and the concentration histories for BRO can be seen in Figure 1C. The logarithms of K^2D are given in Table II. The 95% confidence limits for the log (K^2D) values were usually within ±0.15 of the estimate. The log (K^2D) values for the two different solution volume to polymer surface area ratios agree within experimental error, providing additional evidence that the model is appropriate. Because the volume to surface area ratios were approximately constant (except for one experiment), the log (K^2D) values reflect the trends in compound disappearance rate previously discussed. The K^2D values can be converted to sorption

**Table III. Logarithms of Diffusivity, D (cm² s⁻¹),
Polymer–Water Partition Coefficient, K (Dimensionless), and
Water Solubility, S (mg L⁻¹), for the Halogenated and
Monoaromatic Hydrocarbons in LDPE at 22 °C**

compd[a]	C_∞/C_0	log K exptl[b]	est[c]	log D/cm² s⁻¹ exptl[d]	log S^e/mg L⁻¹ L⁻¹
TET	0.24	1.4	1.5	-8.7	3.5
BEN	0.18	1.5	1.6	-8.1	3.2
BRO	0.17	1.5	1.7	-8.4	3.5
TRI	0.10	1.8	2.2	-8.4	3.2
TOL	0.06	2.1	2.2	-8.4	2.7
EtBEN	0.02	2.5	2.6	-9.1	2.1
p-XYL	0.02	2.5	2.6	-9.0	2.1
HEX	0.01	2.8	2.9	-9.7	1.7
TEY	0.01	2.8	2.7	-9.7	2.2

[a] BEN, benzene; TOL, toluene; EtBEN, ethylbenzene; p-XYL, p-xylene; the other compounds are identified in the first paragraph of Experimental Methods. [b] Calculated by using the following information: $A = 0.372$ cm; $L = 0.053$ cm. [c] The estimated K values were calculated by eq 6 using data from Figure 3 (K_S) and ref 30 and 31 (K_H). [d] The $K^2 D$ values were taken from ref 15 and this work. [e] The water solubilities are for 20 °C (14, 15).

half-times by the formula, $t_{1/2} = 0.585 A^2/K^2 D$. The sorption half-times ranged from less than 20 min for HEX and TEY in LDPE and LAT to over 200 days for BRO and TET in RPVC and PTFE.

For the experiments in which sorption equilibrium was attained, it is possible to calculate K and D by using the following equations: $\alpha = C_\infty/(C_0 - C_\infty)$, $K = A/\alpha L$, and $D = (K^2 D)/K^2$, where C_∞ is the solution concentration at equilibrium. The calculations were performed for the halogenated and monoaromatic hydrocarbons in LDPE; data for the latter compounds were taken from Gillham and O'Hannesin (16). The results (Table III) show that the trends in log K and log D are opposite, in keeping with other studies (23), and that the trend in log ($K^2 D$) is determined by the trend in log K. The logarithms of the water solubilities of the compounds are significantly correlated (0.1% level) with both log K and log ($K^2 D$).

Polymer–Water Partition Coefficients. The purpose of this and the following section is to show that the experimental values of K and D for LDPE are consistent with literature data. In this section, the experimental values for K are compared with literature values derived from Henry's law solubility coefficients and Henry's law constants for air–water partitioning. The following assumptions are implicit: (1) the concentrations of organic compounds used in the experiments were low enough that Henry's law is valid, and (2) K can be calculated by the formula

$$K = K_S K_H \quad (6)$$

where K_S is the Henry's law solubility coefficient for the vapor in the polymer (mol m⁻³ kPa⁻¹) and K_H is the Henry's law constant for air–water partitioning (m³ kPa mol⁻¹). The first assumption is necessary because solubility coefficients for organic vapors in polymers are generally dependent on concentration. It is probably valid because the activities of the organic solutes used in the experiments were of the order of 10⁻³. Further evidence is provided by the nonequilibrium sorption experiments, which showed that sorption rate was independent of initial concentration over the range tested. The second assumption is expected to be valid, because the Henry's law solubility coefficients should not be affected by the small amount of water absorbed by LDPE (<0.01%). Because Henry's law solubility coefficients were not found in the literature for all of the experimental compounds, they were estimated from their
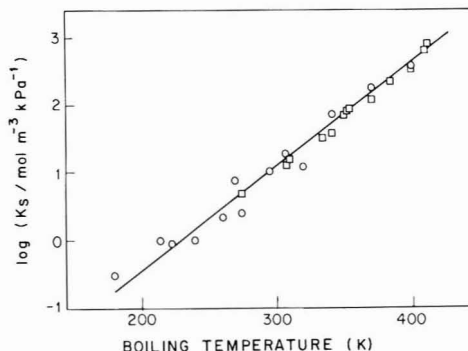
Figure 3. Logarithm of the Henry's law solubility coefficient, K_S (mol m⁻³ kPa⁻¹), versus boiling temperature (K). The solubility coefficients for various compounds in LDPE at 20–25 °C were taken from ref 27 (□) and ref 24 (O). The boiling temperatures were taken from ref 28 and 29.

dependence on the boiling temperature of the compound. This relationship is a consequence of the dependence of the heat of solution of the vapor in the polymer on the heat of condensation of the vapor (23). (See section on temperature dependence of $K^2 D$.)

Henry's law solubility coefficients for a variety of organic compounds in LDPE are plotted against boiling temperature in Figure 3. It is apparent from the figure that a good correlation exists. A regression equation was calculated and used to estimate Henry's law solubility coefficients for the experimental compounds. The polymer–water partition coefficients were then calculated by eq 6, using Henry's law constants for air–water partitioning from McKay and Shiu (30) and Pankow (31). The estimated and the experimental values of log K are given in Table III. There is a good correlation between the two sets of values ($r^2 = 0.93$). The experimental values are on average 0.12 unit (1.3×) lower than the estimated ones. The extent of agreement indicates that the assumptions were not seriously violated.

Polymeric Diffusivities. In this section, the experimental values of D are compared with literature data for diffusivities of organic compounds in LDPE. Many studies of diffusion and permeability in polymers have shown that an increase in penetrant size, in a series of chemically similar penetrants, generally leads to an increase in the solubility and a decrease in the diffusivity in the polymer (23). Because diffusivities for the experimental compounds could not be found in the literature, the relationship between diffusivity and mean molecular diameter was examined. A plot of log D versus mean molecular diameter was constructed by using diffusivities for a variety of gases and volatile organic compounds in LDPE at 20–25 °C gathered from the literature and this work. Mean molecular diameter, d (nm), was calculated by the formula

$$d = (V_M/N)^{1/3} \quad (7)$$

where V_M is the molar volume (nm³ mol⁻¹) and N is Avogrado's number. For the gases, V_M was calculated from the density of the condensed vapor at the boiling temperature; the densities of the organic liquids at 20 °C were obtained from Weast (28).

The plot of log D versus mean molecular diameter for LDPE (Figure 4) resembles plots for rigid poly(vinyl chloride), poly(methyl methacrylate), and polystyrene obtained by Berens and Hopfenberg (32). It is evident from Figure 4 that diffusivity tends to decrease as mean molecular diameter increases. The C_5–C_{18} n-alkanes have
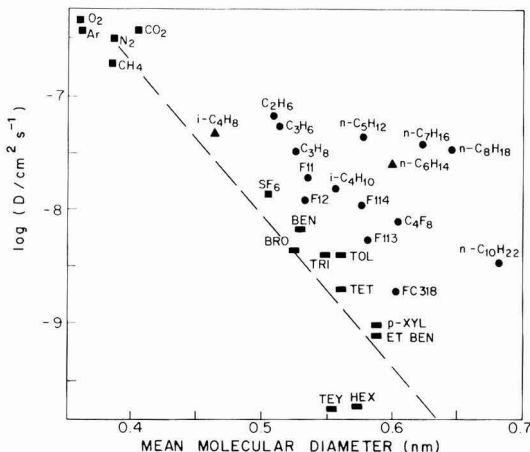
Figure 4. Logarithm of D (cm^2 s^{-1}) versus mean molecular diameter (nm). The diffusivities for various compounds in LDPE at 20–25 °C were taken from ref 27 (●), ref 33 (■), ref 24 (▲), and this work (▬); mean molecular diameters were calculated by eq 7. The broken line represents the (subjective) trend for the more isometric molecules.

diffusivities 1–2 orders of magnitude higher than those of the more isometric molecules of similar mean molecular diameter, because elongated molecules diffuse in an oriented fashion (23, 32). The experimental diffusivities are lower than, but usually within $^1/_2$ order of magnitude of, the literature values for compounds of similar molecular size and shape. It is not obvious why the experimental values are lower. Absorption of water by the polymer and nonplanar geometry would cause the values to be higher. The most likely explanation is mass-transfer resistance in the aqueous phase resulting from insufficient stirring of the solutions. If this is correct, better agreement would be expected for the polymers having lower sorption rates.

Effect of Temperature on Sorption Rate.

It was observed that the log (K^2D) values for LDPE at 22 °C were 0.4–0.8 unit (2.5–6×) higher than those at 10 °C. The temperature dependence of K^2D can be estimated from literature data for the temperature dependences of K and D. Over small temperature ranges, the temperature dependence of D can be represented by the Arrhenius-type relation, $D = D_0 \exp(-E_D/RT)$, where E_D is the apparent activation energy for diffusion (kJ mol^{-1}), T is the absolute temperature (K), and R is the gas constant (0.0083 kJ K^{-1} mol^{-1}). According to eq 6, the temperature dependence of K can be expressed as the product of two exponentials, one for K_S and one for K_H. For K_S the expression is $K_S = K_{S0} \exp(-\Delta H_S/RT)$, where $\Delta H_S = \Delta H_C + \Delta H_{M1}$ (kJ mol^{-1}), ΔH_S is the heat of solution in LDPE, ΔH_C is the heat of condensation, and ΔH_{M1} is the partial molar heat of mixing in LDPE. The expression for K_H is analogous: $K_H = K_{H0} \exp(\Delta H_H/RT)$, where $\Delta H_H = \Delta H_C + \Delta H_{M2}$ (kJ mol^{-1}), ΔH_H is the heat of solution in water, ΔH_C is the heat of condensation, and ΔH_{M2} is the partial molar heat of mixing in water. For condensable organic vapors, ΔH_S and ΔH_H will probably be dominated by ΔH_C. It is therefore assumed that $\Delta H_S + \Delta H_H$ is small in relation to E_D. This fact was verified for Freon 11 (CCl$_3$F) with data from Horacek (27) and Hunter-Smith et al. (34). The activation energy for K^2D is thus approximated by E_D. For the C_5–C_8 n-alkanes and several Freons, E_D ranges from 42 to 84 kJ mol^{-1} (32). This converts to log (K^2D) differences of 0.3–0.6, which is deemed satisfactory agreement with experimental results, because this estimate rests on largely untested assumptions.

Conclusions

The results of the sorption experiments indicate that borosilicate glass is the least likely of the 10 materials tested to elicit sampling artifacts. The results also demonstrate that unprotected metal surfaces have the potential to cause negative sampling bias for polyhalogenated hydrocarbons. The available evidence points toward transformation reactions, but this is not regarded as proven. Stainless steel is less apt to cause sampling bias than either aluminum or galvanized steel. The loss rates observed for stainless steel are lower than those which could cause significant bias in normal monitoring situations. Glass is less durable and stainless steel is heavier and more costly than most organic polymers, however.

All of the polymers tested absorbed halocarbons, but at very different rates. This divergence is most likely related to the diffusivities of the compounds in the polymers. For example, isometric molecules having mean molecular diameters between 0.5 and 0.6 nm have diffusivities between 10^{-16} and 10^{-18} cm^2 s^{-1} in RPVC (32), whereas for LDPE, the diffusivities are 10^{-8}–10^{-9} cm^2 s^{-1} (ref 27 and this work). Our study indicates that flexible polymers are likely to have higher sorption rates than rigid polymers. The apparent relationship between rigidity and diffusivity can be understood by considering that the magnitude of the diffusivity is governed by the energy required to displace the polymer chains sufficiently to enable passage of the diffusant molecules (23). On the basis of the sorption experiments, RPVC would be prefered to PTFE for sampling low activities of halogenated hydrocarbons. However, the magnitudes of the differences in sorption rates may not be accurately reflected by the data in Table II, because the rates were near the lowest that could be determined by the methods employed.

The effective use of sampling equipment constructed from synthetic polymers to monitor organic contaminants in groundwater requires that sorption be minimized. A potentially useful strategy would be to estimate the magnitude of sorption by employing the appropriate sorption constants in a mathematical model based on Fick's laws for the appropriate geometry and boundary constraints. For instance, the model that was used in this paper to quantify K^2D can also be used to estimate the negative bias due to sorption in a stagnant monitoring well (16). The positive bias resulting from the transport of organic contaminants through the wall of a polymer transfer-line tube can be estimated with the model that was used by Holm et al. (35) to predict the invasion of oxygen into sampled groundwater. A model for estimating the negative bias due to sorption in a polymer transfer-line tube could be developed from the principles outlined in Crank (22) and Carslaw and Jaeger (36). This approach requires that reasonably accurate values of the sorption constants can be obtained.

The diffusivities and polymer–water partition coefficients for LDPE were obtained by monitoring the concentrations of the test compounds in a dilute water solution that was exposed to the polymer. These data were compared with diffusivities and Henry's law solubility coefficients taken from the literature. The literature data were obtained by monitoring the pressure change or weight gained by LDPE exposed to a low-pressure vapor of the test compound in the absence of water. The comparison involved certain assumptions, and the degree of consistency found suggests that the assumptions are essentially valid. It appears that water does not substantially alter the diffusivities and Henry's law solubilities of nonpolar organic contaminants in hydrophobic polymers like LDPE.

Diffusivities and solubilities are available for many polymers and compounds of interest from the standpoint of monitoring. When data for particular compounds cannot be found in the literature, empirical relationships like those used here or described elsewhere (23, 37) can be used to estimate the constants from the available data. Our results also indicate that sorption rates are sensitive to temperature, but not to concentration at the low activities employed in the sorption experiments.

The foregoing conclusions are pertinent for low activities of organic contaminants in the environment. At higher activities, as might be encounted near a solvent spill, other problems arise. A polymer that is exposed to high activities of an organic compound that is a good solvent for the polymer, will absorb large quantities of the compound. This was observed in the SEM experiments for BRO in RPVC. The swelling power of various solvents for a given polymer is usually highly variable. For example, RPVC can absorb more than 800% of its weight of methylene chloride, but only 1% of carbon tetrachloride (38). Polymers that have absorbed much solvent are weakened and they represent a potentially strong source of contamination. It is also more difficult to estimate sorption rates at high activities, because they are then often strongly dependent on concentration (23, 24). We observed that the diffusivities of several halocarbons in LDPE were ~1 order of magnitude higher at an activity of 1 than at activities near zero. A much larger difference would be expected for RPVC. Berens (38) found that when RPVC was immersed in various swelling solvents, the rate of approach to equilibrium was several orders of magnitude higher than predicted from the Fickian diffusivities at low activity; solvent transport was Fickian up to activities of 0.25. Parallel studies by Vonk and associates (39–41) indicated that the threshold for the onset of non-Fickian behavior is 0.25 for monoaromatic hydrocarbons and 0.1 for halogenated hydrocarbons. Because it is considerably less subject to swelling by organic solvents, PTFE would be preferred for groundwater monitoring applications when moderately high activities of organic contaminants are anticipated.

Acknowledgments

We wish to thank Hans Kamler and Stephanie O'Hannesin for experimental assistance and James Barker, Robert Huang, Janusz Pawliszyn, and Alfred Rudin for reviewing the manuscript.

Registry No. TRI, 71-55-6; TET, 79-34-5; HEX, 67-72-1; BRO, 75-25-2; TEY, 127-18-4; PVC, 9002-86-2; PTFE, 9002-84-0; NYL, 32131-17-2; PE, 9002-88-4; PP, 9003-07-0; AISI 316, 11107-04-3; Al, 7429-90-5; H_2O, 7732-18-5.

Literature Cited

(1) Barcelona, M. J.; Helfrich, J. A.; Garske, E. E.; Gibb, J. P. *Ground Water Monit. Rev.* **1984**, Spring, 32–41.
(2) Barker, J. F.; Dickhout, R. *Ground Water Monit. Rev.* **1988**, Fall, 112–120.
(3) Barker, J. F.; Patrick, G. C.; Lemon, L.; Travis, G. M. *Ground Water Monit. Rev.* **1987**, Spring, 48–54.
(4) Ho, J. S.-Y. *J.—Am. Water Works Assoc.* **1983**, Nov, 583–586.
(5) Miller, G. D. Uptake and release of lead, chromium and trace level volatile organics exposed to synthetic well casings. In *Proceedings Second Annual Symposium on Aquifer Restoration and Ground Water Monitoring*; National Well Water Assoc.: Worthington, OH, 1982; pp 236–245.
(6) Sykes, A. L.; McAllister, R. A.; Homolya, J. B. *Ground Water Monit. Rev.* **1986**, Fall, 44–47.
(7) Sharom, M. S.; Salomon, K. R. *J. Fish. Aquat. Sci.* **1981**, *38*, 199–204.
(8) Pearsall, K. A.; Eckhardt, A. V. *Ground Water Monit. Rev.* **1987**, Spring, 64–73.
(9) Barcelona, M. J.; Helfrich, J. A.; Garske, E. E. *Anal. Chem.* **1985**, *57*, 460–464.
(10) Barcelona, M. J.; Helfrich, J. A. *Environ. Sci. Technol.* **1986**, *20*, 1179–1184.
(11) Junk, G. A.; Svec, H. J.; Vick, R. D.; Avery, M. J. *Environ. Sci. Technol.* **1974**, *8*, 1100–1106.
(12) Curran, C. M.; Tomson, M. B. *Ground Water Monit. Rev.* **1983**, Summer, 68–71.
(13) Reynolds, G. W. Sorption of chlorinated organics by materials used for groundwater monitoring wells. M.Sc. Project Report, Dept. of Earth Sciences, Univ. of Waterloo, 1985.
(14) Reynolds, G. W.; Gillham, R. W. Absorption of halogenated organic compounds by polymer materials commonly used in ground water monitors. In Proceedings Second Canadian/American Conference on Hydrogeology, Hazardous Wastes in Ground Water: A Soluble Dilemma, Banff, AB, National Well Water Assoc., June 25–29, 1985; pp 125–132.
(15) Gillham, R. W.; O'Hannesin, S. F.; Barker, J. F. Sorption/desorption of soluble constituents of petroleum products by materials used in construction of monitoring wells. American Petroleum Institute Report 4469, Washington, DC, 1988.
(16) Gillham, R. W.; O'Hannesin, S. F. Sorption of aromatic hydrocarbons by materials used in construction of groundwater monitoring wells. ASTM Symposium: Standard Development for Ground Water and Vadose Zone Monitoring Investigations, Albuquerque, NM, Jan 27–29, 1988.
(17) Glaze, W. H.; Lin, C.-C.; Burleson, J. L.; Henderson, J. E.; Mapel, D.; Rawley, R.; Scott, D. R. Optimization of liquid–liquid extraction methods for analysis of organics in water. Project Report, Contract Nos. CR-895472, CR-808562, USEPA/EMSL, Cincinnati, OH, 1983.
(18) Price, F. P.; Gilmore, P. T.; Thomas, E. L.; Laurence, R. L. *J. Polym. Science, Polym. Symp.* **1978**, *63*, 33–44.
(19) Sullivan, K. F.; Atlas, E. L.; Giam, C.-S. *Anal. Chem.* **1981**, *53*, 1718–1719.
(20) Vogel, T. M.; Criddle, C. S.; McCarty, P. L. *Environ. Sci. Technol.* **1987**, *21*, 722–736.
(21) Conover, W. J. *Practical Nonparametric Statistics*, 2nd ed.; John Wiley and Sons: New York, 1980.
(22) Crank, J. *Mathematics of Diffusion*, 2nd ed.; Clarendon: Oxford, UK, 1975.
(23) Rogers, C. E. In *Polymer Permeability*; Comyn, J., Ed.; Elsevier: New York, 1984; Chapter 2.
(24) Rogers, C. E.; Stannett, V.; Szwarc, M. *J. Polym. Science* **1960**, *45*, 61–82.
(25) Windle, A. H. In *Polymer Permeability*; Comyn, J., Ed.; Elsevier: New York, 1984; Chapter 3.
(26) Carman, P. C.; Haul, R. A. W. *Proc. R. Soc. London, Ser. A* **1954**, *222*, 109–118.
(27) Horacek, H. *Die Makromol. Chem.* **1975**, Suppl. 1, 415–439.
(28) Weast, R. C. *Handbook of Chemistry and Physics*, 69th ed.; CRC Press: Boca Raton, FL, 1988.
(29) Dean, J. A. *Lange's Handbook of Chemistry*, 13th ed.; McGraw-Hill: New York, 1985.
(30) Mackay, D.; Shiu, W. Y. *J. Chem. Phys. Ref. Data* **1981**, *10*, 1175–1199.
(31) Pankow, J. F. *Anal. Chem.* **1986**, *58*, 1822–1826.
(32) Berens, A. R.; Hopfenberg, H. B. *J. Membr. Sci.* **1982**, *10*, 283–303.
(33) Michaels, A. S.; Bixler, H. J. *J. Polym. Sci.* **1961**, *50*, 413–439.
(34) Hunter-Smith, R. J.; Balls, P. W.; Liss, P. S. *Tellus* **1983**, *35B*, 170–176.
(35) Holm, T. R.; George, G. K.; Barcelona, M. J. *Ground Water Monit. Rev.* **1988**, Spring, 83–89.
(36) Carslaw, H. S.; Jaeger, J. C. *Conduction of Heat in Solids*; Clarendon: Oxford, UK, 1959.
(37) van Krevelen, D. W.; Hoftyzer, P. J. *Properties of Polymers*, 2nd ed.; Elsevier Press: New York, 1976.

(38) Berens, A. R. *J.—Am. Water Works Assoc.* **1985**, Nov, 57–64.

(39) Vonk, M. W.; Veenendaal, G. *Water Supply* **1983**, *2*, 61–69.

(40) Vonk, M. W. Permeation of organic compounds through pipe materials. Report No. 85, KIWA, Nieuwegein, The Netherlands, (in Dutch), 1985.

(41) Veenendaal, G.; Verheijen, L. A. H. M.; Vonk, M. W. Effects of soil contaminants and piping materials on drinking water quality. Report No. 86, KIWA, Nieuwegein, The Netherlands, 1985.

COMMUNICATIONS

Residual Petroleum and Polychlorobiphenyl Oils as Sorptive Phases for Organic Contaminants in Soils

Stephen A. Boyd* and Shaobai Sun

Department of Crop and Soil Sciences, Michigan State University, East Lansing, Michigan 48824

Introduction

The organic matter fraction of soils and sediments controls the sorptive uptake of nonionic organic contaminants (NOCs) and pesticides from water (*1–3*). Mechanistically, natural organic matter appears to function as a partition medium for the dissolution of NOCs (*1, 2*). The uptake of NOCs by soils and sediments can be described by a simple linear equation of the form $x/m = KC$, where x/m is the solute concentration in soil, C is the equilibrium solute concentration in water, and K is the sorption coefficient. K can be normalized for the fractional organic matter content of soil (f_{om}) to define a new constant $K_{om} = K/f_{om}$. It has been demonstrated that K_{om} values obtained for a compound on different soils converge to a relatively constant value such that K_{om} becomes a unique constant characteristic of the compound (*4*). The relative invariance of the soil K_{om} value demonstrates that the organic matter fraction controls uptake of NOCs by soils, and that organic matter from different soils behaves similarly as a partition medium for NOCs.

The established relationship between organic matter content and sorption of NOCs has greatly simplified the predictions of sorption of NOCs by soils and sediments. Once K_{om} is known for a compound, the K value on any soil or sediment can be estimated simply by knowing f_{om}. Fate and transport models now routinely use K_{om} values to assess the leaching potential of organic contaminants and pesticides.

In this study, the role of residual petroleum and polychlorobiphenyl (PCB) oils as sorptive phases for organic contaminants in soils was evaluated and compared to that of natural soil organic matter. The soil–water distribution coefficients of pentachlorophenol (PCP), toluene, and 2-chlorobiphenyl in actual field soils contaminated with such anthropogenic organic phases are presented here. The results show that both natural organic matter and residual oil components of these soils act as partition media for organic solutes, with the latter being ~10 times more effective as a sorptive phase.

Materials and Methods

Soils. Three soils and a soil particle-size fraction were used in the study. Two soils, designated MG and UP, are from actual wood-preserving sites in Minnesota and Michigan, respectively, and are contaminated with pentachlorophenol. The MG silt + clay sample was obtained by allowing the sand-sized particles to settle out of an aqueous soil slurry. The soil denoted PP is contaminated with Aroclor 1254 as a result of a transformer spill at a Minnesota power plant. The Capac soil is an uncontaminated subsurface soil with a high clay content.

Soil Properties. Pentachlorophenol was extracted with methylene chloride and analyzed as described previously (*5*). The PCB content was measured as described previously (*6*). Oil and grease content was determined by mixing 20 g of soil, acidified to pH 2 with HCl, and 10 g of $MgSO_4$. The sample was extracted with 200 mL of 1,1,2-trichlorotrifluoroethane in a Soxhlet for 20 h. The extract was back-extracted with 0.1 M KCO_3 (pH 12) to remove PCP and then evaporated. The oil and grease remaining was determined gravimetrically. A 1:2 soil–water mixture was used for pH determination. Organic carbon was determined by measuring CO_2 released from combustion; analysis was by Huffman Laboratories, Inc., Golden, CO. The sample was previously extracted with methylene chloride to remove PCP or PCBs and oil/grease. Organic carbon (OC) × 1.74 equals organic matter (OM). Particle-size analysis was by the Michigan State University Soil Testing Laboratory.

Sorption Isotherms. The MG, MG silt + clay, PP, and UP isotherms were obtained by using [ring-^{14}C]PCP, -toluene, or -2-chlorobiphenyl (from Sigma) and the concentrations plotted are for the ^{14}C compound. The Capac isotherm (data not shown) was obtained by adding 5 μL of a [^{14}C]PCP–methanol solution and different volumes of aqueous nonlabeled PCP to soil. Standard batch equilibration isotherms were obtained by mixing from 2 to 10 g of soil, 20 mL of distilled H_2O, and various amounts of PCP, toluene, or 2-chlorobiphenyl in screw-top glass centrifuge tubes that were closed with aluminum foil lined caps. After 24 h, aqueous-phase concentrations were measured by liquid scintillation counting.

Results and Discussion

In studies of PCP sorption by PCP-contaminated soils from former wood-preserving sites we observed that the measured PCP distribution coefficients were much higher

Table I. Soil Properties

property	MG	MG silt + clay	UP	PP	Capac Bt
PCP, ppm	740	2470	624	0	0
organic matter, %					
OC	1.81	12.51	0.29	1.25	0.40
OM	3.15	21.79	0.51	2.18	0.70
oil/grease, %	0.97	7.6	0.24	0	0
PCB, %	0	0	0	0.73	0
pH	7.581	7.353	5.617	8.75	6.668
particle size, %					
sand (0.05–2.0 mm)	90.3	0.7	96.8	47	25
silt (0.002–0.05 mm)	4.9	33.4	2.5	45	45
clay (<0.002 mm)	4.8	65.9	0.7	8	30

than the values predicted in the conventional manner from the K_{om} of PCP and the soil organic matter content. Pentachlorophenol-contaminated soils are numerous, with over 500 sites in the United States alone (7), and these soils typically contain residual petroleum that was used as a carrier for PCP. Many contaminated soils and sediments contain residual oil/grease due to the widespread transport, use, and disposal of petroleum products. Terrestrial petroleum pollution has been estimated at 1.7–8.8 million metric tons per annum (8). Although petroleum biodegradation does occur, it is often far from quantitative, leaving a residual petroleum component (8).

For the sorption of organic contaminants by soils containing residual petroleum, we hypothesized that these soils may be treated as a three-component system consisting of (1) an inert mineral phase, (2) a sorptive natural soil organic matter phase, and (3) a highly sorptive residual petroleum phase. The potential effectiveness of the two sorptive phases can be evaluated by comparing the soil organic matter partition coefficient, K_{om}, to the oil–water partition coefficient, K_{oil}. The K_{oil} should be approximately equal to K_{ow} because both octanol and oil are bulk-phase hydrocarbon media. Comparing K_{om} (18885) and K_{oil} (K_{ow} = 173 780) (9) for PCP suggests that the oil phase could be as much as 10 times more effective than soil organic matter as a partition medium for organic contaminants.

To test this hypothesis, three soils and a soil particle-size fraction were evaluated for the sorption of PCP (Table I). Each sample was analyzed for PCP concentration, natural organic matter content, oil/grease content, pH, and particle size distribution. Table I shows that the MG and UP soils each have high PCP contamination and a significant oil/grease component. The MG silt + clay sample shows that the oil/grease component, and PCP, are associated primarily with the silt and clay fraction. The pristine Capac soil has no PCP contamination and no oil/grease component.

For the soils shown in Table I that have an oil/grease component, the predicted PCP sorption coefficient, K, was expressed as

$$K = f_{om}K_{om} + f_{oil}K_{oil} \qquad (1)$$

where both natural organic matter and the oil/grease component are acting as sorptive phases for PCP as defined by the K_{om} and K_{oil} values. For a partially ionized compound like PCP, the actual overall distribution coefficient, D, can be estimated at any soil pH by using the equation $D = KQ$, where K is the sorption coefficient of the nonionized PCP (pK_a = 4.75), and Q is the fraction of the PCP present in the nonionized form (9). By use of this approach, D values (Table II) were predicted for each soil from the pK_a, K_{om}, and K_{ow} values of PCP and the measured soil organic matter content, oil/grease content, and pH (Table I).

Table II. Measured and Predicted Soil–Water Distribution Coefficients of Pentachlorophenol, Toluene, and 2-Chlorobiphenyl in Soils Containing Residual Petroleum or PCB Oils

soil	compd	distrib coeff	
		measd	pred[a]
MG	PCP	5.79	3.36
MG silt + clay	PCP	42.88	43.09
UP	PCP	72.84	61.29
Capac	PCP	1.60	1.52
MG	toluene	5.52	7.5
PP	toluene	5.66	5.47
PP	2-chlorobiphenyl	702	273

[a] Predicted value from eq 1 assuming $K_{oil} = K_{ow}$. Values of K_{om} and K_{ow} are from ref 4 and 9.
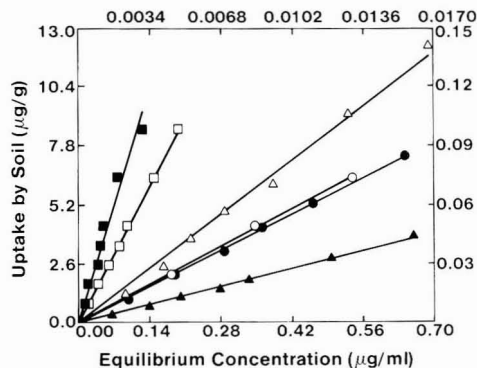

Figure 1. Sorption isotherms of pentachlorophenol (PCP) on the UP soil (■), MG silt + clay (□), and MG soil (▲); 2-chlorobiphenyl on the PP soil (△) and MG soil (●); and toluene on the PP soil (O) and MG soil (●) samples. The left and bottom scales are for PCP, the right and upper scales for toluene, and the left and upper scales for 2-chlorobiphenyl.

To substantiate that the residual petroleum (oil/grease) component was acting as a sorptive phase for PCP, PCP sorption isotherms were measured by using the contaminated soils and, for comparison, the uncontaminated Capac soil. The sorption isotherms shown in Figure 1 for the contaminated soils were obtained by adding [^{14}C]PCP at various concentrations to soil–water mixtures and then measuring [^{14}C]PCP in the aqueous phase at equilibrium. The sorption isotherms obtained were highly linear for all samples (Figure 1), as observed previously for chlorophenol sorption by soils and sediments (9, 10). Because the PCP sorption isotherms are linear, the measured distribution of [^{14}C]PCP represents the overall PCP distribution in the contaminated soils. The experimentally determined values of D are given in Table II, which shows excellent agreement in all cases between the predicted and measured distribution coefficients. For the Capac soil, where no oil phase is present, only natural organic matter is functioning as a sorptive phase for PCP and the distribution coefficient is accurately predicted from the soil organic matter content. For the contaminated soils, consideration of both the oil/grease and soil organic matter components is required to accurately predict the PCP distribution coefficients. The similarity of the measured D values to those predicted by using $K_{oil} = K_{ow}$ shows that the oil/grease component was approximately 10 times more effective than natural organic matter as a sorptive phase for PCP. Similar results were obtained for the sorption of toluene by the MG soil (Figure 1 and Table II). Thus, these results are directly applicable to other organic contaminants (e.g., benzene, toluene, and xylene) found in soils and sediments

where residual petroleum is present.

The sorptive behavior of residual PCB oil (commercial Aroclor) in a PCB-contaminated soil was also evaluated by using the soil denoted PP (Table I). To obtain the predicted K values, the PCB oil–water partition coefficient was again estimated as being approximately equal to K_{ow} (Table II). This assumption appears valid for toluene where the measured sorption coefficient (Table II), obtained from the slope of the linear isotherm (Figure 1), was in excellent agreement with the predicted value. However, for 2-chlorobiphenyl, use of K_{ow} to approximate the PCB oil–water partition coefficient underestimated the observed K (Figure 1 and Table II). The measured K value for 2-chlorobiphenyl corresponds to a log K_{oil} value of ~5 (log K_{ow} = 4.51) and this is entirely reasonable because 2-chlorobiphenyl would be expected to form a more nearly ideal solution in PCB oil than in octanol, making K_{oil} > K_{ow}. In fact, a plot of log K_{ow} versus water solubility for various organic compounds shows that 2-chlorobiphenyl falls below the ideal line by ~0.7 log unit (*11*). Thus, the sorptive behavior of residual PCB oils appears similar in nature to that of residual petroleum. However, in the case of sorption of individual PCB congeners by residual PCB oils, nearly ideal solution behavior is observed and K_{oil} will be greater than K_{ow}; the magnitude of this difference will increase for the more heavily chlorinated PCB congeners (*11*). The resulting effect of residual PCB oils on the soil–water distribution coefficient is dramatic; the K value predicted in the conventional manner, where only soil organic matter is acting as a sorptive phase, is ~37, whereas the observed value is 702.

These results demonstrate that residual petroleum and PCB oils present in soil act as highly effective partition media for organic contaminants. The presence of these highly sorptive anthropogenic organic phases in soils and sediments will significantly increase the immobilization of organic contaminants and thus strongly influence their environmental fate and behavior. The observed soil–water distribution coefficients of organic contaminants were accurately predicted from the soil organic matter content, the oil content (expressed as oil/grease or PCB content), and the solute K_{om} and K_{ow} values. The magnitude of the oil–water partition coefficient makes the residual oil phase a significant sink for organic contaminants in these systems. For accurate prediction of soil–water distribution coefficients in such soils and sediments, the oil compo-

nents, along with the natural organic matter component, must be measured and accounted for individually. The limited effectiveness of soil washing and pump and treat technologies (*12, 13*) for remediating soils contaminated by petroleum spills and PCBs may be related in part to the sorptive behavior of residual oil components as described here.

Literature Cited

(1) Chiou, C. T.; Peters, L. J.; Freed, V. H. *Science* **1979**, *206*, 831–832.
(2) Chiou, C. T.; Porter, P. E.; Schmedding, D. W. *Environ. Sci. Technol.* **1983**, *17*, 227–231.
(3) Karickhoff, S. W.; Brown, D. S.; Scott, T. A. *Water Res.* **1979**, *13*, 241–248.
(4) Chiou, C. T. In *Reactions and Movement of Organic Chemicals in Soils*; Sawhney, B. L., Brown, K., Eds.; Special Publication No. 22; Soil Science Society of America: Madison, WI, 1989; pp 1–29.
(5) Mikesell, M. D.; Boyd, S. A. *Environ. Sci. Technol.* **1988**, *22*, 1411–1414.
(6) Quensen, J. F., III; Tiedje, J. M.; Boyd, S. A. *Science* **1988**, *242*, 752–754.
(7) Cirelli, D. P. In *Pentachlorophenol: Chemistry, Pharmacology and Environmental Toxicology*; Rao, K. R., Ed.; Plenum: New York, 1978; pp 13–18.
(8) Bartha, R. *Microb. Ecol.* **1986**, *12*, 155–172.
(9) Schellenberg, K.; Leuenberger, C.; Schwarzenbach, R. P. *Environ. Sci. Technol.* **1984**, *18*, 652–657.
(10) Lagas, P. *Chemosphere* **1988**, *17*, 205–216.
(11) Chiou, C. T.; Schmedding, D. W. *Environ. Sci. Technol.* **1982**, *16*, 4–10.
(12) Mackay, D. M.; Cherry, J. A. *Environ. Sci. Technol.* **1989**, *23*, 630–636.
(13) Bouchard, D. C.; Enfield, C. G.; Piwoni, M. D. In *Reactions and Movement of Organic Chemicals in Soils*; Sawhney, B. L., Brown, K., Eds.; Special Publication No. 22; Soil Science Society of America: Madison, WI, 1989; pp 349–371.

Ambient Formic Acid in Southern California Air: A Comparison of Two Methods, Fourier Transform Infrared Spectroscopy and Alkaline Trap–Liquid Chromatography with UV Detection

Daniel Grosjean,[*,†] **Ernesto C. Tuazon,**[‡] **and Eric Fujita**[§]

DGA, Inc., 4526 Telephone Road, Suite 205, Ventura, California 93003, Statewide Air Pollution Research Center, University of California, Riverside, California 92521, and Research Division, California Air Resources Board, P.O. Box 2815, Sacramento, California 95812

Introduction

Formic acid is an ubiquitous component of urban smog. Sources of formic acid in urban air include direct emissions from vehicles (*1*) and in situ reaction of ozone with olefins (*2*). Ambient levels of formic acid in southern California air were first measured some 15 years ago by Hanst et al.

(*3*) using long-path Fourier transform infrared spectroscopy (FTIR). All subsequent studies of formic acid in the Los Angeles area have involved the use of two methods, either FTIR (*4–6*) or collection on alkaline traps followed by gas chromatography (*1*), ion chromatography (*7*), or liquid chromatography analysis with UV detection, ATLC–UV (*2, 8*).

The Carbon Species Methods Comparison Study (CSMCS), a multilaboratory air quality study carried out in August 1986 at a southern California smog receptor site

[†] DGA, Inc.
[‡] University of California.
[§] California Air Resources Board.

Table I. Regression Parameters[a]

	all data	excluding 8/15, 0–8 a.m. outlier
no. of observations	39	38
degrees of freedom	37	36
slope ± SE	0.95 ± 0.15	1.07 ± 0.13
intercept ± SE	0.10 ± 1.68	−0.59 ± 1.42
$\bar{X} - \bar{Y}$, mean ± 1 SD	0.13 ± 1.64	0.28 ± 1.39
R^2	0.512	0.645

[a] Y, alkaline trap method; X, FTIR method; units, ppb.

(9), provided an opportunity for direct field comparison of the FTIR and alkaline trap methods. The results of the comparison are presented in this brief report. To our knowledge, no interlaboratory comparison of ambient formic acid measurements involving entirely different sampling *and* analytical methods has been carried out prior to this work. Results of a comparison of sampling methods for ambient formic acid (all participants employed the same analytical method, i.e., standard ion chromatography) have been recently reported (10).

Measurement Methods

Only a brief description of the methods employed is given below. More detailed accounts can be found elsewhere (2, 11).

All measurements were carried out on August 12–21, 1986, in Glendora, CA, 35 km east of Los Angeles, on the Citrus College campus. The alkaline trap sampling units were located on a platform and sampled air 2.5 m above the ground. The FTIR instrument employed on open 25 m base-path multiple-reflection optical system, whose optical axis was also 2.5 m above the ground, parallel to and ~15 m upwind of the platform. The FTIR spectra were recorded at a total path length of 1150 m and a resolution of 0.13 cm^{-1}. Formic acid was measured by its absorption at 1105.0 cm^{-1} after correcting for the interference by a weak absorption band of water.

The FTIR calibration was essentially a determination of the 1105-cm^{-1} absorptivity at the actual resolution of the spectrometer. This calibration, which obeyed Beer–Lambert's law, was carried out in the laboratory with ppm concentrations of HCOOH monomer generated in a 5870-L evacuable chamber equipped with long-path optics (11). At the resolution and path length employed, the detection limit was 1 ppb and the estimated precision was 1.5 ppb.

Alkaline traps consisted of KOH-impregnated 47 mm diameter glass fiber filters mounted downstream of 1.2 μm pore size Teflon filters in open-face dual-filter holders and connected to a calibrated flow meter and a sampling pump. The sampling flow rate was 14 L/min. After sampling, the filters were promptly placed in glass vials capped with Teflon-lined screw caps and containing 10 mL of deionized water and 40 μL of chloroform added as a biocide. Following filter sonication for 10 min in their individual glass vials, aqueous extracts were analyzed by liquid chromatography with a size exclusion column, dilute H_2SO_4 eluent, and ultraviolet detection as is described elsewhere (2). Calibration involved the use of external standards, i.e., aqueous solutions of formate whose concentrations bracketed those relevant to the ambient air samples. Calibration plots (peak height vs concentration) were linear with near-zero intercepts, relative standard deviations on the slope of ±5%, and correlation coefficients of ≥0.99. Collection efficiency was verified with two alkaline filters in series and was 0.89 ± 0.07 for 18 field samples. The detection limit was 0.29 ppb (4-h samples) and 0.15 ppb (8-h samples) and the estimated precision was ±1 ppb for
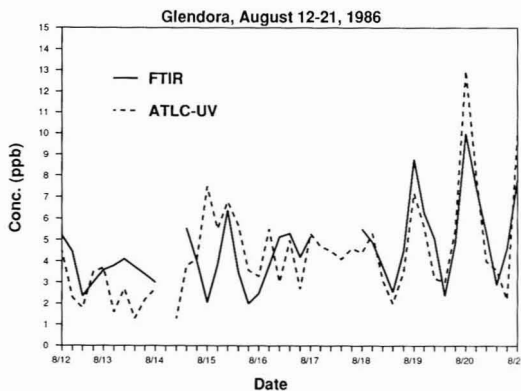

Figure 1. Ambient levels of formic acid, Glendora, CA, August 12–21, 1986, measured by the FTIR and ATLC–UV methods.

HCOOH of ≤5 ppb and ±15% for HCOOH of >5 ppb.

Results and Discussion

The comparison was carried out in a "blind" mode, with both groups reporting their respective results to the California Air Resources Board without prior knowledge of each other's data.

The alkaline trap samples were collected according to a CMSCS-prescribed schedule of five consecutive samples per day, one 8-h sample starting at midnight and four 4-h samples thereafter. FTIR data points, each corresponding to a measurement time of 5 min and initially reported every ~15–20 min and as hourly averages (11), were averaged here over time periods corresponding to those of the 44 alkaline trap samples. Of these, five were excluded due to insufficient FTIR data, yielding 39 FTIR averages.

Time series of ambient formic acid measured by FTIR and by the alkaline trap–liquid chromatography method are plotted together in Figure 1, which indicates reasonable agreement with respect to both ambient concentrations and diurnal variations.

Regression parameters are given in Table I for the entire data set, with and without the single outlier observation of August 15, 0:00–8:00 PDT. There is no significant bias, and the mean difference between the two methods is comparable to the stated precision of the measurements.

Our study, although limited, encompassed a range of conditions (temperature, humidity, levels of copollutants such as ozone, aldehydes, nitric acid, peroxyacetyl nitrate, etc.; see ref 2 for details) that are representative of summertime air quality in southern California. The reasonable agreement between the two methods lends additional confidence in the reliability of formic acid data obtained by both FTIR and ATLC–UV during CSMCS, as well as in data from earlier studies, all involving either FTIR or alkaline trap methods, of ambient levels of formic acid in southern California.

Acknowledgments

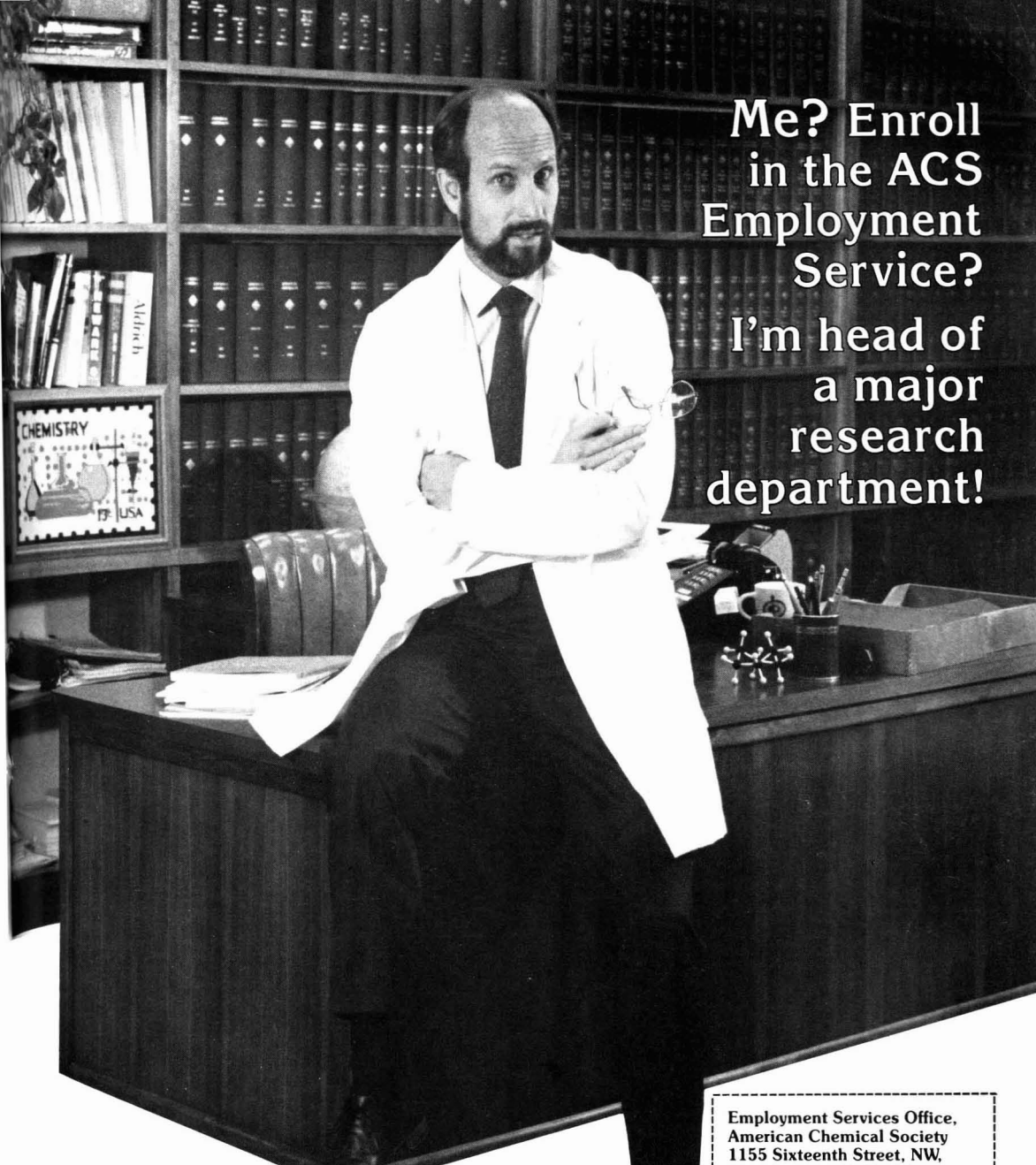We thank D. R. Lawson (ARB) and the CSMCS participants for their support.

Literature Cited

(1) Kawamura, K.; Ng, L. L.; Kaplan, I. R. *Environ. Sci. Technol.* **1985**, *19*, 1082.

(2) Grosjean, D.; Williams, E.; Van Neste, A. Measurements of organic acids in the South Coast Air Basin. Final report to the California Air Resources Board, Agreement A5-177-32, DGA, Inc., Ventura, CA, 1988.

(3) Hanst, P. L.; Wilson, W. E.; Patterson, R. K.; Gay, B. W.; Chaney, L. W.; Burton, C. S. A spectroscopic study of California smog. U.S. EPA report, EPA 650/4-75-006; Research Triangle Park, NC, 1975.

(4) Tuazon, E. C.; Winer, A. M.; Graham, R. A.; Pitts, J. N., Jr. *Adv. Environ. Sci. Technol.* **1980**, *10*, 259.

(5) Tuazon, E. C.; Winer, A. M.; Pitts, J. N., Jr. *Environ. Sci. Technol.* **1981**, *15*, 1232.

(6) Hanst, P. L.; Wong, N. W.; Bragin, J. *Atmos. Environ.* **1982**, *16*, 969.

(7) Grosjean, D. *Atmos. Environ.* **1988**, *22*, 1637.

(8) Grosjean, D. Measurements of low molecular weight carboxylic acids during the Southern California Air Quality Study. Final report to the Coordinating Research Council, Project CRC-SCAQS-2, DGA, Inc. Ventura, CA., 1988.

(9) Lawson, D. R.; Hering, S. V. *Aerosol Sci. Technol.*, in press.

(10) Keene, W. C.; et al. *J. Geophys. Res.* **1989**, *94*, 6457.

(11) Tuazon, E. C. Derivation of formic acid data from FTIR spectra recorded during the 1986 Carbonaceous Species Methods Comparison Study. Final report to the California Air Resources Board, Contract A733-167, U. of California, Riverside, CA, 1989.

Me? Enroll in the ACS Employment Service? **I'm head of a major research department!**

Even for the successful chemist or scientist in an allied field, sometimes the best way to get ahead is to make a change.

The ACS Employment Service offers the opportunity to investigate the possibilities discreetly – and at very low cost.

Our Employment Service is free to all ACS members. If you request confidentiality from current employers or other designated organizations there is a nominal charge.

For more information write, use coupon, or CALL TOLL FREE 800-227-5558

© 1989 Millipore Corporation

How gun cotton and a twist of the wrist made the world a safer place.

In 1855, a German scientist named Fick created quite a stir in the scientific community.

He took a glass rod, dipped it in some gun cotton (nitrocellulose), and literally started "stirring," or rolling the rod. Much to his delight, a thin "sac" formed on the surface of the rod. And the first membrane filter was created.

Fick was excited. Unfortunately, his colleagues weren't. Which explains why it took almost a century for his discovery to make an impact.

Today, refined offsprings of Fick's crude filter monitor workplace and environmental air quality, detect and treat diseases, uncover impurities in foods and drugs, and ensure water supplies are safe to drink.

Surprisingly, these and hundreds of other uses were advanced or

Millipore membranes have led to more rapid, accurate monitoring of coliform densities in water supplies.

developed by one company. Millipore.

But then, maybe it's not a surprise. Anyone who's worked in a lab has probably used a Millipore filter. In fact, over 100 million will be used this year. For good reason, too. Over 120 contaminants

Millipore test kits can detect fine sand and metal particles to ensure airplane fuel reliability.
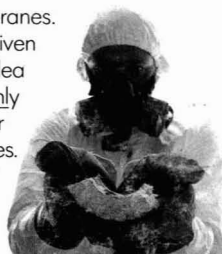
are regulated by the EPA, NIOSH and OSHA. Millipore has membranes to sample them all.

Their filters undergo as many as 25 individual tests.* (More than most people get during a routine physical.)

All this has helped Millipore learn a lot ·

Consistent pore sizes allow Millipore filters to better detect and analyze gas line impurities.

* Depends upon application

about membranes. But it's also given people the idea they're the only manufacturer of membranes. "So," they conclude, "it doesn't matter what brand I buy. It's all Millipore."
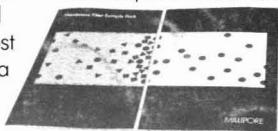
Millipore originated many of the procedures which use membranes for pollution monitoring.

Not so. To ensure you get accurate results—time after time—you've got to ask for Millipore by name.

Try it right now. Call 800-225-1380, or the nearest Millipore office, and ask for a free sample pack, featuring the new Isopore™ track-etched membrane.

After all, it's a lot easier than making your own.

MILLIPORE